The Cardiovascular System and Dioxin Developmental Toxicity in the Zebrafish Embryo

By

Monica Sylvia Yue

A dissertation submitted in partial fulfillment of

the requirements for the degree of

Doctor of Philosophy

(Molecular and Environmental Toxicology)

at the

UNIVERSITY OF WISCONSIN-MADISON

2016

Date of final oral examination: 05/26/2016

The dissertation is approved by the following members of the Final Oral Committee:

Richard E. Peterson, Professor, School of Pharmacy
Christopher A. Bradfield, Professor, Oncology
Chad M. Vezina, Assistant Professor, Comparative Biosciences
Michael R. Taylor, Assistant Professor, Pharmaceutical Sciences
Joan S. Jorgensen, Associate Professor, Comparative Biosciences

ABSTRACT

2,3,7,8-Tetrachlorodibenzo-*p*-dioxin (TCDD) is a lipophilic, persistent, and bioaccumulative environmental contaminant. Zebrafish exposed to TCDD during early life stages develop many toxic effects, including hemorrhages, cardiac malformations, and progressive cardiac failure culminating in circulatory collapse and mortality. Since cardiovascular function is important for the development of organs and tissues it is believed that many of the embryotoxic effects of TCDD are secondary to cardiotoxicity. TCDD toxicity in zebrafish is mediated by activation of the aryl hydrocarbon receptor 2 (AHR2). AHR2 signaling is involved in multiple developmental processes. Thus, it is also likely that TCDD causes toxicity directly in target tissues via aberrant activation of AHR2 and subsequent misregulation of key genes during development. A hallmark of TCDD toxicity is lack of an inflated swim bladder. To investigate the mechanism of this effect, zebrafish embryos were exposed to TCDD and the timecourse of swim bladder development was assessed. In TCDD-treated embryos, swim bladder development was arrested beyond 72 hours post fertilization (hpf), which is concurrent with the onset of TCDD-induced decreases in peripheral blood flow. To determine whether TCDD effects on the swim bladder were secondary to TCDD-induced decreased circulation, swim bladder development was assessed in embryos where cardiac dysfunction was produced by genetic approaches (i.e., *silent heart* morphant; cardiomyocyte-specific constitutively activated AHR signaling, *cmlc2*:caAHR). In such embryos, swim bladder development was inhibited in a pattern reminiscent of that produced by TCDD. At 120 hpf, the swim bladders in all treatment groups (TCDD-exposed, *silent heart* morphants, *cmlc2*:caAHR) were disrupted to a similar extent, indicating that TCDD-induced loss of circulation was sufficient to inhibit swim bladder development. TCDD exposure disrupts development of several vascular structures in zebrafish embryos, and Ahr null mice display vascular defects in the eye and liver. The hypothesis was tested that TCDD exposure disrupts vascular development in the eye and gut of zebrafish embryos. In the

eye, TCDD inhibited anastomosis and altered vessel morphology of the superficial annular vessel (SAV). In the gut, TCDD caused the subintestinal venous plexus (SIVP) to be overgrown and mispatterned. To determine if these TCDD effects on SAV and SIVP development were secondary to TCDD-induced decreases in cardiac output and peripheral circulation, genetic (i.e., *silent heart* morphant) and pharmacologic (i.e., 2,3-butanedione 2-monoxime, BDM) positive controls for cardiac dysfunction were used. Anastomosis of the SAV was disrupted in positive control embryos with inhibited circulation, suggesting that this effect is secondary to TCDD-induced cardiac dysfunction. However, TCDD-induced alterations of SAV vessel morphology and effects in the SIVP were not recapitulated in positive control embryos, suggesting that these TCDD effects are likely caused by mechanisms independent of TCDD-induced circulatory failure. Since cardiac function is an important factor in several of the TCDD effects studied here, the mechanisms that contribute to loss of circulation was also investigated. TCDD inhibits development of the epicardium, the outermost layer of the heart, contributing to the development of cardiac malformations and dysfunction. To better understand the steps involved in epicardium development in zebrafish embryos, the process by which epicardial progenitor cells (i.e., PE cells) migrate to the heart and form the epicardial layer was investigated. PE cells were observed to migrate via formation of a cellular bridge and by the release of cell aggregates. PE clusters could form in the absence of a heartbeat, but failed to migrate or spread over a non-contractile heart. To investigate the factors that influenced PE cell migration, an assay was developed to assess migration of epicardial cells onto hearts isolated from zebrafish embryos *in vitro*. Utilizing this assay it was confirmed that epicardial cells do not migrate onto a non-contractile heart or when myocardial cells were deficient in *tbx5* expression. This suggests that effects in the myocardium can influence epicardial development, highlighting the importance of interactions between these cell types in heart development. Overall, this thesis sheds light on the complex mechanisms of developmental cardiovascular toxicity induced by TCDD in the zebrafish embryo.

DEDICATION

This dissertation is dedicated to my family. To my parents, Kwok To and Drina, who have given me so much love and support, and have inspired me to always challenge myself to work hard to reach my goals. To my sister, Stephanie, who is my lifelong friend and has always encouraged me to be wild, creative, and exceptionally fun (just like her big sis). I also dedicate this dissertation to Ben, who has cheered me on and supported me through all the late nights and weekends, to all my friends near and far, and my cat, Hotpot. Thank you all for the love and support!

ACKNOWLEDGEMENTS

I am truly thankful to my advisor, Richard E. Peterson, for your mentorship, guidance, and kindness. I have gained so much knowledge, both at the bench and beyond it, because of your efforts. I appreciate all the experiences and wonderful stories you have provided me through my graduate school career. I would like to thank each of the members of my committee: Michael R. Taylor, who has supported my research immensely with his knowledge and generosity; Chad Vezina, who has always encouraged me with dynamic and creative ideas; Joan Jorgensen, who has steadfastly supported my ever-changing research projects; and Christopher Bradfield, who has provided me counsel through the most daunting challenges. I appreciate immensely all the guidance and encouragement you have all given me and I consider myself extremely fortunate to be mentored by such bright and wonderful people.

I want to thank all the administration and support staff in the Molecular and Environmental Toxicology Center and the School of Pharmacy for all their help, outreach, and patience. I especially want to thank Mark Marohl for his ever-helpful attitude and friendship. I would also like to thank Warren Heideman for his support early on in my graduate school career.

Thank you to all the members in the lab, past and present, for making every day more enjoyable. I especially want to thank Jessica Plavicki, who has been more than a friend but also a mentor to me. I frankly don't know if I could have done my dissertation without you! You have taught me so much, encouraged me through all my mistakes and demoralizing failures, and inspired me to overcome it all. I also want to thank Kevin Lanham, who always seemed to know what I was confused about and has been so kind and patient in explaining it all to me. I want to thank Joe Gawdzik, for making shared office space fun, always bringing jokes and heady jams to the lab. I also want to thank Tracie Baker, Felipe Burns, Peter Hofsteen, Min-sik Kim, Xinyi Li, and Loes Elemans for being great lab mates, and Dorothy Nesbit

for all her help keeping the fish healthy. In the mouse lab and Taylor lab, I want to thank Robert Moore, Andy Schneider, and Fangzhou Mu for being friendly, helpful, and a lot of fun at all the lab get-togethers.

I am extremely grateful to all my friends who have brightened my life. Thank you to Ashley Brinkman, for being an amazing friend through all the struggles of being a graduate student. Thank you to all my friends that made me feel so loved and welcomed here in Wisconsin: Linda Park, Sarmi Van den Heuvel, Ly Pham, Stella Kim, Heidi Huang, Jonathan Vu, Christine Lien, Elizabeth Thao, Hong and Nancy Vue, Barry Seifert and the trivia crew, Nathan Conn, Jesse Christianson, Tim St. Clair, Javier Velasco, Gene Uenishi, Chantell Evans, Gabby Chaparro, David Banach, Phil and Andrea Hansen, Bryan and Erika Flaherty, Ian and Erin McConnell-Benton, and so many more. I also want to thank my dear friends that have supported me from afar: Kendall "Captain Kinu" McCarthy, Priscilla Mok, and Rosa Trieu. I especially want to thank Benjamin Moderson-Kox, who has been my greatest source of support through all the ups and downs, from driving me home late at night to dinner deliveries to the lab. Your love and encouragement has kept me going these past few years and helped me grow as a person. I cannot express enough the wonderful impact you have had on my life and I will always be grateful for it.

There are still so many more I wish to thank. This has been a grand experience and I consider myself very fortunate that so many brilliant people have contributed to shaping me, supporting me, and guiding me to be where I am today. Thank you all.

TABLE OF CONTENTS

LIST OF FIGURES

CHAPTER II:

CHAPTER III:

CHAPTER IV:

CHAPTER V:

FUTURE DIRECTIONS:

LIST OF TABLES

CHAPTER V:

CHAPTER I: INTRODUCTION

In the 1950s, the Great Lakes region underwent a drastic decline in fish populations. This was most notable in the lake trout (*Salvelinus namaycush*) population, a species that is important to the Great Lakes ecosystem and regional economy. Despite efforts to restock lakes with fish, the lake trout population continued to decline into the late 1970s. Initially it was believed that overfishing and predation was the cause of this severe drop in population. However, it was determined that failed recruitment of lake trout was due to increased sac fry mortality associated with severe pericardial and yolk sac edema, hemorrhages, and craniofacial malformations (Spitsbergen *et al.*, 1991; Walker *et al.*, 1991; Cook *et al.*, 2003; Tillett *et al.*, 2008). These toxic effects closely resembled an edematous syndrome called "blue sac disease", which was first reported in salmonid hatcheries (Wolf, 1969). Further investigation revealed that environmental contamination by halogenated aromatic hydrocarbons (HAHs) with structures and activity similar to 2,3,7,8-tetrachlorodibenzo-*p*-dioxin (TCDD) was the likely cause of blue sac disease and increased mortality in lake trout sac fry (Cook *et al.*, 2003; Tillett *et al.*, 2008).

Fish are among the most sensitive vertebrates to toxicity from exposure to HAHs, especially during early life stages (Peterson *et al*., 1993). In the years since initial reports described the declining lake trout population in the Great Lakes, researchers have gained significant insight into the mechanisms underlying blue sac disease and HAH-induced developmental toxicity in fish species. TCDD and similar HAHs act through activation of the aryl hydrocarbon receptor (AHR) pathway (Hankinson, 1995; Schmidt and Bradfield, 1996). The cardiovascular system is an active site of AHR signaling, and as a result is also a major target of TCDD-induced toxicity mediated by AHR activation (Guiney *et al.*, 1997; Andreasen *et al.*, 2002b; King-Heiden *et al.*, 2012). Proper cardiovascular development and function is essential for survival, and impacts on the individual can translate into broad impacts at the population scale. Thus, understanding the etiology of cardiovascular toxicity can provide insight into the

environmental impacts a contaminant may have on feral fish populations. The following review summarizes current knowledge of how activation of the AHR pathway in fish species causes cardiovascular malformations and defects.

The AHR Pathway

The AHR protein is a member of the basic helix-loop-helix Per-ARNT-Sim (PAS) family of transcription factors (Huang *et al.*, 1993). AHR normally resides in the cytosol in a complex with several chaperone proteins, including p23, XAP2, and a dimer of Hsp90. Upon binding with a ligand, the activated AHR complex translocates into the nucleus where the chaperone proteins are shed and AHR forms a heterodimer with aryl hydrocarbon nuclear receptor translocator (ARNT). The AHR/ARNT complex recognizes and binds to specific sites in the DNA sequence, called xenobiotic response elements (XREs) or AHR response elements (AREs), which leads to chromatin remodeling and recruitment of transcription co-factors to promote gene transcription (Hankinson, 1995; Mimura and Fujii-Kuriyama, 2003; Denison *et al.*, 2011). Members of the PAS family of proteins are involved in sensing and responding to environmental stimuli. As such, it is likely that AHR evolved to respond to environmental compounds by regulating biotransformation and elimination pathways, especially phase I and phase II xenobiotic metabolizing enzymes (Hahn *et al.*, 2002; Mimura and Fujii-Kuriyama, 2003). In addition, AHR is involved in modulating genes involved in cell cycle, cell proliferation, hormone receptor responsiveness, and circadian rhythms (Mimura and Fujii-Kuriyama, 2003; Denison *et al.*, 2011).

AHR pathway components in fish

Fish have multiple AHR genes, which likely arose from a gene duplication event that occurred early in vertebrate evolution (Hahn *et al.*, 2002). Fish have at least two distinct isoforms of AHR, AHR1 and AHR2, which were first identified in killifish (*Fundulus heteroclitus*) and dogfish (*Mustelis canis*) (Hahn *et al.*, 1997). Multiple AHR genes have since been identified and characterized in several other fish

species, including zebrafish (*Danio rerio*), medaka (*Oryzias latipes*), rainbow trout (*Oncorhychus mykiss*), red seabream (*Pagrus major*), and Atlantic tomcod (*Microgadus tomcod*) (reviewed in Hahn *et al.*, 2002; Yamauchi *et al.*, 2005). Phylogenetic analysis indicates that AHR1 is an ortholog of mammalian AHR, while AHR2 is a paralog of AHR1 (Karchner *et al.*, 1999, 2002; Andreasen *et al.*, 2002a). This suggests that multiple functions of mammalian AHR have partitioned between the fish AHR1 and AHR2 forms. Later work has additionally identified two forms of AHR1, AHR1a and AHR1b (Karchner *et al*., 2005). Several studies indicate that AHR2 is the predominant AHR in fish species. In killifish, AHR1 is expressed mostly in the brain, heart, ovary, and testis, while AHR2 is expressed broadly in almost all tissues (Karchner *et al.*, 1999). Similarly, in zebrafish embryos AHR1 expression is limited to the heart, kidney, and liver, while AHR2 is widely expressed in all tissues (Andreasen *et al.*, 2002a).

Fish AHR genes

Multiple studies indicate that AHR2 in fish is primarily responsible for mediating toxicity. *In vitro* binding affinity experiments indicate that zebrafish AHR1a binds poorly to known AHR agonists, such as TCDD or β-napthoflavone (BNF). In contrast, both human AHR and zebrafish AHR1b and AHR2 showed strong binding affinity to TCDD and BNF (Andreasen *et al.*, 2002a; Karchner *et al*., 2005). Transient knockdown of AHR2 expression by injection of a morpholino oligonucleotide (MO) in zebrafish embryos inhibited the onset of developmental toxic effects from exposure to TCDD or BNF (Prasch *et al.*, 2003; Teraoka *et al.*, 2003, 2010; Dong *et al.*, 2004; Antkiewicz *et al.*, 2006). Similar protection from developmental toxicity was observed in killifish and red seabream embryos injected with AHR2 MO and exposed to TCDD or BNF, however no protection was provided when AHR1 MO was injected instead (Yamauchi *et al*., 2006; Clark *et al*., 2010). Recently, a zebrafish AHR2 null line was

developed, *ahr*^{hu3335}. When exposed to TCDD, *ahr*^{hu3335} embryos did not develop hallmark TCDD-induced toxic endpoints (Goodale *et al*., 2012).

Further evidence that AHR2 is the primary isoform in mediating ligand-induced toxicity can be gleaned from studies of fish populations that reside at sites contaminated with HAHs or other AHR agonists. For example, genetic analysis of killifish from streams contaminated with creosote indicated that AHR2 was a recurring target for polymorphisms associated with resistance to TCDD-induced toxicity (Reitzel *et al*., 2014). Similarly, Atlantic tomcod in the HAHs-contaminated Hudson River have a variant of AHR2 that has impaired binding to TCDD (Wirgin *et al*., 2011). In both studies modulation of AHR2 function or signaling was key to continued survival in otherwise toxic environments, reinforcing the role of AHR2 in mediating toxicity.

Although AHR1 is not widely expressed or considered to play a major role in toxicity, it is important to note that some recent research suggests that AHR1 is capable of binding ligands that are not-dioxin-like (i.e., non-traditional AHR ligands), which may result in more subtle toxic endpoints. Zebrafish embryos exposed to a mixture of AHR agonists and antagonists had slightly enhanced toxicity when AHR1a expression was knocked down with MO injection (Garner *et al*., 2013). In addition, *ahr*^{hu3335} null zebrafish exposed to the non-traditional AHR ligand leflunomide showed evidence of binding and activation of AHR1a and AHR1b, although no overt signs of toxicity were observed (Goodale *et al*., 2012).

Fish ARNT genes

Like AHR, fish have multiple ARNT genes, which form heterodimers to activated fish AHR. In zebrafish, there are two forms of ARNT, ARNT1 and ARNT2, with multiple splice variants of each (ARNT1a/b/c, ARNT2a/b/c) (Tanguay *et al*., 2000; Prasch *et al*., 2006). Initially, results from *in vitro*

binding affinity assays suggested that ARNT2b was capable of binding AHR2 and therefore was likely involved in mediating TCDD toxicity (Andreasen *et al*., 2002a). However, it was later revealed through MO experiments that TCDD toxicity requires ARNT1 and not ARNT2 expression (Prasch *et al*., 2006; Antkiewicz *et al*., 2006). Taken together, these data support a paradigm in which ligand binding leads to AHR2 activation, heterodimerization of AHR2 with ARNT1, and, ultimately, altered gene regulation that is sustained, resulting in toxicity.

Gene regulation by AHR activation

After the activated AHR dimerizes with ARNT in the nucleus, the AHR/ARNT complex recognizes and binds to XREs in the DNA sequence, leading to modulation of gene expression. The canonical battery of response genes following exposure to TCDD includes: up-regulation of several phase I enzymes (e.g., cytochrome P450s 1A, 1A2, 1B1) and phase II enzymes (e.g., NADPH, GST-Ya, UGT), altered expression of genes involved in cell proliferation (e.g., TGF-β, IL-1β, PAI-2) and cell cycle regulation (e.g., p27, jun-B, PCNA) (Mimura and Fujii-Kuriyama, 2003; Jönsson *et al*., 2007). The phase I enzyme CYP1A is strongly up-regulated in response to TCDD and other AHR agonists, thus induction of CYP1A mRNA and/or protein activity is widely considered as a marker of AHR activation (Mimura and Fujii-Kuriyama, 2003; Denison *et al*., 2011). In addition, activation of AHR signaling also induces expression of aryl hydrocarbon receptor repressor (AHRR), another member of the PAS family of proteins (Karchner *et al*., 2002). As the name implies, AHRR acts as a repressor of AHR signaling. In zebrafish, AHRRa regulates constitutive AHR signaling during development, while AHRRb regulates genes in the xenobiotic response (Jenny *et al*., 2009).

The induction of cytochrome P450s by AHR activation is a topic of interest because it is suggested that the activity of these enzymes contributes to toxicity by increasing oxidative stress. Some studies have shown a positive correlation between oxidative stress and toxicity from exposure to AHR

agonists (Arzuaga and Elskus, 2010; Goodale *et al*., 2013). Zebrafish and medaka embryos exposed to TCDD or BNF and co-treated with antioxidants, such as N-acetylcysteine and ascorbic acid, showed slight protection against some of the toxic effects induced by TCDD or BNF (Cantrell *et al*., 1996; Kawamura *et al*., 2002; Dong *et al*., 2004; Teraoka *et al*., 2010). Conversely, rainbow trout embryos exposed to the AHR agonist retene and co-treated with various pro-oxidants did not result in increased toxicity (Bauder *et al*., 2005). Multiple studies have additionally shown that inhibition of CYP1A expression in zebrafish embryos does not protect against TCDD-induced toxicity (Carney *et al*., 2004; Antkiewicz *et al*., 2006; Kawamura *et al*., 2002; Xiong *et al*., 2008). Thus, it is possible that CYP1A activity and oxidative stress contributes to toxicity from exposure to AHR agonists, however this effect may be marginal.

AHR Agonists

Halogenated aromatic hydrocarbons

Halogenated aromatic hydrocarbons (HAHs) are lipophilic, persistent, bioaccumulative organic pollutants that contain at least one halogen substitution on a benzene ring. HAHs are produced as by-products in combustion reactions (e.g., municipal and medical waste incinerators, paper bleaching, chemical manufacturing). This family of chemicals includes polychlorinated dibenzo-*p*-dioxins (PCDDs), dibenzofurans (PCDFs), and biphenyls (PCBs). Within these groups, 7 out of 75 possible congeners of PCDDs, 10 out of 135 PCDFs, and 12 out of 209 PCBs are structurally similar and have the ability to bind and activate AHR. The most potent congener of these HAHs is TCDD, hence these compounds are often referred to as dioxin-like compounds (DLCs). The number and position of halogen substitutions influences the ability of a DLC congener to bind to AHR and elicit a toxic response (Van den Berg *et al*., 1998). Work in rainbow trout has shown that mixtures of HAHs can interact in an additive fashion to produce TCDD-like toxicity (Zabel *et al*., 1995a,b; Hornung *et al*., 1999). It is suggested that, because

HAHs are so resistant to metabolism and excretion, exposure to DLCs causes abnormally sustained constitutive activation of AHR and it is this inappropriate signaling that leads to the misregulation of genes culminating in developmental toxicity (Carney *et al*., 2006; King-Heiden *et al*., 2012). Aside from TCDD, other well-studied HAHs that are AHR agonists include: 3,3',4,4',5-pentachlorobiphenyl (PCB126); 3,4,3',4'-tetrachlorobiphenyl (PCB77); 2,3,4,7,8-pentachlorodibenzofuran; and 2,3,7,8-tetrachlorodibenzofuran.

Polycyclic aromatic hydrocarbons

Polycyclic aromatic hydrocarbons (PAHs) are a family of lipophilic environmental pollutants that consist of two or more benzene rings. PAHs are produced from combustion of fossil fuels and organic matter and can be found in coal tar, crude oil, automobile exhaust, and industrial emissions. The toxicity of PAHs is more complex than HAHs. Many PAHs are not AHR agonists, although exposure can lead to toxic effects that appear similar to TCDD-induced toxicity. In general, light PAHs consisting of 2-3 rings (e.g., dibenzothiophene, phenanthrene) cause toxicity in an AHR-independent manner, while heavier 3-5 ring PAHs cause toxicity mediated by AHR (Incardona *et al*., 2011). Zebrafish and rainbow trout embryos exposed to benz[a]anthracene (BaA), BNF, benzo[a]pyrene (BaP), or 7-isopropyl-1-methyl phenanthrene (retene) develop TCDD-like toxicity via activation of AHR2, including strong induction of CYP1A (Billiard *et al*., 2004, 2006; Incardona *et al*., 2006, 2011; Scott *et al*., 2011; Huang *et al*., 2012; Goodale *et al*., 2013). There are of course exceptions. For example, zebrafish exposed to chrysene (4 ring PAH) or benzo[e]pyrene (5 ring PAH) did not exhibit any signs of cardiotoxicity (Incardona *et al*., 2006, 2011).

Unlike HAHs, PAHs are metabolically labile and are substrates of phase I and II enzymes. This can significantly impact toxicity depending on the parent PAH. Knockdown of phase II enzyme GSTp2 in zebrafish embryos increased toxicity of BaP, indicating that elimination via phase II metabolism was an

important protective process influencing toxicity (Garner and Di Giulio, 2012). Similarly, co-exposure of BNF with a CYP1A inhibitor α-naphthoflavone (ANF) has been shown to enhance toxicity in zebrafish embryos (Billiard *et al*., 2006). The ability to rapidly metabolize and remove specific PAHs can vary among species. For example, embryos of olive flounder (*Paralichthys olivaceus*) were much more sensitive to crude oil exposures than the spotted sea bass (*Lateolabrax maculates*) due to a difference in CYP1A metabolic capacity. As a result olive flounder embryos developed a more exaggerated toxic phenotype (Jung *et al*., 2015). Conversely, metabolic processes are sometimes necessary for toxicity, as in the case with pyrene, which causes TCDD-like toxicity in zebrafish embryos that is mediated by AHR2 activation and requires hepatic CYP1A metabolism (Incardona *et al*., 2006). PAHs with substituted derivatives (e.g., alkylation, oxygenation, halogenation) can behave differently than respective un-substituted parent PAHs, including having increased lipophilicity, persistence, and different interactions with AHR and CYP450 enzymes. These PAH derivatives can arise from various environmental transformation processes (e.g., bacterial metabolism in sediments, photooxidation from sun exposure, weathering of crude oil) (Carney *et al*., 2008; Sun *et al*., 2013; Goodale *et al*., 2015). For example, retene is an alkylated derivative of phenanthrene. Rainbow trout embryos exposed to retene show induction of CYP1A and develop AHR-mediated toxicity while exposure to phenanthrene does not (Hawkins *et al*., 2002). In a similar trend, medaka embryos exposed to bacterial metabolites of several PAHs have increased toxicity compared to respective parent PAHs (Carney *et al*., 2008). Finally, oxygenated PAH 7,12-B[a]AQ causes TCDD-like cardiotoxicity in zebrafish embryos and induces expression of several phase I enzymes (Knecht *et al*., 2013; Goodale *et al*., 2015).

In general PAHs tend to be less potent than HAHs, regardless of individual AHR binding affinity (Barron *et al*., 2004). This is likely because activation of AHR leads to rapid induction of pathways that promptly eliminate the PAH itself. Consistent with this hypothesis, chronic exposure of zebrafish and

rainbow trout embryos to PAHs has been shown to closely recapitulate the severity of TCDD-induced toxicity (Billiard *et al*., 1999).

Other AHR agonists

HAHs and PAHs are the most well characterized AHR agonists, although many other AHR agonists have been identified. Examples of naturally occurring AHR agonists include flavonoids from vegetables and fruit (e.g., indole-3-carbonal), tryptophan metabolites (e.g., 6-formyliindolo[3,2-b]carbazole, FICZ), and indirubin (Denison and Nagy 2003; Bergander *et al*., 2003; Brown *et al*., 2015). As many of these ligands occur at low levels in the environment and are rapidly excreted they are often not considered to be of toxicological concern. Recently, it was discovered that solvent extracts of common paper, plastic, and rubber products contain chemicals that can bind and stimulate AHR signaling in zebrafish embryos, resulting in transient expression of xenobiotic response genes like CYP1A. Extracts from rubber also caused toxicity reminiscent of the blue sac disease phenotype (Zhao *et al*., 2013). The exact identity of the chemicals in these solvent extracts is currently unknown, however these findings demonstrate that AHR agonists can be found in a wide variety of sources.

AHR agonists in mixtures

In practice, fish are often exposed to a mixture of contaminants, which can make assessments of environmental risk and hazard challenging. One approach for assessing mixtures of HAHs is to apply the concept of toxic equivalency factors (TEFs). A TEF is the potency of the HAH of interest relative to TCDD. This can be used with concentration data to calculate the cumulative toxic equivalent concentration (TEQ) from all DLCs that an organism may be exposed to (Van den Berg *et al*., 1988). This approach assumes that AHR-active compounds exert toxicity in an additive fashion, which is generally true (Zabel *et al*., 1995b, Walker *et al*., 1996).

However, the TEF approach has limitations and is less applicable to mixtures containing DLC and non-DLC compounds that can sometimes have antagonistic interactions depending on the ratio of compounds in the mixture (Zabel *et al*., 1995b). Since many PAHs and their derivatives can interact with CYP450 enzymes, the presence of CYP450 antagonists or agonists can influence overall toxicity. Killifish embryos exposed to BaP, BNF, or retene and co-exposed to ANF (CYP1A inhibitor) showed enhanced toxicity that could be additive or synergistic in nature depending on the concentration of ANF (Wassenberg and Di Giulio, 2004; Scott and Hodson, 2008). Heterocyclic derivatives of PAHs, which often occur in the environment and do not normally perturb CYP1A activity, have also been shown to enhance toxicity in killifish embryos when exposed in a mixture with AHR agonists (Wassenberg *et al*., 2005). A significant source of PAH contamination is crude oil, which can contain complex mixtures of PAHs that are agonists or antagonists to AHR or CYP450s. In addition, weathering shifts the profile of PAHs in crude oil, generally from a majority of light PAHs to heavy PAHs with more alkylated PAH derivatives. As a result, original crude oil may exert toxicity via AHR-independent pathways, but over time with weathering shift to include AHR-dependent pathways as well (Incardona *et al*., 2011; Jung *et al*., 2013).

Blue Sac Disease Associated with AHR Activation

Blue sac disease, or blue sac syndrome, in fish embryos is characterized by yolk sac and pericardial edema, congestion of peripheral blood circulation, hemorrhage, stunted growth, spinal deformities, craniofacial malformations, and increased mortality post hatching (Spitsbergen *et al*., 1991; Walker *et al*., 1991). The blue sac disease phenotype was first reported in salmon hatcheries, where it was observed that the edema in sac fry sometimes had a milky blue color (Wolf, 1969). Several factors can induce blue sac disease, including elevated ammonia levels, temperature shock, and hypoxia (Spitsbergen

et al., 1991). Today, blue sac disease is most commonly associated with AHR agonist exposures due to the similarity of the blue sac disease phenotype to developmental toxicity caused by DLCs in Great Lakes lake trout sac fry (Spitsbergen *et al*., 1991; Walker *et al*., 1991; Tillett *et al*., 2008). Lake trout and rainbow trout embryos exposed to mixtures of HAHs in ratios similar to what has been reported in Lake Michigan have been shown to develop toxicity comparable to blue sac disease and TCDD toxicity (Walker *et al*., 1996).

While the toxic endpoints of TCDD exposure that make up the blue sac disease phenotype are shared across fish species, different species vary in sensitivity to TCDD toxicity, reflected in the severity of blue sac disease phenotype. Bull trout (*Salvelinus confluentus*), lake trout (*Salvelinus namaycush*), rainbow trout (*Oncorhynchus mykiss*), brook trout (*Salvelinus fontinalis*), lake herring (*Coregonus artedii*), white sucker (*Catostomus commersoni*), northern pike (*Esox lucius*), fathead minnow (*Pimephales promelas*), channel catfish (*Ictalurus punctatus*), medaka, red seabream, and zebrafish all developed blue sac disease following exposure to TCDD, with bull trout being the most sensitive species (Elonen *et al*., 1998; Tanguay *et al*., 2003; Yamauchi *et al*., 2006). Similarly, rainbow trout embryos exposed to retene also develop blue sac disease phenotype (Brinkworth *et al*., 2003; Hodson *et al*., 2007). Atlantic herring (*Clupea harengus*), killifish, fathead minnow, white sucker, rainbow trout, and medaka embryos exposed to various formulations of crude oil, heavy fuel oil, bitumen, and wastewater from oil sands refineries develop blue sac disease phenotypes in a dose-dependent manner, sometimes with induction of CYP1A (Colavecchia *et al*., 2004, 2006; Boudreau *et al*., 2009; Greer *et al*., 2012; Martin *et al*., 2014; Madison *et al*. 2015). These various petroleum formulations are mixtures of PAHs, thus the development of blue sac disease toxicity is often interpreted to suggest presence of AHR agonists.

Cardiovascular Toxicity and Activation of AHR Signaling

The pericardial edema, hemorrhaging, and blood congestion observed in embryos with blue sac disease indicate that the cardiovascular system is a prominent target of AHR-mediated toxicity. Zebrafish embryos exposed to TCDD also exhibited strong induction of CYP1A in the vascular endothelium and heart as early as 48 hours post fertilization (hpf), before most signs of overt toxicity (Andreasen *et al*., 2002b). A variety of cardiovascular defects have been identified in fish species exposed to contaminants that cause aberrant AHR activation and signaling.

Heart malformations

One of the first organs to form during embryogenesis is the heart, and a hallmark of TCDD toxicity is the development of cardiac malformations. Fish have a two-chambered heart consisting of a ventricle and atrium, with an inflow tract (sinus venosus) and outflow tract (bulbus arteriosus). The heart initially forms a tube, which loops to arrange the ventricle next to the atrium (Stainier, 2001; Bakkers, 2011). Zebrafish exposed to TCDD or PCB126 have an un-looped heart with a compacted ventricle, elongated atrium, and reduced bulbus arteriosus (Antkiewicz *et al*., 2005; Grimes *et al*., 2008). Similar observations of heart un-looping have been reported for other fish species exposed to a variety of AHR agonists, including medaka embryos exposed to retene, zebrafish embryos exposed to BaP or BaA, and killifish embryos exposed to BNF or PCB126 (Incardona *et al*., 2006; Clark *et al*., 2010; Huang *et al*., 2012; Mu *et al*., 2014). Although heart malformations often develop concurrent with pericardial edema, experiments have shown that the elongated heart phenotype is not due to pressure caused by edema (Antkiewicz *et al*., 2005). Interestingly, TCDD exposure can cause a normally looped heart to un-loop. Zebrafish embryos with normally looped hearts exposed to TCDD at 72 hpf had un-looped hearts 48 hours later (Carney *et al*., 2006).

In addition to changes in heart shape, multiple studies have observed that heart size is often reduced following exposure to AHR agonists. Rainbow trout embryos exposed to TCDD have a reduced heart size, which can be up to 50% smaller than a control heart at 50 days post fertilization (dpf) (Hornung *et al*., 1999). Similarly, zebrafish and red seabream embryos exposed to TCDD develop smaller hearts than similarly aged controls (Antkiewicz *et al*., 2005; Carney *et al*., 2006; Yamauchi *et al*., 2006). In addition, early work in juvenile yellow perch (*Perca flavescens*) exposed to TCDD showed an increased incidence of cardiac lesions, including necrosis of myocytes (Spitsbergen *et al*., 1988a). Similar cardiac effects, such as cardiac fibrosis and necrosis, have been reported in juvenile zebrafish exposed to a chronic diet of TCDD and examined 42 days later (Liu *et al*., 2014).

The heart is made up of many different cell types. The embryonic heart is organized into three layers: the endocardium (continuous with the vascular endothelium), the myocardium (containing cardiomyocytes responsible for contraction), and the epicardium (outermost layer of the heart) (Stainier, 2001; Bakkers, 2011). Several studies have observed defects in different layers of the heart in response to contaminant exposure.

Effects on the epicardium

While the endocardium and myocardium are derived from the primary heart field and make up the primitive heart tube, the epicardium is derived from a separate pool of progenitors, the proepicardium (PE). These progenitor cells migrate to the heart before spreading over and enveloping the heart to form the epicardium (Serluca, 2008; Brade *et al*., 2013). Several studies have highlighted the epicardium as a target of TCDD toxicity and it may serve as a useful sensor of developmental toxicity (Hofsteen *et al*., 2013b). Early exposure of zebrafish embryos to TCDD causes failure of PE formation and loss of epicardial markers (Plavicki *et al*., 2013). Exposure to TCDD after the PE formed and migrated to the heart inhibited expansion of epicardial cells on the heart, leading to incomplete epicardium formation

(Plavicki *et al*., 2013). Adult zebrafish pre-treated with TCDD were unable to heal from ventricular wounding, a process that requires activation of the epicardial layer (Hofsteen *et al*., 2013a). Similarly, juvenile zebrafish exposed to a sublethal dose of TCDD developed pericardial edema and mild hyperplasia of the ventricular epicardium when assessed as adults (King-Heiden *et al*., 2009).

Effects on the myocardium

Zebrafish embryos exposed to various PAHs (BaA, BaP, retene) or weathered crude oil show induction of CYP1A in the myocardium prior to onset of other cardiac malformations, such as decreased contractility and heart un-looping (Incardona *et al*., 2011; Jung *et al*., 2013). These studies indicate that the myocardium is a key target for AHR activation. One of the earliest effects of TCDD exposure in zebrafish is a decreased number of cardiomyocytes at 48 hpf, which causes a decrease in heart size observed later at 72 hpf (Antkiewicz *et al*., 2005). Similarly, zebrafish embryos exposed to PCB126 had fewer cardiomyocytes compared to controls, as well as reduced myocardial proliferation and cell size (Grimes *et al*., 2008). Activation of AHR in the myocardium can also affect myocardial processes. For example, zebrafish embryos exposed to retene had altered formation of cardiac jelly, which is extracellular matrix secreted by the myocardium. At 36 hpf, the layer of cardiac jelly was reduced, but at 72 hpf there was an excessive amount of cardiac jelly, suggesting inappropriate deposition or clearance of extracelluar matrix by the myocardial cells (Scott *et al*., 2011).

Effects on the endocardium

Interest in the endocardial layer of the heart is often in the context of valve formation and function. Valves are derived from endothelial cells of the endocardium (Hu *et al*., 2000; Bakkers, 2011). Zebrafish embryos exposed to TCDD have improper valve formation, which leads to blood regurgitation between chambers in the heart (Mehta *et al*., 2008). Further examination revealed that endothelial clusters failed to form at the AV and outflow junctions in TCDD-treated embryos at 48 hpf, which is a step

required for valve formation. Expression of *bmp4* and *notch1b*, which is normally restricted to the presumptive valve sites, was instead strongly induced and de-localized in TCDD-treated embryos (Mehta *et al*., 2008). Similar observations of abnormal development at the AV and outflow junctions have been reported for zebrafish embryos exposed to PCB126 (Grimes *et al*., 2008).

Aside from effects on valve development, adult scup and trout exposed to BNF showed strong induction of CYP1A activity specifically in the endocardium, which has not been reported for other fish species (Stegeman *et al*., 1989). This may suggest that in different fish species or at different life stages specific layers in the heart may be more sensitive to altered AHR signaling.

Cardiac dysfunction

Cardiac morphology and function are inextricably related; effects on cardiac function can alter heart morphology and vice versa. Thus, toxic effects on cardiac function and heart morphology often manifest simultaneously. Decreased cardiac output can result from decreased heart rate. Reduction in heart rate has been observed in zebrafish embryos exposed to TCDD or BaP, and red seabream embryos exposed to TCDD (Henry *et al*., 1997; Yamauchi *et al*., 2006; Incardona *et al*., 2011; Huang *et al*., 2012). A recent study has also reported that Bluefin tuna (*Thunnus thynnus*), yellowfin tuna (*Thunnus albacares*), and amberjack (*Seriola dumerili*) embryos that were exposed to weathered crude oil samples from the Deepwater Horizon spill developed a reduced heart rate and irregular atrial arrhythmias (Incardona *et al*., 2014). In many cases, severe reductions in heart rate eventually culminate in complete cardiac standstill and circulatory collapse (Henry *et al*., 1997; Antkiewicz *et al*., 2005, 2006).

Cardiac dysfunction can also arise from decreased stroke volume, which was observed in zebrafish embryos exposed to TCDD and BaP (Antkiewicz *et al*., 2006; Huang *et al*., 2012). Zebrafish embryos exposed to TCDD at 72 hpf also had decreased cardiac output 8 hours after exposure, which

preceded gross changes to heart shape (e.g., un-looping). Microarray analysis of TCDD-exposed hearts 1-2 hours after exposure indicated altered expression of genes involved in proliferation, heart contractility, and heart development (Carney *et al*., 2006). In a similar study involving zebrafish embryos exposed to BaP and non-AHR agonist fluoranthene, microarray analysis of embryo hearts showed significant alteration in genes involved in Ca^{2+} cycling and muscle contractions 2-6 hours after exposure (Jayasundara *et al*., 2015). Taken together these results indicate that activation of AHR in the heart can affect cardiac function, possibly through direct effects on cardiac contractility or through alterations in cardiac morphology and stroke volume.

Circulatory effects

Decreased blood flow has been reported in various peripheral vascular beds in fish species exposed to TCDD, including zebrafish, lake trout, rainbow trout, brook trout, killifish, and medaka (Henry *et al*., 1997; Hornung *et al*., 1999; Guiney *et al*., 2000; Belair *et al*., 2001; Toomey *et al*., 2001; Kawamura *et al*., 2002). Reductions in peripheral blood flow often preceded development of other toxic endpoints, such as severe edema, hemorrhages, and craniofacial malformations (Guiney *et al*., 2000). Zebrafish embryos exposed to TCDD at 72 hpf had decreased blood flow in the intersegmental vessels 12 hour after exposure, and complete loss of circulation by 120 hpf (Carney *et al*., 2006).

In addition to global changes in circulation, several studies have reported specific effects on regional blood flow, which could impact development of surrounding tissues and organs. Lake trout embryos exposed to TCDD have poor perfusion of the yolk vitelline vasculature, which may contribute to failed absorption of the yolk later in development (Walker *et al*., 1991; Guiney *et al*., 2000). In zebrafish, TCDD exposure causes reduced perfusion of the prosencephalic artery and mesencephalic vein as early as 50 hpf. These reductions in blood flow have been correlated with a slight increase in apoptosis in the midbrain at 60 hpf, involves signaling through the thromboxane receptor pathway, and increased

expression of CYP1C1, CYP1C2, and COX2 (Dong *et al*., 2002; Teraoka *et al*., 2009, 2010; Kubota *et al*., 2011). TCDD exposure has also been observed to transiently increase and then decrease blood flow in the hypobranchial artery in zebrafish embryos (Teraoka *et al*., 2002).

Hematopoiesis

Zebrafish embryos exposed to TCDD fail to transition from primitive to definitive hematopoiesis and, consequently, develop anemia (Belair *et al*., 2001). A similar effect was observed when zebrafish embryos were exposed to a high level of retene (Scott *et al*., 2011). The mechanism preventing the transition to definitive hematopoiesis is not known, although several studies have suggested multiple genes that may be involved. *SCL* is a marker of definitive hematopoiesis and was found to be mis-patterned in TCDD-exposed embryos (Belair *et al*., 2001). Alternatively, increased constitutive AHR expression caused by knockdown of AHRRa in zebrafish embryos led to an inappropriate increase in embryonic hemoglobin (*hbbe3*), which may promote continued primitive hematopoiesis beyond when the transition to definitive hematopoiesis would normally occur (Aluru *et al*., 2014). Microarray analysis of zebrafish exposed to TCDD also indicated that micro RNAs involved in erythrocyte maturation (miR-144, miR-451) are significantly repressed when mature erythrocytes should begin appearing in the circulation (Jenny *et al*., 2012).

Even after mature erythrocytes are established in the circulation it appears that juvenile and adult fish remain sensitive to TCDD-induced anemia. Juvenile and yearling rainbow trout exposed to TCDD showed signs of leukopenia, thrombocytopenia, and decreased hematopoiesis in the kidney (Spitsbergen *et al*., 1988b). Similarly, juvenile rainbow trout exposed to a chronic diet of TCDD developed anemia 28 days later (Liu *et al*., 2013).

Effects on the vascular endothelium

The vascular endothelium is likely a key target for TCDD toxicity. CYP1A is strongly induced in the vasculature following TCDD exposure in medaka, lake trout, killifish, and zebrafish embryos, and BNF exposure in scup and rainbow trout (Stegeman *et al.*, 1989; Cantrell *et al*., 1996; Guiney *et al*., 1997; Hornung *et al*., 1999; Toomey *et al*., 2001; Andreasen *et al*., 2002b). Activation of AHR in the endothelium precedes development of other toxic phenotypes, including regional decreases in blood flow and hemorrhaging (Cantrell *et al*., 1996; Hornung *et al*., 1999; Dong *et al*., 2002). In zebrafish, TCDD exposure induced CYP1A mRNA in the endothelium as early as 24 hpf (Andreasen *et al*., 2002b). Microarray analysis of zebrafish embryos exposed to BaA also indicated mis-expression of genes involved in vascular development, suggesting that AHR activation may cause toxicity through this mechanism as well (Goodale *et al*., 2013).

Hemorrhaging and vascular permeability

Hemorrhaging is one of the most visible effects of TCDD toxicity and is an indicator of blue sac disease. Zebrafish, killifish, lake trout, rainbow trout, medaka, and seabream (*Sparus aurata*) embryos exposed to various AHR agonists such as TCDD, retene, and BaP all develop hemorrhages (Spitsbergen *et al*., 1991; Henry *et al*., 1997; Billiard *et al*., 1999; Toomey *et al*., 2001; Brinkworth *et al*., 2003; Kawamura *et al*., 2002; Ortiz-Delgado and Sarasquete, 2004). Hemorrhages may appear anywhere in the vasculature, though the most common tissues where hemorrhaging has been observed include the eye (retrobulbar), head, and yolk sac (Henry *et al*., 1997; Hornung *et al*., 1999; Scott *et al*., 2009). Subcutaneous hemorrhaging has also been reported in juvenile and adult fish exposed to TCDD (Kleeman *et al*., 1988; Liu *et al*., 2013).

It is not known how hemorrhages form in response to AHR activation, though it is suggested that alterations in vessel integrity and vascular permeability are contributing factors. Zebrafish embryos

exposed to TCDD had increased permeability to albumin in the dorsal midbrain (Dong *et al*., 2004). Analysis of TCDD-treated lake trout suggests that edema fluid in the yolk sac is an ultrafiltrate of blood (Guiney *et al*., 2000). Other studies have reported similar altered vascular permeability following exposure to AHR agonists in medaka, killifish, and juvenile seabream (Cantrell *et al*., 1996; Toomey *et al*., 2001; Lauriano *et al*., 2012). It has been proposed that increased vascular permeability leading to hemorrhages is caused by apoptosis or increased oxidative stress in the endothelial cells (Cantrell *et al*., 1996, 1998; Brinkworth *et al*., 2003). However, apoptosis or necrosis of endothelial cells following TCDD exposure has not been reported in other studies even in the presence of hemorrhages and severe edema (Hornung *et al*., 1999; Guiney *et al*., 2000).

Vascular malformations

TCDD has been shown to cause malformations of specific vascular structures. Medaka embryos exposed to TCDD exhibit regression of the yolk vasculature (Kawamura *et al*., 2002). In zebrafish, the common cardinal vein (CCV) is a paired vessel that initially extends across the yolk and connects to the inflow tract of the heart. The CCV is remodeled during development and finally regresses dorsally with the heart (Isogai *et al*., 2001). Zebrafish embryos exposed to TCDD had reduced maximal ventral growth of the CCV. Later, proper remodeling and regression of the CCV was also inhibited (Bello *et al*., 2004). In the brain, zebrafish embryos exposed to TCDD or BNF exhibited concentration-dependent rearrangements in the shape of the prosencephalic artery (Teraoka *et al*., 2010). Interestingly, the levels of TCDD or BNF that caused rearrangements in brain vasculature did not alter vascular development in the tail or trunk, suggesting that vasculature in the brain is much more sensitive to insult from aberrant AHR activation (Teraoka *et al*., 2010).

Sublethal effects of AHR activation on swimming performance

Several fish species exposed to TCDD during early life were reportedly lethargic after hatching (Elonen *et al*., 1998). Recent studies have focused on this facet of AHR agonist toxicity, investigating the impact that contaminants may have on the swimming and metabolic performance in fish. Decreased swimming ability or metabolic efficiency can decrease individual survival and health, especially in fish that have high rates of activity, mobility, and endurance (Incardona *et al*., 2015; Klinger *et al*., 2015).

Embryos are more sensitive to toxic insult than juveniles or adults (Lanham *et al*., 2012). However, exposures to contaminants during early life when key organ systems are developing can lead to adverse effects later in life. Pink salmon (*Oncorhynchus gorbuscha*) and Pacific herring (*Clupea pallasi*) exposed to trace levels of crude oil as embryos developed defects in the outflow tract, compact myocardium, and spongy myocardium as juveniles (Incardona *et al*., 2015). Zebrafish exposed to low levels of weathered crude oil for up to 48 hours as embryos developed subtle changes in heart shape as adults. These subtle morphological changes reduced swimming performance, measured as a reduction in critical swimming velocity (Hicken *et al*., 2011).

Recent studies indicate that even acute exposures for relatively short periods of time can affect juvenile and adult fish. Adult zebrafish exposed to BNF for 48 hours had decreased active metabolic rate, reduced aerobic capacity, decreased cardiac output, and atrioventricular conduction blockade (Gerger *et al*., 2015). Similarly, adult zebrafish exposed to BaP had altered oxygen consumption when swimming and decreased ventricular heart rate (Gerger and Weber, 2015). Juvenile mahi mahi (*Coryphaena hippurus*) exposed to samples of Deepwater Horizon oil also showed decreased swimming efficiency (Mager *et al*., 2014). Mature chub mackerel (*Scomber japonicus*) exposed to weathered crude oil for 96 hours had increased oxygen consumption, likely due to the bioenergetic cost of inducing detoxification pathways (Klinger *et al*., 2015).

RESEARCH PROBLEMS TO BE ADDRESSED

Early life exposure to TCDD causes developmental toxicity in many vertebrate species, with fish being particularly sensitive to TCDD-induced toxicity (Peterson *et al*., 1993). Zebrafish embryos exposed to TCDD develop a variety of cardiovascular defects, highlighting this organ system as a major target of interest. Other notable effects of TCDD exposure include pericardial edema, yolk sac edema, meningeal edema, craniofacial malformations, an un-inflated swim bladder, spinal deformities, growth arrest, and mortality (Henry *et al*., 1997; Antkiewicz *et al*., 2005; King-Heiden *et al*., 2012). The toxic effects of TCDD in fish are mediated by activation of the AHR2 pathway (Prasch *et al*., 2003, 2006; Antkiewicz *et al*., 2006).

A significant feature of TCDD-induced cardiotoxicity in zebrafish embryos is cardiac dysfunction. Cardiac output is reduced at 60 hpf, significantly affecting peripheral circulation by 72 hpf, and eventually culminating in complete loss of circulation at 96-120 hpf (Henry *et al*., 1997; Antkiewicz *et al*., 2005, 2006). Given the importance of circulation in the development of organs and tissues, it is tempting to suggest that many of the effects associated with TCDD developmental toxicity are caused by TCDD-induced repression of cardiac function. However, several studies have shown that this is not necessarily the case. For example, TCDD exposure causes craniofacial malformations and reduced growth of the lower jaw in many fish species (Walker *et al*., 1991; Hornung *et al*., 1999; Henry *et al*., 1997). Initially, it was proposed that these effects were due to decreases in regional circulation in the head and jaw area (Teraoka *et al*., 2002). However, later studies indicate that malformations of the developing jaw and palate are more likely due to TCDD interfering with signaling pathways involved in chondrogenesis and cartilage deposition rather than TCDD-induced effects on circulation (Teraoka *et al*., 2006; Xiong *et al*., 2008; Planchart and Mattingly, 2010; Burns *et al*., 2015).

Another hallmark sign of TCDD developmental toxicity in fish larvae is failure of the swim bladder to inflate. Although lack of swim bladder inflation has been observed in many fish species following exposure to TCDD and other AHR agonists, the mechanism by which this AHR-dependent effect is produced is unknown (Henry *et al*., 1997; Oritz-Delagado *et al*., 2004; King-Heiden *et al*., 2012). Thus, the aim of Chapter II was to characterize the development of the TCDD-induced swim bladder phenotype, and to test the hypothesis that it is secondary to TCDD-induced loss of circulation.

Recent work has identified a novel target of TCDD toxicity: the epicardium. The epicardium plays an important role in heart development and function (Hofsteen *et al*., 2013b). In zebrafish, TCDD exposure inhibits epicardium formation (Plavicki *et al*., 2013). Loss of the epicardium is embryonic lethal and impaired epicardium formation is associated with defects in endocardial valve development, cardiomyocyte proliferation and alignment, development of the coronary vasculature, and heart regeneration (Lie-Venema *et al*., 2007; Gittenberger-de Groot *et al*., 2012; Smart *et al*., 2013). In zebrafish the developmental events leading to epicardium formation are poorly understood. The epicardium is derived from progenitor cells, the proepicardium (PE), which form clusters of cells along the pericardial wall beginning at approximately 50 hpf. These PE cells migrate to the myocardium as the heart develops, eventually forming the epicardial layer (Serulca, 2008). The factors mediating PE cell migration in zebrafish are not known. Hence, the aim of Chapter III was to characterize the migration of PE cells to the heart and investigate factors that may influence this key process in heart development, including expression of epicardial markers and the role of heartbeat on the migration process. Work in Chapter III was done in collaboration with Dr. Jessica Plavicki.

Interactions between the epicardial and myocardial layer have been shown to significantly affect overall heart development (Weeke-Klimp *et al*., 2010; Takahashi *et al*., 2014). Aberrant crosstalk between these neighboring layers in the heart is associated with congenital heart diseases, such as

hypoplastic left heart syndrome and endocardial fibroelastosis (Gittenberger-deGroot *et al*., 2012; Brade *et al*., 2013). However, current approaches to studying epicardial development rarely take into consideration these important cell-cell interactions, especially *in vitro* (Hatcher *et al*., 2004; Pae *et al*., 2008; Ishii *et al*., 2010). Thus, the goal of Chapter IV was to develop an *in vitro* assay to assess epicardial migration using whole hearts from zebrafish embryos. This tool allows for genetic or pharmacological manipulation of epicardial and/or myocardial cells. The assay maintains key cell-cell interactions between heart layers, while enabling independent investigation of cell type-specific factors that may influence the migration of epicardial progenitor cells.

TCDD is known to affect specific vascular structures in fish embryos during early development, such as the yolk vitelline vasculature (Kawamura *et al*., 2002), the common cardinal vein (Bello *et al*., 2004), and the prosencephalic and mesencephalic vessels in the brain (Dong *et al*., 2002; Teraoka *et al*., 2010). Previous work has shown that TCDD exposure causes AHR activation throughout the entire vasculature in zebrafish embryos prior to onset of toxicity (Andreasen *et al*., 2002b). This is perhaps not surprising since research in other model organisms has indicated that the AHR signaling pathway is involved in the development of multiple vascular structures. For example, Ahr null mice develop vascular abnormalities in the eye and liver (Lahvis *et al.*, 2000; Choudhary *et al.*, 2015). Despite this, parallel structures in the zebrafish embryo have heretofore received little attention.

For instance, a hallmark of TCDD exposure in many fish species is failed absorption of the yolk, which likely contributes to increased mortality (Cantrell *et al.*, 1996; Guiney *et al.*, 1997; Henry *et al.*, 1997; Yamauchi *et al.*, 2006). In zebrafish, the gut vasculature, which consists of the subintestinal venous plexus (SIVP), is intimately involved in the transfer of nutrients from the yolk during early development and later contributes to hepatic and intestinal vasculature (Isogai *et al*., 2001). Various studies in fish species involving TCDD exposure or loss of AHR signaling have also reported defects in eye function

and development (Carvalho and Tillitt, 2004; King-Heiden *et al*., 2012; Aluru *et al*., 2014). Thus, the goal of Chapter V was to investigate and characterize malformations in the developing vasculature of the eye and gut of the zebrafish embryo following exposure to TCDD. In addition, since vascular development is closely connected to blood flow and TCDD causes loss of circulation, the role of blood flow on the vascular development of these organs was also examined.

REFERENCES

Aluru, N., Jenny, M.J. and Hahn, M.E., 2014. Knockdown of a zebrafish aryl hydrocarbon receptor repressor (AHRRa) affects expression of genes related to photoreceptor development and hematopoiesis. *Toxicol*. *Sci*. 139, 381-395.

Andreasen, E.A., Hahn, M.E., Heideman, W., Peterson, R.E., Tanguay, R.L., 2002a. The zebrafish (*Danio rerio*) aryl hydrocarbon receptor type 1 is a novel vertebrate receptor. *Mol*. *Pharmacol*. 62, 234–249.

Andreasen, E.A., Spitsbergen, J.M., Tanguay, R.L., Stegeman, J.J., Heideman, W., Peterson, R.E., 2002b. Tissue-specific expression of AHR2, ARNT2, and CYP1A in zebrafish embryos and larvae: effects of developmental stage and 2,3,7,8-tetrachlorodibenzo-*p*-dioxin exposure. *Toxicol*. *Sci*. 68, 403-419.

Antkiewicz, D.S., Burns, C.G., Carney, S.A., Peterson, R.E., Heideman, W., 2005. Heart malformation is an early response to TCDD in embryonic zebrafish. *Toxicol*. *Sci*. 84, 368–377.

Antkiewicz, D.S., Peterson, R.E., Heideman, W., 2006. Blocking expression of AHR2 and ARNT1 in zebrafish larvae protects against cardiac toxicity of 2,3,7,8- tetrachlorodibenzo-*p*-dioxin. *Toxicol*. *Sci*. 94, 175–182.

Arzuaga, X., Elskus, A., 2010. Polluted-site killifish (*Fundulus heteroclitus*) embryos are resistant to organic pollutant-mediated induction of CYP1A activity, reactive oxygen species, and heart deformities. *Environ*. *Toxicol*. *Chem*. 29, 676-682.

Bakkers, J., 2011. Zebrafish as a model to study cardiac development and human cardiac disease. *Cardiovasc*. *Res*. 91,279-288.

Barron, M.G., Heintz, R., Rice, S.D., 2004. Relative potency of PAHs and heterocycles as aryl hydrocarbon receptor agonists in fish. *Mar*. *Environ*. *Res*. 58, 95-100.

Bauder, M.B., Palace, V.P., Hodson, P.V., 2005. Is oxidative stress the mechanism of blue sac disease in retene-exposed trout larvae? *Environ*. *Toxicol*. *Chem*. 24, 694-702.

Belair, C.D., Peterson, R.E., Heideman, W., 2001. Disruption of erythropoiesis by dioxin in the zebrafish. *Dev*. *Dyn*. 222, 581–594.

Bello, S.M., Heideman, W., Peterson, R.E., 2004. 2,3,7,8-Tetrachlorodibenzo-*p*-dioxin inhibits regression of the common cardinal vein in developing zebrafish. *Toxicol*. *Sci*. 78, 258–266.

Bergander, L., Wahlstrom, N., Alsberg, T., Bergman, J., Rannug, A., Rannug, U., 2003. Characterization of in vitro metabolites of the aryl hydrocarbon receptor ligand 6- formylindolo[3,2-b]carbazole by liquid chromatography-mass spectrometry and NMR. *Drug Metab*. *Dispos*. 31, 233-241.

Billiard, S.M., Querbach, K., Hodson, P.V., 1999. Toxicity of retene to early life stages of two freshwater fish species. *Environ*. *Toxicol*. *Chem*. 18, 2070-2077.

Billiard, S.M., Bols, N.C., Hodson, P.V., 2004. *In vitro* and *in vivo* comparisons of fish-specific CYP1A induction relative potency factors for selected polycyclic aromatic hydrocarbons. *Ecotoxicol. Environ*. Saf. 59, 292-299.

Billiard, S.M., Timme-Laragy, A.R., Wassenberg, D.M., Cockman, C., Di Giulio, R.T., 2006. The role of the aryl hydrocarbon receptor pathway in mediating synergistic developmental toxicity of polycyclic aromatic hydrocarbons to zebrafish. *Toxicol. Sci*. 92, 526-536.

Boudreau, M., Sweezey, M.J., Lee, K., Hodson, P.V., Courtenay, S.C., 2009. Toxicity of Orimulsion-400 to early life stages of Atlantic herring (*Clupea harengus*) and mummichog (*Fundulus heteroclitus*). *Environ. Toxicol. Chem*. 28,1206-1217.

Brade, T., Pane, L.S., Moretti, A., Chien, K.R., Laugwitz, K.L., 2013. Embryonic heart progenitors and cardiogenesis. *Cold Spring Harbor Perspect. Med*. 3, a013847.

Brinkworth, L., Hodson, P., Tabash, S., Lee, P., 2003. CYP1A Induction and Blue Sac Disease in Early Developmental Stages of Rainbow Trout (*Oncorhynchus Mykiss*) Exposed to Retene. *J. Toxicol. Environ. Health A* 66, 526-646.

Brown, D.R., Clark, B.W., Garner, L.V., Di Giulio, R.T., 2015. Zebrafish cardiotoxicity: the effects of CYP1A inhibition and AHR2 knockdown following exposure to weak aryl hydrocarbon receptor agonists. *Environ. Sci. Pollut. Res. Int*. 22, 8329-38.

Burns, F.R., Peterson, R.E., Heideman, W., 2015. Dioxin disrupts cranial cartilage and dermal bone development in zebrafish larvae. *Aquat Toxicol*. 164, 52-60.

Cantrell, S.M., Lutz, L.H., Tillitt, D.E., Hannink, M., 1996. Embryotoxicity of 2,3,7,8-tetrachlorodibenzo-*p*-dioxin (TCDD): the embryonic vasculature is a physiological target for TCDD-induced DNA damage and apoptotic cell death in Medaka (*Orizias latipes*). *Toxicol. Appl. Pharmacol*. 141, 23–34.

Cantrell, S.M., Joy-Schlezinger, J., Stegeman, J.J., Tillitt, D.E., Hannink, M., 1998. Correlation of 2,3,7,8-tetrachlorodibenzo-*p*-dioxin-induced apoptotic cell death in the embryonic vasculature with embryotoxicity. *Toxicol. Appl. Pharmacol*. 148, 24–34.

Carney, S.A., Peterson, R.E., Heideman, W., 2004. 2,3,7,8-Tetrachlorodibenzo-*p*-dioxin activation of the aryl hydrocarbon receptor/aryl hydrocarbon receptor nuclear translocator pathway causes developmental toxicity through a CYP1A- independent mechanism in zebrafish. *Mol. Pharmacol*. 66, 512–521.

Carney, S.A., Chen, J., Burns, C.G., Xiong, K.M., Peterson, R.E., Heideman, W., 2006. Aryl hydrocarbon receptor activation produces heart-specific transcriptional and toxic responses in developing zebrafish. *Mol. Pharmacol*. 70, 549-561.

Carney, M.W., Erwin, K., Hardman, R., Yuen, B., Volz, D.C., Hinton, D.E., Kullman, S.W., 2008. Differential developmental toxicity of naphthoic acid isomers in medaka (*Oryzias latipes*) embryos. *Mar. Pollut. Bull*. 57, 255-266.

Carvalho, P.S., Tillitt, D.E., 2004. 2,3,7,8-TCDD effects on visual structure and function in swim-up rainbow trout. *Environ. Sci. Technol*. 38, 6300–6306.

Choudhary, M., Kazmin, D., Hu, P., Thomas, R.S., McDonnell, D.P., Malek, G., 2015. Aryl hydrocarbon receptor knock-out exacerbates choroidal neovascularization via multiple pathogenic pathways. *J. Pathol.* 235, 101-112.

Clark, B.W., Matson, C.W., Jung, D., Di Giulio, R.T., 2010. AHR2 mediates cardiac teratogenesis of polycyclic aromatic hydrocarbons and PCB-126 in Atlantic killifish (*Fundulus heteroclitus*). *Aquat. Toxicol*. 99, 232-240.

Colavecchia, M.V., Backus, S.M., Hodson, P.V., Parrott, J.L., 2004. Toxicity of oil sands to early life stages of fathead minnows (*Pimephales promelas*). *Environ. Toxicol. Chem*. 23, 1709-1718.

Colavecchia, M.V., Hodson, P.V., Parrott, J.L., 2006. CYP1A induction and blue sac disease in early life stages of white suckers (*Catostomus commersoni*) exposed to oil sands. *J. Toxicol. Environ*. *Health A* 69, 967-994.

Cook, P.M., Robbins, J.A., Endicott, D.D., Lodge, K.B., Guiney, P.D., Walker, M.K., Zabel, E.W., Peterson, R.E., 2003. Effects of aryl hydrocarbon receptor-mediated early life stage toxicity on lake trout populations in Lake Ontario during the 20th century. *Environ. Sci. Technol*. 37, 3864–3877.

Denison, M.S., Nagy, S.R., 2003. Activation of the aryl hydrocarbon receptor by structurally diverse exogenous and endogenous chemicals. *Annu. Rev. Pharmacol*. *Toxicol*. 43, 309-334.

Denison, M.S., Soshilova, A.A., He, G., DeGroot, D.E., Zhao, B., 2011. Exactly the same but different: promiscuity and diversity in the molecular mechanisms of action of the aryl hydrocarbon (dioxin) receptor. *Toxicol. Sci*. 124, 1-22.

Dong, W., Teraoka, H., Yamazaki, K., Tsukiyama, S., Imani, S., Imagawa, T., Stegeman, J.J., Peterson, R.E., Hiraga, T., 2002. 2,3,7,8-tetrachlorodibenzo-*p*-dioxin toxicity in the zebrafish embryo: local circulation failure in the dorsal midbrain is associated with increased apoptosis. *Toxicol. Sci*. 69, 191-201.

Dong, W., Teraoka, H., Tsujimoto, Y., Stegeman, J.J., Hiraga, H., 2004. Role of aryl hydrocarbon receptor in mesencephalic circulation failure and apoptosis in zebrafish embryos exposed to 2,3,7,8-tetrachlorodibenzo-*p*-dioxin. *Toxicol. Sci*. 77, 109–116.

Elonen, G.E., Spehar, R.L., Holcombe, G.W., Johnson, R.D., Fernandez, J.D., Erickson, R.J., Tietge, J.E., Cook, P.M., 1998. Comparative toxicity of 2,3,7,8-tetrachlorodibenzo-*p*-dioxin to seven freshwater fish species during early life stage development. *Environ. Toxicol. Chem.* 17, 472–483.

Garner, L.V., Di Giulio, R.T., 2012. Glutathione transferase pi class 2 (GSTp2) protects against the cardiac deformities caused by exposure to PAHs but not PCB-126 in zebrafish embryos. *Comp. Biochem. Physiol. C Toxicol. Pharmacol*. 155, 573-579.

Garner, L.V., Brown, D.R., Di Giulio, R.T., 2013. Knockdown of AHR1A but not AHR1B exacerbates PAH and PCB-126 toxicity in zebrafish (*Danio rerio*) embryos. *Aquat. Toxicol*. 142-143, 336-46.

Gerger, C.J., Thomas, J.K., Janz, D.M., Weber, L.P., 2015. Acute effects of β-naphthoflavone on cardiorespiratory function and metabolism in adult zebrafish (Danio rerio). *Fish Physiol. Biochem*. 41, 289-298.

Gerger, C.J., Weber, L.P., 2015. Comparison of the acute effects of benzo-a-pyrene on adult zebrafish (*Danio rerio*) cardiorespiratory function following intraperitoneal injection versus aqueous exposure. *Aquat. Toxicol*. 165, 19-30.

Gittenberger-de Groot, A.C., Winter, E.M., Bartelings, M.M., Goumans, M.J., DeRuiter, M.C., Poelmann, R.E., 2012. The arterial and cardiac epicardium in development, disease and repair. *Differentiation* 84, 41-53.

Goodale, B.C., La Du, J.K., Bisson, W.H., Janszen, D.B., Waters, K.M., Tanguay, R.L., 2012. AHR2 mutant reveals functional diversity of aryl hydrocarbon receptors in zebrafish. *PLoS One* 7, e29346.

Goodale, B.C., Tilton, S.C., Corvi, M.M., Wilson, G.R., Janszen, D.B., Anderson, K.A., Waters, K.M., Tanguay, R.L., 2013. Structurally distinct polycyclic aromatic hydrocarbons induce differential transcriptional responses in developing zebrafish. *Toxicol. Appl. Pharmacol*. 272, 656-670.

Goodale, B.C., La Du, J., Tilton, S.C., Sullivan, C.M., Bisson, W.H., Waters, K.M., Tanguay, R.L., 2015. Ligand-Specific Transcriptional Mechanisms Underlie Aryl Hydrocarbon Receptor-Mediated Developmental Toxicity of Oxygenated PAHs. *Toxicol. Sci*. 147, 397-411.

Greer, C.D., Hodson, P.V., Li, Z., King, T., Lee, K., 2012. Toxicity of crude oil chemically dispersed in a wave tank to embryos of Atlantic herring (*Clupea harengus*). *Environ. Toxicol. Chem*. 31, 1324-1333.

Grimes, A.C., Erwin, K.N., Stadt, H.A., Hunter, G.L., Gefroh, H.A., Tsai, H.-J., Kirby, M.L., 2008. PCB 126 exposure disrupts zebrafish ventricular and branchial but not early neural crest development. *Toxicol. Sci*. 106, 193–205.

Guiney, P.G., Smolowitz, R.M., Peterson, R.E., Stegeman, J.J., 1997. Correlation of 2,3,7,8-tetrachlorodibenzo-*p*-dioxin induction of cytochrome P4501A in vascular endothelium with toxicity in early life stages of lake trout. *Toxicol. Appl. Pharmacol*. 143, 256-273.

Guiney, P.D., Walker, M.K., Spitsbergen, J.M., Peterson, R.E., 2000. Hemodynamic dysfunction and cytochrome P4501A mRNA expression induced by 2,3,7,8- tetrachlorodibenzo-*p*-dioxin during embryonic stages of lake trout development. *Toxicol. Appl. Pharmacol*. 168, 1–14.

Hawkins, S.A., Billiard, S.M., Tabash, S.P., Brown, R.S., Hodson, P.V., 2002. Altering cytochrome P4501A activity affects polycyclic aromatic hydrocarbon metabolism and toxicity in rainbow trout (*Oncorhynchus mykiss*). *Environ. Toxicol. Chem*. 21, 1845-1853.

Hankinson, O., 1995. The aryl hydrocarbon receptor complex. *Annu. Rev. Pharmacol. Toxicol*. 35, 307-340.

Hahn, M.E., 2002. Aryl hydrocarbon receptors: diversity and evolution. *Chem.-Biol. Interact*. 141, 131-160.

Hahn, M.E., Karchner, S.I., Shapiro, M.A., Perera, S.A., 1997. Molecular evolution of two vertebrate aryl hydrocarbon (dioxin) receptors (AHR1 and AHR2) and the PAS family. *Proc. Natl. Acad. Sci. U.S.A*. 94, 13743-13748.

Hatcher, C.J., Diman, N.Y.G., Kim, M.S., Pennisi, D., Song, Y., Goldstein, M.M., Mikawa, T., Basson, C.T., 2004. A role for Tbx5 in proepicardial cell migration during cardiogenesis. *Physiol. Genomics* 18, 129-140.

Henry, T.R., Spitsbergen, J.M., Hornung, M.W., Abnet, C.C., Peterson, R.E., 1997. Early life stage toxicity of 2,3,7,8-tetrachlorodibenzo-*p*-dioxin in zebrafish (*Danio rerio*). *Toxicol. Appl. Pharmacol*. 142, 56–68.

Hicken, C.E., Linbo, T.L., Baldwin, D.H., Willis, M.L., Myers, M.S., Holland, L., Larsen, M., Stekoll, M.S., Rice, S.D., Collier, T.K., Scholz, N.L., 2011. Sublethal exposure to crude oil during embryonic development alters cardiac morphology and reduces aerobic capacity in adult fish. *Proc. Natl. Acad. Sci. U.S.A*. 108, 7086-7090.

Hodson, P.V., Qureshi, K., Noble, C.A., Akhtar, P., Brown, R.S., 2007. Inhibition of CYP1A enzymes by alpha-naphthoflavone causes both synergism and antagonism of retene toxicity to rainbow trout (*Oncorhynchus mykiss*). *Aquat. Toxicol*. 81, 275-285.

Hofsteen, P., Mehta, V., Kim, M.S., Peterson, R.E., Heideman, W., 2013a. TCDD inhibits heart regeneration in adult zebrafish. *Toxicol. Sci*. 132, 211-221.

Hofsteen, P., Plavicki, J., Peterson, R.E., Heideman, W., 2013b. Epicardium formation as a sensor in toxicology. *J. Dev. Biol*. 1, 112-125.

Hornung, M.W., Spitsbergen, J.M., Peterson, R.E., 1999. 2,3,7,8-Tetrachlorodibenzo-*p*-dioxin alters cardiovascular and craniofacial development and function in sac fry of rainbow trout (*Oncorhynchus mykiss*). *Toxicol. Sci*. 47, 40–51.

Hu, N., Sedmera, D., Yost, H.J., and Clark, E.B., 2000. Structure and function of the developing zebrafish heart. *Anat. Rec*. 260, 148–157.

Huang, Z.J., Edery, I., Rosbash, M., 1993. PAS is a dimerization domain common to Drosophila period and several transcription factors. *Nature* 364, 259-262.

Huang, L., Wang, C., Zhang, Y., Li, J., Zhong, Y., Zhou, Y., Chen, Y., Zuo, Z., 2012. Benzo[a]pyrene exposure influences the cardiac development and the expression of cardiovascular relative genes in zebrafish (*Danio rerio*) embryos. *Chemosphere* 87, 369-75.

Incardona, J.P., Day, H.L., Collier, T.K., Scholz, N.L., 2006. Developmental toxicity of 4-ring polycyclic aromatic hydrocarbons in zebrafish is differentially dependent on AH receptor isoforms and hepatic cytochrome P4501A metabolism. *Toxicol. Appl. Pharmacol*. 217, 308-21.

Incardona, J.P., Linbo, T.L., Scholz, N.L., 2011. Cardiac toxicity of 5-ring polycyclic aromatic hydrocarbons is differentially dependent on the aryl hydrocarbon receptor 2 isoform during zebrafish development. *Toxicol. Appl. Pharmacol*. 257, 242-249.

Incardona, J.P., Gardner, L.D., Linbo, T.L., Brown, T.L., Esbaugh, A.J., Mager, E.M., Stieglitz, J.D., French, B.L., Labenia, J.S., Laetz, C.A. and Tagal, M., 2014. Deepwater Horizon crude oil impacts the developing hearts of large predatory pelagic fish. *Proc. Natl. Acad. Sci. U.S.A*. 111, E1510-E1518.

Incardona, J.P., Carls, M.G., Holland, L., Linbo, T.L., Baldwin, D.H., Myers, M.S., Peck, K.A., Tagal, M., Rice, S.D., Scholz, N.L., 2015. Very low embryonic crude oil exposures cause lasting cardiac defects in salmon and herring. *Sci. Rep*. 5, 13499.

Ishii, Y., Garriock, R.J., Navetta, A.M., Coughlin, L.E., Mikawa, T., 2010. BMP signals promote proepicardial protrusion necessary for recruitment of coronary vessel and epicardial progenitors to the heart. *Dev. Cell* 19, 307-316.

Isogai, S., Horiguchi, M., Weinstein, B.M., 2001. The vascular anatomy of the developing zebrafish: an atlas of embryonic and early larval development. *Dev. Biol*. 230, 278-301.

Jayasundara, N., Garner, L.V.T., Meyer, J.N., Erwin, K.N., Di Giulio, R.T., 2015. AHR2-mediated transcriptomic responses underlying the synergistic cardiac developmental toxicity of PAHs. *Toxicol. Sci.* 143, 469-481.

Jenny, M.J., Karchner, S.I., Franks, D.G., Woodin, B.R., Stegeman, J.J., Hahn, M.E., 2009. Distinct roles of two zebrafish AHR repressors (AHRRa and AHRRb) in embryonic development and regulating the response to 2,3,7,8-tetrachlorodibenzo-*p*-dioxin. *Toxicol Sci.* 110, 426-441.

Jenny, M.J., Aluru, N. and Hahn, M.E., 2012. Effects of short-term exposure to 2,3,7,8-tetrachlorodibenzo-*p*-dioxin on microRNA expression in zebrafish embryos. *Toxicol. Appl. Pharmacol*. 264, 262-273.

Jönsson, M.E., Jenny, M.J., Woodin, B.R., Hahn, M.E., Stegeman, J.J., 2007. Role of AHR2 in the expression of novel cytochrome P450 1 family genes, cell cycle genes, and morphological defects in developing zebra fish exposed to 3,3',4,4',5-pentachlorobiphenyl or 2,3,7,8-tetrachlorodibenzo-*p*-dioxin. *Toxicol Sci*. 100, 180-193.

Jung, J,H., Hicken, C.E., Boyd, D., Anulacion, B.F., Carls, M.G., Shim, W.J., Incardona, J.P., 2013. Geologically distinct crude oils cause a common cardiotoxicity syndrome in developing zebrafish. *Chemosphere* 91, 1146-1155.

Jung, J.H., Kim, M., Yim, U.H., Ha, S.Y., Shim, W.J., Chae, Y.S., Kim, H., Incardona, J.P., Linbo, T.L., Kwon, J.H., 2015. Differential Toxicokinetics Determines the Sensitivity of Two Marine Embryonic Fish Exposed to Iranian Heavy Crude Oil. *Environ. Sci. Technol*. 49, 13639-13648.

Karchner, S.I., Franks, D.G., Hahn, M.E., 2005. AHR1B, a new functional aryl hydrocarbon receptor in zebrafish: tandem arrangement of ahr1b and ahr2 genes. *Biochem. J*. 392, 153-161.

Karchner, S.I., Franks, D.G., Powell, W.H., Hahn, M.E., 2002. Regulatory interactions among three members of the vertebrate aryl hydrocarbon receptor family: AHR repressor, AHR1, and AHR2. *J. Biol. Chem*. 277, 6949-6959.

Karchner, S.I., Powell, W.H., Hahn, M.E., 1999. Identification and functional characterization of two highly divergent aryl hydrocarbon receptors (AHR1 and AHR2) in the teleost *Fundulus heteroclitus*. Evidence for a novel subfamily of ligand-binding basic helix loop helix-Per-ARNT-Sim (bHLH-PAS) factors. *J. Biol. Chem*. 274, 33814-33824.

Kawamura, T., Yamashita, I., 2002. Aryl hydrocarbon receptor is required for prevention of blood clotting and for the development of vasculature and bone in the embryos of medaka fish, *Oryzias latipes*. *Zool. Sci*. 19, 309–319.

King-Heiden, T.C., Spitsbergen, J., Heideman, W., Peterson, R.E., 2009. Persistent adverse effects on health and reproduction caused by exposure of zebrafish to 2,3,7,8-tetrachlorodibenzo-*p*-dioxin during early development and gonad differentiation. *Toxicol. Sci*. 109, 75–87.

King-Heiden, T.C., Mehta, V., Xiong, K.M., Lanham, K.A., Antkiewicz, D.S., Ganser, A., Heideman, W., Peterson, R.E., 2012. Reproductive and developmental toxicity of dioxin in fish. *Mol. Cell. Endocrinol*. 354, 121-138.

Kleeman, J.M., Olson, J.R., Peterson, R.E., 1988. Species differences in 2,3,7,8- tetrachlorodibenzo-*p*-dioxin toxicity and biotransformation in fish. *Fund. Appl. Toxicol*. 10, 206–213.

Klinger, D.H., Dale, J.J., Machado, B.E., Incardona, J.P., Farwell, C.J., Block, B.A., 2015. Exposure to Deepwater Horizon weathered crude oil increases routine metabolic demand in chub mackerel, Scomber japonicus. *Mar. Pollut. Bull*. 98, 259-266.

Knecht, A.L., Goodale, B.C., Truong, L., Simonich, M.T., Swanson, A.J., Matzke, M.M., Anderson, K.A., Waters, K.M., Tanguay, R.L., 2013. Comparative developmental toxicity of environmentally relevant oxygenated PAHs. *Toxicol Appl Pharmacol*. 271, 266-275.

Kubota, A., Stegeman, J.J., Woodin, B.R., Iwanaga, T., Harano, R., Peterson, R.E., Hiraga, T., Teraoka, H., 2011. Role of zebrafish cytochrome P450 CYP1C genes in the reduced mesencephalic vein blood flow caused by activation of AHR2. *Toxicol. Appl. Pharmacol*. 253, 244–252.

Lahvis, G.P., Lindell, S.L., Thomas, R.S., McCuskey, R.S., Murphy, C., Glover, E., Bentz, M., Southard, J., Bradfield, C.A., 2000. Portosystemic shunting and persistent fetal vascular structures in aryl hydrocarbon receptor-deficient mice. *Proc. Natl. Acad. Sci. U.S.A*. 97, 10442-10447.

Lanham, K.A., Peterson, R.E., Heideman, W., 2012. Sensitivity to dioxin decreases as zebrafish mature. *Toxicol. Sci*. 127, 360-370.

Lauriano, E.R., Calò, M., Silvestri, G., Zaccone, D., Pergolizzi, S., Cascio, P.L., 2012. Mast cells in the intestine and gills of the sea bream, *Sparus aurata*, exposed to a polychlorinated biphenyl, PCB 126. *Acta Histochem*., 114, 166-171.

Lie-Venema, H., van den Akker, N., Bax, N.A., Winter, E.M., Maas, S., Kekarainen, T., Hoeben, R.C., deRuiter, M.C., Poelmann, R.E., Gittenberger-de Groot, A.C., 2007. Origin, fate, and function of epicardium-derived cells (EPDCs) in normal and abnormal cardiac development. *Sci. World J.* 7, 1777-1798.

Liu, Q., Rise, M.L., Spitsbergen, J.M., Hori, T.S., Mieritz, M., Geis, S., McGraw, J.E., Goetz, G., Larson, J., Hutz, R.J., Carvan, M.J., 2013. Gene expression and pathologic alterations in juvenile rainbow trout due to chronic dietary TCDD exposure. *Aquat. Toxicol*. 140, 356-368.

Liu, Q., Spitsbergen, J.M., Cariou, R., Huang, C.Y., Jiang, N., Goetz, G., Hutz, R.J., Tonellato, P.J., Carvan, M.J. 3rd., 2014. Histopathologic alterations associated with global gene expression due to chronic dietary TCDD exposure in juvenile zebrafish. *PLoS One* 9, e100910.

Madison, B.N., Hodson, P.V., Langlois, V.S., 2015. Diluted bitumen causes deformities and molecular responses indicative of oxidative stress in Japanese medaka embryos. *Aquat. Toxicol*. 165, 222-230.

Mager, E.M., Esbaugh, A.J., Stieglitz, J.D., Hoenig, R., Bodinier, C., Incardona, J.P., Scholz, N.L., Benetti, D.D., Grosell, M., 2014. Acute embryonic or juvenile exposure to Deepwater Horizon crude oil impairs the swimming performance of mahi-mahi (*Coryphaena hippurus*). *Environ. Sci. Technol*. 48, 7053-7061.

Martin, J.D., Adams, J., Hollebone, B., King, T., Brown, R.S., Hodson, P.V., 2014. Chronic toxicity of heavy fuel oils to fish embryos using multiple exposure scenarios. *Environ. Toxicol. Chem*. 33, 677-687.

Mehta, V., Peterson, R.E., Heideman, W., 2008. 2,3,7,8-Tetrachlorodibenzo-*p*-dioxin exposure prevents cardiac valve formation in developing zebrafish. *Toxicol. Sci*. 104, 303–311.

Mimura, J., Fujii-Kuriyama, Y., 2003. Functional role of Ahr in the expression of toxic effects by TCDD. *Biochim. Biophys. Acta* 1619, 263-268.

Mu, J., Wang, J., Jin, F., Wang, X., Hong, H., 2014. Comparative embryotoxicity of phenanthrene and alkyl-phenanthrene to marine medaka (*Oryzias melastigma*). *Mar. Pollut. Bull*. 85, 505-15.

Ortiz-Delgado, J.B., Sarasquete, C., 2004. Toxicity, histopathological alterations and immunohistochemical CYP1A induction in the early life stages of the seabream, *Sparus aurata*, following waterborne exposure to B(a)P and TCDD. *J. Mol. Histol*. 35, 29-45.

Pae, S.H., Dokic, D., Dettman, R.W., 2008. Communication between integrin receptors facilitates epicardial cell adhesion and matrix organization. *Dev. Dyn*. 237, 962-978.

Peterson, R.E., Theobald, H.M., Kimmel, G.L., 1993. Developmental and reproductive toxicity of dioxins and related compounds: cross-species comparisons. *Crit. Rev. Toxicol*. 23, 283–335.

Planchart, A., Mattingly, C.J., 2010. 2,3,7,8-Tetrachlorodibenzo-*p*-dioxin upregulates FoxQ1b in zebrafish jaw primordium. *Chem. Res. Toxicol*. 23, 480-487.

Plavicki, J., Hofsteen, P., Peterson, R.E., Heideman, W., 2013. Dioxin inhibits zebrafish epicardium and proepicardium development. *Toxicol. Sci*. 131, 558-567.

Prasch, A.L., Teraoka, H., Carney, S.A., Dong, W., Hiraga, T., Stegeman, J.J., Heideman, W., Peterson, R.E., 2003. Aryl hydrocarbon receptor 2 mediates 2,3,7,8- tetrachlorodibenzo-*p*-dioxin developmental toxicity in zebrafish. *Toxicol. Sci*. 76, 138–150.

Prasch, A.L., Tanguay, R.L., Mehta, V., Heideman, W., Peterson, R.E., 2006. Identification of zebrafish ARNT1 homologs: 2,3,7,8-tetrachlorodibenzo-*p*-dioxin toxicity in the developing zebrafish requires ARNT1. *Mol. Pharmacol*. 69, 776-787.

Reitzel, A.M., Karchner, S.I., Franks, D.G., Evans, B.R., Nacci, D., Champlin, D., Vieira, V.M., Hahn, M.E., 2014. Genetic variation at aryl hydrocarbon receptor (AHR) loci in populations of Atlantic killifish (*Fundulus heteroclitus*) inhabiting polluted and reference habitats. *BMC Evol. Biol*. 14, 6.

Schmidt, J. V., Bradfield, C.A., 1996. Ah receptor signaling pathways. *Annu. Rev. Cell Dev. Biol*. 12, 55–89.

Scott, J.A., Hodson, P.V., 2008. Evidence for multiple mechanisms of toxicity in larval rainbow trout (*Oncorhynchus mykiss*) co-treated with retene and alpha-naphthoflavone. *Aquat. Toxicol*. 88, 200-206.

Scott, J.A., Ross, M., Lemire, B.C., Hodson, P.V., 2009. Embryotoxicity of retene in cotreatment with 2-aminoanthracene, a cytochrome P4501A inhibitor, in rainbow trout (*Oncorhynchus mykiss*). *Environ. Toxicol. Chem*. 28, 1304-1310.

Scott, J.A., Incardona, J.P., Pelkki, K., Shepardson, S., Hodson, P.V., 2011. AhR2-mediated, CYP1A-independent cardiovascular toxicity in zebrafish (*Danio rerio*) embryos exposed to retene. *Aquat. Toxicol*. 101, 165-174.

Serluca, F.C., 2008. Development of the proepicardial organ in zebrafish. Dev. Biol. 315, 18-27.

Smart, N., Dubé, K.N., Riley, P.R., 2013. Epicardial progenitor cells in cardiac regeneration and neovascularisation. *Vascul. Pharmacol*. 58, 164-173.

Spitsbergen, J.M., Kleeman, J.M., Peterson, R.E., 1988a. 2,3,7,8-Tetrachlorodibenzo-*p*-dioxin toxicity in yellow perch (*Perca flavescens*). *J. Toxicol. Environ. Health* 23, 359-383.

Spitsbergen, J.M., Kleeman, J.M., Peterson, R.E., 1988b. Morphologic lesions and acute toxicity in rainbow trout (*Salmo Gairdneri*) treated with 2,3,7,8-tetrachlorodibenzo-*p*-dioxin. *J. Toxicol. Environ. Health* 23, 333-358.

Spitsbergen, J.M., Walker, M.K., Olson, J.R., Peterson, R.E., 1991. Pathologic alterations in early life stages of lake trout, *Salvelinus namaycush*, exposed to 2,3,7,8-tetrachlorodibenzo-*p*-dioxin as fertilized eggs. *Aquat. Toxicol*. 19, 41–72.

Stainier, D.Y., 2001. Zebrafish genetics and vertebrate heart formation. *Nat. Rev. Genet*. 2, 39-48.

Stegeman, J.J., Miller, M.R., Hinton, D.E., 1989. Cytochrome P450IA1 induction and localization in endothelium of vertebrate (teleost) heart. *Mol. Pharmacol*. 36, 723-729.

Sun, J.L., Zeng, H., Ni, H.G., 2013. Halogenated polycyclic aromatic hydrocarbons in the environment. *Chemosphere* 90, 1751-1759.

Takahashi, M., Yamagishi, T., Narematsu, M., Kamimura, T., Kai, M., Nakajima, Y., 2014. Epicardium is required for sarcomeric maturation and cardiomyocyte growth in the ventricular compact layer mediated by transforming growth factor β and fibroblast growth factor before the onset of coronary circulation. *Congenit. Anom*. 54, 162-171.

Tanguay, R.L., Andreasen, E., Heideman, W., Peterson, R.E., 2000. Identification and expression of alternatively spliced aryl hydrocarbon nuclear translocator 2 (ARNT2) cDNAs from zebrafish with distinct functions. *Biochim. Biophys. Acta* 1494, 117–128.

Tanguay, R.L., Andreasen, E., Walker, M.K., Peterson, R.E., 2003. Dioxin toxicity and aryl hydrocarbon receptor signaling in fish. *In*: Schecter, A., Gasiewicz, T.A. (Eds.), Dioxins and Health. John Wiley & Sons, New Jersey, pp. 603–628.

Teraoka, H., Dong, W., Ogawa, S., Tsukiyama, S., Okuhara, Y., Niiyama, M., Ueno, N., Peterson, R.E., Hiraga, T., 2002. 2,3,7,8-Tetrachlorodibenzo-*p*-dioxin toxicity in the zebrafish embryo: altered regional blood flow and impaired lower jaw development. *Toxicol. Sci*. 65, 192–199.

Teraoka, H., Dong, W., Tsujimoto, Y., Iwasa, H., Endoh, D., Ueno, N., Stegeman, J.J., Peterson, R.E., Hiraga, T., 2003. Induction of cytochrome P450 1A is required for circulation failure and edema by 2,3,7,8-tetrachlorodibenzo-*p*-dioxin in zebrafish. *Biochem. Biophys. Res. Commun*. 304, 223-8.

Teraoka, H., Dong, W., Okuhara, Y., Iwasa, H., Shindo, A., Hill, A.J., Kawakami, A., Hiraga, T., 2006. Impairment of lower jaw growth in developing zebrafish exposed to 2,3,7,8-tetrachlorodibenzo-*p*-dioxin and reduced hedgehog expression. *Aquat. Toxicol*. 78, 103-113.

Teraoka, H., Kubota, A., Dong, W., Kawai, Y., Yamazaki, K., Mori, C., Harada, Y., Peterson, R.E., Hiraga, T., 2009. Role of cyclooxygenase 2-thromboxane pathway in 2,3,7,8-tetrachlorodibenzo-*p*-dioxin-induced decrease in mesencephalic vein blood flow in the zebrafish embryo. *Toxicol. Appl. Pharmacol*. 234, 33–40.

Teraoka, H., Ogawa, A., Kubota, A., Stegeman, J.J., Peterson, R.E., Hiraga, T., 2010. Malformation of certain brain blood vessels caused by TCDD activation of Ahr2/Arnt1 signaling in developing zebrafish. *Aquat. Toxicol*. 99, 241–247.

Tillitt, D.E., Cook, P.M., Giesy, J.P., Heideman, W., Peterson, R.E., 2008. Reproductive impairment of great lakes lake trout by dioxin-like chemicals. *In*: Di Giulio, R.T., Hinton, D.E. (Eds.), Toxicology of Fishes. CRC Press, Boca Raton, Florida, pp. 819– 875.

Toomey, B.H., Bello, S., Hahn, M.E., Cantrell, S., Wright, P., Tillitt, D.E., Di Giulio, R.T., 2001. 2,3,7,8-Tetrachlorodibenzo-*p*-dioxin induces apoptotic cell death and cytochrome P4501A expression in developing *Fundulus heteroclitus* embryos. *Aquat. Toxicol*. 53, 127-138.

Van den Berg, M., Birnbaum, L., Bosveld, A.T., Brunstrom, B., Cook, P., Feeley, M., Giesy, J.P., Hanberg, A., Hasegawa, R., Kennedy, S.W., et al., 1998. Toxic equivalency factors (TEFs) for PCBs, PCDDs, PCDFs for humans and wildlife. *Environ. Health Perspect*. 106, 775-792.

Walker, M.K., Spitsbergen, J.M., Olsen, J.R., Peterson, R.E., 1991. 2,3,7,8-Tetrachlorodibenzo-*p*-dioxin (TCDD) toxicity during early life stage development of lake trou (*Salvelinus namaycush*). *Can. J. Fish. Aquat. Sci*. 48, 875-883.

Walker, M.K., Cook, P.M., Butterworth, B.C., Zabel, E.W., Peterson, R.E., 1996. Potency of a complex mixture of polychlorinated dibenzo-*p*-dioxin, dibenzofuran, and biphenyl congeners compared to 2,3,7,8-tetrachlorodibenzo-*p*-dioxin in causing fish early life stage mortality. *Fundam. Appl. Toxicol*. 30, 178-86.

Wassenberg, D.M., Di Giulio, R.T., 2004. Synergistic embryotoxicity of polycyclic aromatic hydrocarbon aryl hydrocarbon receptor agonists with cytochrome P4501A inhibitors in *Fundulus heteroclitus*. *Environ. Health Perspect*. 112, 1658-1664.

Wassenberg, D.M., Nerlinger, A.L., Battle, L.P., Di Giulio, R.T., 2005. Effects of the polycyclic aromatic hydrocarbon heterocycles, carbazole and dibenzothiophene, on *in vivo* and *in vitro* CYP1A activity and polycyclic aromatic hydrocarbon-derived embryonic deformities. *Environ. Toxicol. Chem*. 24, 2526-2532.

Weeke-Klimp, A., Bax, N.A., Bellu, A.R., Winter, E.M., Vrolijk, J., Plantinga, J., Maas, S., Brinker, M., Mahtab, E.A., Gittenberger-de Groot, A.C., van Luyn, M.J., 2010. Epicardium-derived cells enhance proliferation, cellular maturation and alignment of cardiomyocytes. *J. Mol. Cell. Cardiol*. 49, 606-616.

Wirgin, I., Roy, N.K., Loftus, M., Chambers, R.C., Franks, D.G., Hahn, M.E., 2011. Mechanistic basis of resistance to PCBs in Atlantic tomcod from the Hudson River. *Science* 331, 1322-1325.

Wolf, K., 1969. Blue-sac Disease of Fish, US Fish and Wildlife Service, Fish Disease Leaflet. No. 15, pp. 1–4.

Xiong, K.M., Peterson, R.E., Heideman, W., 2008. Aryl hydrocarbon receptor-mediated downregulation of Sox9b causes jaw malformations in zebrafish embryos. *Mol*. *Pharmacol*. 74, 1544–1553.

Yamauchi, M., Kim, E.Y., Iwata, H., Tanabe, S., 2005. Molecular characterization of the aryl hydrocarbon receptors (AHR1 and AHR2) from red seabream (*Pagrus major*). *Comp*. *Biochem. Physiol. C Toxicol. Pharmacol*. 141, 177-187.

Yamauchi, M., Kim, E.Y., Iwata, H., Shima, Y., Tanabe, S., 2006. Toxic effects of 2,3,7,8-tetrachlorodibenzo-*p*-dioxin (TCDD) in developing red seabream (*Pagrus major*) embryo: an association of morphological deformities with AHR1, AHR2 and CYP1A expressions. *Aquat. Toxicol*. 80, 166-179.

Zabel, E.W., Cook, P.M., Peterson, R.E., 1995a. Toxic equivalency factors of polychlorinated dibenzo-p-dioxin, dibenzofuran, and biphenyl congeners based on early life stage mortality in rainbow trout (*Oncorhynchus mykiss*). *Aquat. Toxicol*. 13, 315–328.

Zabel, E.W., Walker, M.K., Hornung, M.W., Clayton, M.K., Peterson, R.E., 1995b. Interactions of polychlorinated dibenzo-*p*-dioxin, dibenzofuran, and biphenyl congeners for producing rainbow trout early life stage mortality. *Toxicol. Appl. Pharmacol*. 134. 204-213.

Zhao, B., Bohonowych, J.E., Timme-Laragy, A., Jung, D., Affatato, A.A., Rice, R.H., Di Giulio, R.T., Denison, M.S., 2013. Common commercial and consumer products contain activators of the aryl hydrocarbon (dioxin) receptor. *PLoS One*. 8, e56860.

CHAPTER II:

DIOXIN INHIBITION OF SWIM BLADDER DEVELOPMENT IN ZEBRAFISH: IS IT SECONDARY TO HEART FAILURE?

Monica S. Yue, Richard E. Peterson, and Warren Heideman

Aquatic Toxicology. (2015) **162**, 10-17.

ABSTRACT

The swim bladder is a gas-filled organ that is used for regulating buoyancy and is essential for survival in most teleost species. In zebrafish, swim bladder development begins during embryogenesis and inflation occurs within 5 days post fertilization (dpf). Embryos exposed to 2,3,7,8-tetrachlorodibenzo-*p*-dioxin (TCDD) before 96 hours post fertilization (hpf) developed swim bladders normally until the growth/elongation phase, at which point growth was arrested. It is known that TCDD exposure causes heart malformations that lead to heart failure in zebrafish larvae, and that blood circulation is a key factor in normal development of the swim bladder. The adverse effects of TCDD exposure on the heart occur during the same period of time that swim bladder development and growth occurs. Based on this coincident timing, and the dependence of swim bladder development on proper circulatory development, we hypothesized that the adverse effects of TCDD on swim bladder development were secondary to heart failure. We compared swim bladder development in TCDD-exposed embryos to: (1) *silent heart* morphants, which lack cardiac contractility, and (2) transiently transgenic *cmlc2*:caAHR-2AtRFP embryos, which mimic TCDD-induced heart failure via heart-specific, constitutive activation of AHR signaling. Both of these treatment groups, which were not exposed to TCDD, developed hypoplastic swim bladders of comparable size and morphology to those found in TCDD-exposed embryos. Furthermore, in all treatment groups swim bladder development was arrested during the growth/elongation phase. Together, these findings support a potential role for heart failure in the inhibition of swim bladder development caused by TCDD.

INTRODUCTION

2,3,7,8-Tetrachlorodibenzo-*p*-dioxin (TCDD or dioxin) is a lipophilic, halogenated aromatic hydrocarbon that is persistent, bioaccumulative, and ubiquitously found in the environment. It is the most potent of the halogenated aromatic hydrocarbons (HAHs) (Hankinson, 1995). These compounds are agonists of the aryl hydrocarbon receptor (AHR). When activated by TCDD, AHR translocates into the nucleus, forms a heterodimer with aryl hydrocarbon nuclear translocator (ARNT), and binds to recognition sites on the DNA sequence, leading to regulation of gene expression (Nguyen and Bradfield, 2008; Schmidt and Bradfield, 1996; Tanguay *et al.*, 2005).

TCDD has been observed to adversely affect the development of many vertebrate species, and fish are especially sensitive to TCDD developmental toxicity (Elonen *et al.*, 1998; Peterson *et al.*, 1993; Walker and Peterson, 1994). Adverse developmental effects of TCDD in fish larvae include heart malformations and heart failure, pericardial edema, yolk sac edema, meningeal edema, hemorrhage, craniofacial malformations, growth arrest, and mortality (reviewed in King-Heiden *et al.*, 2012). One of the hallmark effects of TCDD developmental toxicity in fish larvae is failure of the swim bladder to inflate properly (Henry *et al.*, 1997; Oritz-Delagado *et al.*, 2004).

The swim bladder is present in approximately half of all modern teleost fish species (Denton, 1961). It is a gas-filled sac located dorsal to the gut, used to regulate buoyancy and occasionally for acoustic sensation (Alexander, 1993; Evans, 1925; Zeddies and Fay, 2005). It is crucial for survival in most fish species because it minimizes energy required to maintain vertical position in the water column (Alexander, 1972). Aside from TCDD, exposure to other AHR agonists such as PCB126 also inhibits swim bladder inflation in zebrafish (Jönsson *et al.*, 2012).

In zebrafish, development of the swim bladder occurs in three phases: budding, growth/elongation, and inflation (Winata *et al.*, 2009). Budding phase lasts from 36-65 hours post fertilization (hpf) and involves initiation of the swim bladder bud, which forms as an evagination of the foregut and consists entirely of epithelial cells. The growth/elongation phase (65-96 hpf) involves elongation of the swim bladder bud to form the pneumatic duct, and growth of the swim bladder. At this stage three distinct tissue layers form in the swim bladder: an epithelial layer (from the bud), surrounded by a mesenchymal layer, followed by an outer mesothelium (Finney *et al.*, 2006; Winata *et al.*, 2009). Each layer has unique expression of gene markers and coordinated growth and organization occurs via crosstalk between the layers using signals, such as hedgehog and Wnt (Winata *et al.,* 2009; Winata *et al.*, 2010). The final inflation phase involves inflation of the single-chambered swim bladder (presumptive posterior chamber) at 96-120 hpf via air-gulping (Goolish and Okutake, 1999; Winata *et al.*, 2009). Later, at 20-21 days post fertilization (dpf), inflation of the anterior chamber occurs, and development of the two-chambered swim bladder as seen in adults is complete (Robertson *et al.*, 2007; Winata *et al.*, 2009).

While it is well known that TCDD exposure inhibits inflation of the swim bladder, the potential mechanisms underlying this observed phenotype have not been elucidated. It was previously assumed that TCDD acts directly on the swim bladder, either by interference with development of presumptive swim bladder cells or by causing cellular necrosis in the swim bladder. However, Winata *et al.* (2010) showed that normal blood circulation plays an important role in swim bladder development. This is significant because TCDD causes heart malformations that culminate in heart failure and a complete loss of circulation (Antkiewicz *et al.*, 2005; Belair *et al.*, 2001; Henry *et al.*, 1997). Therefore, we hypothesized that TCDD-induced heart failure impairs development of the swim bladder secondary to circulatory failure.

Here we show that TCDD impairs development of the swim bladder in zebrafish larvae by arresting swim bladder development during the growth/elongation phase. We propose that this effect may be secondary to TCDD-induced heart failure because the two effects temporally coincide. In support of this hypothesis, we show that *silent heart* morphant larvae and transiently transgenic *cmlc2*:caAHR-2AtRFP larvae, neither one exposed to TCDD, also develop heart failure and disrupted swim bladder development. In addition, the impaired swim bladder development of these larvae temporally coincides with effects observed in TCDD-exposed embryos. Furthermore, these larvae phenocopied the gross morphology and histology of disrupted swim bladder development in TCDD-exposed embryos.

MATERIALS AND METHODS

Zebrafish and TCDD exposure

Embryos were obtained from adult zebrafish (*Danio rerio*) housed and maintained according to methods described by Westerfield (2000). AB wild-type strain zebrafish were used in all experiments unless otherwise indicated. Eggs were collected within 4 h of spawning and fertilized eggs were placed into a large petri dish with egg water (60 μg/ml Instant Ocean Sea Salts with 0.2 ppm methylene blue) until appropriate age for use in experiments was reached. Clean water changes were made daily.

Zebrafish embryos or larvae were statically exposed in water to either TCDD (1 ng/ml) or vehicle (0.1% dimethyl sulfoxide, DMSO) for 1 h in 4 ml glass scintillation vials, with gentle rocking. Ten embryos or larvae were present per ml of dosing solution, with a total of 20 embryos or larvae in each vial. After 1 h exposure to TCDD or vehicle, embryos or larvae were rinsed with TCDD-free water at least three times and placed in 100 mm petri dishes with clean water. Embryos and larvae were raised, with daily water changes, until the age when measurements were made (48, 72, 96, or 120 hpf).

All procedures involving zebrafish were approved by the Animal Care and Use Committee of the University of Wisconsin-Madison and adhered to the National Institute of Health's "Guide for the Care and Use of Laboratory Animals."

Silent heart **morphants**

Silent heart (*sih*; cardiac troponin T2, *tnnt2*) morpholino was obtained from Gene Tools (Philomath, OR). A 2 nM morpholino solution was prepared and microinjected into fertilized AB strain eggs at the 1-2 cell stage, as previously described (Carney *et al.*, 2004; Antkiewicz *et al.*, 2006). The Gene Tools standard control morpholino (control MO) was used as a control. Embryos were screened for incorporation of morpholino at 48 hpf.

Heart-specific constitutively activated AHR transient transgenic fish, *cmlc2*:caAHR-2AtRFP

Newly fertilized AB strain eggs were microinjected with either *cmlc2*:caAHR-2AtRFP or *cmlc2*:caAHR^{-dbd}-2AtRFP DNA plasmid construct (negative control), designed and generously donated by Dr. Kevin Lanham (Lanham *et al.*, 2014). Briefly, the *cmlc2*:caAHR-2AtRFP construct constitutively activates AHR signaling in cells expressing the cardiomyocyte-specific *cmlc2* (myosin light chain 7, *myl7*) promoter, and production of red fluorescent protein (RFP) is used as an indicator of successful construct incorporation and therefore activation of AHR signaling. The *cmlc2*:caAHR^{-dbd}-2AtRFP construct served as a negative control and is similar to the *cmlc2*:caAHR-2AtRFP construct except for an insertion mutation in the Rgs domain that disrupts DNA binding and hence there is no constitutive activation of AHR signaling. Construct injections were done as previously described by Lanham *et al.* (2012). Embryos were screened at 48 hpf for use in experiments.

Histology

Embryos or larvae were euthanized using tricaine (MS 222, Sigma) and fixed in 4% parafomaldehyde in phosphate buffered solution (PBS) overnight at 4 ^{o}C. Embryos were then dehydrated in a graded ethanol series and stored at -20 ^{o}C until time for processing. To align samples for sagittal sectioning, stored embryos were re-hydrated into PBS in a graded series, oriented laterally in 0.5% agarose under a dissecting microscope, and completely dehydrated into ethanol before embedding into paraffin. Sections were made in 8 μm thickness, stained with hematoxylin and eosin (H&E), and mounted on glass microscope slides with permount as previously described (King Heiden *et al.*, 2009).

Imaging and analysis of swim bladder areas

At age 120 hpf, DMSO- and TCDD-treated larvae were placed in 3% methylcellulose to characterize TCDD-induced effects on the swim bladder. Live imaging and imaging of H&E sections were done using an Olympus SZX16 camera mounted on an Olympus DP72 epifluorescent microscope with cellSens Digital Imaging software.

Swim bladder area was measured using Image J software from images of H&E sections taken at 12.4x magnification. Only images of sections where the pneumatic duct was clearly visible were used for swim bladder area analysis, and such a section image from an individual fish that met this requirement was considered n = 1 for that cohort for statistics.

Statistics

Student's t-test was used to compare mean swim bladder area in TCDD-treated embryos dosed at 4, 24, 48, 72, or 96 hpf to DMSO-treated embryos (control) dosed at the same time. Data were square-root transformed and checked with the F-test before analysis in order to meet the condition of homoscedasticity required for Student's t-test. Significance was set at $p \leq 0.01$. One-way analysis of

variance (ANOVA) followed by Tukey's HSD test was conducted to compare swim bladder area in TCDD-treated embryos, *silent heart* morphants, *cmlc2*:caAHR-2AtRFP transient transgenic embryos, and their respective controls. These data were not transformed for analysis, as all required conditions for ANOVA were met. Significance was set at $p \leq 0.01$. All cohorts had a sample size of n = 10 to 13. All statistical analyses were done using GraphPad Prism statistics software.

RESULTS

TCDD exposure impairs swim bladder development

Exposure to TCDD causes developmental toxicity in zebrafish larvae, which is clearly manifested by 120 hpf (Fig. 1). Many of these effects were reviewed by King-Heiden *et al.* (2012), and include heart malformations culminating in heart failure and vasculature malformations (not shown), craniofacial and jaw malformations, pericardial edema, yolk sac edema, and meningeal edema (Fig. 1B, black arrow heads). Of particular interest for the present study is the inflated swim bladder, which is clearly visible in control embryos exposed to DMSO (Fig. 1A, white arrow head). Conversely, the swim bladder is either absent or uninflated in the representative TCDD-exposed larvae (Fig. 1B, white arrow head).

To investigate the effect of TCDD on development of the swim bladder, zebrafish embryos were exposed to DMSO (vehicle control) or TCDD for 1 h beginning at 4 hpf and collected at different stages of swim bladder development (Fig. 2). In control fish the swim bladder bud is observed forming from a dorsal evagination of the foregut at 48 hpf (Fig. 2A). The bud elongates to form the pneumatic duct that connects to the primitive swim bladder by 72 hpf, which shows a thick-walled morphology (Fig. 2B). The swim bladder then enters a period of growth where it increases in size and layers of the swim bladder wall become thinner (Fig. 2C). Between 96 and 120 hpf the swim bladder inflates, at which point it is easily

identifiable in free-swimming larvae (Fig. 1A, Fig. 2D). Embryos exposed to TCDD seem to develop a swim bladder normally until 72 hpf (Fig. 2E-H). More specifically, initiation of the swim bladder bud at 48 hpf, followed by bud elongation and initial growth at 72 hpf appears to occur normally (Fig. 2E-F). However, further development is severely impaired beyond 72 hpf, such that by 120 hpf the swim bladder is significantly smaller than in similarly-aged controls and is not inflated (Fig. 2G-H). The swim bladder of the TCDD-exposed embryo at 120 hpf has morphology similar to a developing swim bladder at 72 hpf: a small, uninflated sac with thick walls (compare Fig. 2B and 2H). Overall, this suggests that TCDD does not affect initiation, elongation, or early growth of the swim bladder bud; rather arrests development of the swim bladder at 72 hpf, just before it enters the phase of extensive growth.

Swim bladder development is sensitive to the time of TCDD exposure

To determine whether there is a specific window of time in which swim bladder development is particularly sensitive to TCDD, zebrafish embryos were exposed to either DMSO or TCDD at different ages, and swim bladder size and histology were assessed at 120 hpf. All embryos exposed to DMSO developed fully inflated swim bladders of comparable size by 120 hpf (Fig. 3A, G). In contrast, embryos exposed to TCDD at 4, 24, or 48 hpf had hypoplastic swim bladders at 120 hpf (Fig. 3B-D). These swim bladders had morphology comparable to developing swim bladders at 72 hpf, and were significantly smaller than their respective DMSO-exposed controls at 120 hpf (Fig. 3G, $p \leq 0.01$). Embryos exposed to TCDD at 96 hpf were able to develop an inflated swim bladder that was comparable in size and morphology to control at both 120 hpf (Fig. 3F, G), and up until mortality at approximately 168 hpf when assessment of swim bladder development ended (data not shown). Embryos exposed to TCDD at 72 hpf, when extensive growth of the swim bladder begins, were able to develop a small, partially-inflated swim bladder by 120 hpf (Fig. 3E). These swim bladders were still significantly smaller than control (Fig. 3G, p

≤ 0.01) and displayed morphology intermediate between TCDD-treated embryos exposed at earlier ages (4, 24, or 48 hpf) and control embryos (compare Fig. 3E to 3A-D).

Overall, these results suggest that the developing swim bladder is most sensitive to TCDD-induced disruption of development when TCDD exposure occurs prior to 72 hpf. TCDD exposure at 96 hpf is ineffective in disrupting swim bladder development, while exposure at 72 hpf is only partially effective.

Swim bladder development is impaired in the *silent heart* morphant

The *silent heart* morphant lacks cardiac contractility and develops many gross morphological characteristics by 120 hpf that are similar to embryos exposed to TCDD at 4 hpf, including an un-looped heart, heart failure, pericardial edema, and an uninflated swim bladder. In the present study, embryos injected with control MO developed swim bladders normally, such that by 120 hpf an inflated swim bladder was clearly visible (Fig. 4A-D). In contrast, *silent heart* morphants had a hypoplastic swim bladder at 120 hpf (Fig. 4E-H). In the *silent heart* morphant, initiation of swim bladder bud, elongation, and initial growth of the primitive swim bladder progressed normally through 48 and 72 hpf (Fig. 4E-F). At these ages the *silent heart* morphant had morphology indistinguishable from control (compare Fig. 4A-B and 4E-F). Beginning at 96 hpf, the *silent heart* morphant swim bladder did not increase in size, nor did it transition to the thinner-walled morphology typically seen in controls at 120 hpf (compare Fig. 4C-D and 4G-H).

Swim bladder development is impaired in transient transgenic fish where AHR signaling is constitutively activated in the heart

Since impaired development of the swim bladder in *silent heart* morphants resembled impaired swim bladder development in TCDD-exposed embryos, we investigated whether TCDD-induced heart

failure was sufficient to impair swim bladder development. However, it is not possible to limit TCDD exposure to only one organ, such as the heart, without simultaneously exposing other organs, such as the developing swim bladder, to TCDD as well. TCDD causes embryo toxicity in zebrafish by activating AHR signaling (Prasch *et al.*, 2003; Prasch *et al.*, 2006). The *cmlc2*:caAHR-2AtRFP transient transgenic zebrafish embryo phenocopies TCDD-induced heart malformations and heart failure, in the absence of TCDD, by constitutively activating AHR signaling in only the heart myocytes (Lanham *et al.*, 2014). It is important to note that AHR signaling is not activated in any other cell types, including the developing swim bladder, in embryos expressing this heart-specific, constitutively active, AHR construct (Lanham *et al.*, 2014).

Control embryos injected with a nonfunctional construct, *cmlc2*:caAHR^{-dbd}-2AtRFP, which contains a mutated DNA binding domain that prevents activation of constitutively activated AHR signaling in the heart (Lanham *et al.*, 2014), develop normal swim bladders that inflate by 120 hpf (Fig. 5A-D). In contrast, at 120 hpf, *cmlc2*:caAHR-2AtRFP embryos with constitutively active AHR signaling in the heart produced the previously reported heart failure and malformation (not shown) and developed hypoplastic, uninflated swim bladders (Fig. 5H). The latter, transient transgenic embryos, displayed normal initiation of swim bladder bud formation, elongation, and initial growth of the swim bladder until 72 hpf, after which further development was significantly impaired (Fig. 5E-H). The *cmlc2*:caAHR-2AtRFP larvae swim bladder at 96 and 120 hpf had similar size and thick-walled morphology to the 72 hpf developing swim bladder, suggesting development had been arrested at this age (Fig. 5G-H).

Swim bladder development is inhibited in zebrafish larvae when heart failure is induced by: TCDD exposure, *silent heart* morpholino, or heart-specific constitutively activated AHR signaling

It is well known that circulatory failure due to TCDD-induced heart malformation and heart failure plays an important role in TCDD developmental toxicity in zebrafish larvae (Carney *et al.*, 2006;

King-Heiden *et al.*, 2012; Lanham *et al.*, 2014). To determine if impaired cardiac function is capable of inhibiting swim bladder development, we compared the area of the swim bladder at 120 hpf, relative to control, in larvae with TCDD-, *silent heart* morphant-, and *cmlc2*:caAHR-2AtRFP-induced heart failure. In all three treatment groups, swim bladder area was significantly reduced at 120 hpf compared to the respective control group (Fig. 6). In addition, swim bladder areas in all control groups were not significantly different from each other, nor were swim bladder areas in the three treatment groups significantly different from one another (Fig. 6).

Figure 1. Zebrafish embryos exposed to TCDD do not develop an inflated swim bladder by 120 hpf.

Embryos exposed to (A) 0.1% DMSO for 1 h at 4 hpf develop a functional, inflated, single-chamber swim bladder by age 120 hpf (white arrow head). In contrast, embryos exposed to (B) TCDD (1 ng/ml) for 1 h at 4 hpf have an undeveloped, uninflated swim bladder (white arrow head). In addition, there are craniofacial malformations and meningeal, pericardial, and yolk sac edema (B, black arrow heads). Scale bars represent 500 μm.

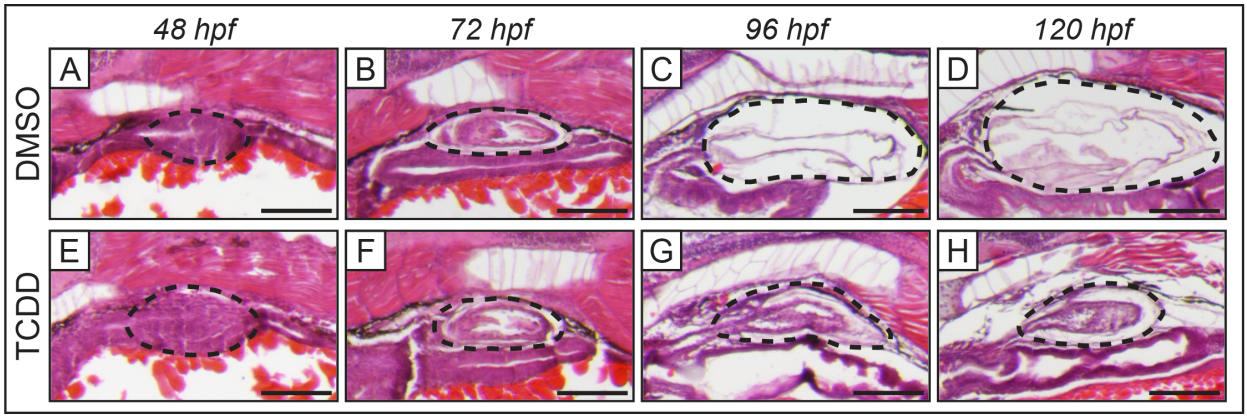

Figure 2. Exposure to TCDD arrests development of the swim bladder during the growth/elongation phase in embryonic zebrafish.

Histology of swim bladder development in embryos at 48, 72, 96, and 120 hpf when exposed for 1 h beginning at 4 hpf to DMSO (control, A-D) or TCDD (1 ng/ml, E-H). Normal swim bladder development is observed in embryos exposed to DMSO: initiation of swim bladder bud from foregut (A), bud elongation and growth (B), and inflation (C-D). TCDD-exposed embryos have developing swim bladder morphology indistinguishable from control at 48 and 72 hpf (E-F), suggesting that TCDD does not interrupt budding and initial growth of the swim bladder bud. Swim bladder development in TCDD-exposed larvae is impaired beyond 72 hpf (G-H). By 120 hpf the TCDD-exposed swim bladder is smaller, uninflated, and has morphology more similar to the 72 hpf swim bladder than control at 120 hpf. Black dotted outlines indicate developing swim bladder, scale bars represent 100 μm. In all panels, the representative embryos are positioned laterally, with anterior to the left.

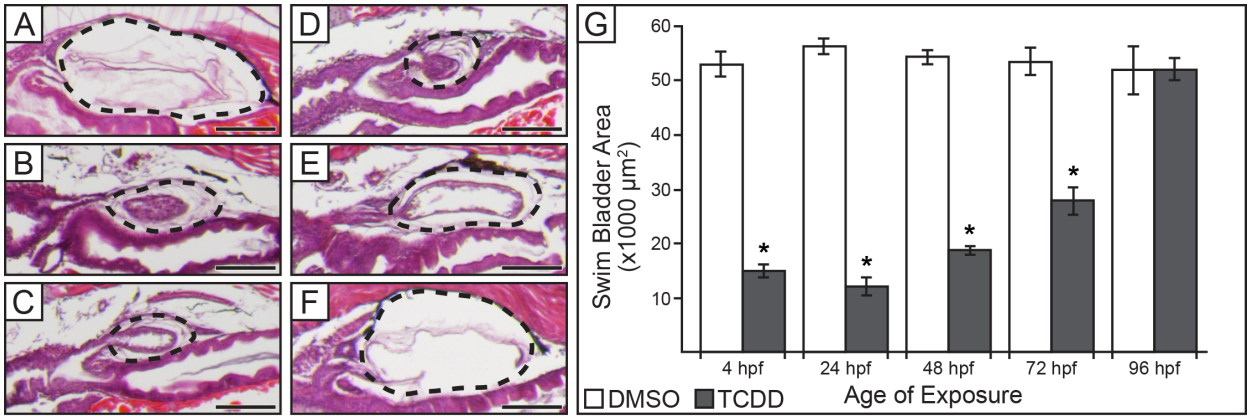

Figure 3. TCDD inhibits swim bladder development when exposure occurs before 96 hpf.

(A-F) Histology of swim bladders at 120 hpf when exposed to either (A) DMSO, or (B-F) TCDD. Exposure to TCDD was started at either: (B) 4, (C) 24, (D) 48, (E) 72, or (F) 96 hpf. Black dotted outlines indicate swim bladder, scale bars represent 100 µm. (G) Mean area of swim bladders (± SEM, n = 10 to 13) at 120 hpf when exposed to DMSO or TCDD at 4, 24, 48, 72, or 96 hpf. Swim bladder areas were measured from H&E sections where the pneumatic duct was clearly visible. Embryos exposed to TCDD before 96 hpf had swim bladders significantly reduced in size, while embryos exposed to TCDD beginning at 96 hpf had swim bladder areas similar to control. Presence of an asterisk indicates swim bladder area in the TCDD-treated group is significantly less than control ($p \leq 0.01$).

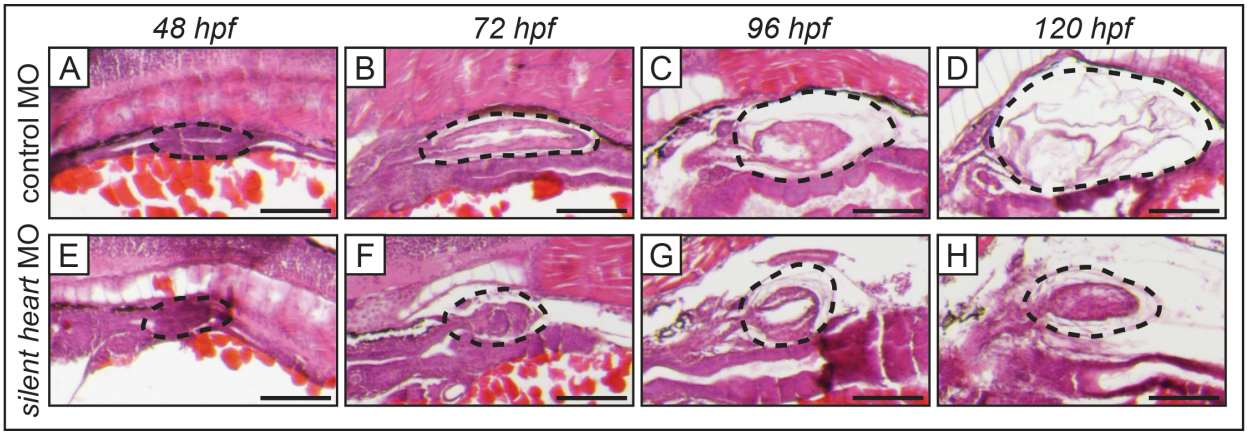

Figure 4. Swim bladder development is impaired in *silent heart* morphants.

Histology of swim bladder development of *silent heart* morphants with heart failure (E-H), and embryos injected with control MO (A-D), at 48 to 120 hpf. Control embryos developed swim bladders normally. *Silent heart* morphants underwent normal swim bladder budding (E), elongation, and initial growth (F), however, subsequent growth beginning at 96 hpf was disrupted (G-H). By 120 hpf the *silent heart* morphant swim bladder is significantly smaller and has thick-walled morphology (H) compared to control (D). Black dotted outlines indicate developing swim bladder, scale bars represent 100 μm.

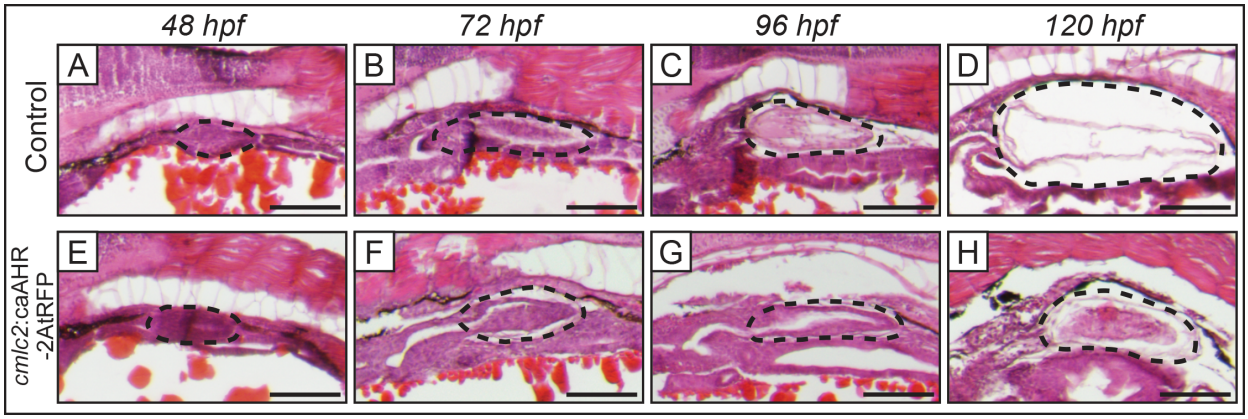

Figure 5. Swim bladder development is impaired in *cmlc2*:caAHR-2AtRFP transient transgenic fish.

Histology of swim bladder development in transient transgenic fish where AHR signaling was constitutively activated only in heart myocytes expressing the cardiomyocyte-specific gene *cmlc2* (*cmlc2*:caAHR-2AtRFP, E-H), and embryos injected with a nonfunctional *cmlc2*:caAHR^{-dbd}-2AtRFP control plasmid (Control, A-D), at 48 to 120 hpf. Control embryos developed swim bladders normally (A-D). Conversely, *cmlc2*:caAHR-2AtRFP embryos had normal swim bladder budding, elongation, and initial growth (E-F), but development was disrupted beginning at 96 hpf (G-H). By 120 hpf the *cmlc2*:caAHR-2AtRFP larvae had distinctly smaller swim bladders whose morphology was different from control. Black dotted outlines indicate developing swim bladder, scale bars represent 100 μm.

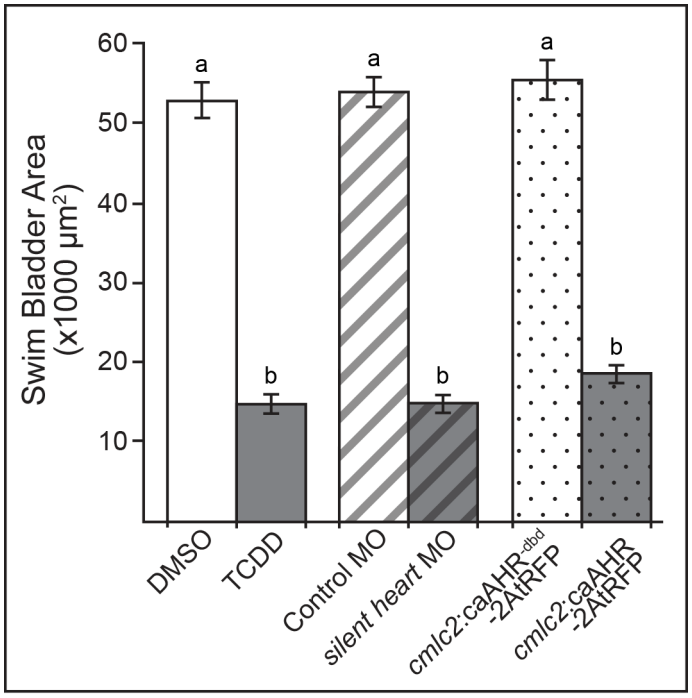

Figure 6. Swim bladder area in TCDD-exposed embryos is similar to embryos with impaired cardiac function.

Swim bladder area (mean ± SEM, n = 10 to 13) was measured at 120 hpf in embryos exposed to: TCDD at 4 hpf (TCDD, solid gray), *silent heart* morphants (*silent heart* MO, gray with black stripes), and *cmlc2*:caAHR-2AtRFP transient transgenic larvae (*cmlc2*:caAHR-2AtRFP, gray with black dots). Embryos exposed to DMSO at 4 hpf (solid white), injected with a control morpholino (Control MO, white with gray stripes), or control plasmid (*cmlc2*:caAHR^{-dbd}-2AtRFP, white with gray dots) served as a control for each treatment group, respectively. Different lower case letters indicate significant difference between groups ($p \leq 0.01$).

DISCUSSION

TCDD impairs swim bladder development during the growth/elongation phase

When TCDD exposure began as early as 4 hpf, the initial steps in swim bladder development did not seem to be affected; swim bladder bud initiation, elongation, and early growth of the primitive swim bladder occurred on time. The gross morphology and histology of the TCDD-exposed developing swim bladder was indistinguishable from control up to 72 hpf. However, beyond this stage of development swim bladder growth was significantly impaired; TCDD-exposed larvae at 96 and 120 hpf had abnormally small, underdeveloped swim bladders that were similar in gross morphology and histology to the 72 hpf swim bladder of control larvae.

The effects of TCDD on swim bladder development were found to depend on the timing of exposure. Exposure to TCDD beginning at 96 hpf, when the growth phase has been completed and the swim bladder is beginning inflation, failed to impair swim bladder development. Additionally, TCDD exposure beginning at 96 hpf did not cause the inflated swim bladder to become uninflated, which suggests that TCDD does not affect cells and tissues involved in maintaining the inflated swim bladder.

Embryos exposed to TCDD before the beginning of the growth/elongation phase (at 4, 24, or 48 hpf) had swim bladders with severely impaired development at 120 hpf. More specifically, swim bladder area was significantly smaller, and gross morphology and histology of the swim bladder at 120 hpf were strikingly abnormal, resembling the control swim bladder at 72 hpf. Larvae exposed to TCDD beginning at 72 hpf, had swim bladders that displayed an intermediate phenotype when evaluated at 120 hpf; these swim bladders at 120 hpf were only partially inflated, significantly reduced in size, and had walls that were thicker than control.

Taken together, these results highlight the early growth/elongation phase, between 65 and 72 hpf when formation and organization of the three swim bladder tissue layers occurs, as the sensitive window for TCDD-induced inhibition of swim bladder development. TCDD exposure beyond this time, at 96 hpf, is not effective in disrupting swim bladder development.

Potential role of TCDD-induced decrease in cardiac output on swim bladder development

Exposure to TCDD at 4 hpf did not produce detrimental effects on the swim bladder until after 72 hpf. Consistent with this observation, embryos exposed to TCDD at 4, 24, or 48 hpf exhibit normal blood circulation until 72 hpf, at which time a significant decrease in peripheral blood flow is observed (Henry *et al.*, 1997; Prasch *et al.*, 2003; Teraoka *et al.*, 2002). These reductions may be the result of TCDD interference with heart valve formation, which leads to blood regurgitation, an effect that begins to manifest at 60 hpf, and is significantly observed at 72 hpf (Mehta *et al.*, 2008). In addition, stroke volume and cardiac output in embryos exposed to TCDD at 4 hpf may begin to decline at 60 hpf and progressively worsen with time. TCDD exposure also interferes with formation of the heart epicardium beginning around this time, which plays an important role in normal heart function and development (Plavicki *et al.*, 2013). Normal peripheral circulation is known to be important for swim bladder development (Winata *et al.*, 2010). Considering this, it is possible that TCDD-induced impairment of blood circulation, which manifests specifically when the swim bladder begins to undergo growth and organization of the three tissue layers, plays an important role in inhibiting swim bladder development.

Swim bladder development in embryos exposed to TCDD at 72 hpf was less affected than in embryos exposed to TCDD at earlier ages. Previously, Carney *et al.* (2006) showed that exposing embryos to TCDD beginning at 72 hpf did not seem to have any deleterious effects on cardiac output 4 hours later. However, beginning 8 hours post exposure, at 80 hpf, there were significant decreases in stroke volume and cardiac output, which continued to worsen with time. Thus, it is likely that embryos

exposed to TCDD at 72 hpf had significant decreases in blood circulation, that began after the most sensitive stage of swim bladder development, leading to the formation of less severely affected swim bladders at 120 hpf.

In another study by Jönsson *et al.* (2012), zebrafish embryos injected with an Ahr2 morpholino were exposed to PCB126, a full AHR agonist. Although the Ahr2 morpholino loses effectiveness at approximately 72 to 96 hpf, this partial knockdown of Ahr2 was still sufficient to block the adverse effects of PCB126 on swim bladder development (Jönsson *et al.*, 2012).

Sensitive window for TCDD inhibition of swim bladder development coincides with formation of mesenchymal and outer mesothelial swim bladder tissues

The growth/elongation phase in swim bladder development (65-96 hpf) may be particularly sensitive because it is when the mesenchymal and outer mesothelial layers are forming and crosstalk of signals between these layers, and the existing epithelial layer, play an important role in their organization and growth. Disorganization of the mesenchymal layer caused by impaired hedgehog signaling leads to a disorganized and underdeveloped outer mesothelium (Winata *et al.*, 2009). At the same time, Wnt signals from both mesenchyme and outer mesothelium seem to play an important role in coordinating growth of the epithelial layer (Yin *et al.*, 2011). Henry *et al.* (1997) observed a lack of mesenchymal layer in the uninflated swim bladders of TCDD-exposed zebrafish embryos at 104 hpf, and Winata *et al.* (2010) observed significantly disorganized mesenchymal and outer mesothelial layers in both the *cloche* mutant and *silent heart* morphant.

Is inhibition of swim bladder development by TCDD secondary to TCDD-induced heart failure?

Due to the similar timing during zebrafish embryo/larval development of TCDD-induced heart and circulatory failure and arrested swim bladder development, we hypothesized that TCDD arrests swim

bladder development secondary to heart failure. Previous research has shown that these responses to TCDD are mediated through AHR signaling (Prasch *et al.*, 2003; Prasch *et al.*, 2006). In support of our hypothesis, we show that heart-specific constitutive activation of AHR signaling, which phenocopies heart failure caused by TCDD, but in the absence of TCDD exposure (Lanham *et al.*, 2014), inhibited swim bladder development in a manner that was essentially indistinguishable from that of TCDD when assessed at 48, 72, 96 and 120 hpf. This demonstrates that it is not necessary to activate AHR signaling in the developing swim bladder itself to disrupt swim bladder development. Rather, constitutive activation of AHR signaling in the heart alone, leading to circulatory failure, is sufficient to impair swim bladder development. This, of course, does not eliminate the possibility that TCDD-induced activation of AHR signaling in the swim bladder itself may be capable of disrupting swim bladder development. Rather, it shows that swim bladder development can be inhibited indirectly by causing circulatory failure that coincides temporally with vulnerable stages of swim bladder development.

To investigate this latter possibility further, we assessed how swim bladder development was affected in the *silent heart* morphant, which lacks cardiac contractility and therefore also lacks circulation (Sehnert *et al.*, 2002). We showed that heart failure produced in *silent heart* morphant larvae also was accompanied by impaired swim bladder development that follows a similar time course to that of TCDD, and when AHR signaling was constitutively activated in the heart. These results are consistent with observations by Winata *et al.* (2010), who found that impaired swim bladder development occurred secondary to circulatory failure in *cloche* mutants, which lack circulation due to inhibition of endothelial cell and hematopoietic progenitor differentiation (Stainier *et al.*, 1995; Winata *et al.*, 2010).

Thus, zebrafish larvae assessed at 120 hpf, where heart failure was induced by TCDD exposure, *silent heart* MO, or heart-specific constitutive activation of AHR signaling, developed swim bladders smaller than their respective controls. Gross morphology and histology of the 120 hpf swim bladders in

each treatment group resembled each other, and a control swim bladder at 72 hpf. These findings suggest that swim bladder development was arrested in all groups at this stage of development.

It should be noted that the work presented here does not prove that inhibition of swim bladder development in TCDD-exposed zebrafish was entirely secondary to heart failure, or that direct effects of TCDD on the swim bladder were not involved. TCDD was not present in experiments involving the *silent heart* morphant and the *cmcl2*:caAHR-2AtRFP larvae. The only condition that was common to these two treatment groups and the TCDD group was heart failure. In this context it is striking that the: time course of inhibited swim bladder development, reduced swim bladder area, swim bladder gross morphology and histology, and lack of swim bladder inflation in *silent heart* morphant and *cmcl2*:caAHR-2AtRFP larvae were essentially similar to that of larvae with TCDD-induced heart failure. Together, these various results strongly suggest that the observed inhibitory effects of TCDD on swim bladder development could be secondary to heart malformation culminating in heart failure.

CONCLUSIONS

It has been widely documented that embryonic exposure to TCDD in the developing zebrafish results in failure of the swim bladder to inflate. Here we propose that TCDD produces this effect on the swim bladder by arresting development early in the growth/elongation stage (65-72 hpf), which occurs prior to inflation. Embryos exposed to TCDD before this stage develop hypoplastic swim bladders that are significantly reduced in size. However, swim bladder development rapidly becomes less sensitive to the effects of TCDD exposure after 72 hpf, such that embryos exposed to TCDD at 96 hpf have swim bladders that seem to develop and function normally. Thus, TCDD does not block initiation of swim bladder formation, nor the survival or differentiation of mature swim bladder cells after inflation.

The timing during development, for TCDD-induced disruption of swim bladder development, is similar to that for TCDD-induced circulation failure. However, what cannot be determined from experiments using TCDD alone is whether the effects of TCDD on swim bladder development are direct or indirect. In support of an indirect effect, we investigated the effect of circulatory failure on swim bladder development in *silent heart* morphants and larvae with heart-specific constitutively activated AHR signaling (*cmlc2*:caAHR-2AtRFP) that were not exposed to TCDD. Swim bladder development in these larvae was compared to larvae exposed to TCDD. We found that in all treatment groups circulatory failure was sufficient to arrest swim bladder development; the resultant phenotype and time course of effects was similar among all treatment groups. Thus, it is possible for TCDD to impair development of one organ, the swim bladder, secondary to causing dysfunction in a different organ, the heart. These findings provide new insights into the complex mechanisms by which TCDD induces developmental toxicity.

ACKNOWLEDGEMENTS

This research was funded by the National Institute for Environmental Health Sciences training grant (T32 ES007015) and (R01 ES012716) to W.H. and R.E.P. The authors wish to thank Dr. Kevin Lanham for providing DNA plasmid constructs for use in experiments, as well as his helpful advice. We also wish to thank Dr. J. Plavicki, Dr. P. Hofsteen, Dr. F. Burns, K. Behrens, and D. Nesbit for expert advice and general support in conducting this research and preparing this publication.

REFERENCES

Alexander, R.M.,1972. The energetics of vertical migration by fishes. *Symp. Soc. Exp. Biol*. 26, 273–294.

Alexander, R.M., 1993. Buoyancy, in: Evans, D.H. (Eds.), *The physiology of fishes*. CRC Press, Boca Raton, pp. 75-97.

Antkiewicz, D.S., Burns, C.G., Carney, S.A., Peterson, R.E., Heideman, W., 2005. Heart malformation is an early response to TCDD in embryonic zebrafish. *Toxicol. Sci*. 84, 368–377.

Antkiewicz, D.S., Peterson, R.E., Heideman, W., 2006. Blocking expression of AHR2 and ARNT1 in zebrafish larvae protects against cardiac toxicity of 2,3,7,8-tetrachlorodibenzo-*p*-dioxin. *Toxicol. Sci*. 94, 175-182.

Belair, C.D., Peterson, R.E., Heideman, W., 2001. Disruption of erythropoiesis by dioxin in the zebrafish. *Dev. Dyn*. 222, 581-594.

Carney, S.A., Chen, J., Burns, C.G., Xiong, K.M., Peterson, R.E., Heideman, W., 2006. Aryl hydrocarbon receptor activation produces heart-specific transcriptional and toxic responses in developing zebrafish. *Mol. Pharmacol*. 70, 549-561.

Carney, S.A., Peterson, R.E., Heideman, W., 2004. 2,3,7,8-Tetrachlorodibenzo-*p*-dioxin activation of the aryl hydrocarbon receptor/aryl hydrocarbon receptor nuclear translocator pathway causes developmental toxicity through a CYP1A-independent mechanism in zebrafish. *Mol. Pharmacol*. 66, 512-521.

Denton, E.J., 1961. The buoyancy of fish and cephalopods. *Prog. Biophys. Biophys. Chem*. 11, 177-234.

Elonen, G.E., Sphear, R.L., Holcombe, G.W., Johnson, R.D., 1998. Comparative toxicity of 2,3,7,8-tetrachlorodibenzo-*p*-dioxin to seven freshwater species during early life-stage development. *Environ. Toxicol. Chem*. 17, 472-483.

Evans, H.M., 1925. A contribution to the anatomy and physiology of the air-bladder and Weberian ossicles in cyprinidae. *Proc. R. Soc. London, Ser. B* . 97, 545-576.

Finney, J.L., Robertson, G.N., McGee, C.A., Smith, F.M., Croll, R.P., 2006. Structure and autonomic innervation of the swim bladder in the zebrafish (*Danio rerio*). *J. Comp. Neurol*. 495, 587-606.

Goolish, E.M., Okutake, K., 1999. Lack of gas bladder inflation by the larvae of zebrafish in the absence of an air-water interface. *J. Fish Biol*. 55, 1054-1063.

Hankinson, O., 1995. The aryl hydrocarbon receptor complex. *Annu. Rev. Pharmacol. Toxicol*. 35, 307-340.

Henry, T.R., Spitsbergen, J.M., Hornung, M.W., Abnet, C.C., Peterson, R.E., 1997. Early life stage toxicity of 2,3,7,8-tetrachlorodibenzo-*p*-dioxin in zebrafish (*Danio rerio*). *Toxicol. Appl. Pharmacol*. 142, 56–68.

Jönsson, M.E., Kubota, A., Timme-Laragy, A.R., Woodin, B., Stegeman, J.J., 2012. Ahr2-dependence of PCB126 effects on the swim bladder in relation to expression of CYP1 and cox-2 genes in developing zebrafish. *Toxicol. Appl. Pharmacol*. 265, 166-174.

King-Heiden, T.C., Mehta, V., Xiong, K.M., Lanham, K.A., Antkiewicz, D.S., Ganser, A., Heideman, W., Peterson, R.E., 2012. Reproductive and developmental toxicity of dioxin in fish. *Mol. Cell. Endocrinol*. 354, 121-138.

King Heiden, T.C., Spitsbergen, J., Heideman, W., Peterson, R.E., 2009. Persistent adverse effects on health and reproduction caused by exposure of zebrafish to 2,3,7,8-tetrachlorodibenzo-*p*-dioxin during early development and gonad differentiation. *Toxicol. Sci*. 109, 75–87.

Lanham, K.A., Peterson, R.E., Heideman, W., 2012. Sensitivity to dioxin decreases as zebrafish mature. *Toxicol. Sci*. 127, 360-70.

Lanham, K.A., Plavicki, J., Peterson, R.E., Heideman, W., 2014. Cardiac Myocyte-Specific AHR Activation Phenocopies TCDD-Induced Toxicity in Zebrafish. *Toxicol. Sci*. 141, 141-154.

Mehta, V., Peterson, R. E., and Heideman, W., 2008. 2,3,7,8-Tetrachlorodibenzo-*p*-dioxin exposure prevents cardiac valve formation in developing zebrafish. *Toxicol. Sci*. 104, 303–311.

Nguyen, L.P., Bradfield, C.A., 2008. The search for endogenous activators of the aryl hydrocarbon receptor. *Chem. Res. Toxicol*. 21, 102–116.

Ortiz-Delgado, J.B., Sarasquete, C., 2004. Toxicity, histopathological alterations and immunohistochemical CYP1A induction in the early life stages of the seabream, *Sparus aurata*, following waterborne exposure to B(a)P and TCDD. *J. Mol. Histol*. 35, 29–45.

Peterson, R. E., Theobald, H. M., and Kimmel, G. L., 1993. Developmental and reproductive toxicity of dioxins and related compounds: Cross-species comparisons. *Crit. Rev. Toxicol*. 23, 283–335.

Plavicki, J., Hofsteen, P., Peterson, R.E., Heideman, W., 2013. Dioxin inhibits zebrafish epicardium and proepicardium development. *Toxicol. Sci*. 131, 558–567.

Prasch, A.L., Tanguay, R.L., Mehta, V., Heideman, W., Peterson, R.E., 2006. Identification of zebrafish ARNT1 homologs: 2,3,7,8-tetrachlorodibenzo-*p*-dioxin toxicity in the developing zebrafish requires ARNT1. *Mol. Pharmacol*. 69, 776–787.

Prasch, A.L., Teraoka, H., Carney, S.A., Dong, W., Hiraga, T., Stegeman, J.J., Heideman, W., Peterson, R.E., 2003. Aryl hydrocarbon receptor 2 mediates 2,3,7,8-tetrachlorodibenzo-*p*-dioxin developmental toxicity in zebrafish. *Toxicol. Sci*. 76, 138–150.

Robertson, G.N., McGee, C.A.S., Dumbarton, T.C., Croll, R.P., Smith, F.M., 2007. Development of the swimbladder and its innervation in the zebrafish, *Danio rerio*. *J. Morphol*. 268, 967-985.

Schmidt, J. V., Bradfield, C.A., 1996. Ah receptor signaling pathways. *Annu. Rev. Cell Dev. Biol*. 12, 55–89.

Sehnert, A.J., Huq, A., Weinstein, B.M., Walker, C., Fishman, M., Stainier, D.Y.R., 2002. Cardiac troponin T is essential in sarcomere assembly and cardiac contractility. *Nat. Genet*. 31, 106-10.

Stainier, D.Y., Weinstein, B.M., Detrich, H.W. 3rd, Zon, L.I., Fishman, M.C., 1995. Cloche, an early acting zebrafish gene, is required by both the endothelial and hematopoietic lineages. *Development*. 121, 3141-50.

Tanguay, R. L., Andreasen, E. A., Walker, M. K., Peterson, R. E., 2005. Dioxin toxicity and aryl hydrocarbon receptor signaling in fish, in: Schecter, A., Gasiewicz, T.A. (Eds.), *Dioxins and Health*. John Wiley & Sons, Inc., New York, pp. 603-628.

Teraoka, H., Dong, W., Ogawa, S., Tsukiyama, S., Okuhara, Y., Niiyama, M., Ueno, N., Peterson, R.E., Hiraga, T., 2002. 2,3,7,8-Tetrachlorodibenzo-*p*-dioxin toxicity in the zebrafish embryo: altered regional blood flow and impaired lower jaw development. *Toxicol. Sci*. 65, 192-199.

Walker, M.K., Peterson, R.E., 1994. Aquatic toxicity of dioxins and related chemicals, in: Schecter, A. (Ed.), *Dioxins and Health*. Plenum Press, New York, pp. 347-387.

Westerfield, M., 2000. The Zebrafish Book. A Guide for the Laboratory Use of Zebrafish (*Danio rerio*), fourth ed. Univ. of Oregon Press, Eugene, OR.

Winata, C.L., Korzh, S., Kondrychyn, I., Korzh, V., Gong, Z., 2010. The role of vasculature and blood circulation in zebrafish swimbladder development. *BMC Dev. Biol*. 10, 3.

Winata, C.L., Korzh, S., Kondrychyn, I., Zheng, W., Korzh, V., Gong, Z., 2009. Development of zebrafish swimbladder: The requirements of Hedgehog signaling in specification and organization of the three tissue layers. *Dev. Biol*. 331, 222-36.

Yin, A., Korzh, S., Winata, C.L., Korzh, V., Gong, Z., 2011. Wnt signaling is required for early development of zebrafish swimbladder. *PLoS One*. 30, e18431.

Zeddies, D.G., Fay, R.R., 2005. Development of the acoustically evoked behavioral response in zebrafish to pure tones. *J. Exp. Biol*. 208, 1363-1372.

CHAPTER III:

MULTIPLE MODES OF PROEPICARDIAL CELL MIGRATION REQUIRE HEARTBEAT

Jessica S. Plavicki, Peter Hofsteen, Monica S. Yue, Kevin A. Lanham, Richard E. Peterson, Warren Heideman

BMC Developmental Biology. (2015) **14**, 18.

This work was done in collaboration with Dr. Jessica Plavicki.

My contribution is presented in the Figures 7, 8, 9 and Figure S2.

ABSTRACT

Background

The outermost layer of the vertebrate heart, the epicardium, forms from a cluster of progenitor cells termed the proepicardium (PE). PE cells migrate onto the myocardium to give rise to the epicardium. Impaired epicardial development has been associated with defects in valve development, cardiomyocyte proliferation and alignment, cardiac conduction system maturation and adult heart regeneration. Zebrafish are an excellent model for studying cardiac development and regeneration; however, little is known about how the zebrafish epicardium forms.

Results

We report that PE migration occurs through multiple mechanisms and that the zebrafish epicardium is composed of a heterogeneous population of cells. Heterogeneity is first observed within the PE and persists through epicardium formation. Using *in vivo* imaging, histology and confocal microscopy, we show that PE cells migrate through a cellular bridge that forms between the pericardial mesothelium and the heart. We also observed the formation of PE aggregates on the pericardial surface, which were released into the pericardial cavity. It was previously reported that heartbeat-induced pericardiac fluid advections are necessary for PE cluster formation and subsequent epicardium development. We manipulated heartbeat genetically and pharmacologically and found that PE clusters clearly form in the absence of heartbeat. However, when heartbeat was inhibited the PE failed to migrate to the myocardium and the epicardium did not form. We isolated and cultured hearts with only a few epicardial progenitor cells and found a complete epicardial layer formed. However, pharmacologically inhibiting contraction in culture prevented epicardium formation. Furthermore, we isolated control and *silent heart* (*sih*) morpholino (MO) injected hearts prior to epicardium formation (60 hpf) and co-cultured these hearts with

"donor" hearts that had an epicardium forming (108 hpf). Epicardial cells from donor hearts migrated on to control but not *sih* MO injected hearts.

Conclusions

Epicardial cells stem from a heterogeneous population of progenitors, suggesting that the progenitors in the PE have distinct identities. PE cells attach to the heart via a cellular bridge and free-floating cell clusters. Pericardiac fluid advections are not necessary for the development of the PE cluster, however heartbeat is required for epicardium formation. Epicardium formation can occur in culture without normal hydrodynamic and hemodynamic forces, but not without contraction.

BACKGROUND

The proepicardium is a cluster of cardiac progenitor cells that develops adjacent to the heart and migrates onto the heart to form the outermost layer, the epicardium [1,2]. After the epicardium has formed, a subset of epicardial cells undergo epithelial-to-mesenchymal transitioning (EMT) and contribute to the development and maturation of many cardiac cell types, such as cardiac fibroblasts, endothelial cells, and vascular smooth muscle cells [3-7]. Disruptions in epicardial development are associated with defects in endocardial valve development, heart looping, cardiomyocyte proliferation and alignment, development of the coronary vasculature, cardiac conduction system maturation, and cardiac regeneration (reviewed in [8-12]).

PE development and migration have primarily been studied using the chick and mouse models. In chick, the PE forms asymmetrically on the right sinus horn and migrates to the dorsal surface of the ventricular myocardium via an extracellular matrix bridge, which connects the PE and myocardium [13-16]. Epicardial coverage proceeds over the myocardium in a sheet-like manner [17]. Studies of Xenopus and the axolotl find that PE cell migration in amphibians also occurs via a bridge [18,19]. However, it has been debated whether murine PE cell migration occurs through a mechanism involving direct contact between the PE and myocardium or, alternatively, through free-floating PE-cell aggregates. In the latter model, aggregates are released into the pericardial space and attach at various sites on the myocardium creating “epicardial islands” [20]. Epicardial islands spread out and are ultimately stitched together to form an epicardial sheet covering the myocardium. Work by Rogers *et al.* [21] argues that the mouse epicardium forms, as in the in chick, through villi that protrude from the mouse PE and contact the myocardium directly. Movement of the beating heart transfers the PE villi onto the myocardium. In the same study, PE cell aggregates were also observed, indicating more than one mode of transfer occurs during epicardial development, which was also suggested in an earlier study by Komiyama *et al.* [20].

Zebrafish form a PE on the pericardial wall, adjacent to the atrioventricular (AV) junction [1,22]. However, in zebrafish, how epicardial progenitor cells migrate onto the zebrafish myocardium remains poorly understood. In this work, we show that PE cells migrate to the heart using both direct contact and the release of free-floating aggregates. We find that a PE cluster located at the AV junction forms a cellular bridge between the pericardial mesothelium and the heart. Additional PE clusters form near the venous pole, are released into the pericardial space, and subsequently attach to the heart.

Although it has previously been reported that pericardial fluid forces acting on the mesothelium are required to induce the formation of PE clusters and direct epicardial morphogenesis [23], we found that PE clusters clearly form without a heartbeat. However, without a heartbeat, the PE cells failed to migrate onto and across the heart. To determine if specific pericardial fluid forces or hemodynamic forces were necessary for epicardium formation, we isolated hearts just as the first epicardial progenitors had attached, and grew these hearts in culture. Starting from only a few pioneer progenitors, a complete epicardial layer formed *in vitro*, thus indicating the pericardial fluid forces and hemodynamic forces are not necessary for directing epicardial development.

To examine if heartbeat was need for epicardial cell migration, we developed an *in vitro* epicardial cell migration assay to test whether epicardial cells can migrate from a donor heart onto a younger recipient heart, which had not yet formed an epicardium. Indeed, epicardial cells were able to migrate onto control recipient hearts, but not onto recipient hearts in which heartbeat was inhibited. Together our results show the critical importance of myocardial contraction for PE migration and epicardium formation.

RESULTS

Normal PE and epicardium development and migration in zebrafish

Consistent with previous findings, the PE could be observed at 50 hpf [1] and steadily increased in size through 72 hpf, a point at which we repeatedly observed PE clusters near the AV junction forming a cellular bridge between the myocardium and pericardium. This was apparent in still images (Figure 1A), live videos (Additional file 1: Video 1), H&E-stained sections (Figure 1B), and confocal images using a *tcf21*:DsRed2 epicardial cell reporter (Figure 1C-D).

By 84 hpf, after the initial establishment of epicardial cells on the ventricle, we found that *tcf21*+ cells were still present on the pericardial wall near the AV junction protruding towards the heart (Figure 2B and C). In addition to the PE cluster at the AV junction, we consistently observed *tcf21*+ PE clusters that formed near the venous pole as well as additional smaller clusters forming on the pericardial wall closer to the ventricle (Figure 2A). We frequently observed *tcf21*+ cells or cell aggregates moving within the pericardial space. Clusters of *tcf21*+ cells were observed on the pericardial wall and within the pericardial space from 74 hpf (Figure 2A) to 120 hpf (Figure 2C). Together, our results provide support for both cellular bridge and floating aggregate models of PE migration.

Zebrafish PE and epicardium are composed of a heterogeneous population of cells

The murine PE and epicardium are composed of heterogeneous populations of cells that have divergent roles during heart development [24]. As shown in Figure 1C, we observed evidence for similar heterogeneity during zebrafish epicardial development. A close-up confocal z-stack and orthogonal slice of the PE at 72 hpf (Figure 1D) shows that not all cells within the PE cluster expressed *tcf21*. An optical slice generated along the line indicated by the “X”, orthogonal to the plane of the image, shows a cross-

section of the PE with both *tcf21*+ and *tcf21*- cells. These results indicate that differences between PE cells exist prior to reaching the myocardium.

Heterogeneous *tcf21* expression was also found in the epicardium at later stages of development. At 1-week post fertilization (wpf), distinct sections of the epicardium, while clearly marked by the epicardial reporter *pard3*:EGFP, lacked *tcf21* expression (Figure 3A-A"). These *tcf21*- regions of epicardium persisted over time. Continuous regions of *tcf21*- cells on the heart surface could be seen covering the trabeculated myocardium at 2 wpf (Figure 3B-B') and at 6 wpf (Figure 3C-C"). We observed similar results using another known epicardial marker, *tbx18* [18,25,26]. Again, while some epicardial cells showed strong expression of *tbx18*, others had weak expression or lacked *tbx18* expression completely (Additional file 2: Figure S1). Based on the observed *tcf21* and *tbx18* expression patterns in the juvenile epicardium, we conclude that the developing epicardium is composed of a heterogeneous population of cells.

Spatial and temporal progression of zebrafish epicardium formation

We followed the path of epicardium development over time using the *pard3*:EGFP reporter to mark the developing epicardium and ALCAM staining to visualize the underlying myocardium. We consistently found that epicardial progenitors first migrated onto and over the ventricle to form a ventricular epicardium. At 78, 84, and 96 hpf, epicardial cells were only found overlying the ventricle (Figure 4A-D). It was not until 120 hpf that epicardial cells were detected on the atrium (Figure 4E). Epicardial cells were clearly present on both heart chambers by one week; however, even then epicardial coverage was incomplete (Figure 4F). The epicardium continued to mature over the ensuing weeks (see also Figure 3B-C").

Heartbeat and epicardium development

Heartbeat is necessary for important steps in heart development, including valve cushion formation [27]. We manipulated the heartbeat genetically by using *sih* MOs to completely and specifically blocking heart contractions to determine whether a heartbeat is needed for epicardium development. As an alternative approach, we pharmacologically inhibited contractions using BDM [27]. BDM treatment dramatically reduced heart contractility when present in the water, but once removed, heart contractions resumed.

We first examined PE development in *sih* MO and BDM treated larvae at 72 hpf. Brightfield images clearly show PE clusters in control, *sih* MO-injected and BDM-treated larvae (Figure 5A-C), indicating that inhibiting heartbeat did not prevent PE development. We examined 10 individuals for each condition, and observed a PE in 10/10 fish for the control, *sih* MO, and BDM groups. Furthermore, if BDM was present during the period in which the PE cluster forms (24-72 hpf), and then removed afterwards, the epicardium appeared normal at 120 hpf (not shown).

To confirm that the cells seen adjacent to the heart in the brightfield images were in fact specified PE cells, we injected *sih* MOs into the *tcf21*:DsRed2 reporter line (Figure 5D and E). We examined control and *sih* MO-injected larvae at 72 hpf and could clearly identify *tcf21*+ PE clusters in 15 out of 15 larvae in each group (Figure 5D and E). Together, our results demonstrate that heartbeat is not necessary for PE specification or cluster formation.

Although the PE developed in the absence of heartbeat when we examined the *sih* MO-injected *tcf21*:DsRed2 larvae at 96 hpf we found that the epicardium had not formed (Figure 5F and G). Consistent with our finding at 72 hpf, we found PE-like clusters of *tcf21*:DsRed2+ cells at the venous pole at 96 hpf (arrowhead in Figure 5G).

We repeated the *sih* MO injection experiment with embryos from a second epicardial reporter line, *pard3*:EGFP. Again, at 96 hpf *pard3*:EGFP + epicardial cells were easily detected on the ventricles of control hearts, but never on the hearts of *sih* morphants. As with the previous experiment, we often observed what appeared to be small PE-like clusters in the pericardial cavity (arrowhead in Figure 5I) and near the venous pole (not shown). We did not observe the formation of a PE bridge in *sih* morphants, but did observe incidences where free-floating aggregates were present in the pericardial cavity. Using BDM, we impaired heartbeat during different stages of epicardial development (Figure 6). BDM treatment from 48-120 hpf also blocked epicardium formation (Figure 6B). If we waited until 72 hpf to add BDM, we found some epicardial cells on the ventricle at 120 hpf (Figure 6C); however, epicardium formation was incomplete and epicardial cells were not detected on the atrium. This suggests that inhibiting heartbeat with BDM halted expansion of the epicardial layer.

Epicardium formation on isolated hearts

To test whether pericardial fluid forces are necessary to direct epicardium formation, we examined whether epicardial development could occur on isolated hearts *in vitro*. Isolation of hearts from *tcf21*:DsRed2 larvae at 74 hpf yielded intact ventricles carrying along 2-4 *tcf21*+ pioneer epicardial cells (Figure 7A). Placed in culture, these hearts continued to beat and over the next few days developed complete *tcf21*+ epicardiums *in vitro* (Figure 7B and C). If the hearts were removed prior to PE migration, 40-48 hpf, with no *tcf21*+ cells, they continued to beat, but the epicardium did not form (not shown). We confirmed our findings by extracting *pard3*:EGFP and *tbx18*:DsRed2 hearts at 74 hpf and following epicardial development *in vitro*. Again, we observed the formation of a complete epicardial layer on cultured hearts (Additional file 3: Figure S2 A and B). To determine if epicardial cells were dividing in culture, we stained *pard3*:EGFP cultured hearts for phospho-histone H3 (pH3) and, indeed, found pH3-positive epicardial cells (Additional file 3 Figure S2A).

As with the *in vivo* experiments, we found that contractility was essential for epicardium expansion *in vitro*. For these experiments we isolated hearts with a few epicardial progenitors attached (74 hpf; Figure 8A) and cultured hearts in the presence and absence of BDM to manipulate heart contractility. In the control heart, the epicardial cells expanded over the entire ventricle (Figure 8B and D). In contrast, while the original *tcf21*+ cells remained on the BDM-treated heart, they did not expand (Figure 8C and E).

Epicardial migration assay

To further explore the necessity of heartbeat during epicardium formation, we developed an *in vitro* epicardial migration assay. In this assay, we co-cultured isolated donor hearts carrying *tcf21*:DsRed2 epicardial cells (108 hpf) with *cmlc2*:GFP recipient hearts isolated from either control or *sih* MO embryos. The recipient hearts were isolated earlier than in the previous experiment, at 60 hpf, before epicardial cells were present on the myocardium (Figure 9A). We found that epicardial cells from donor hearts could migrate onto control recipient hearts (Figure 9B, C, and D). However, epicardial cells from donor hearts did not migrate onto recipient *sih* MO hearts in which the heartbeat was inhibited (Figure 9E, F, G). Together, these findings indicate that the heartbeat itself, independent of its effects on pericardial fluid forces, is necessary for epicardial cell migration.

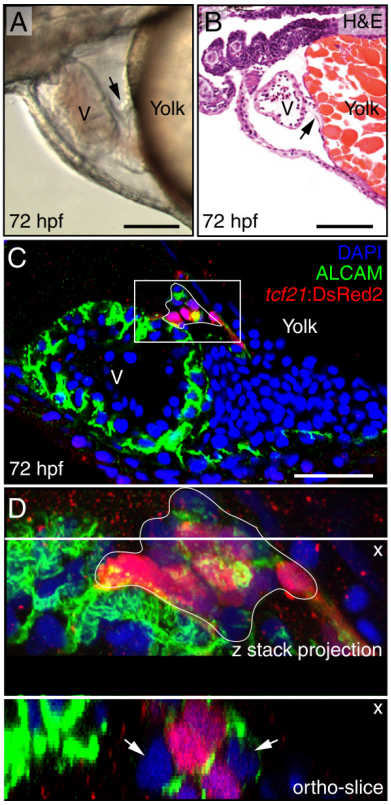

Figure 1. PE migration occurs through a cellular bridge to the heart. Lateral views of zebrafish hearts at 72 hpf.

(A) Brightfield image of a live heart (n = 10). Arrow indicates the PE. (B) H&E stained section through heart and pericardium (n = 5). Arrow indicates the PE. (C-D) Confocal images of whole-mount fixed zebrafish. Epicardial cells marked with immunostaining for DsRed2 (red), which is driven by the *tcf21* promoter. Nuclei are stained with DAPI (blue) and cardiomyocytes are marked with *activated cell adhesion molecule* (ALCAM; green). (C) The PE, which is outlined, forms a bridge between the ventricle and the pericardial wall (n = 10). (D) Magnified Z-stack projection and orthogonal slice of area boxed in C. Orthogonal slice at line indicated by "x" shows cross-section of cells below the line. White arrows indicate cells within the PE cluster that are not expressing *tcf21*. For all panels, anterior is to the left and V is ventricle. Scale bars = 50 microns.

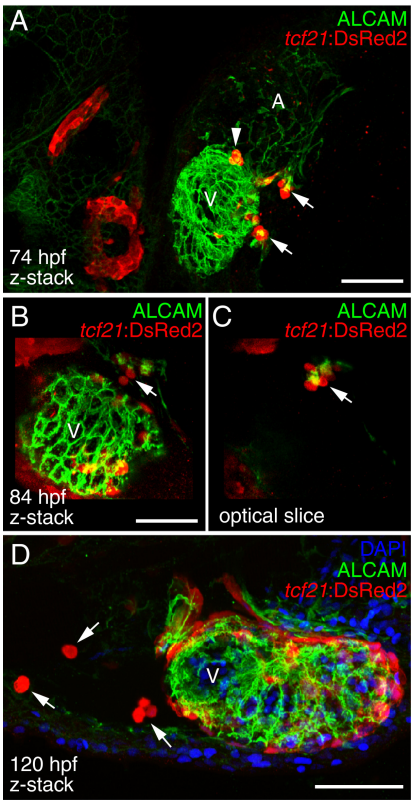

Figure 2. Ongoing PE cluster formation.

Ventral (A) and lateral (B-D) views of hearts from *tcf21*:DsRed2 larvae. PE and epicardial cells are marked with immunostaining for DsRed2 (red) and cardiomyocytes are marked with ALCAM (green). Nuclei are stained with DAPI (blue) in panel D. (A) Confocal z-stack of heart at 74 hpf. Epicardial cells have attached to the ventricle and additional PE clusters (arrows) are forming. A PE aggregate (arrowhead) that has been released into the pericardial cavity is located near the atrioventricular (AV) junction (n = 10). (B) Confocal z-stack of a ventricle at 84 hpf. Epicardial cells are established on the ventricle. PE cells clustered on the pericardial wall projecting towards the heart (n = 10). (C) A single optical slice taken from the z-stack, showing the persisting PE cluster (arrow). (D) PE cell aggregates (white arrows) in the pericardial cavity at 120 hpf (n = 7). For all panels, anterior is to the left and V is ventricle. Scale bars = 50 microns.

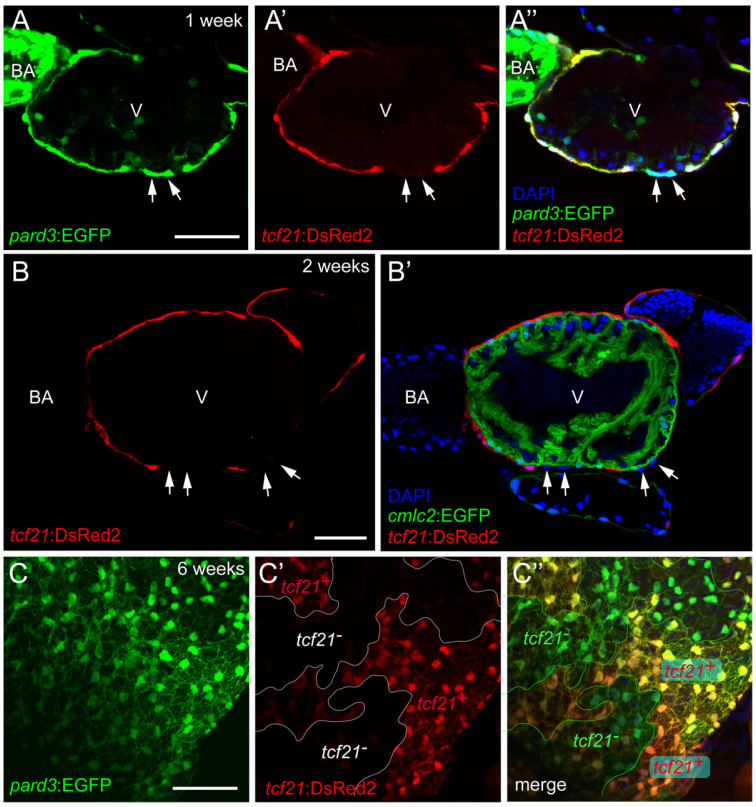

Figure 3. Heterogeneous *tcf21* expression within the developing epicardium.

Confocal images of the developing zebrafish epicardium. (A-A") Lateral view of a 1-week *pard3*:EGFP; *tcf21*:DsRed2 heart (n = 10). (A) Epicardial cells are marked with *pard3*:EGFP (green). (A') Immunostaining for DsRed2 (red). (A") Merge of A and A' with DAPI staining (nuclei; blue). Arrows indicate *pard3*+/*tcf21*- epicardial cells. (B-B') Ventral view of a 2-week *cmlc2*:EGFP; *tcf21*:DsRed2 heart (n = 5). (B) Epicardial cells are marked with immunostaining for DsRed2 (red). (B') *cmlc2*:EGFP; *tcf21*:DsRed2 heart with DAPI staining (nuclei; blue). *tcf21*-/DAPI + epicardial cells (arrows) are seen overlying the myocardium. (C-C") Ventricular epicardium from a 6-week old zebrafish heart (n = 5). (C) Epicardial cells are marked with *pard3*:EGFP (green). (C') Immunostaining for DsRed2 (red). (C") Merge of C and C'. For all panels: V is ventricle, BA is bulbus arteriosus. Scale bars = 50 microns.

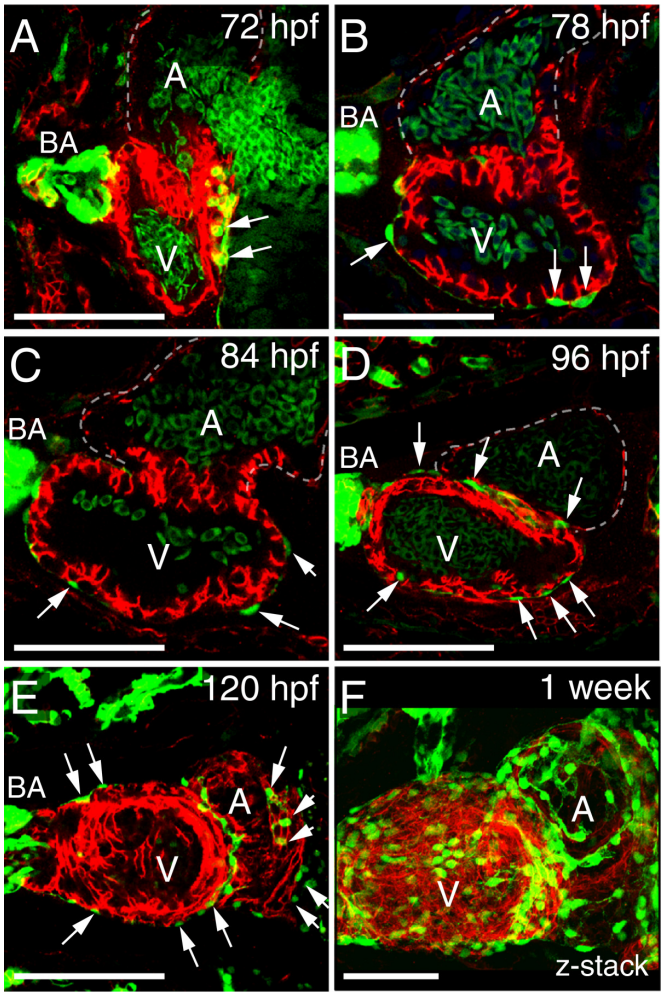

Figure 4. Normal progression of epicardium formation. Ventral views of zebrafish hearts.

(A-F) Epicardial cells are marked with *pard3* (EGFP; green) and cardiomyocytes are marked with ALCAM (red). Confocal images from 72-120 hpf are optical slices showing progressive epicardium coverage (white arrows) proceeding across the ventricle (V) and then onto the atrium (A) at 120 hpf. The z-series at one-week shows epicardial cells on the ventricle and atrium, however epicardium coverage is not complete. For all panels, with anterior to the left and BA is bulbus arteriosus. Scale bars = 50 microns. For each time point n = 5.

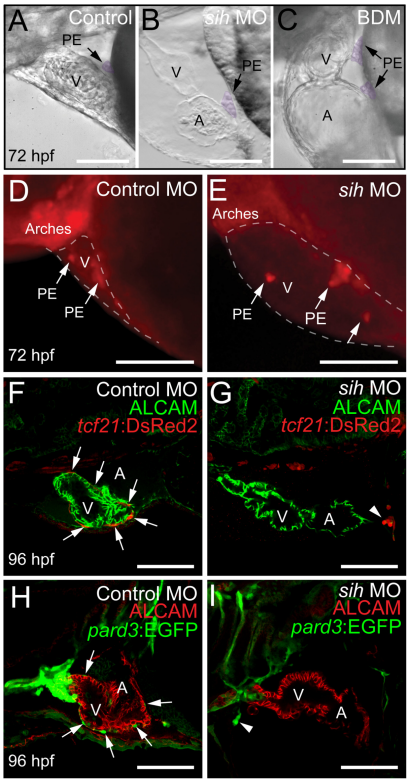

Figure 5. Heartbeat is not required for PE cluster formation, but is necessary for epicardium development.

Lateral views of zebrafish hearts with anterior to the left. (A-C) Brightfield micrographs showing hearts from control (A), *sih* MO (B), and BDM-treated (C) fish at 72 hpf. The PE clusters are pseudo colored purple and indicated by arrows (n = 10 per group). (D and E) Epifluorescence images showing hearts from control (D) and *sih* MO-treated (E) fish at 72 hpf, using the *tcf21*:DsRed2 reporter to reveal PE clusters (arrows) (n = 15 per group). The pericardial space is outlined with a dashed line. (F-I) Confocal images of embryos treated with control and *sih*-MO collected at 96 hpf (n = 12 per group). (F and G) *tcf21*:DsRed2 is red and ALCAM is green. (H and I) *pard3*:EGFP is green and ALCAM is red. Arrows indicate epicardial cells developing across the ventricle. Arrows indicate small PE clusters expressing *tcf21* or *pad3*. For all panels, V is ventricle; A, Atrium; BA, bulbus arteriosus. Scale bars = 50 microns.

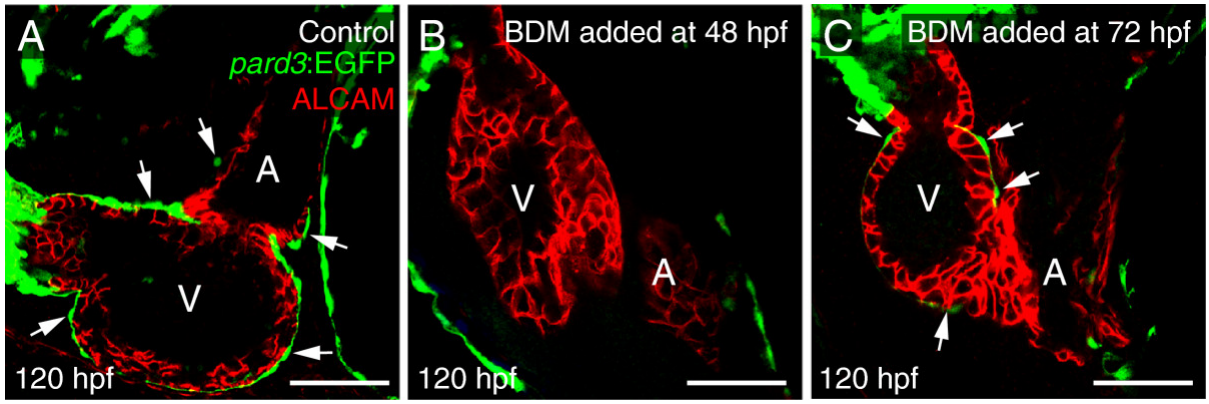

Figure 6. Inhibiting heartbeat impairs expansion of the epicardium.

Lateral confocal images of zebrafish hearts at 120 hpf with anterior to the left. The epicardial marker, *pard3*, is green and ALCAM (cardiomyocytes) is red. Arrows in panels A and C indicate epicardial cells on the ventricle (n = 7 per group). (A) Control. (B) BDM added at 48 hpf and maintained to the end of the experiments. (C) BDM added at 72 hpf and maintained to the end of the experiments. For all panels, V is ventricle; A, Atrium. Scale bars = 50 microns.

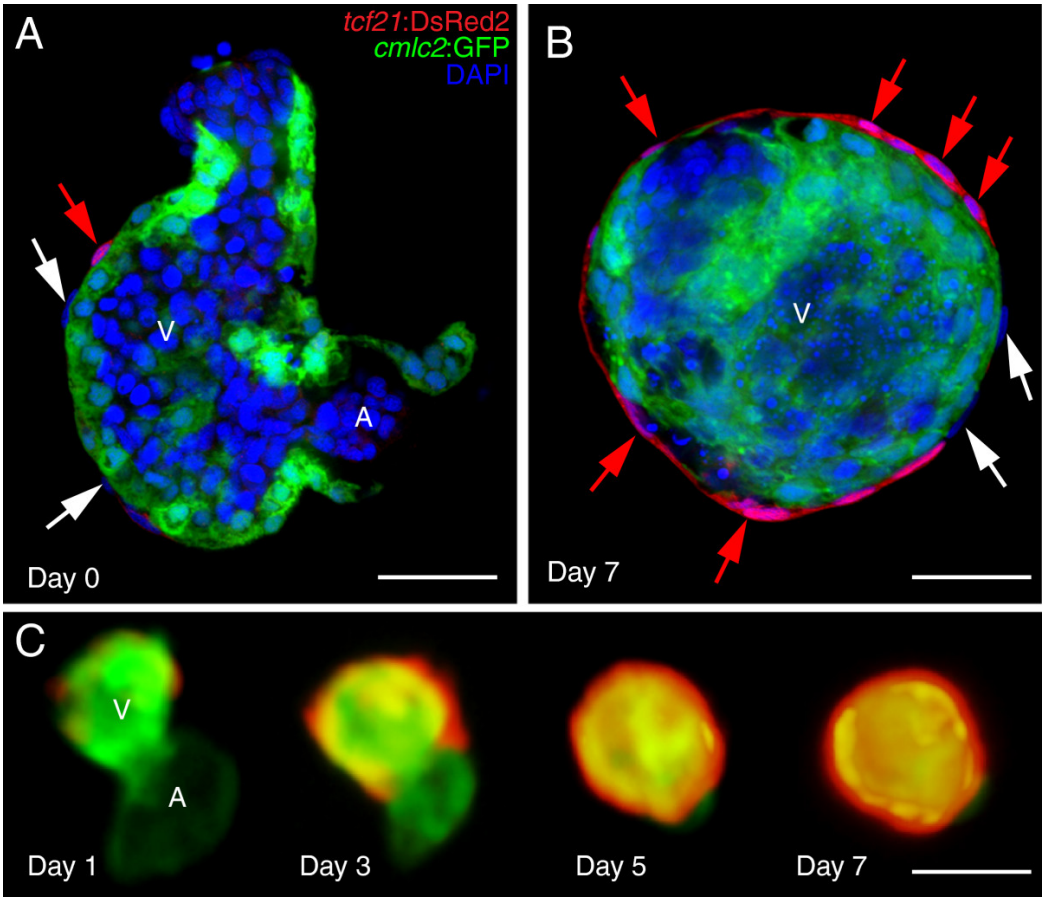

Figure 7. Epicardium formation on isolated hearts *in vitro*.

Hearts from *cmlc2*:EGFP; *tcf21*:DsRed2 larvae were extracted and placed in culture for 7 days. (A) Representative confocal image of a single ventricle prior at the time of isolation (Day 0; n = 10). (B) Confocal image of a fixed ventricle after 7 days in culture (n = 10). (C) Epifluorescent images tracking epicardium formation in culture. Images shown are from days 1, 3, 5 and 7 (n = 10). *tcf21*:DsRed2 marks epicardial cells (red) and *cmlc2*:EGFP marks cardiomyocytes (green). DAPI (DNA) is in blue in A and B. Arrows indicate epicardial cells that are *tcf21*+ (red arrows) or *tcf21*- (white arrows), which are identifiable by DAPI staining and their flattened epicardial cell morphology. Scale bars = 50 microns.

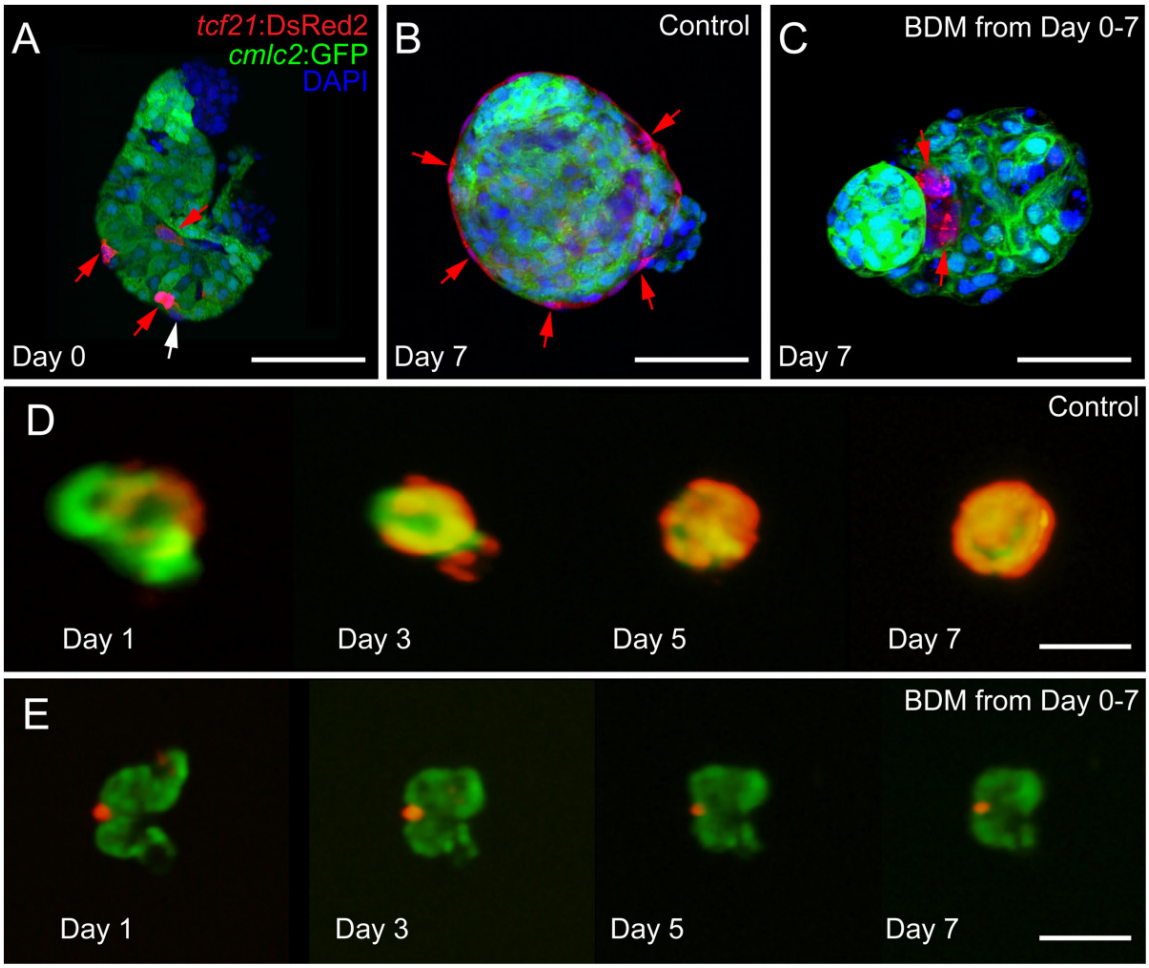

Figure 8. Inhibiting contraction prevents epicardial development *in vitro*.

Hearts from *cmlc2*:EGFP; *tcf21*:DsRed2 larvae were extracted and placed in culture with or without BDM. (A, B, and C) Confocal images of fixed hearts were collected at the time of isolation (A) and after 7 days (B and C) in culture. (B and D) Control hearts (n = 14). (C and E) BDM treated hearts (n = 14). *tcf21*:DsRed2 marks epicardial cells (red) and *cmlc2*:EGFP marks cardiomyocytes (green). DAPI (DNA) is in blue in A-C. Scale bars in A-C = 25 microns. Scale bars in D and E = 50 microns.

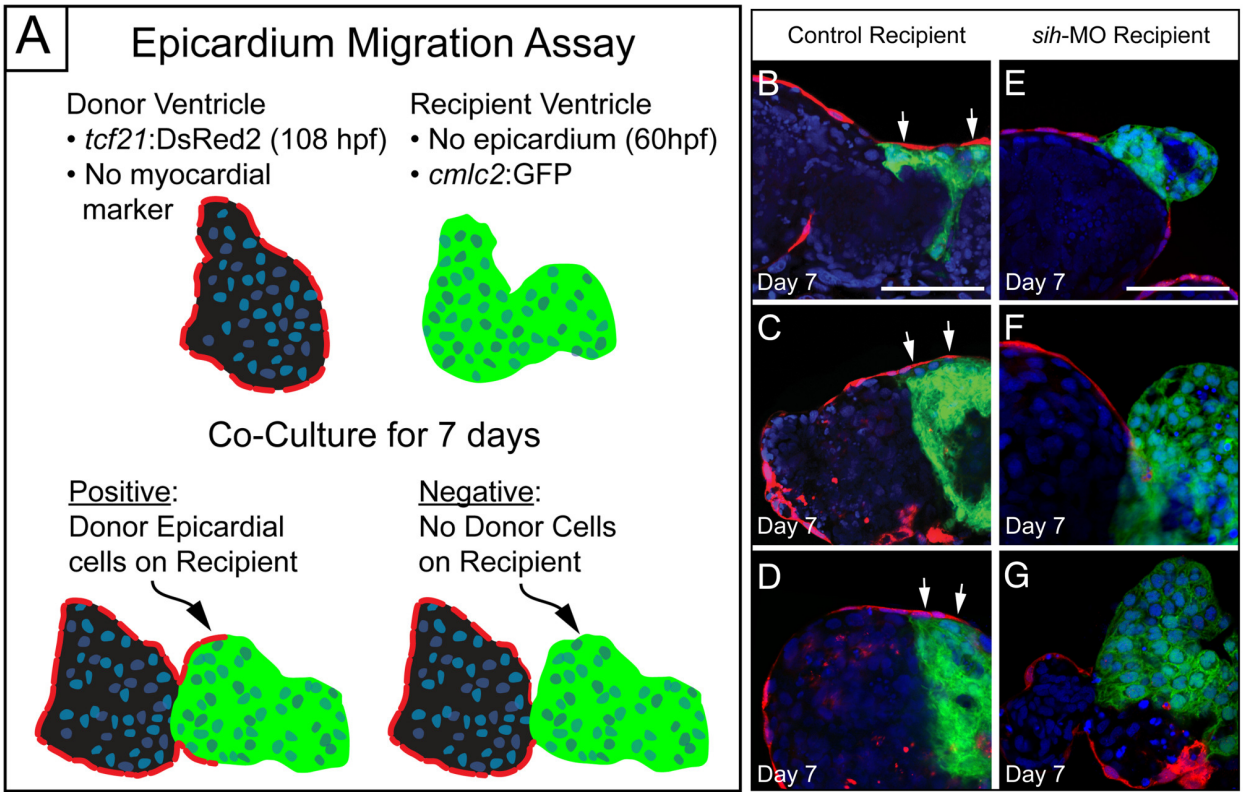

Figure 9. Epicardial cells from donor hearts do not migrate onto *sih* recipient hearts.

(A) Schematic of our epicardial cell migration assay. Control *tcf21*:DsRed2 donor hearts (108 hpf) were co-cultured with either control or *sih* injected *cmlc2*:GFP recipient hearts (60 hpf). (B, C, D) Epicardial cells from control donors migrate onto control recipient hearts (n = 7). (E, F, G) Epicardial cells from control donors do not migrate onto *sih* recipient hearts (n = 7).

<http://bmcdevbiol.biomedcentral.com/articles/10.1186/1471-213X-14-18>

Additional file 1: Movie 1. The PE bridge *in vivo*.

Lateral views of zebrafish at 72 hpf with anterior to the left. A PE cluster is simultaneously attached to both the pericardial wall and the ventricle.

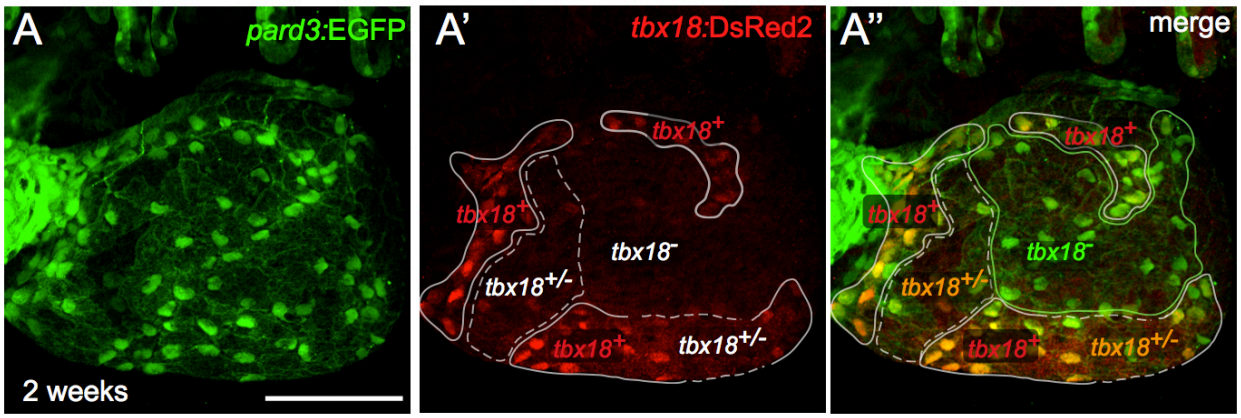

Additional file 2: Figure S1. Heterogeneous *tbx18* expression within the developing epicardium.

(A-A") Lateral view of 2-week *pard3*:EGFP; *tbx18*:DsRed2 heart. Epicardial cells are marked with *pard3*:EGFP (green) and immunostaining for DsRed2 (red). *tbx18* is expressed in a subset of epicardial cells (n = 5). Scale bars = 50 microns.

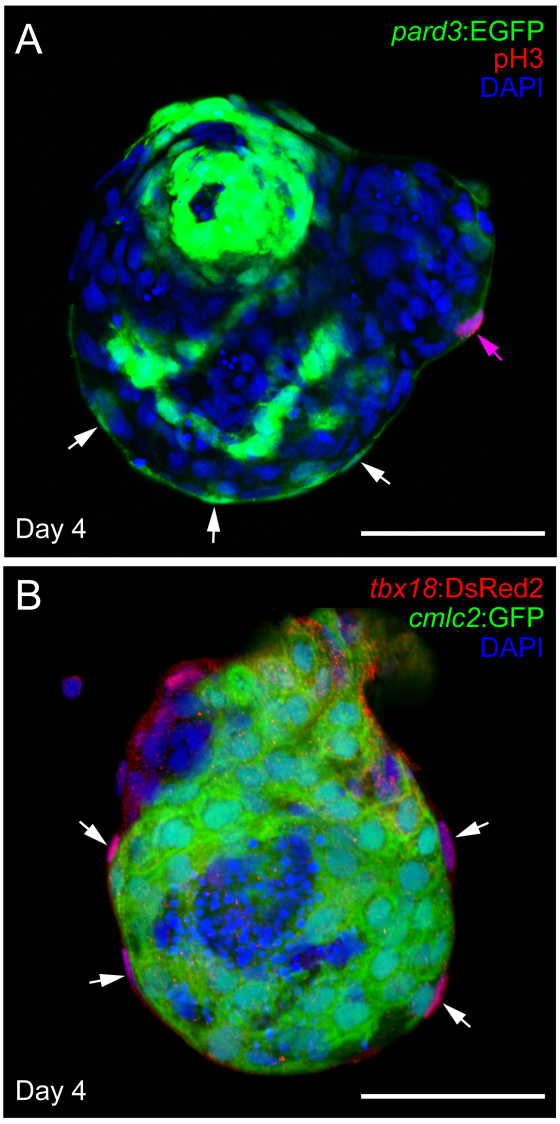

Additional file 3: Figure S2. Epicardial formation *in vitro* using additional epicardial markers.

(A) *pard3*:EGFP (n = 12) and (B) *tbx18*:DsRed2; *cmlc2*:GFP (n = 5) hearts isolated at 72 hpf and grown in culture for 4 days. (A) Cultured *pard3*:EGFP were stained with pH3 to examine cell division. Cell division was seen in the epicardium (A) as well as the myocardium (not shown). DAPI (DNA) is blue in A and B. Scale bars = 50 microns.

DISCUSSION

In this work we describe zebrafish PE migration and epicardium development in detail. As in other vertebrates, a PE forms, the progenitors migrate to the heart, and cells envelop the myocardium. We find that in zebrafish that PE migration occurs through both a cellular bridge and the release of PE aggregates into the pericardial cavity. Similar to murine epicardium development, we observe heterogeneous gene expression in the PE [24] and continue to observe heterogeneous gene expression in the developing larval and juvenile epicardium. We find the epicardium first forms over the ventricle and then begins to cover the atrium. Formation of the epicardium begins after the basic organization of the heart has been established and the heart is beating. We found that, as with valve development [27], heartbeat was essential for epicardium formation. The PE formed in the absence of the heartbeat, but epicardial progenitors failed to migrate to the myocardium, and the epicardium did not form.

Bridge and clusters

In the chick embryo, the PE migrates towards the myocardium by an extracellular matrix bridge [13]. In the mouse there is evidence for PE cell migration through both direct contact as well as free-floating PE cell aggregates [28]. In our experiments, the zebrafish PE protrudes towards the heart and makes direct contact with the myocardium forming a cellular bridge. Our finding with zebrafish suggests that teleosts develop a similar proepicardial bridge as reported in avians [13], amphibians [18,19,29], lamprey, dogfish [30], sturgeon [31] and the rat [32]. We also observed the release of PE cell aggregates during epicardium development, which indicates that multiple modes of PE migration occur during zebrafish epicardium development. Dual mechanisms have also been observed in mouse [20], axolotls [19], and dogfish [30].

Heterogeneity

In mice, the lineages of subsets of cells originating in the PE have been traced during development and found to contribute to different cell types in the heart including cardiac fibroblasts, smooth muscle, pericytes, subepicardial EPDCs, and perivascular cells such as the smooth muscle of the outflow tract. [16,24,33-35]. However, whether epicardial cells contribute to formation of cardiac muscle has been controversial [25,36-40]. The most significant evidence that the epicardium does not contribute to muscle comes from tracing epicardial cells with the *tcf21* marker. Our work clearly shows that not all epicardial cells are *tcf21*+. We observed cellular heterogeneity beginning within the PE and persisting through epicardium development. The *tcf21*- cells observed in the epicardium potentially descended from the *tcf21*- cells originally detected in the PE. Lineage tracing of the *tcf21*- cells, to complement what we know about the *tcf21*+ cells in the epicardium, will be needed to fully understand how epicardial progenitors contribute to zebrafish heart structures.

The role of heartbeat in epicardial development

Inhibiting heartbeat prevented the epicardium from forming, however it did not prevent the specification of PE cells or the development of PE clusters. If the heartbeat was stopped later in development, established epicardial cells remained on the heart surface but did not migrate and expand further across the heart.

Our findings are consistent with the report that PE cells are specified in *sih* morphants [1]. However, our work contradicts the conclusion from Peralta *et al.* [23] that PE cluster formation requires heartbeat induced pericardial fluid forces. We note that we used different techniques and markers, and scored for PE cluster formation later in development, which may explain the differences between the two reports. We initially used brightfield microscopy as well as video microscopy to identify PE cluster formation in live embryos suspended in methylcellulose. PE formation was clearly evident in samples

both with and without heartbeat. After observing PE cluster formation in these samples, we injected *sih* MO into a known PE marker line, *tcf21*:DsRed2 and confirmed that the observed clusters were composed of specified PE cells. Together, our findings demonstrate that heartbeat is not necessary for PE cluster formation. However, our results are in agreement with Peralta *et al.* [23] that the heartbeat is needed for epicardium formation.

Although it has been proposed that heartbeat has an indirect impact on the epicardium through hydrodynamic forces generated within the pericardium, our results with hearts cultured *in vitro* lead us to doubt this. Clearly the heartbeat itself is needed, but none of the specific flow patterns of blood or pericardial fluid are present *in vitro*, nor are factors found in the pericardial space that might promote adhesion and proliferation. Yet the epicardial layer formed nonetheless: as long as the beat continued. We were also able to show that the transfer of epicardial cells from a donor to a recipient heart was heartbeat dependent. Since epicardial cell migration does not occur in the absence of heartbeat, we speculate that the cardiomyocyte surface may be altered due to the loss of regular beating.

In addition, inhibiting heartbeat may alter the expression of signaling molecules and/or their receptors, which may be needed for PE migration. In chick, *bone morphogenetic proteins* (*bmp*) signals emanating from the myocardium direct PE protrusion and attachment [41]. Planar cell polarity also known to play an important role in PE cell migration and it may be that signals from the myocardium induce polarity in migrating PE cells. We consistently observed that the initially spherical PE cells acquired an oblong, planar shape as they encountered the myocardial surface. When contractility was blocked *in vivo*, PE cells adjacent to the myocardium remained rounded. In mice, loss of the planar cell polarity protein *Par3* results in failure of PE cell migration [42]. In zebrafish, Serluca showed that knockdown of the cell polarity genes *heart and soul* (*has*/*aPKC*/*PRKCl*) and *nagie oko* (*nok*) resulted in defects in PE morphogenesis [1].

CONCLUSIONS

We show that PE migration occurs through multiple modes, including a cellular bridge that forms between the pericardial wall and the heart near the AV junction. Consistent with Peralta *et al.* [23], we observe the development of multiple PEs and the release of progenitor cell aggregates into the pericardial space. We find that the epicardium first envelops the ventricle before moving across the atrium. The presence of a heartbeat is not required for PE formation, but it is necessary for expansion of the epicardium across the myocardium. The formation of PE clusters in the absence of a heartbeat and the finding that epicardial growth and expansion occurs across hearts *in vitro*, rule out pericardiac fluid advections as a critical requirement for epicardium development. Heart contraction, however, was required for epicardial formation *in vitro* and *in vivo*.

METHODS

Zebrafish strains

Adult zebrafish lines were maintained and zebrafish embryos were reared and housed according to procedures described by [43]. The AB wild type line was used unless otherwise indicated. Transgenic lines used: *pard3*:EGFP [*ET*(*krt4*:*EGFP*)^{sqet27}] [44], *tcf21*:DsRed2 [*Tg*(*tcf21*:*DsRed2*)^{pd37}] [40], and *cmlc2*:EGFP [*Tg*(*cmlc2*:*EGFP*)^{f1}] [45]. All procedures involving animals were approved by the Animal Care and Use Committee of the University of Wisconsin-Madison, and adhered to the National Institutes of Health's "Guide for the Care and Use of Laboratory Animals".

Immunohistochemistry and confocal microscopy

Antibody staining was performed as previously described [46,47]. Primary antibodies were used at the following dilutions: mouse anti- *activated leukocyte cell adhesion molecule* (ALCAM/zn5; ZIRC)

1:50, rabbit anti-DsRed (AnaSpec, Fremont, CA) at 1:200 in phosphate buffered saline with 0.03% triton and 4% bovine serum albumin (PBT). Secondary anti mouse antibodies (Alexa 488, Alexa 568; Invitrogen) were used at 1:200 dilution in PBT. Embryos were mounted in Vectashield or Vectashield with Dapi (Vector Laboratories). Confocal images were collected on an Olympus Fluoview FV1000 microscope. Brightest point projections were made using Olympus Fluoview software and images were processed using Adobe Photoshop. Optical sections in z-series were collected at 0.52 μm intervals.

PE imaging

Live embryos were imaged as previously described [47]. Briefly, fish were imaged at 72 hpf in 3% methylcellulose using a Nikon TE300 inverted microscope attached to a Princeton Instruments Micromax CCD camera. Videos were collected using MotionsScope software and analyzed using Metamorph software.

Morpholinos and 2,3-butanedione 2-monoxime (BDM)

All morpholino oligonucleotides (MOs; Gene Tools, LLC) were used as previously reported [48,49]. The TNNT2 MO (5' CAT GTT TGC TCT GAT CTG ACA CGC A 3') was designed to block the translational start site of zebrafish cardiac troponin 2 (*tnnt2*; *silent heart*, *sih*). The standard Gene Tools Control MO (5'-CCT CTT ACC TCA GTT ACA ATT TAT A-3') was used to control for non-specific responses. One-cell embryos were injected with 2 ng of MO. 2,3-Butanedione 2-monoxime (BDM, Sigma Aldrich) was used at a final concentration of 10 mM embryo water.

Tissue culture

Hearts from *cmlc2*:GFP and *tcf21*:DsRed2 larvae were isolated at 60 hpf and 108 hpf, respectively, as previously described [50]. Hearts were mixed in a 1:2 ratio of *tcf21*:DsRed2 to *cmlc2*:GFP hearts and placed in culture plates with matrigel (thin gel coating method, BD Biosciences).

Heart cultures were incubated at 28°C with 5% CO_2 in cell culture media containing Leibovitz's L-15 (Fisher) with 10% fetal bovine serum (Sigma) and 4x penicillin/streptomycin (Invitrogen). Cultures were monitored daily and media was refreshed every other day. Images were obtained with an Olympus DP72 camera mounted on an Olympus SZX16 epifluorescence stereo microscope with cellSens software. On Day 7 in culture, heart clusters were removed and fixed in 4% paraformaldehyde and immediately prepped for immunohistochemistry.

COMPETING INTERESTS

The authors declare that they have no competing interests.

AUTHORS' CONTRIBUTIONS

JP & MSY carried out the immunohistochemistry and JP collected all the confocal images. JP and PH performed the morpholino injections. MSY developed the heart culture protocol. MSY, JP and PH performed the *in vitro* BDM and heart culture experiments. PH conducted the PE brightfield imaging experiments. JP, KAL, PH, MSY, REP and WH participated in the study design, data analysis and writing of the manuscript. All authors read and approved the final manuscript.

ACKNOWLEDGEMENTS

We thank Dorothy Nesbit for execellent oversight and care of the zebrafish facility, and Drs. Vladamir Korzh, Kenneth Poss, and C. Geoffrey Burns for providing the *pard3*:EGFP, *tcf21*:DsRed2, and

cmlc2:GFP transgenic zebrafish lines respectively. We thank Maggie Shuda, Erica Christensen, John K. Samson and Paul Forslyn for technical support.

REFERENCES

1. Serluca FC: Development of the proepicardial organ in the zebrafish. *Dev Biol* 2008, **315**(1):18-27.

2. Bakkers J: Zebrafish as a model to study cardiac development and human cardiac disease. *Cardiovasc Res* 2011, **91**(2):279-288.

3. Vincent SD, Buckingham ME: How to make a heart: the origin and regulation of cardiac progenitor cells. *Curr Top Dev Biol* 2010, **90**:1-41.

4. Srivastava D, Olson EN: A genetic blueprint for cardiac development. *Nature* 2000, **407**(6801):221-226.

5. Olson EN: Gene regulatory networks in the evolution and development of the heart. *Science* 2006, **313**(5795):1922-1927.

6. Buckingham M, Meilhac S, Zaffran S: Building the mammalian heart from two sources of myocardial cells. *Nat Rev Genet* 2005, **6**(11):826-835.

7. Martin-Puig S, Wang Z, Chien KR: Lives of a heart cell: tracing the origins of cardiac progenitors. *Cell Stem Cell* 2008, **2**(4):320-331.

8. Gittenberger-de Groot AC, Winter EM, Bartelings MM, Jose Goumans M, Deruiter MC, Poelmann RE: The arterial and cardiac epicardium in development, disease and repair. *Differentiation* 2012, **84**(1):41-53.

9. Smart N, Riley PR: The epicardium as a candidate for heart regeneration. *Future Cardiol* 2012, **8**(1):53-69.

10. Smart N, Dube KN, Riley PR: Epicardial progenitor cells in cardiac regeneration and neovascularisation. *Vascul Pharmacol* 2012, **58**(3):164-173.

11. Riley PR: An epicardial floor plan for building and rebuilding the mammalian heart. *Curr Top Dev Biol* 2012, **100**:233-251.

12. Lie-Venema H, van den Akker NM, Bax NA, Winter EM, Maas S, Kekarainen T, Hoeben RC, DeRuiter MC, Poelmann RE, Gittenberger-de Groot AC: Origin, fate, and function of epicardium-derived cells (EPDCs) in normal and abnormal cardiac development. *Sci World J* 2007, **7**:1777-1798.

13. Nahirney PC, Mikawa T, Fischman DA: Evidence for an extracellular matrix bridge guiding proepicardial cell migration to the myocardium of chick embryos. *Dev Dyn* 2003, **227**(4):511-523.

14. Sakaguchi T, Kikuchi Y, Kuroiwa A, Takeda H, Stainier DY: The yolk syncytial layer regulates myocardial migration by influencing extracellular matrix assembly in zebrafish. *Development* 2006, **133**(20):4063-4072.

15. Manner J: The development of pericardial villi in the chick embryo. *Anat Embryol* (Berl) 1992, **186**(4):379-385.

16. Manner J: Does the subepicardial mesenchyme contribute myocardioblasts to the myocardium of the chick embryo heart? A quail-chick chimera study tracing the fate of the epicardial primordium. *Anat Rec* 1999, **255**(2):212-226.

17. Hiruma T, Hirakow R: Epicardial formation in embryonic chick heart: computer-aided reconstruction, scanning, and transmission electron microscopic studies. *Am J Anat* 1989, **184**(2):129-138.

18. Jahr M, Schlueter J, Brand T, Manner J: Development of the proepicardium in Xenopus laevis. *Dev Dyn* 2008, **237**(10):3088-3096.

19. Fransen ME, Lemanski LF: Epicardial development in the axolotl, Ambystoma mexicanum. *Anat Rec* 1990, **226**(2):228-236.

20. Komiyama M, Ito K, Shimada Y: Origin and development of the epicardium in the mouse embryo. *Anat Embryol* 1987, **176**(2):183-189.

21. Rodgers LS, Lalani S, Runyan RB, Camenisch TD: Differential growth and multicellular villi direct proepicardial translocation to the developing mouse heart. *Dev Dyn* 2008, **237**(1):145-152.

22. Hu N, Sedmera D, Yost HJ, Clark EB: Structure and function of the developing zebrafish heart. *Anat Rec* 2000, **260**(2):148-157.

23. Peralta M, Steed E, Harlepp S, González-Rosa JM, Monduc F, Ariza-Cosano A, Cortés A, Rayón T, Gómez-Skarmeta JL, Zapata A, Vermot J, Mercader N: Heartbeat-driven pericardiac fluid forces contribute to epicardium morphogenesis. *Curr Biol* 2013.

24. Katz TC, Singh MK, Degenhardt K, Rivera-Feliciano J, Johnson RL, Epstein JA, Tabin CJ: Distinct compartments of the proepicardial organ give rise to coronary vascular endothelial cells. *Dev Cell* 2012, **22**(3):639-650.

25. Cai CL, Martin JC, Sun Y, Cui L, Wang L, Ouyang K, Yang L, Bu L, Liang X, Zhang X, Stallcup WB, Denton CP, McCulloch A, Chen J, Evans SM: A myocardial lineage derives from Tbx18 epicardial cells. *Nature* 2008, **454**(7200):104-108.

26. Liu J, Stainier DY: Tbx5 and Bmp signaling are essential for proepicardium specification in zebrafish. *Circ Res* 2010, **106**(12):1818-1828.

27. Bartman T, Walsh EC, Wen KK, McKane M, Ren J, Alexander J, Rubenstein PA, Stainier DY: Early myocardial function affects endocardial cushion development in zebrafish. *PLoS Biol* 2004, **2**(5):E129.

28. Schulte I, Schlueter J, Abu-Issa R, Brand T, Manner J: Morphological and molecular left-right asymmetries in the development of the proepicardium: a comparative analysis on mouse and chick embryos. *Dev Dyn* 2007, **236**(3):684-695.

29. Tandon P, Miteva YV, Kuchenbrod LM, Cristea IM, Conlon FL: Tcf21 regulates the specification and maturation of proepicardial cells. *Development* 2013, **140**(11):2409-2421.

30. Pombal MA, Carmona R, Megias M, Ruiz A, Perez-Pomares JM, Munoz-Chapuli R: Epicardial development in lamprey supports an evolutionary origin of the vertebrate epicardium from an ancestral pronephric external glomerulus. *Evol Dev* 2008, **10**(2):210-216.

31. Icardo JM, Guerrero A, Duran AC, Colvee E, Domezain A, Sans-Coma V: The development of the epicardium in the sturgeon *Acipenser naccarii*. *Anat Rec* (Hoboken) 2009, **292**(10):1593-1601.

32. Nesbitt T, Lemley A, Davis J, Yost MJ, Goodwin RL, Potts JD: Epicardial development in the rat: a new perspective. *Microsc Microanal* 2006, **12**(5):390-398.

33. Dettman RW, Denetclaw W Jr, Ordahl CP, Bristow J: Common epicardial origin of coronary vascular smooth muscle, perivascular fibroblasts, and intermyocardial fibroblasts in the avian heart. *Dev Biol* 1998, **193**(2):169-181.

34. Mikawa T, Gourdie RG: Pericardial mesoderm generates a population of coronary smooth muscle cells migrating into the heart along with ingrowth of the epicardial organ. *Dev Biol* 1996, **174**(2):221-232.

35. Gittenberger-de Groot AC, Vrancken Peeters MP, Mentink MM, Gourdie RG, Poelmann RE: Epicardium-derived cells contribute a novel population to the myocardial wall and the atrioventricular cushions. *Circ Res* 1998, **82**(10):1043-1052.

36. Zhou B, Ma Q, Rajagopal S, Wu SM, Domian I, Rivera-Feliciano J, Jiang D, von Gise A, Ikeda S, Chien KR, Pu WT: Epicardial progenitors contribute to the cardiomyocyte lineage in the developing heart. *Nature* 2008, **454**(7200):109-113.

37. Zhou B, Pu WT: More than a cover: epicardium as a novel source of cardiac progenitor cells. *Regen Med* 2008, **3**(5):633-635.

38. Limana F, Zacheo A, Mocini D, Mangoni A, Borsellino G, Diamantini A, De Mori R, Battistini L, Vigna E, Santini M, Loiaconi V, Pompilio G, Germani A, Capogrossi MC: Identification of myocardial and vascular precursor cells in human and mouse epicardium. *Circ Res* 2007, **101**(12):1255-1265.

39. Merki E, Zamora M, Raya A, Kawakami Y, Wang J, Zhang X, Burch J, Kubalak SW, Kaliman P, Izpisua Belmonte JC, Chien KR, Ruiz-Lozano P: Epicardial retinoid X receptor alpha is required for myocardial growth and coronary artery formation. *Proc Natl Acad Sci* U S A 2005, **102**(51):18455-18460.

40. Kikuchi K, Gupta V, Wang J, Holdway JE, Wills AA, Fang Y, Poss KD: tcf21+ epicardial cells adopt non-myocardial fates during zebrafish heart development and regeneration. *Development* 2011, **138**(14):2895-2902.

41. BMP signals promote proepicardial protrusion necessary for recruitment of coronary vessel and epicardial progenitors to the heart. *Dev Cell* 2010, **19**(2):307-316.

42. Hirose T, Karasawa M, Sugitani Y, Fujisawa M, Akimoto K, Ohno S, Noda T: PAR3 is essential for cyst-mediated epicardial development by establishing apical cortical domains. *Development* 2006, **133**(7):1389-1398.

43. Westerfield M: The Zebrafish Book. A Guide for the Laboratory Use of Zebrafish (*Danio rerio*). 3rd edition. 1995.

44. Poon KL, Liebling M, Kondrychyn I, Garcia-Lecea M, Korzh V: Zebrafish cardiac enhancer trap lines: new tools for in vivo studies of cardiovascular development and disease. *Dev Dyn* 2010, **239**(3):914-926.

45. Burns CG, Milan DJ, Grande EJ, Rottbauer W, MacRae CA, Fishman MC: High-throughput assay for small molecules that modulate zebrafish embryonic heart rate. *Nat Chem Biol* 2005, **1**(5):263-264.

46. Dong J, Feldmann G, Huang J, Wu S, Zhang N, Comerford SA, Gayyed MF, Anders RA, Maitra A, Pan D: Elucidation of a universal size-control mechanism in Drosophila and mammals. *Cell* 2007, **130**(6):1120-1133.

47. Plavicki J, Hofsteen P, Peterson RE, Heideman W: Dioxin inhibits zebrafish epicardium and proepicardium development. *Toxicol Sci* 2013, **131**(2):558-567.

48. Antkiewicz DS, Peterson RE, Heideman W: Blocking expression of AHR2 and ARNT1 in zebrafish larvae protects against cardiac toxicity of 2,3,7,8-tetrachlorodibenzo-*p*-dioxin. *Toxicol Sci* 2006, **94**(1):175-182.

49. Prasch AL, Teraoka H, Carney SA, Dong W, Hiraga T, Stegeman JJ, Heideman W, Peterson RE: Aryl hydrocarbon receptor 2 mediates 2,3,7,8-tetrachlorodibenzo-*p*-dioxin developmental toxicity in zebrafish. *Toxicol Sci* 2003, **76**(1):138-150.

50. Burns CG, MacRae CA: Purification of hearts from zebrafish embryos. *Biotechniques* 2006, **40**(3):274-278.

CHAPTER IV:

A CO-CULTURE ASSAY OF EMBRYONIC ZEBRAFISH HEARTS TO ASSESS MIGRATION OF EPICARDIAL CELLS *IN VITRO*

Monica S. Yue, Jessica S. Plavicki, Xin-yi Li, Richard E. Peterson, and Warren Heideman

BMC Developmental Biology. (2015) **15**, 50.

ABSTRACT

Background

The vertebrate heart consists of three cell layers: the innermost endothelium, the contractile myocardium and the outermost epicardium. The epicardium is vital for heart development and function, and forms from epicardial progenitor cells (EPCs), which migrate to the myocardium during early development. Disruptions in EPC migration and epicardium formation result in a number of cardiac malformations, many of which resemble congenital heart diseases in humans. Hence, it is important to understand the mechanisms that influence EPC migration and spreading in the developing heart. *In vitro* approaches heretofore have been limited to monolayer epicardial cell cultures, which may not fully capture the complex interactions that can occur between epicardial and myocardial cells *in vivo*.

Results

Here we describe a novel *in vitro* co-culture assay for assessing epicardial cell migration using embryonic zebrafish hearts. We isolated donor hearts from embryonic zebrafish carrying an epicardial-specific fluorescent reporter after epicardial cells were present on the heart. These were co-cultured with recipient hearts expressing a myocardial-specific fluorescent reporter, isolated prior to EPC migration. Using this method, we can clearly visualize the movement of epicardial cells from the donor heart onto the myocardium of the recipient heart. We demonstrate the utility of this method by showing that epicardial cell migration is significantly delayed or absent when myocardial cells lack contractility and when myocardial cells are deficient in *tbx5* expression.

Conclusions

We present a method to assess the migration of epicardial cells in an *in vitro* assay, wherein the migration of epicardial cells from a donor heart onto the myocardium of a recipient heart in co-culture is monitored

and scored. The donor and recipient hearts can be independently manipulated, using either genetic tools or pharmacological agents. This allows flexibility in experimental design for determining the role that target genes/signaling pathways in specific cell types may have on epicardial cell migration.

BACKGROUND

The heart is one of the first organs to form in vertebrate embryogenesis and during early development consists of three major cell layers: endocardium, myocardium, and epicardium. The endocardial and myocardial cells originate from populations of mesodermal cells that migrate from the midbrain-hindbrain boundary to form the linear heart tube [1,2]. These cardiogenic mesoderm cells form the ventricle, atrium, outflow tract myocardium, and contribute to the cardiac conduction system [3]. The epicardium originates from a different population of cells, the proepicardium (PE), a transitory structure of progenitor cells arising from coelomic mesenchyme of the septum transversum [3]. Epicardial progenitor cells (EPCs) from the PE migrate onto the bare myocardium and envelop the heart, forming the epicardium. There are two known mechanisms of cell migration from the PE to the heart: 1) the release of free-floating EPC aggregates that land on the myocardium (e.g., mouse); 2) the formation of a tissue bridge between the PE and myocardium (e.g., chick). Both mechanisms of PE cell migration are observed in some species (e.g., zebrafish, axolotl) [4-6]. As the heart develops, a subset of epicardial cells undergo epithelial-to-mesenchymal transition and invade the subepicardial space. These mesenchymal cells, called epicardium-derived cells (EPDCs), are important for normal heart maturation and have been shown to differentiate into interstitial cardiac fibroblasts, coronary vascular smooth muscle cells, and adventitial fibroblasts. Though somewhat controversial, it is suggested that EPDCs also contribute to the coronary endothelium, valve development, myocardial cells, and Purkinje fiber differentiation [4,7].

Congenital heart disease, which affects between 0.4-5% of live births, is often due to defective cardiac morphogenesis involving problems with cardiac progenitor cells [3]. There has been increasing interest on epicardium formation and importance of the epicardium in subsequent heart development [7]. Ablation of the PE inhibits epicardium formation, causing an array of cardiac malformations that resemble malformations observed in human congenital heart disease. For example, chicks lacking an

epicardium developed thin compact myocardia similar to human left ventricular non-compaction cardiomyopathy [8]. Aberrant crosstalk between the epicardial layer and underlying myocardial and endocardial cells has been implicated in several congenital diseases, such as hypoplastic left heart syndrome and endocardial fibroelastosis [3,7].

In vivo approaches to studying PE migration and epicardium formation often include microsurgery to ablate the PE or the use of physical barriers to block migration. Manipulation of specific genes involved in signaling or cell adhesion has also been used to assess involvement in PE formation [5,8-10]. However, the genes of interest, including *Wt1*, *Tbx18*, *Tcf21*, are expressed during development in other organs besides the heart: the use of mutants or morpholino oligonucleotide (MO) knockdown produces effects wherever the target gene is normally expressed. This creates a concern that the results have been influenced by altered gene expression not specific to heart cells [7,9,11].

Common *in vitro* approaches involve excising the PE or heart segment and monitoring effects on EPC migration in culture [9,12,13]. One advantage of this approach is the ease with which signaling factors can be added to the culture media to assess effects on migration [9]. In addition, it avoids the problem of off-target effects in gene manipulation experiments. However, most of these studies have focused on the effects of factors in the culture medium, rather than on the cell-cell interactions between epicardial cells and myocardial cells, which have been shown to play an important role in heart development *in vivo* [6,8,14].

Here we describe an *in vitro* assay to assess and quantify the migration of epicardial cells from a donor heart onto the bare myocardium of a recipient heart. In this assay, the important cell-cell interactions between different cell types remain intact. Because the technique cultures multiple cell types, differentiated cell phenotypes are better preserved [15], allowing the hearts to remain healthy in culture

for several days. This permits for lengthy observations, not possible with most *in vitro* approaches. In this method, the source of migrating epicardial cells is different from the source of target myocardial cells, making it possible to manipulate either or both types of cells independently.

We use embryonic zebrafish as the source of hearts. This is advantageous for several reasons: zebrafish produce large numbers of offspring, embryonic hearts can be efficiently isolated, externally fertilized eggs allow for gene manipulation with MO or CRISPR-Cas9, and there is clear observation of effects during early development. Additionally, a variety of transgenic lines are readily available [1].

In this report, we demonstrate key features of this assay by assessing the ability of epicardial cells from a donor heart (marked with *tcf21*:DsRed2) to migrate onto the myocardial surface of a recipient heart (marked with *cmlc2*:EGFP). We show the normal course of migration, and how migration was inhibited when the recipient hearts were extracted from embryos injected with MOs against *silent heart* (*sih*), and *tbx5*. *Sih* morphants lack a heartbeat [16]. *Tbx5*, which is expressed in multiple tissues in the heart, has been implicated in EPC migration *in vivo* [12]. Because this approach maintains the multiple cell types of the *in vivo* setting, yet allows for manipulation of individual cell types, this assay can be used to identify not only genes important in epicardial formation, but also where they function.

METHODS

Zebrafish

Embryos were obtained from adult zebrafish (*Danio rerio*) housed and maintained according to guidelines described in Westerfield (2000) [17]. Embryos were harvested at 84 hours post fertilization (hpf) for obtaining "donor hearts". These hearts were obtained from the transgenic line *tcf21*:DsRed2 [*Tg(tcf21:DsRed2)*^{pd37}], which marks epicardial cells with a red fluorescent protein. The "recipient hearts"

were collected from 60 hpf embryos from the transgenic line *cmlc2*:EGFP [*Tg(cmlc2:EGFP)*^{f1}], which marks myocardial cells with a green fluorescent protein (Fig. 1A).

The *silent heart* (*sih*; cardiac troponin T2, *tnnt2*) and *tbx5* (T-box 5) MOs were obtained from Gene Tools (Philomath, OR). The Gene Tools standard control morpholino (control MO) was used as a control. The MO sequences were: *sih*, 5' CATGTTTGCTCTGATCTGACACGA 3' [16]; *tbx5*, 5' GAAAGGTGTCTTCACTGTCCGCCAT 3' [18]; control MO, 5' CCTCTTACCTCAGTTACAATTTATA 3'. A 2 nM MO solution was prepared with either the *sih*, *tbx5*, or control MO, and microinjected into *cmlc2*:EGFP eggs in the 1-2 cell stage. Microinjections were done as previously described [19]. Eggs were collected into a petri dish with autoclave-sterilized egg water (60 µg/ml Instant Ocean Sea Salts with 0.2 ppm methylene blue). Embryos were screened for MO incorporation at 48 hpf, and only MO positive embryos were used. Clean water changes were made daily.

All procedures involving zebrafish were approved by the Animal Care and Use Committee of the University of Wisconsin-Madison and adhered to the National Institute of Health's "Guide for the Care and Use of Laboratory Animals."

Culture media and plate preparation

Culture medium consisted of Leibovitz's L-15 medium (Life Technologies) supplemented with 10% fetal bovine serum (Life Technologies) and 4x penicillin/streptomycin (Fisher Scientific). The culture medium was filtered through a disposable sterile filter unit, and stored at 4 ^{o}C prior to use. Conical-bottom 60-well plates with lids (Electron Microscopy Sciences) were pre-plated with a mix made from Matrigel basement membrane matrix mix (Corning), with a protein concentration diluted to 4 mg/mL in 1X DMEM (Corning) and supplemented with 4x penicillin/streptomycin. The matrigel mix was prepared ahead of time in a sterile hood and stored at -20^{o} C. On the culture start day, the matrigel

mix was thawed and plated onto a culture dish following the manufacturer-recommended thin gel coating method. Each well required approximately 10 μL of matrigel mix to coat. After the culture dish was set (37 ^{o}C, 30 minutes) it was stored in the cell culture incubator (28 ^{o}C, 5% CO_2) until time for placement of hearts into culture.

Isolation of embryonic hearts and placement into culture

Hearts were extracted from embryos according to methods adapted from Burns and MacRae [20]. Briefly, 50 to 80 embryos were lightly anesthetized with tricaine (MS 222, Sigma-Aldrich) and placed into a 1.7 mL microcentrifuge tube. Excess water was drawn off and 1 mL of culture medium was added. The microcentrifuge tube with embryos was placed beneath a 5 mL syringe fitted with a 19-gauge needle, adjusted such that the beveled end of the needle aligned with the 0.25 mL mark on the microcentrifuge tube. The syringe was gently pumped up and down, bringing culture media and embryos into and out of the syringe, in a rhythm guided by beats on a metronome. Hydrodynamic shear forces remove the hearts from the bodies. These forces are proportional to the rate of flow through the needle, and inversely proportional to the needle diameter, thus the rate of syringe pumping is critical. All contents from the syringe and microcentrifuge tube were then quantitatively emptied from the syringe with washes and filtered through a 105 micron nylon mesh (Component Supply) to separate the bodies and other large debris from the hearts in the filtrate. If necessary, the media was filtered again with a 37 micron nylon mesh (Component Supply) to retain the hearts on the filter and remove smaller debris. Hearts in medium were placed in a Petri dish and collected using a micropipettor with the aid of an Olympus SZX16 epifluorescence stereomicroscope and the EGFP or RFP heart markers, and placed temporarily into a droplet of fresh culture media until all hearts had been collected. The efficiency of heart extraction yields varied depending on the number of strokes (total number of draws and expulsions) and rate of plunger motion; these factors differed depending on the age and treatment of the embryos. Donor hearts from 84

hpf *tcf21*:DsRed2 embryos required approximately 70 strokes (35 draws and 35 expulsions) at a rate of 60 beats per minute (bpm) according to a metronome. Recipient hearts from 60 hpf control MO *cmlc2*:EGFP embryos required approximately 50 strokes at a rate of 60 bpm. Recipient hearts from 60 hpf embryos injected with *sih* MO or *tbx5* MO were considerably more vulnerable to over-shearing that can destroy the tissue, and as such required between 40 to 50 strokes at 40 bpm for extraction.

Once all donor (*tcf21*:DsRed2) and recipient (control, *sih*, or *tbx5* MO *cmlc2*:EGFP) hearts were collected, 5 µL of fresh culture media was added to each well of the prepared culture dish. One donor heart and one recipient heart were added to each well with a minimal carry over of extra medium using a micropipettor. Sterilized forceps were used to gently arrange the hearts so that they lay side-by-side, with the ventricles in contact. This work was done under a dissecting microscope. After placement of hearts into culture was completed the culture dish was gently returned to the incubator, avoiding disturbances that might separate donors from recipients.

Culture conditions

Culture medium was refreshed on a daily basis by removing up to 5 µL of old medium and adding 5 to 8 µL of fresh culture medium (Fig. 1C). The culture dish was carefully monitored for signs of contamination and any questionable samples were removed and not used for analysis. As previously mentioned, the cell culture incubator was maintained at 28 ^{o}C with 5% CO_2.

Assay imaging and scoring

Beginning on the day after hearts were placed in culture, images of each well were obtained daily (Day 1 through Day 7 in culture) using an Olympus DP72 camera mounted on an Olympus SZX16 epifluorescence stereo microscope with cellSens software (Fig. 1C). Images were processed using Adobe Photoshop (Adobe). The migration of epicardial cells (red) from the donor heart onto the myocardium of

a recipient heart (green) was scored by an experimenter blinded to sample identity (Fig. 1D). Scoring was based on a scale from 0 to 7: 0 = no migration of epicardial cells was observed during the duration of culture; 1 = epicardial cells were only observed on the recipient myocardium on Day 7; 2 = migration of epicardial cells began on Day 6 and continued to expand coverage of the recipient myocardium through Day 7; 3 = migration began on Day 5, etc.; 4 = migration began on Day 4, etc.; 5 = migration began on Day 3, etc.; 6 = migration began on Day 2, etc.; 7 = migration began on Day 1, etc.

Assay analysis

Each culture dish well containing one donor and one recipient heart that remained in contact throughout the seven days in culture was considered n = 1 for statistics. In order to assess whether data for each treatment group could be pooled from two experimental replicates, two-way analysis of variance was conducted to confirm that variation from different experimental days did not have an effect. Since both the experimental day and interaction variables were not significant ($p \leq 0.05$) for both *sih* MO and *tbx5* MO groups and their respective controls, replicate data sets were pooled. The pooled sample size for the control vs. *sih* MO group was n = 13 to 14, and the pooled sample size for control vs. *tbx5* MO group was n = 14 to 19. Student's *t*-test was used to compare the pooled migration scores of control MO recipient hearts with respective *sih* MO or *tbx5* MO recipient hearts. *F*-test was used to check homoscedasticity of data and significance was set at $p \leq 0.05$. All statistical analysis was conducted with GraphPad Prism statistics software (GraphPad Software).

Immunohistochemistry

On Day 7, the donor/recipient hearts from each well were collected from the culture dish and processed for confocal imaging using a method from Plavicki *et al*. [6] (Fig. 1E). Primary antibody rabbit anti-DsRed2 (AnaSpec) was used in a 1:200 dilution in PBT (0.3 % Triton X-100 in phosphate buffered saline) buffer. Secondary antibody, anti-rabbit Alexa 568 antibody (Invitrogen), was used in a 1:100

dilution in PBT buffer. Confocal images were collected with an Olympus Fluoview FV1000 microscope. Brightest point projections were made using Olympus Fluoview software (Olympus) and images were processed in Adobe Photoshop (Adobe).

RESULTS

To verify that migration from a donor heart to a recipient heart can be assessed *in vitro*, we collected normal donor hearts from *tcf21*:DsRed2 embryos and placed them in culture with control MO recipient hearts from *cmlc2*:EGFP embryos. In zebrafish, EPCs begin migrating to the ventricle between 60-72 hpf. By 96 hpf, epicardial cells cover most of the ventricle, and, by 120 hpf, also cover most of the atrium. Hence, donor hearts were collected at 84 hpf, a time point at which epicardial cells were present and actively spreading on the ventricle. In contrast, recipient hearts were collected at 60 hpf before EPCs began migrating to the ventricle in order to prevent recipient-epicardial cells from confounding our results. To confirm that recipient hearts extracted at 60 hpf lacked epicardial cells, we examined hearts from embryos with both a red epicardial marker, *tcf21*:DsRed2, and green myocardial marker, *cmlc2*:EGFP. Hearts extracted from *cmlc2*:EGFP; *tcf21*:DsRed2 embryos at 60 hpf lacked epicardial cells on the ventricle and atrium (n = 10). Neither *tcf21*+ cells nor DAPI-stained cells with the flattened epicardial cell phenotype were observed on the myocardia of these hearts (Additional File 1: Figure S1 A). In addition, we confirmed that recipient hearts did not contain cells that were capable of independently differentiating into epicardial cells after 7 days in the presented culture conditions. Hearts from 60 hpf *cmlc2*:EGFP; *tcf21*:DsRed2 embryos that were individually maintained in culture for 7 days did not have any *tcf21*+ cells or DAPI-stained cells with the epicardial phenotype present on their myocardia (n = 8, Additional File 1: Figure S1 B).

Scoring for epicardial cell migration was assessed by the increasing overlap between red epicardial signal (*tcf21*+) and green myocardial signal (*cmlc2*+) over time (Fig. 2A-C). In control experiments, epicardial cell migration was observed in 12 of 13 samples (controls for *sih* MO cohort) and 17 of 19 samples (controls for *tbx5* MO cohort). In general, epicardial cells from control samples showed clear signs of migration onto recipient myocardia between Day 4 and 5 (Figs. 2A, and 3). This was reflected in the scoring: average migration scores for control samples were 3.615 (SEM ±0.385) for the *sih* MO cohort, and 3.737 (SEM ±0.445) for the *tbx5* MO cohort (Fig. 3). In contrast, no migration was observed at all in 5 of 14 samples in the *sih* MO group. If migration occurred it was minimal and significantly delayed, beginning in most cases between Day 6 and 7 (Fig. 2B). This was reflected in a significantly lower average migration score of 1.786 (SEM ±0.435) (Fig. 3). Similarly, there was no migration in 6 of 14 samples in the *tbx5* MO group. Again, in those cases in which migration occurred the area of overlap was small and migration was significantly delayed, beginning in most cases on Day 6, with an average migration score of 2.000 (SEM ±0.584) (Fig. 3).

While migration can be readily observed with normal fluorescence microscopy, it can be difficult to determine whether the merged signal is due to true overlap of spreading epicardial cells in contact with the underlying myocardia; a merged signal can also result when the two tissues are simply positioned above and below each other but not in actual contact. Thus, migration was confirmed using confocal microscopy to examine samples on Day 7 for the presence of *tcf21*+ epicardial cells on top of, and associated closely with, the myocardial cells of recipient hearts (Fig. 2D-F). Donor epicardial cells (red) were observed covering recipient myocardial cells (green) in control samples (yellow arrows, Fig. 2D). In contrast, many recipient hearts from the *sih* MO and *tbx5* MO groups did not have any observable donor epicardial cells covering the labeled myocardial cells (Fig. 2E-F).

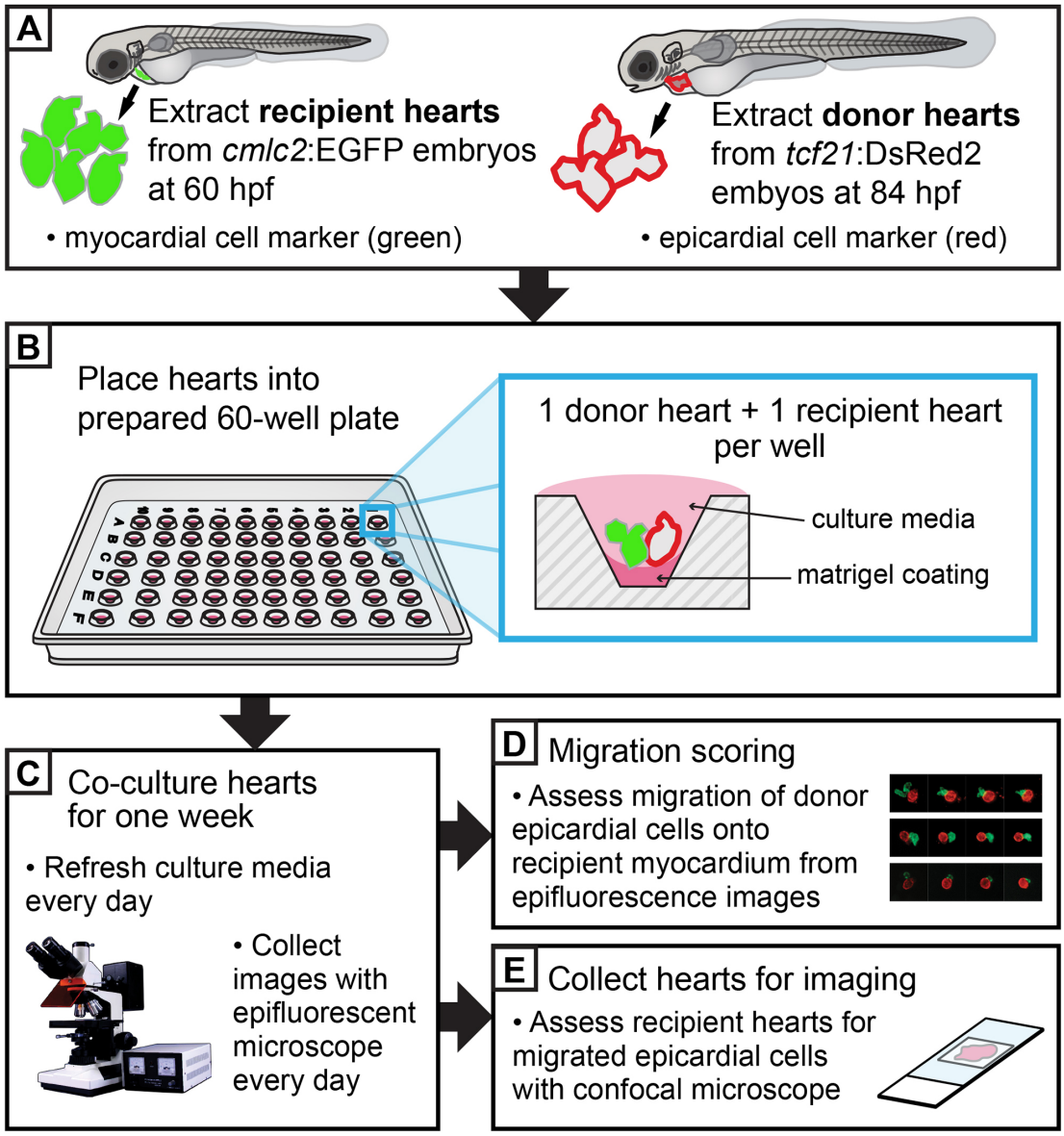

Figure 1. Overview schematic of the *in vitro* co-culture assay for assessing migration of epicardial cells.

(A) Hearts are extracted from embryonic zebrafish. Recipient hearts are collected from *cmlc2*:EGFP embryos, which have a green myocardial cell marker. These hearts are extracted at 60 hpf, prior to the migration of epicardial progenitor cells (EPCs), such that extracted hearts have bare myocardia. Donor

hearts are collected from *tcf21*:DsRed2 embryos, which have a red epicardial cell marker. These hearts are extracted at 84 hpf, after migration of EPCs has begun, such that extracted hearts carry some epicardial cells that are actively spreading. Recipient and/or donor embryos may be pre-treated before isolation of hearts according to experimental design. For example, in this report the recipient hearts came from embryos that were injected with MOs affecting expression of specific genes. (B) Collected hearts are placed in a prepared 60-well cell culture dish. Each well has been pre-coated with a thin layer of matrigel basement membrane mix, and contains one donor and one recipient heart, submerged in culture medium. The donor and recipient hearts are arranged such that the ventricles are in contact. (C) Donor and recipient hearts are co-cultured for one week. Each day the culture media is refreshed and images of each culture well are imaged with an epifluorescence microscope. (D) Epifluorescence images are scored in a blinded fashion for the migration of donor epicardial cells onto recipient myocardial cells. (E) After 7 days in culture, heart samples are fixed and stained for immunohistochemistry. Each sample is analyzed with confocal microscopy for presence of donor epicardial cells that have migrated onto recipient myocardia to verify positive migration.

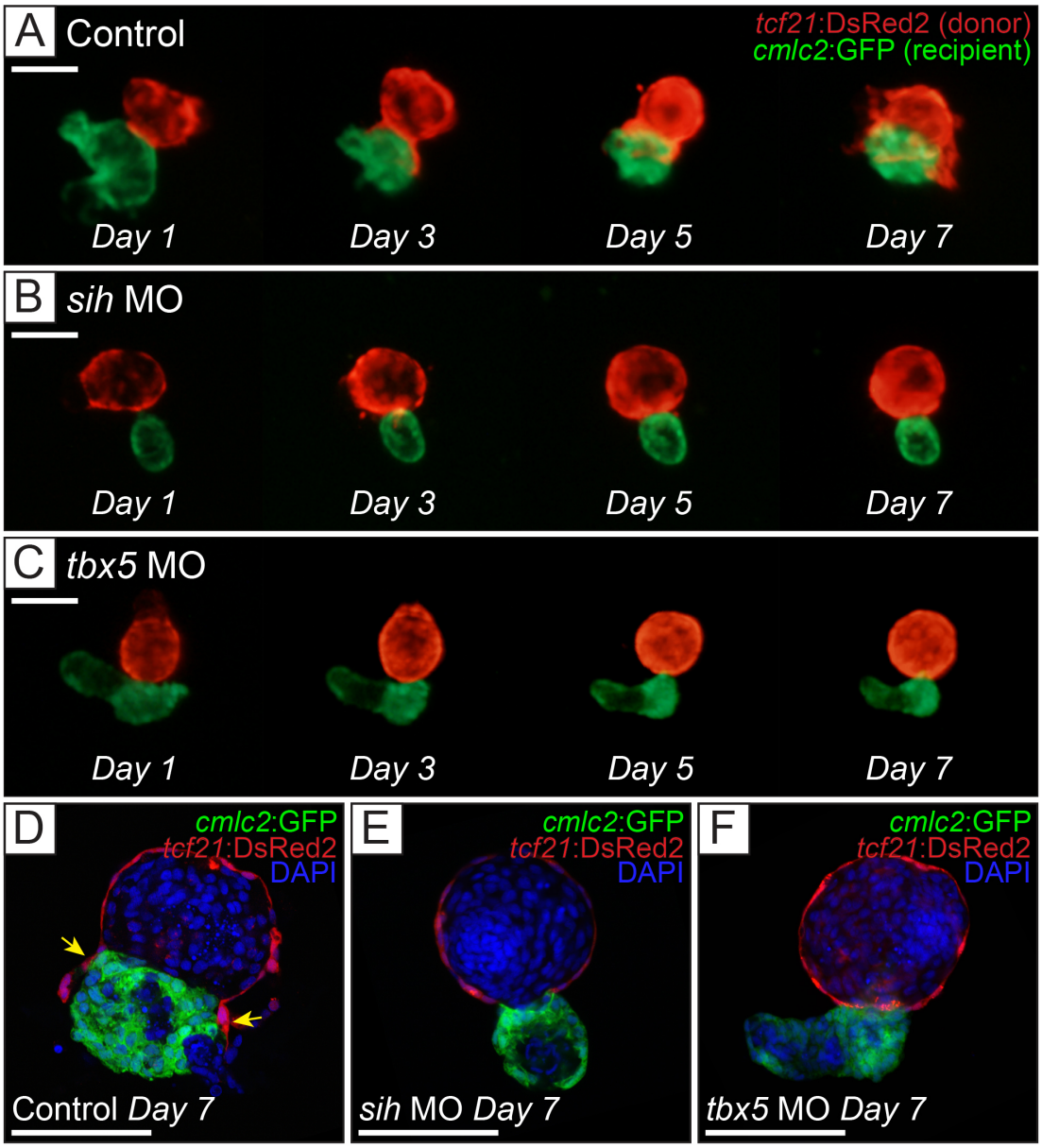

Figure 2. Migration of epicardial cells from donor hearts onto control, *sih*, or *tbx5* MO recipient hearts.

(A-C) Fluorescence images taken on Days 1, 3, 5, and 7 in culture show progression of epicardial cell migration. Red (*tcf21*:DsRed2) shows epicardial cells from the donor, green (*cmlc2*:EGFP) shows

recipient myocardial cells. (A) Migration of donor epicardial cells onto a control MO recipient heart is apparent by Day 5 in culture. The merged red-on-green signal, appearing yellow, is significantly noticeable by Day 7. There does not appear to be any significant migration of donor epicardial cells onto either the *sih* MO recipient heart (B) or the *tbx5* MO heart (C) throughout the 7 days in culture. (D-F) Confocal microscopy images of donor/recipient heart samples after 7 days in culture. Red indicates *tcf21*:DsRed2 donor epicardial cells, green indicates *cmlc2*:EGFP recipient myocardial cells, blue indicates DNA (DAPI stain). (D) Confocal microscopy verifies the presence of donor epicardial cells that have migrated onto the control MO recipient myocardium (yellow arrows). In contrast, there does not seem to be any donor epicardial cells on the *sih* MO recipient heart (E) or the *tbx5* MO recipient heart (F), which is consistent with the epifluorescence images. In this figure, single hearts were followed throughout the 7-day time course in panels A-C, and were then collected to produce the confocal images shown in panels D-F. Scale bars in all images represent 100 μm.

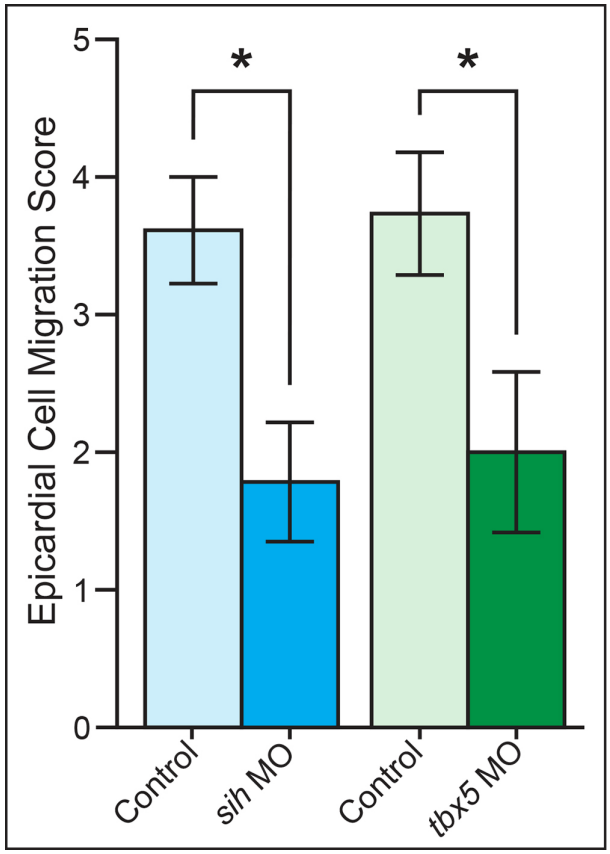

Figure 3. Migration scores for *sih* and *tbx5* MO recipient hearts are significantly lower than respective controls.

Each sample was scored for migration of epicardial cells as described in the Methods. Bar graphs show average migration score for each group, error bars represent standard error of the mean (SEM), asterisk indicates that the treatment group is significantly different from its respective control (Student's *t*-test, $p \leq 0.05$).

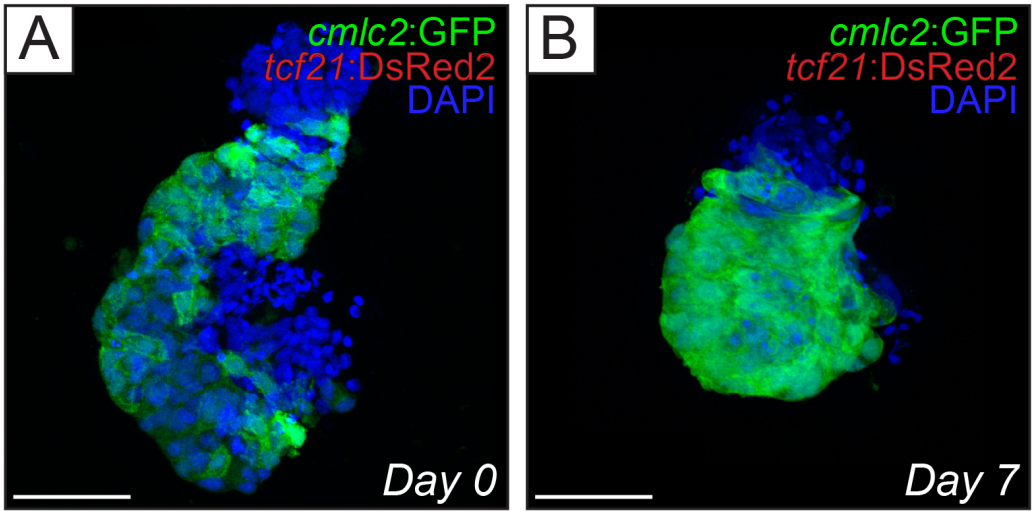

Additional File: Figure S1. Hearts extracted at 60 hpf lack epicardial cells.

(A and B) Confocal micrographs of *cmlc2*:EGFP; *tcf21*:DsRed2 hearts extracted at 60 hpf . Images show brightest point projections from confocal z-series. (A) *cmlc2*:EGFP; *tcf21*:DsRed2 hearts before being placed into culture (Day 0). (B), *cmlc2*:EGFP; *tcf21*:DsRed2 hearts after 7 days in culture (Day 7). There were no epicardial cells (red) observed on the heart myocardia (green) at Day 0 or Day 7. In addition, there were no observed *tcf21*- cells with the stereotypical flattened phenotype of epicardial cells present on top of the myocardium (blue, DAPI nuclear staining). Scale bars in all images represent 50 μm.

DISCUSSION

The heartbeat is halted in *sih* morphants [16]. Our results show that epicardial cell migration is significantly delayed or inhibited when the myocardial cells do not contract. This supports our previous results, which showed that pharmacological inhibition of heartbeat inhibited migration of PE cells and spreading of epicardial cells over the myocardium, both *in vitro* and *in vivo* [6]. A similar co-culture assay comparing migration of epicardial cells onto normal and *sih* MO recipient hearts was also presented in those experiments [6]. We have developed the assay further to increase precision: instead of mixing a large number of donor and recipient hearts in a 24-well culture dish, we have refined the method into using only one donor and one recipient heart per well in a culture dish. This reduces the number of hearts needed per experiment, and reduces the risk of widespread contamination across many hearts. This also addresses potential concerns that neighboring hearts could influence migration, for example, by locally increasing the concentration of a secreted paracrine factor.

Although *tbx5* is expressed in several cardiac tissues, many studies have focused on investigating the role of *tbx5* expression in the PE [12]. In zebrafish, *tbx5a* is required for PE specification, a process that also involves BMP (bone morphogenetic protein) signals [21]. In the chick, *tbx5* expression is regulated in concert with initiation and cessation of cell migration. Either reducing or increasing *tbx5* expression in PE explants could inhibit EPC migration, *in vivo* and *in vitro* [12]. The investigators assessed *in vitro* migration as the ability of an epicardial monolayer of cells to spread out (migrate) in a cell culture dish. However, this approach does not provide for the crosstalk that may occur with myocardial cells, which also express *tbx5* [12]. Here, we show that inhibiting expression of *tbx5* in the myocardium alone is sufficient to substantially affect epicardial cell migration. Our results add to our overall understanding of *tbx5* in epicardium development.

It is important to recognize that in the presented assay the age of the recipient myocardial cells is different than that of the migrating donor epicardial cells, an interaction that does not happen in natural circumstances. It was necessary to use younger recipient myocardial cells in this assay so that recipient hearts lacked epicardial cells, which could influence the migration of donor epicardial cells and confound the interpretation of results. In chick models, it is possible to remove the source of epicardial cells by blocking or ablating the PE using microsurgery techniques [8, 10]. However this is difficult to replicate in zebrafish larvae. The size of the zebrafish PE is considerably smaller, making physical manipulations logistically challenging. Furthermore, multiple PEs form over multiple days of development and contribute to the zebrafish epicardium [6]. Therefore, a single ablation event cannot remove the PE.

Another possible approach is to genetically ablate epicardial cells from the recipient heart *in vivo* before extraction and placement into culture with a same-age donor heart. For example, bacterial nitroreductase can be expressed in epicardial tissues using the *tcf21* promoter to convert nontoxic metronidazole into a cytotoxin in *tcf21*+ cells [22]. However, complete ablation of epicardial cells is difficult, especially given the regenerative capacity of the zebrafish heart, as surviving epicardial cells are capable of repopulating the epicardium [22,23]. Given these challenges, we felt that using the 60 hpf recipient heart was appropriate for the intended scope of this assay.

It is desirable to use genetic tools and techniques to study developmental processes such as epicardium formation *in vivo,* however, these genetic approaches rely on the availability of a cell-specific marker to drive expression of a recombinase, transcriptional factor, or other activating enzyme in a discrete expression pattern [24,25]. While there are well-documented examples of myocardial-specific markers (e.g., *cmlc2*), there are no known PE- or EPC-specific markers that are not expressed in other tissues during development. Most common markers of the epicardial lineage, *Wt1*, *Tbx18*, *Tcf21*, are

expressed in other tissues, including the liver, kidney, pectoral fin mesenchyme, developing palate, and pharyngeal arches [26-29]. Furthermore, the PE and epicardium are composed of heterogeneous populations of cells [30], for example, there are both *tcf21*+ and *tcf21*- cells in the zebrafish epicardium [6]. Therefore, a truly precise genetic approach would require targeted modifications using intersectional epicardial markers (e.g., use a dual recombinase approach to target gene expression in cells that are both *tcf21*+ and *tbx18*+). Designing and establishing such highly specific transgenic lines would take considerable time and effort. Hence, *in vitro* approaches, such as the one presented here, are desirable as comparatively faster and less logistically complex alternatives. The presented assay can aide in identifying candidate genes involved in EPC migration and provide insight into the tissue-specific role of these genes, while using readily available genetic tools.

CONCLUSIONS

In conclusion, we have developed an assay that can assess epicardial cell migration *in vitro* by co-culture of a donor and recipient heart. Our assay uses whole hearts in culture, allowing for important cell-to-cell interactions between the epicardial and myocardial cells. Given that donor and recipient hearts come from different individuals, these cells can be uniquely manipulated in order to determine how effects in each cell type can influence EPC/epicardial cell migration. In addition to genetic manipulation, signaling factors, blocking antibodies, or pharmacologic agents can be readily added to the hearts before or after placement in culture media. Using our assay, we demonstrated that epicardial cell migration was inhibited when myocardial cells lacked contractility (*sih* MO). In addition, we demonstrated that lack of *tbx5* expression in myocardial cells alone was sufficient to inhibit epicardial cell migration.

AUTHOR CONTRIBUTIONS

M.S.Y., J.P., and X.L. were responsible for the planning and execution of laboratory work, collection and processing of data, and preparation of the manuscript. W.H. and R.E.P. directed research, provided supervision, intellectual input and funding. All authors participated in the interpretation of results and approve of the submitted manuscript.

ACKNOWLEDGEMENTS

This research was funded by the National Institute for Environmental Health Sciences grants (T32 ES007015) and (R01 ES012716) to W.H. and R.E.P. The authors wish to thank Dr. K. Lanham, Dr. T. Baker, Dr. F. Burns, J. Gawdzik, and J. Gilbertson for advice and general support in conducting this research.

COMPETING INTERESTS

The authors declare no competing interests.

REFERENCES

1. Bakkers J: Zebrafish as a model to study cardiac development and human cardiac disease. *Cardiovasc Res* 2011, **91**:279-288.

2. Stainier DY: Zebrafish genetics and vertebrate heart formation. *Nat Rev Genet* 2001, **2**:39-48.

3. Brade T, Pane LS, Moretti A, Chien KR, Laugwitz KL: Embryonic heart progenitors and cardiogenesis. *Cold Spring Harbor Perspect Med* 2013, **3**:a013847.

4. Carmona R, Guadix JA, Cano E, Ruiz-Villalba A, Portillo-Sánchez V, Pérez-Pomares JM, *et al*. The embryonic epicardium: an essential element of cardiac development. *J Cell Mol Med* 2010, **14**:2066-2072.

5. Nahirney PC, Mikawa T, Fischman DA: Evidence for an extracellular matrix bridge guiding proepicardial cell migration to the myocardium of chick embryos. *Dev Dyn* 2003, **227**:511-523.

6. Plavicki JS, Hofsteen P, Yue MS, Lanham KA, Peterson RE, Heideman W: Multiple modes of proepicardial cell migration require heartbeat. *BMC Dev Biol* 2014, **14**:18.

7. Gittenberger-de Groot AC, Winter EM, Bartelings MM, Goumans MJ, DeRuiter MC, Poelmann RE: The arterial and cardiac epicardium in development, disease and repair. *Differentiation* 2012, **84**:41-53.

8. Takahashi M, Yamagishi T, Narematsu M, Kamimura T, Kai M, Nakajima Y: Epicardium is required for sarcomeric maturation and cardiomyocyte growth in the ventricular compact layer mediated by transforming growth factor β and fibroblast growth factor before the onset of coronary circulation. *Congenital anomalies* 2014, **54**:162-171.

9. Ishii Y, Garriock RJ, Navetta AM, Coughlin LE, Mikawa T: BMP signals promote proepicardial protrusion necessary for recruitment of coronary vessel and epicardial progenitors to the heart. *Dev Cell* 2010, **19**:307-316.

10. Männer J, Schlueter J, Brand T. Experimental analyses of the function of the proepicardium using a new microsurgical procedure to induce loss-of-proepicardial-function in chick embryos: *Dev Dyn* 2005, **233**:1454-1463.

11. van Wijk B, van den Hoff M: Epicardium and myocardium originate from a common cardiogenic precursor pool. *Trends Cardiovasc Med* 2010, **20**:1-7.

12. Hatcher CJ, Diman NY, Kim M-S, Pennisi D, Song Y, Goldstein MM, *et al*. A role for Tbx5 in proepicardial cell migration during cardiogenesis. *Physiol Genomics* 2004, **18**:129-140.

13. Pae SH, Dokic D, Dettman RW: Communication between integrin receptors facilitates epicardial cell adhesion and matrix organization. *Dev Dyn* 2008, **237**:962-978.

14. Weeke-Klimp A, Bax NAM, Bellu AR, Winter EM, Vrolijk J, Plantinga J, *et al*. Epicardium-derived cells enhance proliferation, cellular maturation and alignment of cardiomyocytes. *J Mol Cell Cardiol* 2010, **49**:606-616.

15. Eid H, Larson DM, Springhorn JP, Attawia MA, Nayak RC, Smith TW, *et al*. Role of epicardial mesothelial cells in the modification of phenotype and function of adult rat ventricular myocytes in primary coculture. *Circ Res* 1992, **71**:40-50.

16. Sehnert AJ, Huq A, Weinstein BM, Walker C, Fishman M, Stainier DYR: Cardiac troponin T is essential in sarcomere assembly and cardiac contractility. *Nat Genet* 2002, **31**:106-110.

17. Westerfield M. The zebrafish book: a guide for the laboratory use of zebrafish (*Danio rerio*). 4th ed. Eugene: University of Oregon Press; 2000.

18. Garrity DM, Childs S, Fishman MC: The heartstrings mutation in zebrafish causes heart/fin Tbx5 deficiency syndrome. *Development* 2002, **129**:4635-4645.

19. Carney SA, Peterson RE, Heideman W: 2,3,7,8-Tetrachlorodibenzo-*p*-dioxin activation of the aryl hydrocarbon receptor/aryl hydrocarbon receptor nuclear translocator pathway causes developmental toxicity through a CYP1A-independent mechanism in zebrafish. *Mol Pharmacol* 2004, **66**:512-521.

20. Burns CG, MacRae CA: Purification of hearts from zebrafish embryos. *BioTechniques* 2006, **40**:274.

21. Liu J, Stainier DYR: Tbx5 and Bmp signaling are essential for proepicardium specification in zebrafish. *Circ Res* 2010, **106**:1818-1828.

22. Wang J, Cao J, Dickson AL, Poss KD: Epicardial regeneration is guided by cardiac outflow tract and Hedgehog signalling. *Nature* 2015, **522**:226-330.

23. Lepilina A, Coon AN, Kikuchi K, Holdway JE, Roberts RW, Burns CG, *et al*. A dynamic epicardial injury response supports progenitor cell activity during zebrafish heart regeneration. *Cell* 2006, **127**:607-619.

24. Gerety SS, Breau MA, Sasai N, Xu Q, Briscoe J, Wilkinson DG: An inducible transgene expression system for zebrafish and chick. *Development* 2013, **140**:2235-2243.

25. Rocha A, Ruiz S, Estepa A, Coll JM: Application of inducible and targeted gene strategies to produce transgenic fish: a review. *Mar Biotechnol* 2004, **6**:118-127.

26. Drummond IA, Majumdar A, Hentschel H, Elger M, Solnica-Krezel L, Schier AF, *et al*. Early development of the zebrafish pronephros and analysis of mutations affecting pronephric function. *Development* 1998, **125**:4655-4667.

27. Serluca FC, Fishman MC: Pre-pattern in the pronephric kidney field of zebrafish. *Development* 2001, **128**:2233-2241.

28. Begemann G, Gibert Y, Meyer M, Ingham PW: Cloning of zebrafish T-box genes tbx15 and tbx18 and their expression during embryonic development. *Mech Dev* 2002, **114**:137-141.

29. Lee G-H, Chang M-Y, Hsu C-H, Chen Y-H: Essential roles of basic helix-loop-helix transcription factors, Capsulin and Musculin, during craniofacial myogenesis of zebrafish. *Cell Mol Life Sci* 2011, **68**:4065-4078.

30. Katz TC, Singh MK, Degenhardt K, Rivera-Feliciano J, Johnson RL, Epstein JA, *et al*. Distinct compartments of the proepicardial organ give rise to coronary vascular endothelial cells. *Dev Cell* 2012, **22**:639-650.

CHAPTER V:

TCDD EXPOSURE ALTERS THE GROWTH AND MORPHOLOGY OF DEVELOPING OCULAR AND SUBINTESTINAL VASCULATURE IN THE ZEBRAFISH EMBRYO

Monica S. Yue, Richard E. Peterson, Jessica S. Plavicki

ABSTRACT

Aryl hydrocarbon receptor (AHR) signaling is necessary for proper development of the hepatic, retinal, and renal vasculature. Exposure to 2,3,7,8-tetrachlorodibenzo-*p*-dioxin (TCDD), the prototypic agonist of AHR, causes vascular malformations in the head and heart. Here we investigated effects of TCDD exposure on the developing vasculature in the superficial system of the eye and the subintestinal venous plexus (SIVP) of the gut in zebrafish embryos. At 72 hours post fertilization (hpf), TCDD exposure inhibited closure of the superficial annular vessel (SAV) in the eye. In addition, TCDD caused alterations in SAV morphology, including changes in shape, texture, and increased variation in vessel thickness at 60 and 72 hpf. In the gut, TCDD exposure led to excessive growth and incorrect patterning of the SIVP. At 48-72 hpf, SIVP area and number of compartments was significantly higher in TCDD-treated embryos compared to controls. At 54-72 hpf, SIVP length was also significantly higher in TCDD-treated embryos compared to controls. Since blood flow affects vascular development and TCDD exposure impairs circulation, we investigated whether the observed TCDD-induced eye and SIVP phenotypes were recapitulated in embryos with inhibited circulation. Loss of circulation resulted in failure of the SAV to close. However, vessel morphology in the SAV was distinctly different from both control and TCDD-treated embryos. In particular, vessel lumens were absent in embryos where circulation was inhibited, however vessel lumens were observed in TCDD-treated embryos. The SIVP in embryos with inhibited circulation was either smaller or not significantly different than respective controls, which is contradictory to the effects observed in the SIVP of TCDD-treated embryos. Overall, these findings indicate that TCDD-induced SAV and SIVP phenotypes are not secondary to circulatory impairment and support alternative mechanisms of toxicity whereby TCDD exposure and AHR activation interact with key signaling pathways involved in vascular development.

INTRODUCTION

2,3,7,8-Tetrachlorodibenzo-*p*-dioxin (TCDD) is a persistent, bioaccumulative halogenated aromatic hydrocarbon that is found ubiquitously in the environment. TCDD is the prototypic agonist of the aryl hydrocarbon receptor (AHR), thus TCDD toxicity is mediated via activation of AHR signaling (Hankinson, 1995; Schmidt and Bradfield, 1996; Prasch *et al.*, 2003, 2006). Fish are particularly sensitive to TCDD toxicity during early life stages. Fish embryos exposed to TCDD develop a condition called blue sac disease, which is characterized by edema, hemorrhaging, craniofacial malformations, and mortality (Elonen *et al.*, 1998; Walker and Peterson, 1994).

Proper vascular development is crucial for survival as it is required to transport oxygen, nutrients, hormones, metabolic products, and immune cells to various organ systems throughout the body. Abnormal development of vasculature is often associated with disease, highlighting the importance of understanding the mechanisms influencing its development (Wilkinson and van Eeden, 2014). AHR null mice have vascular anomalies in the eye, liver, and kidney, indicating that AHR signaling is necessary for the normal development of vascular systems during organogenesis (Lahvis *et al.*, 2000; Choudhary *et al.*, 2015).

Given the role of AHR in vascular development, it has long been proposed that the developing vasculature is a primary target for TCDD toxicity. CYP1A, a widely accepted marker of AHR activation, is strongly induced in the vasculature following TCDD exposure in medaka (Cantrell *et al.*, 1996), lake trout (Guiney *et al.*, 1997), killifish (Toomey *et al.*, 2001), and zebrafish embryos (Andreasen *et al.*, 2002). In zebrafish, TCDD exposure induced CYP1A mRNA in the endothelium as early as 24 hours post fertilization (hpf), preceding any signs of toxicity, and co-localized with AHR2 expression (Andreasen *et al.*, 2002). In addition, various studies have demonstrated that TCDD exposure can affect the development of specific vascular structures, including regression of the yolk vasculature (Cantrell *et al.*,

1996), retrobulbar capillary hemorrhaging (Guiney *et al.*, 2000), decreased blood perfusion in the dorsal midbrain (Dong *et al.*, 2002), inhibited growth and remodeling of the common cardinal vein (Bello *et al.*, 2004), and malformation of the prosencephalic artery (Teraoka *et al.*, 2010). Here we investigate the effects of TCDD exposure on the vasculature of the developing eye and intestine in zebrafish embryos, which have heretofore never been characterized in detail.

As mentioned above, studies in AHR null mice have highlighted the developing ocular and hepatic vasculature as particularly sensitive to perturbations in AHR signaling. More specifically, AHR null mice have inappropriate neovascularization of the choroidal network in the eye (Choudhary *et al.*, 2015), and also have a patent ductus venosus in the liver, which is a fetal vascular structure that is normally resolved shortly after birth (Lahvis *et al.*, 2000). In zebrafish, the embryonic eye consists of the hyaloid and superficial vascular systems. The hyaloid system eventually gives rise to the retinal vasculature, while the superficial system is remodeled into the choroidal vessel network (Isogai *et al.*, 2001; Kitambi *et al.*, 2009). In the gut, zebrafish develop a subintestinal venous plexus (SIVP), which is structurally similar to the vitelline veins in mouse (Goi and Childs, 2016; Crawford *et al.*, 2010). The SIVP in zebrafish is a bilateral vascular structure that supports transfer of nutrients from the yolk sac during early development. Later on, the SIVP is remodeled to provide blood flow to the digestive tract and also contributes to the development of hepatic sinusoids and the portal veins (Isogai *et al.*, 2001).

Here we show that TCDD exposure affects development of ocular and intestinal vasculature. In the eye, TCDD inhibits closure of the superficial annular vessel (SAV), the central structure of the superficial vascular system, and alters vessel morphology of the SAV. In the gut, TCDD causes excessive growth and incorrect patterning of the SIVP. Effects of TCDD on the closure of the SAV may be secondary to TCDD-induced reductions in circulation. However, other effects in the SAV and SIVP may

have a different mechanism of toxicity, as inhibition of blood flow was insufficient to recapitulate these TCDD-induced phenotypes.

MATERIALS AND METHODS

Zebrafish and TCDD exposure

Embryos were obtained from adult zebrafish (*Danio rerio*) housed and maintained according to methods described by Westerfield (2000). The following transgenic lines were used: *kdrl*:DsRed2 [*Tg(flk1:DsRed2)*^{pd27}] (Kikuchi *et al.*, 2011), and *fli1a*:EGFP [*Tg(fli1a:EGFP)*^{y1}] (Lawson and Weinstein, 2002) crossed with *gata1a*:DsRed [*Tg(gata1a:DsRed)*^{sd2}] (Traver *et al.*, 2003). Eggs were collected within 1 hour (h) of spawning and fertilized eggs were placed into a petri dish with egg water (0.03% Instant Ocean Sea Salts).

At 4 hpf, zebrafish embryos were statically exposed in water to either TCDD (1 ng/ml) or vehicle (0.1% dimethyl sulfoxide, DMSO) for 1 h in 4 ml glass scintillation vials while gently rocking. Ten embryos were present per ml of dosing solution with a total of 40 embryos in each vial. After 1 h exposure to TCDD or vehicle, embryos were rinsed three times with TCDD-free egg water and placed into petri dishes. Embryos were raised in egg water with 0.003% 1-phenyl-2-thiourea (PTU, Sigma) to inhibit formation of pigment. Water changes were made daily.

All procedures involving zebrafish were approved by the Animal Care and Use Committee of the University of Wisconsin-Madison and adhered to the National Institute of Health's "Guide for the Care and Use of Laboratory Animals."

Morpholinos and 2,3-butanedione 2-monoxime (BDM) treatment

Silent heart (*sih*; cardiac troponin T2, *tnnt2*) morpholino (MO) was obtained from Gene Tools (Philomath, OR). Embryos were microinjected with prepared MO solutions (4 ng/embryo) at the 1-2 cell stage, as previously described (Sehnert *et al.*, 2002; Plavicki *et al.*, 2014; Yue *et al.*, 2015). The Gene tools standard control morpholino (MO) was used as a control. The MO sequences were: *sih*/*tnnt2*, 5' CATGTTTGCTCTGATCTGACACGA 3' (Sehnert *et al.*, 2002); control MO, 5' CCTCTTACCTCAGTTACAATTTATA 3'. Embryos were screened for MO incorporation at 48 hpf.

For experiments involving 2,3-butanedione 2-monoxime (BDM, Sigma), a 15 mM BDM solution was prepared with egg water and 0.003% PTU. At 60 hpf, embryos were placed into new petri dishes, with 10 embryos per dish, and maintained in either regular PTU egg water or in the 15 mM BDM solution until assessment at 72 hpf.

Live confocal imaging

To visualize development of vascular structures, embryos were anesthetized in 0.02% tricaine (MS-222, Sigma) and mounted in glass bottom petri dishes using 1.2% low melting point agarose (Sigma). Confocal imaging was performed on an inverted Nikon A1R scanning laser confocal microscope and analyzed using NIS-Elements AR4.30 software. To assess developing ocular vasculature, embryos were mounted in lateral orientation and z-stacks were acquired at 54, 60, and 72 hpf. Z-stacks spanned 77-134 μm with z-sections collected at 2.85 μm. To assess the developing SIVP, embryos were mounted in dorsal-lateral orientation on the left and right sides, and z-stacks were acquired at 48, 54, 60, and 72 hpf. Z-stacks spanned 68-128 μm with z-sections collected at 2.85 μm. Maximum intensity projections and volume depth color-coding were done using NIS-Elements AR4.30 software and images were processed in Adobe Photoshop.

Analysis of the superficial annular vessel (SAV)

The SAV was assessed using z-stacks collected from live confocal imaging of *kdrl*:DsRed2 embryos. A researcher blinded to the age and treatment of samples scored for the incidence of complete SAV closure. To assess morphology of the SAV, the diameter of the SAV vessel was measured at multiple points between the dorsal radial vessel (DRV), nasal radial vessel (NRV), and ventral radial vessel (VRV). Since the posterior side of the SAV (i.e., VRV-DRV) does not form in all of the samples, only the vessel diameters on the anterior side of the SAV (i.e., DRV-NRV and NRV-VRV) were measured. To control for variability stemming from different developmental stages and/or treatments, we took advantage of the ring-like structure of the SAV to select comparable points for consistently measuring vessel diameter. The length of SAV between the DRV and VRV was arbitrarily divided into 20 sectors by 21 lines that radiated from a "center". The "center" point was defined as the base of the hyaloid vascular system, where the various branching vessels coalesce into the singular hyaloid artery. NIS-Elements software 3D volume rendering allowed for sample z-stacks to be digitally oriented such that the "center" consistently aligned with the center of the presumptive SAV ring. The point where each of the 21 radiating lines intersected with the SAV was where vessel diameter was measured. From these measurements the average vessel diameter and variation in vessel diameters (indicated by coefficient of variation) were calculated for each sample and grouped by treatment. Schematic examples are shown in Figure 3A'-B'.

Analysis of the subintestinal venous plexus (SIVP)

The developing SIVP was assessed using z-stacks collected from live confocal imaging of *fli1a*:EGFP; *gata1a*:DsRed embryos. Quantification of area, length and number of compartments in the SIVP for the right and left sides were similar to those performed by Goi and Childs (2016). Area of the SIVP was defined as the area spanning from the posterior cardinal vein (PCV) to the ventral edges of the

SIVP, indicated by *fli1a*:EGFP expression. Length of the SIVP was defined as the perpendicular distance from the PCV to the ventral apex of the SIVP. To evaluate patterning of the SIVP, the number of compartments that formed between secondary vessels in the SIVP were counted. For consistency, area, length, and number of compartments were assessed between the same 7 somites in all samples. Schematic examples are shown in Figure 6A'-C'.

Statistics

One-way analysis of variance (ANOVA) followed by Tukey's HSD test was used to compare DMSO- and TCDD-treated embryos for incidence of SAV closure, average SAV vessel diameter, variation in SAV vessel diameter, area of SIVP, length of SIVP, and number of SIVP compartments at ages ranging from 48-72 hpf. Significance was set at $p \leq 0.05$. Student's t-test was used to compare SIVP area, length, and number of compartments in embryos exposed to BDM and *sih* morphants, with their respective controls, at age 72 hpf. Significance was set at $p \leq 0.05$. For assessments of ocular vasculature: n = 15 for DMSO- and TCDD-treated embryos; n = 6 for control and BDM-treated embryos; n = 6 for control and *sih* morphants. For assessments of SIVP on left and right sides: n = 5 to 7 for DMSO- and TCDD-treated embryos; n = 4 for control and BDM-treated embryos; n = 4 to 5 for control and *sih* morphants. All statistics analyses were done using GraphPad Prism statistics software.

RESULTS

TCDD exposure inhibits closure of the superficial annular vessel (SAV) in the eye

Early life TCDD exposure has previously been reported to disrupt the development of vascular structures during organogenesis (Cantrell *et al.*, 1996; Dong *et al.*, 2002; Bello *et al.*, 2004, Teraoka *et al.*, 2010). To investigate the effects of TCDD on developing ocular vasculature, zebrafish embryos were

exposed to either DMSO (vehicle control, 0.1%) or TCDD (1 ng/ml, waterborne) for 1 h at 4 hpf and assessed at different stages of ocular vascular development (Figure 1). Focus was placed on development of the superficial vascular system, which is stereotypically patterned and easily characterized. During normal development, the SAV develops into a ring-like structure that connects flow from three radial vessels (dorsal radial vessel, DRV; nasal radial vessel, NRV; ventral radial vessel, VRV). At 54 hpf the SAV has formed between the DRV-NRV and NRV-VRV (Figure 1A). Growing tips extend from the DRV and VRV (Figure 1A-B, blue arrowheads) and eventually coalesce to form a complete SAV structure by 72 hpf (Figure 1C, asterisk). In TCDD-treated embryos at 54 hpf the anterior side of the SAV has formed between the DRV-NRV and NRV-VRV (Figure 1D). Growing vessel tips are apparent, however unlike in DMSO-treated controls, these tips often fail to coalesce. By 72 hpf the SAV in TCDD-treated embryos is incomplete (Figure 1F). To confirm that this effect was significant, a researcher blinded to both sample age and treatment scored for closure of the SAV in DMSO- and TCDD-treated embryos at 54, 60, and 72 hpf (Figure 1H). Scoring revealed that the percent of DMSO-treated embryos with SAV closure increased over time, such that by 72 hpf there was 93±7% successful closure of the SAV. In contrast, the percent of TCDD-treated embryos with SAV closure did not significantly increase over time. By 72 hpf, the percent of TCDD-treated embryos with successful SAV closure was 47±13%, significantly lower than similarly-aged DMSO-treated controls ($p \leq 0.05$). Together these results indicate that TCDD exposure inhibits closure of the SAV in the developing superficial vascular system of the eye.

TCDD exposure alters SAV vessel morphology

To further characterize how TCDD exposure alters SAV development, we examined vessel morphology in greater detail (Figure 2). High magnification confocal micrographs revealed differences in vessel shape and texture. At 72 hpf, DMSO-treated embryos had relatively smooth SAV vessel texture with a clearly visible, continuous lumen (Figure 2A-A”’). In contrast, at 72 hpf, the SAV in TCDD-

treated embryos had a rougher texture and winding shape (Figure 2B-B"'). Filopodia appeared to extend randomly outwards (Figure 2B', B") and in some regions the lumen appeared highly constricted (Figure 2B"'). Note that the TCDD-treated sample in Figure 2 is an example of a completely formed SAV and is shown so that parallel comparisons of all SAV regions could be made between representative DMSO- vs. TCDD-treated samples. Even when the SAV closes successfully in TCDD-treated embryos, the vessel is rougher and meandering in shape, which would likely increase turbidity of blood flow and decrease circulatory efficiency.

In order to quantify the morphological changes observed in the SAV of TCDD-treated embryos, a system was devised to measure vessel thickness at comparable, regular intervals along the anterior portion of the SAV (see Materials and Methods for a detailed description). An example of measurements taken from a DMSO- and TCDD-treated embryo is shown in Figure 3A-A' and Figure 3B-B', respectively. Averaging vessel diameters in DMSO- vs. TCDD-treated samples indicated that the mean vessel diameter was not significantly different between treatments at 54-72 hpf. However, when the variation in vessel diameters in each sample was assessed a difference emerged (Figure 3C). The variation in vessel diameters for each sample was described using the coefficient of variation (calculated as the standard deviation divided by sample mean, expressed as a percentage). At 60 and 72 hpf the variation in vessel diameters was significantly higher in TCDD-treated samples than in age-matched DMSO controls. Together these findings indicate that TCDD exposure altered vessel morphology in the SAV, increasing variation in the shape and vessel diameter at 60-72 hpf.

Inhibiting circulation is insufficient to recapitulate all TCDD-induced SAV phenotypes

TCDD exposure induces severe cardiotoxicity, including reductions in cardiac output culminating in complete loss of circulation (Henry *et al.*, 1997; Antkiewicz *et al.*, 2005, 2006). Since normal blood flow is vital for vascular development, we investigated whether the effects observed in the SAV could be

recapitulated when circulation was repressed (Figure 4). Circulation was inhibited pharmacologically, via exposure to BDM (Bartman *et al.*, 2004; Plavicki *et al.*, 2014), or genetically, with injection of *sih* MO (Sehnert *et al.*, 2002). It was previously reported that TCDD exposure significantly decreases cardiac output beginning at 60 hpf (Antkiewicz *et al.*, 2006). Therefore, we simulated TCDD-induced effects on circulation by exposing embryos to 15mM BDM beginning at 60 hpf, which caused near complete loss of heart contractility (data not shown). Heartbeat and circulation are absent in *sih* morphants (Sehnert *et al.*, 2002). Respective controls for each treatment were not different from one another (DMSO, No BDM, Control MO). At 72 hpf, the SAV in control embryos closed normally and vessels appear smooth with clearly visible lumens (Figure 4A, C, E; asterisk). In contrast, at 72 hpf the SAV failed to close in TCDD-treated, BDM-treated, and *sih* MO embryos (Figure 4B, D, F). However, the vessel morphology of the SAV in TCDD-treated embryos differed from that in BDM-treated and *sih* MO embryos. As described above, the SAV in TCDD-treated embryos appeared rough, winding in shape, with a visible (albeit occasionally constricted) lumen. In contrast, the vessels in BDM-treated and *sih* MO embryos appeared smooth, dense, and lacked a defined luminal space (compare Figure 4B to D, F). In addition, the superficial radial vessels (DRV, NRV, VRV) in *sih* MO embryos were severely reduced and in some cases completely degenerated (data not shown). Furthermore, although it was not the focus of this report, the hyaloid system was drastically reduced in both BDM-treated and *sih* MO embryos. This was distinct from the hyaloid system in TCDD-treated embryos, which did not appear grossly different from DMSO-treated controls. Overall these data suggest that effects in the SAV cannot be solely attributed to secondary effects from TCDD-induced reductions in circulation.

TCDD exposure leads to aberrant growth and incorrect patterning of the SIVP

A hallmark of TCDD early life developmental toxicity is failure of the yolk sac to absorb, which has been observed in multiple fish species (Spitsbergen *et al.*, 1991; Cantrell *et al.*, 1996; Guiney *et al.*,

1997; Henry *et al.*, 1997; Yamauchi *et al.*, 2006). In zebrafish, the SIVP is intimately involved in the absorption of nutrients from the yolk sac during the first few days of development, and later contributes to blood flow of the digestive tract and hepatic vasculature (Isogai *et al.*, 2001). Thus, we investigated whether TCDD exposure affected development of the SIVP.

Zebrafish embryos with endothelial (*fli1a*:EGFP) and erythrocyte (*gat1a*:DsRed) markers were exposed to either DMSO (vehicle control, 0.1%) or TCDD (1 ng/ml, waterborne) at 4 hpf and the left SIVP was assessed at 48-72 hpf (Figure 5). In DMSO-treated controls at 48 hpf, endothelial cells have already formed the primitive structure of the SIVP, which extends ventrally from the posterior cardinal vein (PCV) (Figure 5A). The primary subintestinal vein (SIV), which at this stage runs mostly parallel to the PCV, is identifiable. Additional interconnected secondary vessels make up the rest of the vascular plexus, forming several "compartments". Over time, the SIVP increases in area and length, spreading ventrally (Figure 5B-D). Blood begins to perfuse the SIVP at approximately 60 hpf (Figure 5C). By 72 hpf remodeling of secondary vessels forms a basket-like structure, with most secondary vessels forming connections directly between the primary SIV and PCV. In addition, there is rapid blood flow throughout the SIVP (Figure 5D). In TCDD-treated embryos, the SIVP appears to sprout normally and spreads ventrally at 48 hpf (Figure 5E). However, the SIVP quickly expands to cover an area and length beyond the range of similarly aged controls (Figure 5F-H). Blood is observed to perfuse the SIVP normally at approximately 60 hpf (Figure 5G). Between 48-72 hpf the primary SIV is poorly defined and the secondary vessels appear disorganized. By 72 hpf a high number of compartments persist between secondary vessels (Figure 5H). Although not a precise assessment of blood flow, z-stacks from live confocal imaging can provide a general sense of flow rate: the slow-scanning laser can only capture partial snapshots of moving blood cells. Thus, rapidly moving cells appear as red "hatch marks" within the vessel lumens, as seen in DMSO-treated controls at 72 hpf (Figure 5D), and indicate normal blood

circulation. In contrast, slow-moving or stationary blood cells appear as rounded shapes, as seen in TCDD-treated embryos at 60 and 72 hpf (Figure 5G-H), indicating slow or nonexistent circulation. A similar phenotype was observed in the right SIVP of DMSO- vs. TCDD-treated embryos (Supplemental Figure S1, A-H).

In order to quantify effects observed in the SIVP of TCDD-treated embryos, the area, length, and number of compartments in the left SIVP was assessed at 48, 54, 60, and 72 hpf (Figure 6). Quantification was done in a manner similar to Goi and Childs (2016), and an example of each of the measurements acquired in this study is shown in a DMSO-treated sample (Figure A'-C'). The area and number of compartments in the SIVP was significantly higher in TCDD-treated embryos compared to DMSO-treated controls at 48-72 hpf (Figure 6A, C; $p \leq 0.05$). The length of the SIVP was also significantly higher in TCDD-treated embryos at 54-72 hpf (Figure 6B; $p \leq 0.05$). Similar results were observed when SIVP area, length, and number of compartments were measured in the right SIVP of DMSO- vs. TCDD-treated embryos (Supplemental Figure S1, I-K). Overall, this suggests that both the growth and patterning of the SIVP are affected by TCDD exposure.

TCDD-induced effects on the SIVP are not phenocopied by inhibition of circulation

As mentioned above, TCDD exposure leads to reduced cardiac output beginning at 60 hpf, which eventually culminates in complete circulatory collapse (Antkiewicz *et al.*, 2005, 2006). Therefore, we investigated whether the observed SIVP phenotype following TCDD exposure could be recapitulated by inhibiting circulation beginning at 60 hpf (via exposure to BDM), or when circulation was entirely lost (using *sih* MO) (Figure 7). The left SIVP developed normally in DMSO-treated embryos and embryos that were not exposed to BDM (No BDM) (Figure 7A, C). The SIVP in control MO embryos was reduced compared to other controls, although at 72 hpf circulation and patterning appeared normal (Figure 7B). TCDD-treated embryos developed a phenotype as described above: by 72 hpf the SIVP extended over a

large area beyond that of controls, had a large number of poorly organized compartments, and lacked apparent circulation (Figure 7B; Table 1). Interestingly, BDM-treated and *sih* MO embryos developed different characteristics. At 72 hpf, the SIVP of BDM-treated embryos was not significantly different in area, length, or number of compartments than respective controls (Figure 7D; Table 1; $p \leq 0.05$). In *sih* MO embryos, only the length and number of compartments was significantly reduced compared to respective controls (Figure 7F; Table 1; $p \leq 0.05$). In general, there was a trend of smaller SIVP area and length in BDM-treated and *sih* MO embryos, compared to their respective controls, which is the opposite of what was observed in TCDD-treated embryos (Table 1). In addition, the SIVP vessel morphology in BDM-treated and *sih* MO embryos differed from TCDD-treated embryos. When circulation was inhibited by BDM or *sih* MO, the vessels became dense and lacked identifiable lumens (Figure 7D, F). In contrast, even though TCDD-treated embryos had markedly decreased or stagnant circulation at 72 hpf, the vessel lumens were still clearly visible (Figure 7B). Similar trends were observed in the right SIVP of embryos exposed to the same treatments (Supplemental Figure S2, Table S1). Overall, this suggests that the effects of TCDD exposure on the SIVP are unlikely to be secondary to TCDD-induced reductions in circulation.

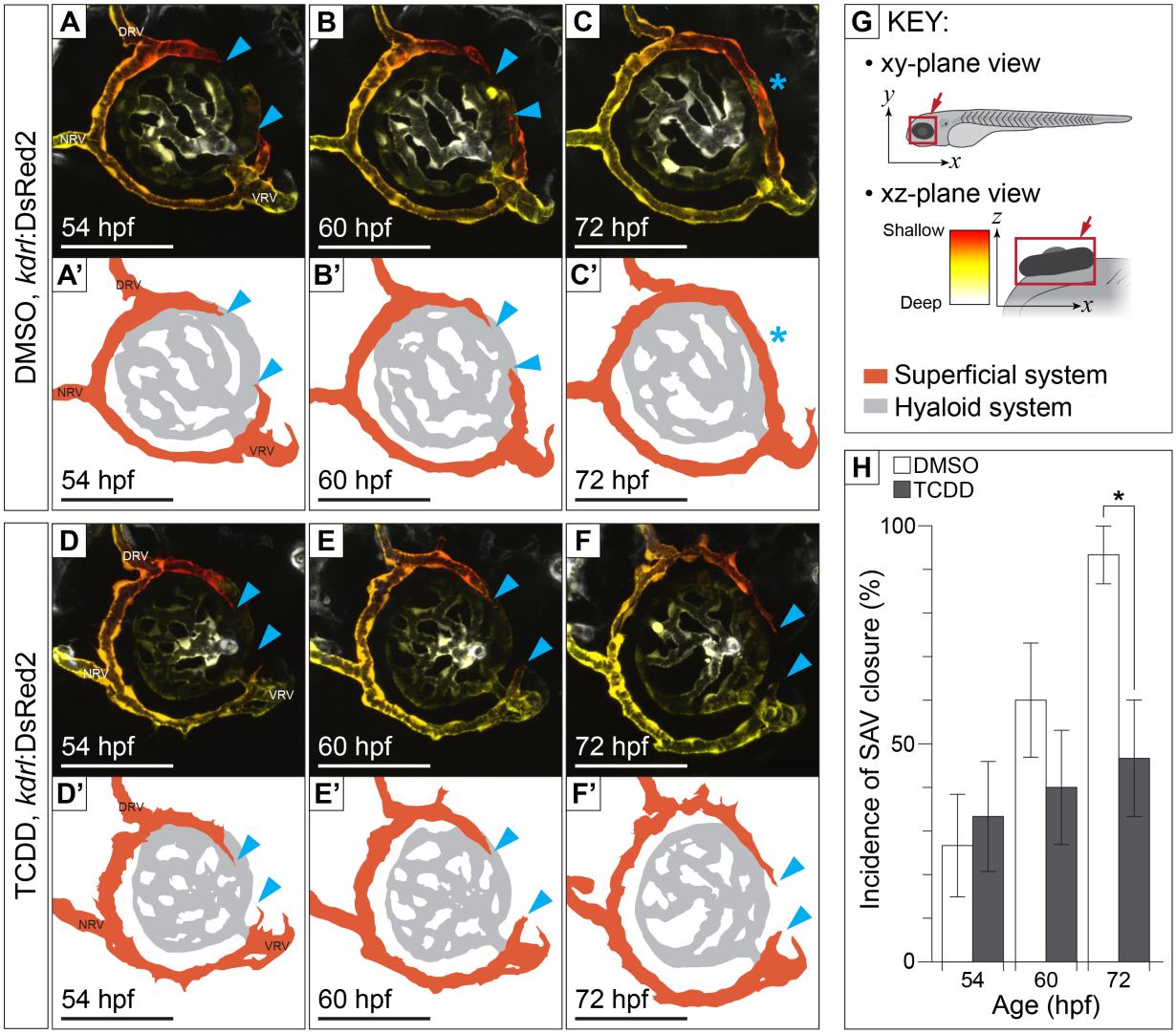

Figure 1. TCDD exposure inhibits closure of the superficial annular vessel (SAV) in the eye.

Transgenic *kdrl*:DsRed2 embryos were exposed to either (A-C) DMSO (0.1%), or (D-F) TCDD (1 ng/ml, waterborne) at 4 hpf and the development of the superficial vascular system was assessed at 54, 60, and 72 hpf. (A-F) Maximum intensity projections of live confocal imaging are shown. *kdrl* expression is depth color-coded to distinguish between deep vs. shallow structures (see key, G). (A'-F') Schematics show the developing superficial (orange) and hyaloid (gray) vascular systems in (A-F), respectively. At

52 hpf, radial vessels of the superficial system connect to the dorsal, anterior, and ventral portions of the SAV in both DMSO- and TCDD-treated fish (A, A'; D, D'). The growing tips of the SAV are indicated by blue arrowheads. (B, B') In DMSO-treated fish, the growing tips extend and eventually coalesce. (C, C') At 72 hpf the SAV is complete and forms a ring-like vessel that connects flow between all three radial vessels of the superficial system (asterisk). In contrast, by 72 hpf the SAV is incomplete in TCDD-treated fish and the vessel tips remain apart (F, F'; blue arrowheads). (H) The incidence of SAV closure is significantly decreased in TCDD-treated fish at 72 hpf (ANOVA, $p \leq 0.05$; significance indicated by asterisk). Representative images are shown (n = 15). All images are orientated laterally with anterior to the left. Scale bars = 100 μm. Abbreviations: dorsal radial vessel (DRV), nasal radial vessel (NRV), ventral radial vessel (VRV).

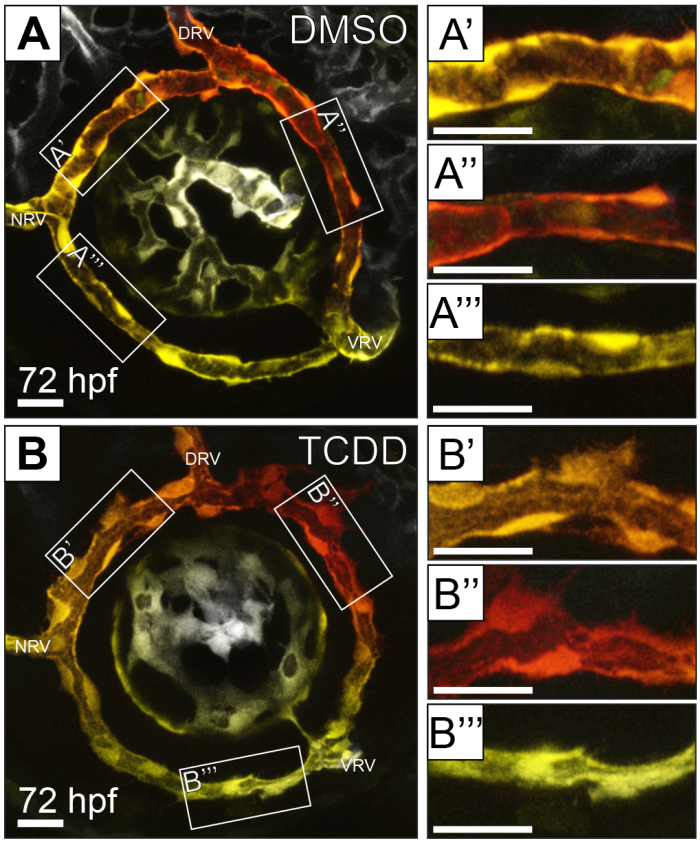

Figure 2. SAV morphology is abnormal in TCDD-treated fish.

Embryos exposed to (A) DMSO (0.1%), or (B) TCDD (1 ng/ml) at 4 hpf develop different vessel morphologies by 72 hpf. (A-B) Maximum intensity projections from live confocal imaging of *kdrl*:DsRed2 embryos are shown. *kdrl* expression is depth color-coded (see Figure 1G for key). (A'-A''') High magnification images of the boxes in (A) of different regions of the SAV in a DMSO-treated fish show that the vessel is uniformly smooth throughout and has a clearly defined lumen. (B'-B''') In contrast, high magnification images of the boxes in (B) of the SAV in a TCDD-treated fish show a rough vessel surface and tortuous shape with varying lumen thickness at different points along the structure. Representative images are shown. All images are orientated laterally with anterior to the left. Scale bars = 25 μm. Abbreviations: dorsal radial vessel (DRV), nasal radial vessel (NRV), ventral radial vessel (VRV).

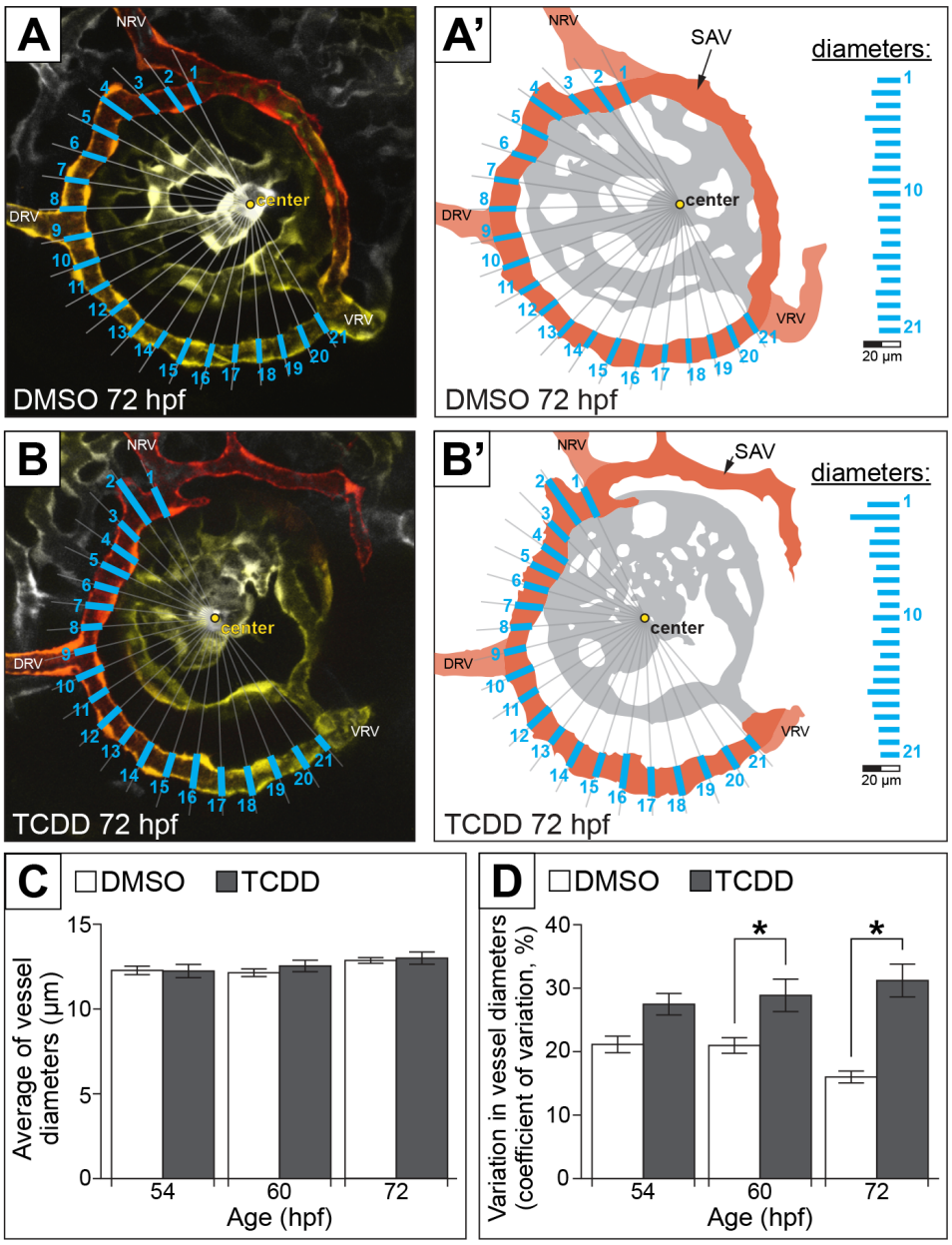

Figure 3. TCDD exposure increases the variation in vessel diameters measured along the SAV.

The diameter of the SAV vessel was measured at multiple points between the DRV-NRV-VRV in embryos exposed to DMSO or TCDD (1 ng/ml) at 4 hpf. A detailed description of the method for vessel diameter measurements is described in the Materials and Methods section. Representative examples of

(A) DMSO- and (B) TCDD-treated fish are shown. (A', B') Schematic diagrams of vessel measurements in (A) and (B), respectively. Vessel diameters are aligned in a column to illustrate the variation in diameters along the length of SAV that was assessed. (C) The average SAV vessel diameter is not significantly different between DMSO- and TCDD-treated fish. (D) However, the variation in vessel diameter is significantly greater in TCDD-treated fish at 60 and 72 hpf, as indicated by higher coefficients of variation. Significance indicated by asterisk (ANOVA, $p \leq 0.05$). All images are orientated laterally with anterior to the left. Abbreviations: superficial annular vessel (SAV), dorsal radial vessel (DRV), nasal radial vessel (NRV), ventral radial vessel (VRV).

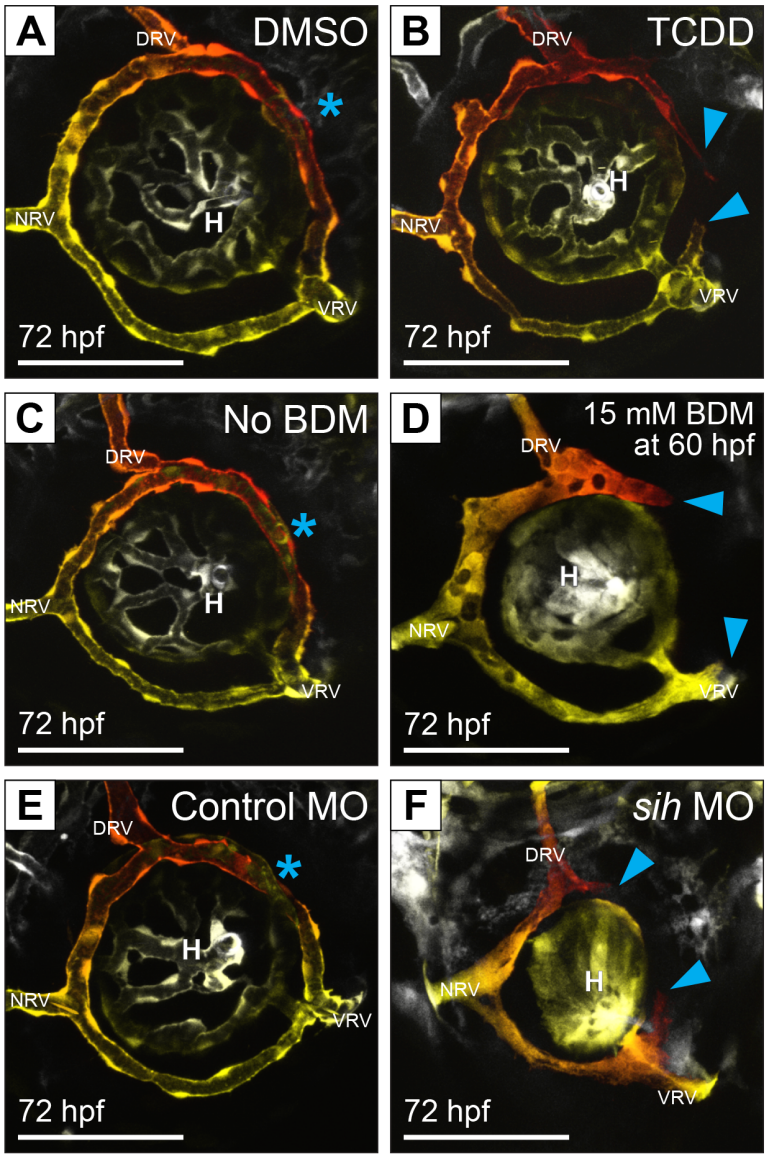

Figure 4. TCDD-induced effects on the SAV are not completely secondary to TCDD-induced depression of circulation.

The development of the superficial vascular system in *kdrl*:DsRed2 embryos exposed to different treatments was assessed at 72 hpf: (A) DMSO or (B) TCDD exposure at 4 hpf; (C) raised in normal conditions (i.e., No BDM) or (D) raised in 15 mM BDM beginning at 60 hpf; microinjected with (E)

Control MO or (F) *sih*/*tnnt2* MO. (A-F) Maximum intensity projections from live confocal imaging are shown with depth color-coding (see Figure 1G for key). The SAV is closed and developed normally in DMSO-treated, No BDM, and Control MO embryos (A, C, E; asterisk). In contrast, the SAV is incompletely closed in embryos with reduced or absent circulation (B, D, F; blue arrowheads). The morphology of vessels in TCDD-treated embryos is different than in BDM-treated and *sih* MO embryos. The TCDD-treated SAV has a rough surface, tortuous shape, and visible lumen (B). In contrast, when circulation was inhibited beginning at 60 hpf by BDM (D) or continuously in *sih* MO (F) all vessels in the superficial system developed a smooth texture, appearing dense, and lacking visible lumens. In addition, the hyaloid system is significantly underdeveloped. Images are representative, orientated laterally with anterior to the left. Scale bars = 100 μm. Abbreviations: dorsal radial vessel (DRV), nasal radial vessel (NRV), ventral radial vessel (VRV), hyaloid system (H).

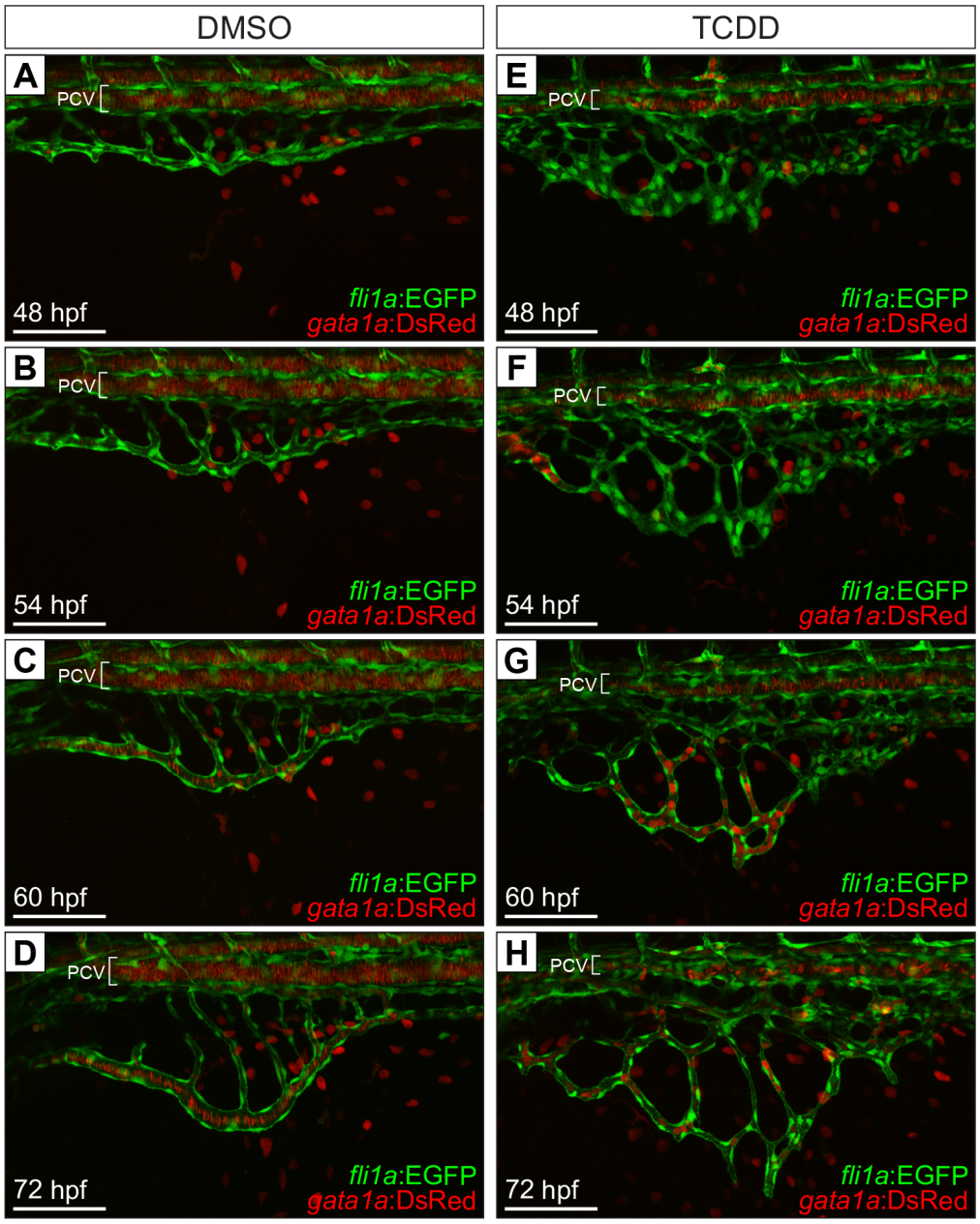

Figure 5. TCDD exposure causes aberrant growth and patterning of the subintestinal venous plexus (SIVP).

Transgenic *fli1a*:EGFP; *gata1a*:DsRed embryos were exposed to either (A-D) DMSO (0.1%), or (E-H) TCDD (1 ng/ml, waterborne) at 4 hpf and the development of the SIVP was assessed at 48, 54, 60, and 72

hpf. *fli1a* (green) is an endothelial marker and *gata1a* (red) is an erythrocyte marker. (A-H) Maximum intensity projections from live confocal imaging of the left SIVP are shown. (A-D) In DMSO-treated embryos the developing SIVP emerges from the posterior cardinal vein (PCV) and spreads ventrally. The SIVP consists of a primary subintestinal vessel (SIV) that forms the main anterior-to-posterior loop, and inter-connected secondary vessels that form compartments. The SIVP is not perfused until approximately 60 hpf (C). By 72 hpf, the secondary vessels have remodeled into an organized "basket" of parallel vessels connecting the primary SIV and the PCV, with rapid blood flow visible (D). In TCDD-treated embryos the SIVP appears to sprout normally from the PCV (E) and rapidly spreads ventrally. However, the secondary vessels are poorly organized, evident by the high number of compartments that persists over time (E-H). Circulation begins at approximately the same time as in DMSO-treated controls (G), however perfusion is poor at 72 hpf (H). Furthermore, the SIVP in TCDD-treated embryos is overgrown, covering a greater area and distance than similarly aged DMSO-treated controls (E-H). In addition, the primary SIV is poorly defined (E-H). Representative images are shown (n = 5 to 7). All images are orientated dorsal-laterally with anterior to the left. Scale bars = 100 μm. Abbreviations: posterior cardinal vein (PCV).

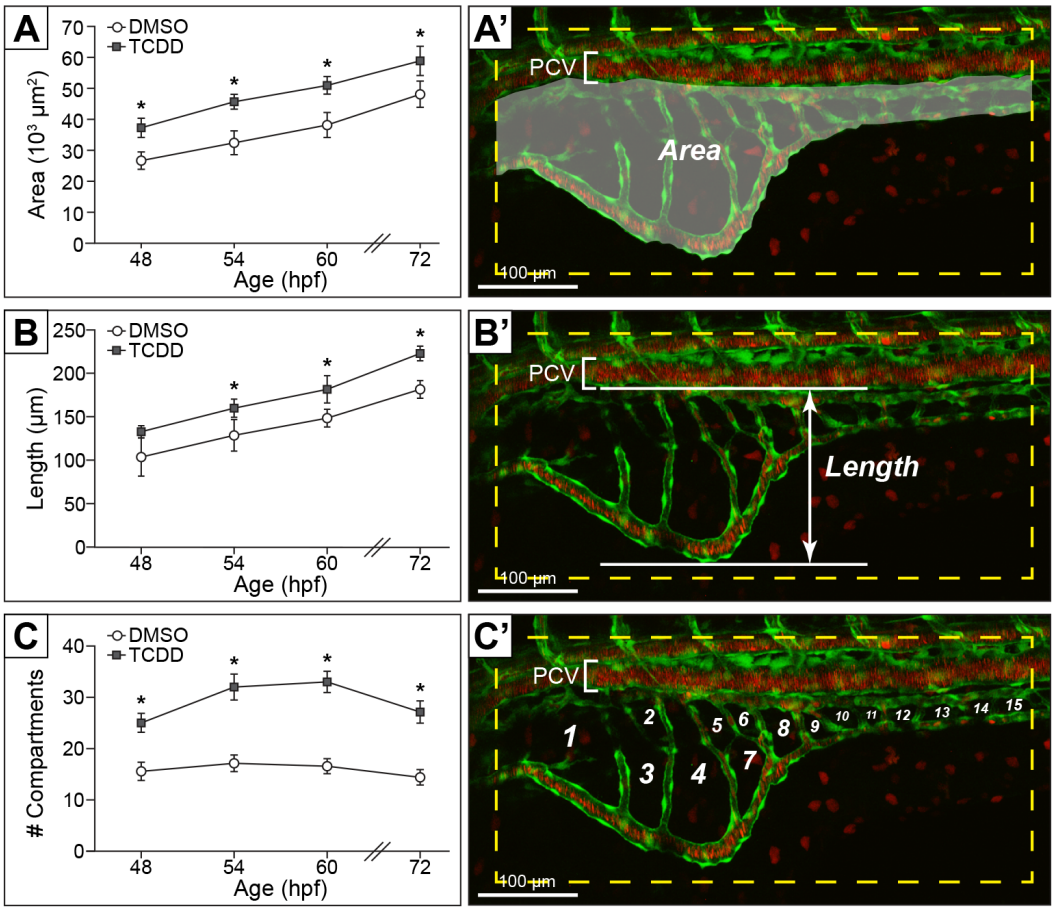

Figure 6. TCDD exposure increases the area, length, and number of compartments in the SIVP.

The SIVP was assessed as described in the Methods and Materials sections at 48, 54, 60, and 72 hpf in DMSO- and TCDD-treated embryos. The average area of the left SIVP (A) and number of compartments (C) is significantly greater at 48-72 hpf in TCDD-treated embryos. The average length of the left SIVP (B) is significantly greater in TCDD-treated embryos at 54-72 hpf. Significance is indicated with an asterisk (ANOVA, $p \leq 0.05$). (A'-C') Examples of measurements in (A-C) are shown, respectively, in a DMSO-treated fish (*fli1a*:EGFP; *gata1a*:DsRed). Yellow dashed box shows region of assessment. All images are orientated dorsal-laterally with anterior to the left. Scale bars = 100 µm. Abbreviations: posterior cardinal vein (PCV).

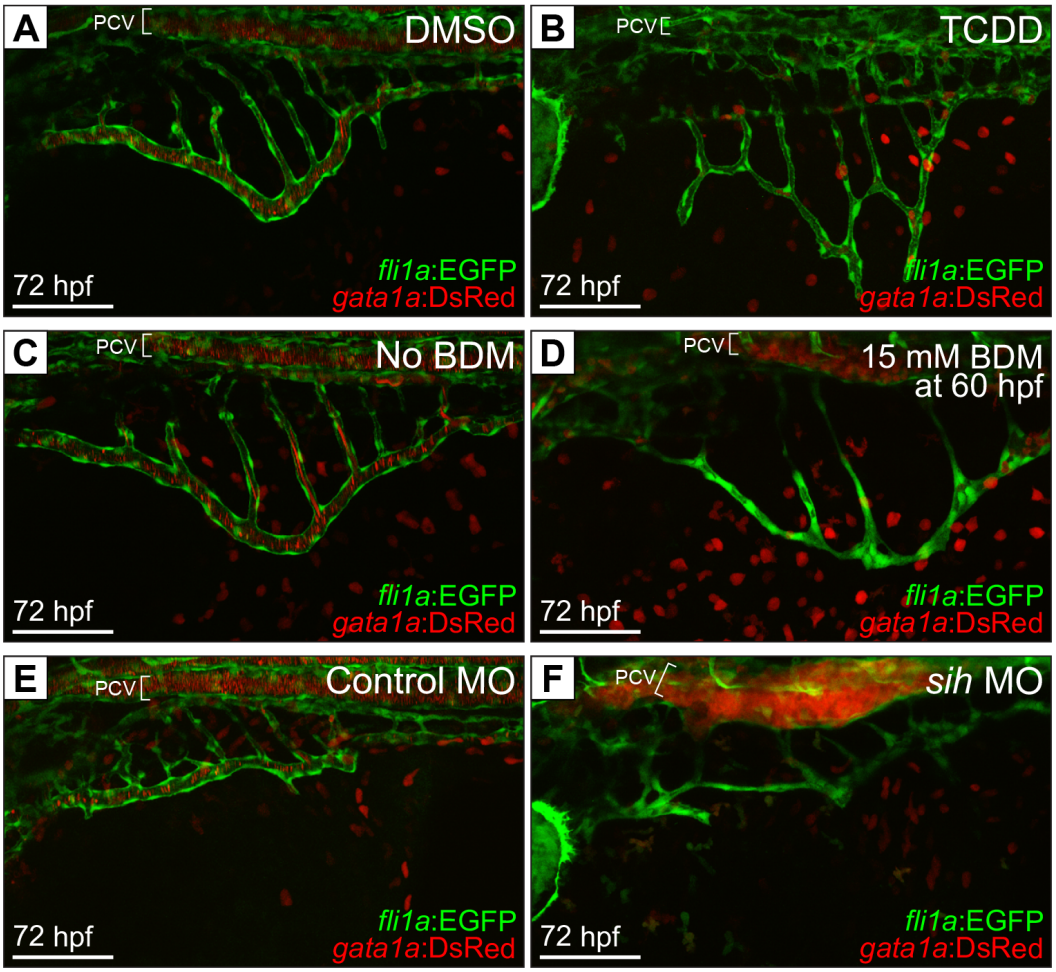

Figure 7. TCDD-induced effects on the SIVP are unlikely to be secondary to TCDD-induced reductions in circulation.

The development of the left SIVP was compared in age 72 hpf *fli1a*:EGFP; *gata1a*:DsRed embryos given different treatments: (A) DMSO or (B) TCDD exposure at 4 hpf; (C) raised in normal conditions (i.e., No BDM) or (D) raised in 15 mM BDM beginning at 60 hpf; (E) microinjected with Control MO or (F) *sih*/*tnnt2* MO. (A-F) Maximum intensity projections from live confocal imaging are shown. At 72 hpf, the SIVP developed normally in DMSO-treated and No BDM embryos (A, C). The SIVP in TCDD-treated embryos appears overgrown and is very poorly perfused (B). In contrast, embryos treated with BDM (D)

appear to have similar SIVP area, length, and number of compartments as their respective No BDM control embryos (C). The SIVP of Control MO embryos is notably reduced in size compared to other controls (A, C vs. E), however the SIVP of the *sih* MO is even more diminished and appears poorly organized (F). In treatments where circulation was inhibited by BDM or *sih* MO the vessels of the SIVP are smooth, condensed, and lack visible lumens (D, F), which is dissimilar to the TCDD-treated SIVP where the lumen of primary and secondary vessels is still visible (B). In addition, stagnant blood is observed pooling in the PCV in only BDM-treated and *sih* MO embryos (D, F). Images are representative, oriented dorsal-laterally with anterior to left. Scale bars = 100 μm. Abbreviations: posterior cardinal vein (PCV).

Table 1. Effects of TCDD, BDM, or *sih* Morpholino Treatment on Morphologic Development of the Left Subintestinal Venous Plexus (SIVP) in Zebrafish Larvae at 72 hpf [Δ]

	SIVP Area (10^3 μm^2)	SIVP Length (μm)	SIVP Compartments (number)
DMSO[†]	48.1 ±1.7	182 ±5	14 ±1
TCDD[†]	58.9 ±1.8*	223 ±7*	27 ±1*
No BDM[‡]	55.6 ±2.5	190 ±7	14 ±1
BDM[‡]	43.5 ±6.9	152 ±18	13 ±1
Control MO[‡]	31.7 ±0.7	126 ±4	17 ±1
sih MO[‡]	26.3 ±2.5	95 ±11*	11 ±2*

[Δ] All values are mean ± SE (n = 4 to 7).
* Significantly different from respective control ($p \leq 0.05$).
[†] Analysis done by ANOVA followed by Tukey's HSD test.
[‡] Analysis done by Student's t-test.

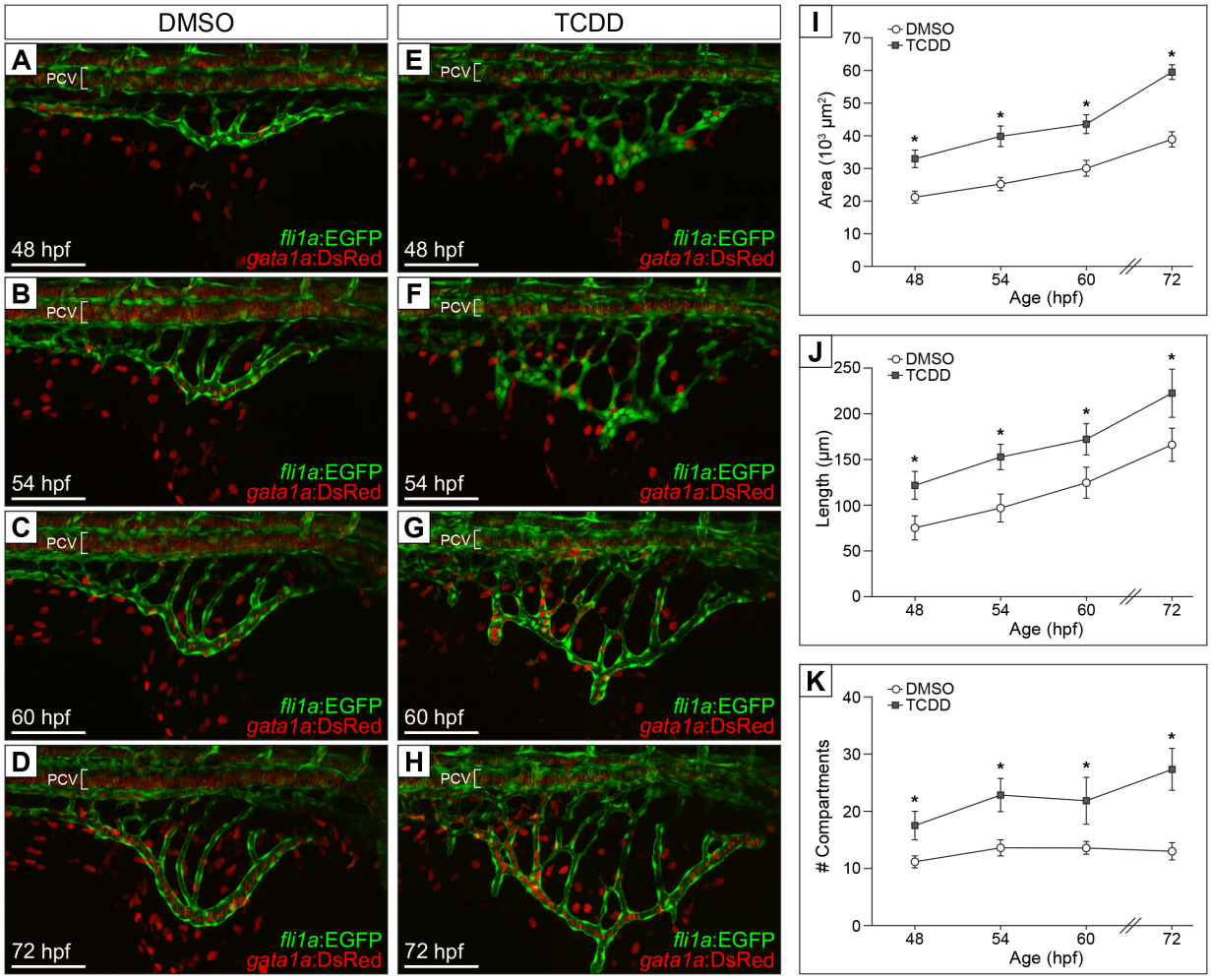

Supplemental Figure S1. TCDD exposure causes aberrant growth and patterning of the right SIVP.

Transgenic *fli1a*:EGFP; *gata1a*:DsRed embryos were exposed to either (A-D) DMSO (0.1%), or (E-H) TCDD (1 ng/ml, waterborne) at 4 hpf and the development of the SIVP was assessed at 48, 54, 60, and 72 hpf. *fli1a* (green) is an endothelial marker and *gata1a* (red) is an erythrocyte marker. (A-H) Maximum intensity projections from live confocal imaging of the right SIVP are shown. (I-K) Measurements of SIVP area, length, and number of compartments in DMSO- and TCDD-treated embryos. The observed phenotypes in the right SIVP are similar to the phenotypes reported for the left SIVP (Figures 5 and 6). (A-D) In DMSO-treated embryos the developing SIVP emerges from the PCV and spreads ventrally. By

72 hpf, secondary vessels have remodeled into parallel vessels connecting the primary SIV and the PCV, with rapid blood flow visible (D). In TCDD-treated embryos the SIVP sprouts normally from the PCV (E) and rapidly spreads ventrally. The secondary vessels are poorly organized, evident by the high number of compartments that persists over time (E-H). The SIVP in TCDD-treated embryos is overgrown (E-H), and there is poor circulation (G-H). The average area (I), length (J), and number of compartments (K) of the right SIVP are significantly greater at 48-72 hpf in TCDD-treated embryos (asterisk; ANOVA, $p \leq 0.05$). Representative images are shown (n = 5 to 7). All images are orientated dorsal-laterally with anterior to the right. Scale bars = 100 μm. Abbreviations: posterior cardinal vein (PCV).

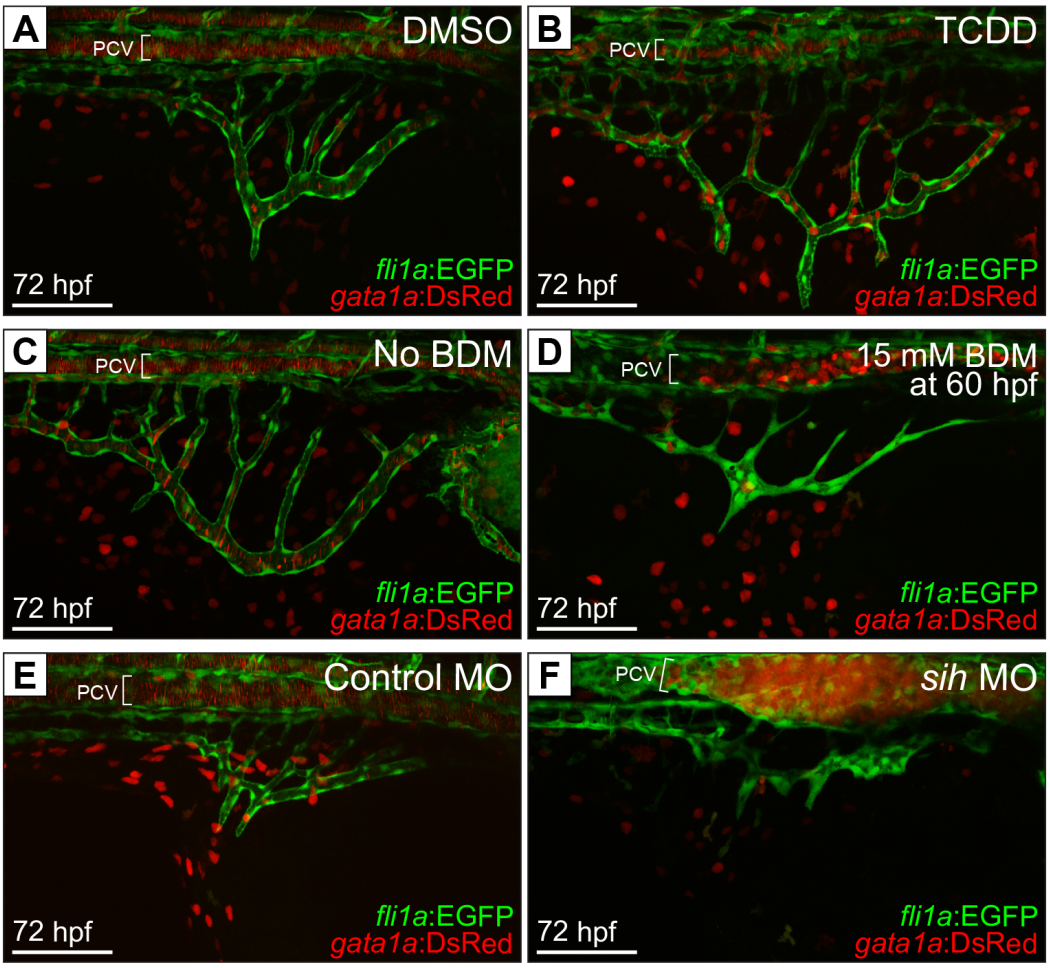

Supplemental Figure S2. TCDD-induced effects on the right SIVP are unlikely to be secondary to TCDD-induced reductions in circulation.

The development of the right SIVP was compared at 72 hpf in *fli1a*:EGFP; *gata1a*:DsRed embryos given different treatments: (A) DMSO or (B) TCDD exposure at 4 hpf; (C) raised in normal conditions (i.e., No BDM) or (D) raised in 15 mM BDM beginning at 60 hpf; (E) microinjected with Control MO or (F) *sih*/*tnnt2* MO. (A-F) Maximum intensity projections from live confocal imaging are shown. Results are similar to findings presented for the left SIVP (Figure 7). At 72 hpf, the right SIVP developed normally in DMSO-treated and No BDM embryos (A, C). The right SIVP is reduced in the Control MO embryos

compared to other controls (DMSO, No BDM), but appears properly patterned (E). The SIVP in TCDD-treated embryos is overgrown, with a high number of compartments, and is poorly perfused (B). In contrast, embryos treated with BDM (D) have a smaller SIVP with fewer compartments than respective No BDM controls (C). The SIVP of the *sih* MO appears similar in area, length, and number of compartments to respective Control MO (E-F). However, the organization of compartments is variable. In treatments where circulation was inhibited by BDM or *sih* MO, the vessels of the SIVP are smooth and lack clear lumens (D, F). In contrast, the lumen is still visible in the SIVP of TCDD-treated embryos (B). Stagnant blood is observed pooling in the PCV in BDM-treated and *sih* MO embryos (D, F). Images are representative, oriented dorsal-laterally with anterior to right. Scale bars = 100 μm. Abbreviations: posterior cardinal vein (PCV).

Table S1. Effects of TCDD, BDM, or *sih* Morpholino Treatment on Morphologic Development of the Right Subintestinal Venous Plexus (SIVP) in Zebrafish Larvae at 72 hpf [Δ]

	SIVP Area (10^3 μm^2)	SIVP Length (μm)	SIVP Compartments (number)
DMSO[†]	38.9 ±2.3	166 ±8	14 ±1
TCDD[†]	59.5 ±2.2*	223 ±11*	27 ±1*
No BDM[‡]	42.1 ±3.8	203 ±5	15 ±1
BDM[‡]	31.7 ±1.1*	164 ±16	12 ±0*
Control MO[‡]	28.7 ±2.3	119 ±6	14 ±1
sih MO[‡]	28.5 ±2.6	122 ±19	12 ±1

[Δ] All values are mean ± SE (n = 4 to 7).
* Significantly different from respective control ($p \leq 0.05$).
[†] Analysis done by ANOVA followed by Tukey's HSD test.
[‡] Analysis done by Student's t-test.

DISCUSSION

TCDD affects vessel development in the SAV of the eye

In this study we investigated the effects of TCDD exposure on the development of the superficial vascular system. We focused on the development of the SAV, which is the central ring-like structure of the superficial system that connects flow between three radial vessels (DRV, NRV, VRV), and the hyaloid system via the hyaloid vein.

At 54 hpf, the anterior portion of the SAV in both DMSO- and TCDD-treated embryos was properly formed, including the portions of the SAV between the DRV-NRV and NRV-VRV. Growing tips were observed at the junctions of the SAV-DRV and SAV-VRV. In DMSO-treated embryos, the growing tips extended over time and eventually coalesced to form a complete SAV by 72 hpf. However, even when extension of the growing tips was observed between 54-60 hpf, in many TCDD-treated embryos the tips failed to coalesce and the SAV remained incompletely formed by 72 hpf. To determine if this effect was significant, a reviewer blinded to both age and treatment of samples scored for closure of the SAV. Previous reports describing the development of the SAV suggest that closure of the "ring" can occur as early as 52-53 hpf (Kaufman *et al.*, 2015). In agreement with this, we observed 27±12% of DMSO-treated embryos with successful SAV closure at 54 hpf. A similar percent of embryos with SAV closure was observed in the TCDD treatment group at 54 hpf (33±13%). The percent of control embryos with SAV closure increased over time in the DMSO treatment group, such that by 72 hpf nearly all embryos had a completely formed SAV (93±7%). Although there was a slight trend of increased percent of TCDD-treated embryos with SAV closure over time, by 72 hpf it was still significantly lower (47±13%) than in similarly aged controls.

Even when the SAV closed normally in TCDD-treated embryos, the morphology of the vessel itself appeared different from DMSO-treated controls. In general, the SAV in DMSO-treated embryos appeared smooth, with a visible continuous lumen, and relatively uniform vessel thickness throughout the length of the SAV. In contrast, the SAV in TCDD-treated embryos had a rough texture, with a meandering shape. Although the lumen was visible there was variation in vessel thickness, appearing dilated or constricted at various points along the length of the SAV. To better characterize this effect, we measured the vessel diameter along several points of the SAV between the DRV-NRV-VRV. The mean vessel diameter was not significantly different between treatments. However, there was significantly greater variation in vessel diameters within samples of the TCDD-treated group at 60 and 72 hpf. This variability in vessel shape could impact flow patterns within the vessel, for example by disrupting laminar flow. Fluid modeling of vessels with varying degrees of stenosis indicates that as little as 30% stenosis of vessel diameter can increase peak blood velocity and wall shear stress (Li *et al.*, 2007). Alterations in shear stress or flow type can affect mechanotransduction signaling. At present it is unclear how this may impact development in embryonic endothelial cells. In adult vascular systems, there is a growing body of evidence implicating the importance of normal blood flow patterns in vascular sprouting, remodeling, maintenance of arterial vs. venous identity, and regulation of Notch signaling (Jones, 2011a,b). It is therefore likely that the alterations in embryonic vessel morphology observed here could impact downstream developmental events and have important physiological consequences.

TCDD causes excessive growth and incorrect patterning of the SIVP

Development of the SIVP in zebrafish involves phases of sprouting, migration, growth, and remodeling (Lenard *et al.*, 2015; Goi and Childs, 2016). The SIVP begins to form at approximately 30 hpf through the coalescence of endothelial cells that have migrated ventrally from the PCV (Goi and Childs, 2016). From here, the primary vessel (or primary SIV) forms and migrates ventrally across the surface of

the yolk sac. Interconnecting secondary vessels form within the plexus, which at first have a honeycomb-like appearance that later expands to form large compartments between vessels. At approximately 3 days post fertilization (dpf) these compartments are remodeled and the secondary vessels align in parallel, connecting flow directly from the PCV to the primary SIV. Beyond this stage there are notable differences in the development and remodeling of the right and left SIVPs, which develop specifically into the hepatic sinusoids (left) and the intestinal vasculature (right) (Isogai *et al.*, 2001).

In this study we focused our assessment to the developmental stages prior to the overt divergence of left and right SIVP development that begins after 3 dpf. In DMSO-treated embryos we observed the primary SIV growing and migrating ventrally (48 hpf), the formation and expansion of compartments between secondary vessels (54-60 hpf), and finally minor remodeling of the SIVP (72 hpf). TCDD exposure affected all stages of SIVP development in both the left and right SIVP. As early as 48 hpf and continuing to 72 hpf, the left SIVP area and number of compartments in TCDD-treated embryos was significantly higher than in similarly aged controls. At 54 hpf through to 72 hpf, the left SIVP length was also significantly greater in TCDD-treated embryos compared to controls. In the right SIVP, area, length, and number of compartments was significantly higher in TCDD-treated embryos at 48-72 hpf. Overall, these results indicate that TCDD exposure leads to an overgrown SIVP that is incorrectly patterned. Interestingly, in the left SIVP, the number of compartments in TCDD-treated embryos increased slightly between 48-60 hpf, and then decreased between 60-72 hpf, suggesting that some remodeling may have occurred. However, this was limited and the SIVP was organized differently than in DMSO-treated controls. This trend was not observed in the right SIVP.

In addition to changes in the size and spread of the SIVP, TCDD exposure altered the morphology of the primary SIV. In DMSO-treated embryos this vessel is clearly identifiable at all stages of development as the leading edge of the expanding SIVP. By 72 hpf, the primary SIV is noticeably

larger than the secondary vessels, with blood rapidly flowing through it. In contrast, the primary SIV in TCDD-treated embryos remained poorly defined, in part due to interruptions in the shape of the vessel by extending lamellipodia. By 72 hpf this vessel was not remarkably different than most secondary vessels in the TCDD-treated SIVP. Interestingly, blood was observed to perfuse the SIVP of TCDD-treated embryos at approximately the same time as in DMSO-treated embryos (60 hpf), although circulation was slower and generally nonexistent by 72 hpf.

Role of circulation on TCDD-induced effects in the SAV and SIVP

Blood circulation can influence multiple aspects of vascular development, including angiogenic sprouting, arterial-venous identity, and vessel pruning (Jones, 2011a,b; Kocchan *et al.*, 2013). In zebrafish, early exposure to TCDD ultimately leads to complete loss of circulation by 96-120 hpf, beginning with decreased cardiac output at 60 hpf (Antkiewicz *et al.*, 2006). Therefore, we tested whether the observed SAV and SIVP phenotypes in TCDD-treated embryos were secondary to a TCDD-induced decrease in circulation. To investigate this possibility we assessed the development of the SAV and SIVP in embryos where circulation was inhibited in two scenarios: 1) when circulation was repressed beginning at 60 hpf via exposure to BDM, 2) when circulation was completely inhibited via *sih* MO.

When circulation was inhibited by either BDM treatment or *sih* MO, the SAV failed to close at 72 hpf. This suggests that the TCDD-induced inhibition of SAV closure may in fact be a secondary effect due to TCDD-induced decreases in cardiac output. However, circulatory changes cannot account for other effects observed in this study, e.g., the alterations in vessel morphology in the SAV, and the growth and patterning of the SIVP.

A drastic difference between TCDD-treated embryos and BDM-treated or *sih* MO embryos was the morphology of the vessels in both the SAV and SIVP. In BDM-treated and *sih* MO embryos the

vessels had a smooth texture and appeared to lack a visible lumen. In some *sih* MO embryos, the radial vessels in the superficial system were also regressed, and in both BDM-treated and *sih* MO embryos the hyaloid system was significantly reduced. Neither of these additional effects was observed in TCDD-treated embryos. Recent work by Gebala *et al.* (2016) showed that blood flow drives formation of lumens during sprouting angiogenesis. Thus it is possible that in *sih* MO embryos the lumens in the SAV never form even though the vessels themselves are present and patterned correctly. Inhibiting circulation starting at 60 hpf in the BDM-treated embryos resulted in a vessel morphology that was very similar to that of *sih* MO embryos. This suggests that blood flow may also have a significant role in maintaining lumens and vessel integrity after circulation has been established, which is in agreement with current models that emphasize the importance of fluid forces and hemodynamics in the signaling, growth, and remodeling of vessels (Jones, 2011a,b). Given this paradigm, it is perhaps even more striking that the vessels in the SAV and SIVP of TCDD-treated embryos maintained lumens despite significantly decreased cardiac output and peripheral trunk circulation at 60 and 72 hpf, respectively (Antkiewicz *et al.*, 2006; Henry *et al.*, 1997).

The effects on SIVP growth and patterning following TCDD exposure similarly do not appear to be secondary to TCDD-induced reduction in blood flow. In BDM-treated embryos there was a trend of smaller SIVP area, length, and number of compartments as compared to similarly aged controls. In *sih* MO embryos there was a trend of smaller left SIVP area, and the left SIVP length and number of compartments was significantly lower than controls. In the right SIVP, there was also a slight trend of smaller SIVP in *sih* MO embryos compared to controls. Our results with *sih* MO embryos were somewhat incongruous with findings from Lenard *et al.* (2015), which reported that the SIVP in *sih* MO embryos was not significantly different from controls in growth or patterning. It is possible that this discrepancy stems from variation in test fish. Our control MO cohort had unexpectedly reduced SIVP development

compared to other control fish at the same age (i.e., DMSO-treated or No BDM embryos), so it is possible that unknown stressors innately present in this cohort affected the *sih* MO embryos more than usual, leading to the reduced SIVP development observed here. Nevertheless, in BDM-treated and *sih* MO embryos there was an overall trend of either decreased or not significantly different growth and patterning of the SIVP. This is the opposite of what was observed in TCDD-treated embryos where the SIVP was consistently larger and incorrectly patterned compared to DMSO-treated controls. In addition, these effects were present before perfusion of the SIVP was observed (54-60 hpf), or when TCDD caused reductions in blood flow (60-72 hpf).

Overall, the weight of evidence suggests that altered vessel morphology in the SAV and SIVP, as well as the excessive growth and incorrect patterning in the SIVP, are not secondary effects from TCDD-induced reduction in blood flow. Rather, our results suggest that alternative mechanisms may be involved.

Potential targets of TCDD and AHR activation in the developing vasculature of the eye and intestine

There are many signaling pathways that are involved in normal vascular development. Vascular endothelial growth factor (Vegf) signaling, for example, is involved in endothelial cell proliferation, migration, and survival (Hirashima, 2009) and is often required to guide angiogenic sprouting (Gerhardt *et al.*, 2003). Notch signaling is closely linked to vascular remodeling and arterial identity (Hirashima, 2009). In addition, the balance of specific ligand stimulation (either by JAG1 or Dll4) in Notch signaling can influence lumen formation (Pandey *et al.*, 2015). Bone morphogenetic protein (BMP) signaling is involved in promoting ventral sprouting of the caudal venous plexus in zebrafish, is known to crosstalk with multiple signaling pathways during vascular development, and has been directly linked to vascular disorders in humans (Garcia de Vinuesa *et al.*, 2016).

It is proposed that aberrant activation of the AHR signaling pathway by TCDD leads to corruption of gene expression patterns involved in developmental processes, thus manifesting as developmental toxicity (Carney *et al.*, 2006; King-Heiden *et al.*, 2012). In zebrafish, TCDD developmental toxicity is mediated by activation of AHR2 (Prasch *et al.*, 2003, 2006). As several of the effects observed in this study are unlikely secondary to repressed circulation, we instead propose that these effects are the result of TCDD-induced AHR2 activation causing inappropriate signaling in one or several of the pathways involved in vascular development.

Recent studies emphasize that Vegfa-Vegfr2 signaling and BMP signaling are key factors in regulating SIVP sprouting, growth, and patterning (Koenig *et al.*, 2016; Goi and Childs, 2016). *Vegfaa* is expressed in the endoderm along the yolk, while its receptors *kdrl* and *kdr* are expressed in the SIVP vessels (Koenig *et al.*, 2016). Loss of expression of Vegfa homologs (*vegfaa*, *vegfab*) or Vegfr2 receptors (*kdrl*, *kdr*) leads to reductions in SIVP growth and mispatterning, with the severity depending on the homolog (Koenig *et al.*, 2016; Goi and Childs, 2016). Similarly, *bmp4* is expressed in the nearby developing gut concurrent to SIVP development (Zeng and Childs, 2012). Inhibition of BMP signaling with small molecule exposure reduced SIVP growth, although patterning did not appear to be affected (Goi and Childs, 2016).

In this study, we observed excessive growth and incorrect patterning of the SIVP in TCDD-treated embryos. Previous work has shown that TCDD exposure induces delocalized expression of *bmp4* in the heart, and likely contributes to malformation of endothelial-derived heart valves (Mehta *et al.*, 2008). A similar mechanism could mediate the observed SIVP phenotype. Misregulated increase in BMP expression or increased sensitivity to BMP signaling in the vascular endothelium could encourage excessive growth of the SIVP. Alternatively, expression of various components of the Vegf signaling pathway could be misregulated by TCDD/AHR2 activation. For example, while not required for SIVP

development, *vegfr3*/*flt4* is also expressed in the SIVP vessels (Koenig *et al.*, 2016). Thus, inappropriate expression of the complimentary ligand, *vegfc*, in the endoderm could promote excessive growth of the SIVP. Since loss of *kdrl* can reduce the number of cells in the SIVP (Koenig *et al.*, 2016) the opposite may occur if *kdrl* was over-expressed, or if guiding cues *vegfaa*/*b* were increased. This could also induce incorrect patterning of the SIVP that was observed in TCDD-treated embryos. Finally, the lack of proper SIVP remodeling in TCDD-treated embryos indicates possible misregulation of Notch signaling, which is known to be involved in vascular remodeling. However, this seems unlikely since Goi and Childs (2016) demonstrated that exposure to two different Notch inhibitors did not affect SIVP development.

In both the SAV and SIVP the morphology of vessels in TCDD-treated embryos was altered. Specifically in the SAV, the vessel appeared rough, the shape was meandering, and there was significantly higher variation in vessel diameter within each sample. The mechanism by which TCDD exposure may be altering vessel shape and diameter is unclear. In adults, vessel morphology can be influenced by extracellular matrix proteins, vascular smooth muscle cells, endothelial nitric oxide synthase (eNOS), or blood flow (Jones, 2011a). However, these same factors may not be applicable to embryonic vasculature. Smooth muscle cells differentiate at later stages of development, and various studies have suggested conflicting effects of eNOS induction or inhibition during embryonic development (Jones, 2011a,b). Nevertheless, TCDD has been shown to decrease expression of *sox9b*, a regulator of extracellular matrix proteins, in the developing heart and jaw of zebrafish (Hofsteen *et al.*, 2013; Xiong *et al.*, 2008; Burns *et al.*, 2015). Perhaps a similar pathway involving misregulation of extracellular matrix components via the TCDD/AHR2 pathway is involved in creating the effects on embryonic vessel morphology observed here.

The vessel lumens in TCDD-treated embryos remained intact despite TCDD-induced reductions in circulation, which contrasted sharply with apparent loss of vessel lumens in BDM-treated embryos. This effect was surprising considering other effects induced by TCDD exposure on vessel morphology seem to encourage non-laminar flow conditions that can lead to vessel degeneration or possibly rupture (Jones, 2011a,b). Work from Zhong *et al.* (2011) may offer a clue to this paradox. Using small molecule screening with zebrafish embryos, Zhong *et al.* (2011) discovered that activity of MEK1/2 and Vegfr2 worked in combination to support vessel integrity. Given the role of Vegfa-Vegfr2 in the SIVP, it seems plausible that TCDD exposure affects the Vegf signaling pathway. Furthermore, studies have indicated two-way crosstalk exists between AHR signaling and MAP kinase pathways (Puga *et al.*, 2009). Although still uncertain, cumulatively these findings suggest a possible mechanism whereby TCDD/AHR2 activation supports lumen integrity through altered Vegf and MAP kinase signaling.

We have presented several potential targets that may be involved in the TCDD-induced effects in the developing SAV and SIVP. Unfortunately, it was beyond the scope of this study to pursue these hypothetical mechanisms for TCDD-induced toxicity. However, these conjectures represent many interesting avenues for future research and investigation.

CONCLUSIONS

Vascular development is essential for growth, development, and survival. TCDD exposure is known to adversely affect the development of various vascular structures in multiple fish species. In this study we demonstrated that TCDD exposure disrupts development of the superficial vascular system of the eye and the SIVP in the gut in zebrafish embryos. In the eye, TCDD exposure significantly inhibited closure of the SAV. The morphology of this vessel was also affected, including alterations in general

shape, texture, and increased variation in vessel diameter. In the developing gut, TCDD exposure caused excessive growth and incorrect patterning of the SIVP.

TCDD exposure causes decreased cardiac output and inhibition of circulation, therefore we compared TCDD-treated embryos to embryos where circulation was impaired by BDM exposure or *sih* MO. Inhibition of circulation by BDM exposure or *sih* MO was insufficient to fully recapitulate effects observed in the SAV and SIVP of TCDD-treated embryos. Inhibition of SAV closure was observed in both BDM-treated and *sih* MO embryos, suggesting that this effect is secondary to TCDD-induced decreases in circulation. However, alterations to vessel morphology in the SAV and the overgrowth and mispatterning of the SIVP were distinctly different in TCDD-treated embryos compared to BDM-treated or *sih* MO embryos. Overall, this supports a mechanism of toxicity different from TCDD-induced repression of blood flow. We propose that TCDD-induced activation of the AHR signaling pathway likely interacts with other pathways involved in vascular development, such as Vegf and BMP, resulting in the effects observed here. Determining the precise mechanisms by which these vascular phenotypes emerge will be an interesting area of research for future studies to explore.

ACKNOWLEDGEMENTS

Support for this research was provided by the Graduate School and the Office of the Vice Chancellor for Research and Graduate Education at the University of Wisconsin-Madison with funding from the Wisconsin Alumni Research Foundation. This research was also supported by a National Institute for Environmental Health Sciences grant (K99 ES023848) to J.S.P. The authors wish to thank Dr. M.R. Taylor, Dr. K. Lanham, J. Gawdzik, F. Mu, and L. Elemans for helpful conversations, advice, and

general support in conducting this research. The authors also thank K. Hausman, C. Patz, and H. Stellrecht for help in maintaining zebrafish.

REFERENCES

Andreasen, E.A., Spitsbergen, J.M., Tanguay, R.L., Stegeman, J.J., Heideman, W., Peterson, R.E., 2002. Tissue-specific expression of AHR2, ARNT2, and CYP1A in zebrafish embryos and larvae: effects of developmental stage and 2,3,7,8-tetrachlorodibenzo-*p*-dioxin exposure. *Toxicol. Sci.* 68, 403-419.

Antkiewicz, D.S., Burns, C.G., Carney, S.A., Peterson, R.E., Heideman, W., 2005. Heart malformation is an early response to TCDD in embryonic zebrafish. *Toxicol. Sci.* 84, 368–377.

Antkiewicz, D.S., Peterson, R.E., Heideman, W., 2006. Blocking expression of AHR2 and ARNT1 in zebrafish larvae protects against cardiac toxicity of 2,3,7,8-tetrachlorodibenzo-*p*-dioxin. *Toxicol. Sci.* 94, 175-182.

Bartman, T., Walsh, E.C., Wen, K., McKane, M., Ren, J., Alexander, J., Rubenstein, P.A., Stainier, D.Y.R., 2004. Early myocardial function affects endocardial cushion development in zebrafish. *PLoS Biol.* 2, 673-681.

Bello, S.M., Heideman, W., Peterson, R.E., 2004. 2,3,7,8-Tetrachlorodibenzo-*p*-dioxin inhibits regression of the common cardinal vein in developing zebrafish. *Toxicol. Sci.* 78, 258-266.

Burns, F.R., Peterson, R.E., Heideman, W., 2015. Dioxin disrupts cranial cartilage and dermal bone development in zebrafish larvae. *Aquat. Toxicol.* 164, 52-60.

Cantrell, S.M., Lutz, L.H., Tillitt, D.E., Hannink, M., 1996. Embryotoxicity of 2,3,7,8-tetrachlorodibenzo-*p*-dioxin (TCDD): the embryonic vasculature is a physiological target for TCDD-induced DNA damage and apoptotic cell death in medaka (*Orizias latipes*). *Toxicol. Appl. Pharmacol.* 141, 23-34.

Carney, S.A., Chen, J., Burns, C.G., Xiong, K.M., Peterson, R.E., Heideman, W., 2006. Aryl hydrocarbon receptor activation produces heart-specific transcriptional and toxic responses in developing zebrafish. *Mol. Pharmacol.* 70, 549-561.

Choudhary, M., Kazmin, D., Hu, P., Thomas, R.S., McDonnell, D.P., Malek, G., 2015. Aryl hydrocarbon receptor knock-out exacerbates choroidal neovascularization via multiple pathogenic pathways. *J. Pathol.* 235, 101-112.

Crawford, L.W., Foley, J.F., Elmore, S.A., 2010. Histology atlas of the developing mouse hepatobiliary system with emphasis on embryonic days 9.5-18.5. *Toxicol. Pathol.* 38, 872-906.

Dong, W., Teraoka, H., Yamazaki, K., Tsukiyama, S., Imani, S., Imagawa, T., Stegeman, J.J., Peterson, R.E., Hiraga, T., 2002. 2,3,7,8-Tetrachlorodibenzo-*p*-dioxin toxicity in the zebrafish embryo: local circulation failure in the dorsal midbrain is associated with increased apoptosis. *Toxicol. Sci.* 69, 191-201.

Elonen, G.E., Sphear, R.L., Holcombe, G.W., Johnson, R.D., 1998. Comparative toxicity of 2,3,7,8-tetrachlorodibenzo-*p*-dioxin to seven freshwater species during early life-stage development. *Environ. Toxicol. Chem.* 17, 472-483.

Garcia de Vinuesa, A., Abdelilah-Seyfried, S., Knaus, P., Zwijsen, A., Bailly, S., 2016. BMP signaling in vascular biology and dysfunction. *Cytokine Growth Factor Rev.* 27, 65-79.

Gebala, V., Collins, R., Geudens, I., Phng, L., Gerhardt, H., 2016. Blood flow drives lumen formation by inverse membrane blebbing during angiogenesis *in vivo*. *Nat*. *Cell Biol*. 18, 443-450.

Gerhardt, H., Golding, M., Fruttiger, M., Ruhrberg, C., Lundkvist, A., Abramsson, A., Jeltsch, M., Mitchell, C., Alitalo, K., Shima, D., Betsholtz, C., 2003. VEGF guides angiogenic sprouting utilizing endothelial tip cell filopodia. *J*. *Cell Biol*. 161, 1163-1177.

Goi, M., Childs, S.J., 2016. Patterning mechanisms of the sub-intestinal venous plexus in zebrafish. *Dev*. *Biol*. 409, 114-128.

Guiney, P.G., Smolowitz, R.M., Peterson, R.E., Stegeman, J.J., 1997. Correlation of 2,3,7,8-tetrachlorodibenzo-*p*-dioxin induction of cytochrome P4501A in vascular endothelium with toxicity in early life stages of lake trout. *Toxicol*. *Appl*. *Pharmacol*. 143, 256-273.

Guiney, P.D., Walker, M.K., Spitsbergen, J.M., Peterson, R.E., 2000. Hemodynamic dysfunction and cytochrome P4501A mRNA expression induced by 2,3,7,8-tetrachlorodibenzo-*p*-dioxin during embryonic stages of lake trout development. *Toxicol*. *Appl*. *Pharmacol*. 168, 1-14.

Hankinson, O., 1995. The aryl hydrocarbon receptor complex. *Annu*. *Rev*. *Pharmacol*. *Toxicol*. 35, 307-340.

Henry, T.R., Spitsbergen, J.M., Hornung, M.W., Abnet, C.C., Peterson, R.E., 1997. Early life stage toxicity of 2,3,7,8-tetrachlorodibenzo-*p*-dioxin in zebrafish (*Danio rerio*). *Toxicol*. *Appl*. *Pharmacol*. 142, 56-68.

Hirashima, M., 2009. Regulation of endothelial cell differentiation and arterial specification by VEGF and Notch signaling. *Anat*. *Sci*. *Int*. 84, 95-101.

Hofsteen, P., Plavicki, J., Johnson, S.D., Peterson, R.E., Heideman, W., 2013. Sox9b is required for epicardium formation and plays a role in TCDD-induced heart malformation in zebrafish. *Mol*. *Pharmacol*. 84, 353-360.

Isogai, S., Horiguchi, M., Weinstein, B.M., 2001. The vascular anatomy of the developing zebrafish: an atlas of embryonic and early larval development. *Dev*. *Biol*. 230, 278-301.

Jones, E.A.V., 2011. Mechanical factors in the development of the vascular bed. *Respir*. *Physiol*. *Neurobiol*. 178, 59-65.

Jones, E.A.V., 2011. The initiation of blood flow and flow induced events in early vascular development. *Semin*. *Cell Dev*. *Biol*. 22, 1028-1035.

Kaufman, R., Weiss, O., Sebbagh, M., Ravid, R., Gibbs-Bar, L., Yaniv, K., Inbal, A., 2015. Development and origins of zebrafish ocular vasculature. *BMC Dev*. *Biol*. 15, 18.

Kikuchi, K., Holdway, J.E., Major, R.J., Blum, N., Dahn, R.D., Begemann, G., Poss, K.D., 2011. Retinoic acid production by endocardium and epicardium is an inquiry response essential for zebrafish heart regeneration. *Dev*. *Cell* 20, 397-404.

King-Heiden, T.C., Mehta, V., Xiong, K.M., Lanham, K.A., Antkiewicz, D.S., Ganser, A., Heideman, W., Peterson, R.E., 2012. Reproductive and developmental toxicity of dioxin in fish. *Mol*. *Cell*. *Endocrinol*. 354, 121-138.

Kitambi, S.S., McCulloch, K.J., Peterson, R.T., Malicki J.J., 2009. Small molecule screen for compounds that affect vascular development in the zebrafish retina. *Mech*. *Dev*. 126, 464-477.

Kocchan, E., Lenard, A., Ellertsdottir, E., Herwig, L., Affolter, M., Belting, H., Siekmann, A.F., 2013. Blood flow changes coincide with cellular rearrangements during blood vessel pruning in zebrafish embryos. *PLoS One* 8, e75060.

Koenig, A.L., Baltrunaite, K., Bower, N.I., Rossi, A., Stainier, D.Y.R., Hogan, B.M., Sumanas, S., 2016. Vegfa signaling promotes zebrafish intestinal vasculature development through endothelial cell migration from the posterior cardinal vein. *Dev*. *Biol*. 411, 115-127.

Lahvis, G.P., Lindell, S.L., Thomas, R.S., McCuskey, R.S., Murphy, C., Glover, E., Bentz, M., Southard, J., Bradfield, C.A., 2000. Portosystemic shunting and persistent fetal vascular structures in aryl hydrocarbon receptor-deficient mice. *Proc*. *Natl*. *Acad*. *Sci*. *U.S.A*. 97, 10442-10447.

Lawson, N.D., Weinstein, B.M., 2002. *In vivo* imaging of embryonic vascular development using transgenic zebrafish. *Dev*. *Biol*. 248, 307-318.

Lenard, A., Daetwyler S., Betz, C., Ellertsdottir, E., Belting, H., Huisken, J., Affolter, M., 2015. Endothelial cell self-fusion during vascular pruning. *PLoS Biol*. 3, e1002126.

Li, M.X., Beech-Brandt, J.J., John, L.R., Hoskins, P.R., Easson, W.J., 2007. Numerical analysis of pulsatile blood flow and vessel wall mechanics in different degrees of stenoses. *J. Biomech*. 40, 3715-3724.

Mehta, V., Peterson, R. E., and Heideman, W., 2008. 2,3,7,8-Tetrachlorodibenzo-*p*-dioxin exposure prevents cardiac valve formation in developing zebrafish. *Toxicol. Sci*. 104, 303-311.

Pandey, R., Botros, M.A., Nacev, B.A., Albig, A.R., 2015. Cyclosporin A disrupts notch signaling and vascular lumen maintenance. *PLoS One* 10, e0119279.

Plavicki, J.S., Hofsteen, P., Yue, M.S., Lanham, K.A., Peterson, R.E., Heideman, W. 2014. Multiple modes of proepicardial cell migration require heartbeat. *BMC Dev*. *Biol*. 14, 18.

Prasch, A.L., Tanguay, R.L., Mehta, V., Heideman, W., Peterson, R.E., 2006. Identification of zebrafish ARNT1 homologs: 2,3,7,8-tetrachlorodibenzo-*p*-dioxin toxicity in the developing zebrafish requires ARNT1. *Mol*. *Pharmacol*. 69, 776-787.

Prasch, A.L., Teraoka, H., Carney, S.A., Dong, W., Hiraga, T., Stegeman, J.J., Heideman, W., Peterson, R.E., 2003. Aryl hydrocarbon receptor 2 mediates 2,3,7,8-tetrachlorodibenzo-*p*-dioxin developmental toxicity in zebrafish. *Toxicol*. *Sci*. 76, 138-150.

Puga, A., Ma, C., Marlowe, J.L., 2009. The aryl hydrocarbon receptor cross-talks with multiple signal transduction pathways. *Biochem*. *Pharmacol*. 77, 713-722.

Schmidt, J. V., Bradfield, C.A., 1996. Ah receptor signaling pathways. *Annu*. *Rev*. *Cell Dev*. Biol. 12, 55-89.

Sehnert, A.J., Huq, A., Weinstein, B.M., Walker, C., Fishman, M., Stainier, D.Y.R., 2002. Cardiac troponin T is essential in sarcomere assembly and cardiac contractility. *Nat*. *Genet*. 31, 106-10.

Spitsbergen, J.M., Walker, M.K., Olson, J.R., Peterson, R.E., 1991. Pathologic alterations in early life stages of lake trout, *Salvelinus namaycush*, exposed to 2,3,7,8-tetrachlorodibenzo-*p*-dioxin as fertilized eggs. *Aquat. Toxicol*. 19, 41-72.

Teraoka, H., Ogawa, A. Kubota, A., Stegeman, J.J., Peterson, R.E., Hiraga, T., 2010. Malformation of certain brain blood vessels caused by TCDD activation of Ahr2/Arnt1 signaling in developing zebrafish. *Aquat*. *Toxicol*. 99, 241-247.

Toomey, B.H., Bello, S., Hahn, M.E., Cantrell, S., Wright, P., Tillitt, D.E., Di Giulio, R.T., 2001. 2,3,7,8-Tetrachlorodibenzo-*p*-dioxin induces apoptotic cell death and cytochrome P4501A expression in developing *Fundulus heteroclitus* embryos. *Aquat*. *Toxicol*. 53, 127-138.

Traver, D., Paw, B.H., Poss, K.D., Penberthy, W.T., Lin, S., Zon, L.I., 2003. Transplantation and in vivo imaging of multilineage engraftment in zebrafish bloodless mutants. *Nat*. *Immunol*. 4, 1238-1246.

Walker, M.K., Peterson, R.E., 1994. Aquatic toxicity of dioxins and related chemicals, *in*: Schecter, A. (Ed.), *Dioxins and Health*. Plenum Press, New York, pp. 347-387.

Westerfield, M., 2000. The Zebrafish Book. A Guide for the Laboratory Use of Zebrafish (*Danio rerio*), fourth ed. Univ. of Oregon Press, Eugene, OR.

Wilkinson, R. N., van Eeden, F. J., 2014. The zebrafish as a model of vascular development and disease. *Prog. Mol. Biol. Transl. Sci*. 124, 93-122.

Xiong, K.M., Peterson, R.E., Heideman, W., 2008. Aryl hydrocarbon receptor-mediated down-regulation of sox9b causes jaw malformation in zebrafish embryos. *Mol. Pharmacol*. 74, 1544-1553.

Yamauchi, M., Kim, E., Iwata, H., Shima, Y., Tanabe, S., 2006. Toxic effects of 2,3,7,8-tetrachlorodibenzo-*p*-dioxin (TCDD) in developing red seabream (*Pagrus major*) embryo: an association of morphological deformities with AHR1, AHR2 and CYP1A expressions. *Aquat. Toxicol*. 80, 166-179.

Yue, M.S., Peterson, R.E., Heideman, W., 2015. Dioxin inhibition of swim bladder development in zebrafish: is it secondary to heart failure? *Aquat. Toxicol*. 162, 10-17.

Zeng, L., Childs, S.J., 2012. The smooth muscle microRNA miR-145 regulates gut epithelial development via a paracrine mechanism. *Dev. Biol*. 367, 178–186.

Zhong, H., Wang, D., Wang, N., Rios, Y., Huang, H., Li, S., Wu, X., Lin, S., 2011. Combinatory action of VEGFR2 and MAP kinase pathways maintains endothelial-cell integrity. *Cell Res*. 21, 1080-1087.

SUMMARY

TCDD and other DLCs are global environmental contaminants that cause developmental toxicity in fish and other vertebrate species (Peterson *et al.*, 1993). Fish embryos exposed to DLCs develop an edematous syndrome known as blue sac disease, characterized by pericardial and yolk sac edema, craniofacial malformations, hemorrhage, spinal deformities, congestion of peripheral blood flow, stunted growth, and increased mortality. Previous work has shown that TCDD toxicity is AHR-mediated (Poland *et al*., 1976; Hankinson, 1995; Schmidt and Bradfield, 1996) and in zebrafish involves activation of AHR2/ARNT1 (Prasch *et al*., 2003, 2006; Antkiewicz *et al*., 2006).

A major endpoint of TCDD-induced blue sac disease in fish embryos is cardiotoxicity. In the zebrafish embryo, exposure to TCDD causes decreased heart size, heart un-looping, ventricular compaction, elongation of the atrium, inhibition of valve formation, reduced development of the bulbus arteriosus, reduced heart rate, and decreased cardiac output culminating in ventricular standstill and circulatory collapse (Henry *et al*., 1997; Belair *et al*., 2001; Antkiewicz *et al*., 2005, 2006; Carney *et al*., 2006; Mehta *et al*., 2008; King-Heiden *et al*., 2012). Considering the importance of cardiovascular function in embryonic development, it was initially proposed that many of the adverse effects associated with blue sac disease were secondary to defects in cardiovascular development and function. However, some of the observed phenotypes result from direct action of TCDD on the affected tissues. For instance, several studies have shown that reduced growth of the lower jaw following exposure to TCDD is most likely due to TCDD-induced effects on chondrogenesis and cartilage deposition as opposed to ancillary effects from alterations in regional blood flow (Teraoka *et al*., 2006; Xiong *et al*., 2008; Planchart and Mattingly, 2010; Burns *et al*., 2015). Candidate genes that are misregulated by TCDD exposure and likely

involved in the development of craniofacial malformations have been identified and include *sox9b* and *foxQ1b* (Xiong *et al*., 2008; Planchart and Mattingly, 2010; Burns *et al*., 2015).

A hallmark of TCDD and DLC toxicity is the lack of an inflated swim bladder, which has been reported in multiple fish species (Henry *et al*., 1997; Elonen *et al*., 1998; Oritz-Delagado *et al*., 2004; King-Heiden *et al*., 2012). It was assumed that this effect resulted from TCDD-induced cardiotoxicity, however this has never been fully investigated. In light of revelations regarding the mechanism of TCDD-induced jaw malformation, work in Chapter II focused on the mechanism of failed swim bladder inflation.

To understand the progression of TCDD-induced effects on the swim bladder, zebrafish embryos were exposed to TCDD at 4 hpf and assessed at 48, 72, 96, and 120 hpf. TCDD did not affect swim bladder development up to 72 hpf: swim bladder bud initiation from the gut, elongation to form the pneumatic duct, and initial growth of the swim bladder chamber occurred normally despite TCDD exposure. However, after 72 hpf development of the swim bladder was arrested, such that by 120 hpf it was smaller than in DMSO control embryos of the same age. In addition, gross morphology of the TCDD-exposed swim bladder at 120 hpf was similar to that at 72 hpf, including a thick chamber wall and lack of inflation. To determine if there was a window of development where the swim bladder was most sensitive to TCDD, embryos were exposed at 4, 24, 48, 72, and 96 hpf, and swim bladder development was assessed at 120 hpf. Embryos exposed to TCDD between 4 and 48 hpf developed swim bladders at 120 hpf that were similar, smaller than control, and with a gross morphology comparable to a control swim bladder at 72 hpf. In embryos exposed to TCDD at 96 hpf, swim bladder development progressed normally and was similar in size and morphology to control. Embryos exposed to TCDD at 72 hpf developed swim bladders at 120 hpf that had an intermediate phenotype: smaller than control, but not as severe as the phenotype in embryos exposed to TCDD between 4 and 48 hpf. Together, these experiments highlight the “growth/elongation phase” of swim bladder development, 65-96 hpf, as the most sensitive to

disruption caused by TCDD. The mesenchymal and mesothelial layers of the swim bladder form at this time, and crosstalk between these layers and the epithelial layer of the initial swim bladder bud are necessary for normal growth and organization of the organ (Winata *et al*., 2009; Yin *et al*., 2011). It is important to note that this window of sensitivity coincides with the onset of TCDD-induced loss of circulation (Henry *et al*., 1997; Antkiewicz *et al*., 2006) and previous reports have indicated that normal circulation is an important factor for swim bladder development (Winata *et al*., 2010). Thus, to determine if the TCDD-induced effects on the swim bladder were secondary to TCDD-induced decreases in blood flow, swim bladder development in embryos with impaired cardiac function was also examined. To simulate TCDD-induced cardiotoxicity, transient transgenic embryos expressing cardiomyocyte-specific constitutively active AHR signaling (*cmlc2*:caAHR) were used. These *cmlc2*:caAHR embryos phenocopied several TCDD-induced toxic endpoints, including cardiac dysfunction and loss of circulation (Lanham *et al*., 2014). In addition to the *cmlc2*:caAHR embryos, *silent heart* (*sih*) morphants, which never develop a heartbeat or circulation, were also assessed (Sehnert *et al*., 2008). Both the *cmlc2*:caAHR transient transgenic embryos and the *sih* morphants had impaired swim bladder development that progressed temporally in a manner similar to that observed in TCDD-exposed embryos. In all treatments swim bladder bud initiation and elongation occurred normally but beyond 72 hpf development was arrested, resulting in an un-inflated swim bladder at 120 hpf. Furthermore, the size and morphology of swim bladders from the three treatment groups −TCDD, *cmlc2*:caAHR, and *sih* morphant− were similar at 120 hpf. Overall, these experiments demonstrated that TCDD-induced loss of circulation was sufficient to arrest development of the swim bladder and inhibit inflation.

Recent studies have identified the epicardium in the heart as a target of TCDD toxicity and zebrafish embryos exposed to TCDD do not form an epicardium (Plavicki *et al*., 2013; Hofsteen *et al*., 2013b). The onset of TCDD-induced cardiac dysfunction and several cardiac malformations coincides

with the window of epicardial development, implying that these cardiac defects may be due to lack of epicardium formation (Plavicki *et al*., 2013; Hofsteen *et al*., 2013b). However, the development of the epicardium in zebrafish embryos is poorly understood. Similar to the chick and mouse, in zebrafish the epicardium is derived from a pool of extracardiac progenitors, called the proepicardium (PE) (Komiyama *et al*., 1987; Männer, 1992; Nahirney *et al*., 2003; Rodgers *et al*., 2008; Serluca, 2008). During early development, PE cells migrate onto the heart, spreading over the myocardium and eventually enveloping the heart entirely (Serluca, 2008). The mechanisms that direct PE migration and spreading in zebrafish are unknown. To better understand this process, Chapter III focused on characterizing the steps involved in PE cell migration in zebrafish embryos. In zebrafish, PE cells were observed migrating via two mechanisms: 1) formation of a cellular bridge between the PE on the pericardial wall and the heart myocardium, and 2) release of free-floating PE cell clusters into the pericardial space that land and attach onto the myocardium. Similar modes of PE migration have been observed in other species, including chick, mouse, and axolotl (Komiyama *et al*., 1987; Fransen and Lemanski, 1990; Nahirney *et al*., 2003). In zebrafish, epicardial progenitors began migrating at approximately 60 hpf, first spreading over the ventricle followed by the atrium, and covering most of the heart by 120 hpf. It was also observed that the epicardium consists of a heterogeneous population of cells. To determine if heartbeat influenced PE formation and/or epicardial development, different stages of PE/epicardial development were assessed in embryos with inhibited heartbeat. These included *sih* morphants and embryos raised in 2,3-butanedione 2-monoxime (BDM), a pharmacological agent that inhibits heart contraction (Bartman *et al*., 2004; Sehnert *et al*., 2008). In both *sih* morphants and BDM-treated embryos PE clusters were observed forming along the pericardial wall. However, these PE cells were unable to migrate. Even at 120 hpf no epicardial cells were observed on the myocardium of hearts that lacked heartbeat. Thus, while the PE specification and clustering occurs independent of heartbeat, heart contraction is required for migration of PE cells. This was counter to what was previously proposed by Peralta *et al*., (2013), namely, that pericardial fluid

forces driven by heartbeat were required for PE cluster formation and epicardial spreading. To determine if this was the case, embryonic hearts were isolated and raised in culture under conditions that paralleled *in vivo* experiments. Using an *in vitro* culture approach, it was observed that epicardial cells could proliferate and spread over a beating heart, forming an epicardium, in the absence of pericardial fluid forces. In contrast, this did not occur when contraction of the isolated hearts was inhibited with BDM. Furthermore, epicardial cells from a normal heart were able to migrate onto and spread over the myocardium of a neighboring heart *in vitro*. However, similar migration did not occur when the neighboring heart was non-contractile (e.g., heart from a *sih* morphant). Based on results presented in Chapter III a paradigm of zebrafish epicardium development was constructed: 1) PE cells form clusters along the pericardial wall in a process that is independent of heartbeat; 2) beginning at approximately 60 hpf, PE cells migrate to the heart via formation of a cellular bridge, or by releasing cell aggregates, in a process that requires heart contractility; 3) PE cells on the heart proliferate and spread over the ventricle and then the atrium, eventually enveloping the heart and forming the epicardium, in a process that also requires heart contraction.

The assay used to assess migration of epicardial cells *in vitro*, presented in Chapter III, was developed further (Chapter IV) to improve precision and address current logistical challenges in the study of epicardial development. A major obstacle in this area of research is the lack of a PE/epicardial-specific genetic marker. Most common markers of the epicardial lineage, including *Wt1*, *Tbx18*, and *Tcf21*, are expressed in tissues outside the heart during development, including the liver, kidney, pectoral fin mesenchyme, developing palate, and pharyngeal arches (Drummond *et al*., 1998; Serluca and Fishman, 2001; Begemann *et al*., 2002; Lee *et al*., 2011). Thus, using any of these epicardial markers in genetic manipulation experiments *in vivo* could cause unintended off-target effects that may confound interpretation of results. In addition, findings from Chapter III revealed that the epicardium consists of a

heterogeneous population of cells and do not express these known epicardial markers uniformly (e.g., *Tcf21*). Thus, to completely target epicardial cells with a desired transgene, a complex intersectional gene expression approach is required (e.g., using dual recombinases to target cells that are both *Tcf21*+ and *Tbx18*+). As a result of these challenges, several studies have explored *in vitro* approaches that use epicardial cells in culture. However, most of these *in vitro* approaches involve monolayer cell cultures that ignore important cell-cell interactions that occur between migrating epicardial cells and the myocardial cells beneath them; crosstalk between these neighboring layers in the heart are known to play an important role in normal heart development (Weeke-Klimp *et al*., 2010; Gittenberger-deGroot *et al*., 2012; Brade *et al*., 2013; Takahashi *et al*., 2014).

The assay presented in Chapter IV offers a method to assess epicardial migration *in vitro* while maintaining important cell-cell interactions by using whole embryonic hearts. To demonstrate proof of concept, the assay was used to assess whether epicardial cells could migrate onto a heart deficient in *tbx5* expression. Although *tbx5* is expressed in myocardial and epicardial tissues, studies have heretofore only focused on the role of epicardial *tbx5* expression during heart development. In zebrafish, *tbx5a* is required for PE specification in a process that involves BMP signaling (Liu and Stainier, 2010). In chick, epicardial *tbx5* expression is tightly regulated in time with migration of epicardial cells (Hatcher *et al*., 2004). Here it was demonstrated that loss of myocardial *tbx5* expression is sufficient to significantly reduce epicardial migration *in vitro*. As another proof of concept, and in accordance with results reported in Chapter III, the *in vitro* assay confirmed that myocardial contraction (i.e., heartbeat) was required for epicardial migration to occur. This *in vitro* epicardial migration assay provides a useful tool for investigating how target genes or signaling pathways in specific cell types in the heart affect migration of epicardial progenitor cells.

Previous work has shown that TCDD causes AHR activation in the vasculature of zebrafish embryos early in development, preceding the onset of toxicity (Andreasen *et al*., 2002b). Several studies have also demonstrated that TCDD exposure can affect the development of specific vascular structures in fish embryos. For example, TCDD exposure causes regression of the yolk vasculature in medaka (Kawamura *et al*., 2002), inhibits growth and regression of the common cardinal vein in zebrafish (Bello *et al*., 2004), and causes regional repression of blood flow and rearrangements in shape of the prosencephalic vein in the dorsal midbrain of zebrafish (Teraoka *et al*., 2010). Together these findings indicate that the vasculature is likely a key target of TCDD toxicity. Furthermore, studies in mouse suggest that AHR signaling is involved in normal vascular development (Lahvis *et al*., 2000; Choudhary *et al.*, 2015). Thus, since TCDD induces toxicity via activation of AHR signaling it seems likely that direct effects on vascular development would be observed following exposure to TCDD.

Ahr null mice have abnormal vascular development in the eye and the liver, displaying fetal vascular structures that are improperly remodeled (Lahvis *et al*., 2000; Choudhary *et al.*, 2015). In Chapter V, parallel vascular structures were examined and characterized in zebrafish embryos exposed to TCDD. In the eye, TCDD exposure inhibited closure of the superficial annular vessel (SAV) at 72 hpf and altered SAV vessel morphology, appearing rough in texture with a meandering shape. In addition, vessel thickness was highly variable, with the luminal space appearing dilated or constricted at different points along the vessel length. In zebrafish, the subintestinal venous plexus (SIVP) is involved in the transfer of nutrients during early development and later undergoes remodeling, contributing to both hepatic and intestinal vasculature (Isogai *et al*., 2001). In embryos exposed to TCDD, the SIVP became overgrown and mis-patterned, indicating improper remodeling. To determine if circulation, which is reduced by TCDD exposure, was influencing the development of these vascular structures the SAV and SIVP were examined at 72 hpf in positive control embryos with inhibited blood flow to see if the same

effects of TCDD could be recapitulated. Blood flow was inhibited in positive control embryos using two methods: 1) injection of *sih* morpholino oligonucleotide and 2) exposure to BDM. To simulate TCDD-induced reductions in circulation, embryos were exposed to BDM beginning at 60 hpf when TCDD causes decreases in cardiac output (Antkiewicz *et al*., 2006). In the eye, the SAV failed to close in both *sih* morphants and BDM-treated embryos, suggesting that this effect was indeed secondary to TCDD-induced decreases in blood flow. However, other effects in the SAV and SIVP were not recapitulated in *sih* morphants or BDM-treated embryos. Unlike TCDD-treated embryos, morphology of the SAV in *sih* morphants and BDM-treated embryos appeared smooth, dense, and lacked a visible lumen. In addition, the SIVP in *sih* morphants and BDM-treated embryos was either slightly reduced in size or not significantly different from controls and was generally patterned normally. Overall this suggested that TCDD-induced alterations in SAV vessel morphology, and the excessive growth and mis-patterning of the SIVP are unlikely secondary effects of TCDD-induced loss of circulation. Instead, these findings indicate that TCDD exposure and/or activation of AHR may interfere with signaling pathways involved in vascular maintenance and growth, such as Vegf or BMP signaling (Koenig *et al*., 2016; Goi and Childs, 2016).

FUTURE DIRECTIONS

Does AHR activation in the vasculature cause toxicity?

Understanding the mechanisms behind TCDD-induced toxicity can offer insight into the role of AHR signaling during development and how aberrant activation of this pathway can contribute to the development of congenital diseases. Part of understanding the mechanisms of TCDD-induced toxicity includes identifying which cell types are primary targets. This can be challenging due to the nature of

TCDD and the broad expression of AHR in essentially all cells of vertebrate organisms (Hankinson, 1995). It is not possible to limit TCDD exposure to specific tissues. In zebrafish, TCDD exposure causes global activation of AHR. Although induction of CYP1A can suggest likely key targets of TCDD, this is at best correlative information (Andreasen *et al*., 2002b). Fortunately, advances in zebrafish genetic tools allows for increasingly precise approaches to help distinguish where TCDD exerts toxic effects. One such tool is the constitutively activated AHR (caAHR$^{ZF/M}$) construct developed by Dr. Lanham (Lanham *et al*., 2014). This construct is a fusion of the zebrafish AHR2 DNA binding and dimerization domains with the transcriptional activation domain of a constitutively active mutant mouse Ahr^{b1} receptor (McGuire *et al*., 2001). Heart-specific caAHR signaling can be achieved by using the cardiomyocyte-specific *cmlc2* promoter to drive expression of the caAHR$^{ZF/M}$ construct (*cmlc2*:caAHR$^{ZF/M}$) in the zebrafish embryo. This resulted in phenocopying many TCDD-induced toxic endpoints, including pericardial and yolk sac edema, heart malformations, reduction of peripheral blood flow, and eventual circulatory collapse (Lanham *et al*., 2014), thus indicating that the myocardium is a major target of TCDD. Overexpression of wild-type zebrafish AHR2 can also produce agonist-independent activity (Abnet *et al*., 1999; Tanguay *et al*., 1999; Andreasen *et al*., 2002a). As such, cardiomyocyte-specific over-expression of AHR2 (*cmlc2*:AHR2) also resulted in TCDD-like cardiotoxicity, although the resultant phenotype was milder than that of *cmlc2*:caAHR or TCDD treatment groups. Although cardiomyocyte-specific activation of AHR signaling recapitulated many TCDD developmental toxicity endpoints, hemorrhaging was not observed in *cmlc2*:caAHR or *cmlc2*:AHR2 embryos. Hemorrhaging is a hallmark of TCDD toxicity and blue sac disease in fish embryos (Henry *et al*., 1997; Elonen *et al*., 1998; King-Heiden *et al*., 2012). Several studies have implicated the vascular endothelium as a site of TCDD-induced AHR activity but how this may contribute to specific endpoints of TCDD toxicity is still unknown (Cantrell *et al*., 1996; Hornung *et al*., 1999; Guiney *et al*., 2000; Andreasen *et al*., 2002b; Dong *et al*., 2002).

In order to determine whether activation of AHR signaling in endothelial cells mediates the hemorrhaging phenotype in TCDD-exposed fish it is necessary to investigate what happens when AHR signaling is activated only in endothelial cells. This can be achieved by using an endothelial-specific promoter, such as *kdrl*, to drive expression of caAHR$^{ZF/M}$ or overexpression of wild-type AHR2 in the developing vasculature. Some headway has already been made in this area, and *kdrl*:caAHR and control *kdrl*:caAHR^{-dbd} constructs have been made (Figure 1A). In the study by Lanham *et al*. (2014), transient expression *cmlc2*:caAHR$^{ZF/M}$ was sufficient to elicit caAHR signaling and cause toxicity. However, injections of the *kdrl*:caAHR and control *kdrl*:caAHR^{-dbd} constructs to make transient transgenics were not successful due to very poor expression. This is likely because transient experiments produce mosaic expression. In addition, the vascular endothelium consists of a large number of cells spread across the entire embryo, and therefore mosaic expression of the injected construct would likely be "diluted."

In order to guarantee broad and uniform expression of the desired constructs in the endothelium it is necessary to establish stable transgenic lines. Lanham *et al*., (2014) reported that it was not feasible to establish stable transgenic lines of *cmlc2*:caAHR zebrafish because founders died of cardiovascular failure and the few individuals that survived had very low fecundity. It is probable that full expression of endothelial-specific caAHR would make it difficult or impossible to generate stable transgenic lines. Therefore, an alternate transgenic approach, such as utilizing the Gal4/UAS system (Figure 1B) or Tet-On system (Figure 1C), is a better strategy. Using this approach, one transgenic line is generated in which yeast Gal4 is expressed under the control of an endothelial-specific promoter (*kdrl*:Gal4). In a complimentary transgenic line, the upstream activating sequence of Gal4, UAS, drives expression of caAHR (or other desired constructs like caAHR^{-dbd}, AHR2, etc.) and a reporter (2A-EGFP). In the absence of Gal4, expression of caAHR does not occur, thereby avoiding toxicity that may inhibit establishment of a stable transgenic line. Crossing the Gal4 and UAS lines results in offspring that carry

both the *kdrl*:Gal4 and UAS:caAHR, leading to endothelial-specific expression of caAHR (and reporter) (Figure 1B). A parallel set of transgenic lines can be established using the Tet-On system. Similar to the Gal4/UAS system, one line provides endothelial specificity (e.g., *kdrl*:rtTA) and the other complimentary line contains the caAHR construct (e.g., TRE:caAHR) (Figure 1C). In addition to tissue-specificity, the Tet-On system also offers temporal control of transgene expression. In the Tet-On system, rtTA protein will only bind to the complimentary TRE sequence in the presence of doxycycline, which can be added to the zebrafish water at the experimenter's discretion. An example of a 3 dpf embryo from crossing potential founder *kdrl*:rtTA and TRE:caAHR fish is shown in (Figure 2), where doxycycline was added shortly after fertilization. Expression of caAHR, indicated by the EGFP reporter, is confined to the vasculature, which is marked by *kdrl*:DsRed2.

Different Gal4 or rtTA lines can also be crossed with respective UAS or TRE lines to investigate the effects of caAHR signaling and/or AHR2 over-expression in other tissues besides the vascular endothelium. For example, several studies have already used Gal4 in combination with the neuronal marker *elavl3/HuC* (Akerboom *et al*., 2012), the glial marker *gfap* (Shimizu *et al*., 2015), and the liver marker *fabp1a* (Nath *et al*., 2015). Together, these transgenic lines provide powerful tools to explore the effects of activated AHR signaling in a variety of tissues and at specific stages of development.

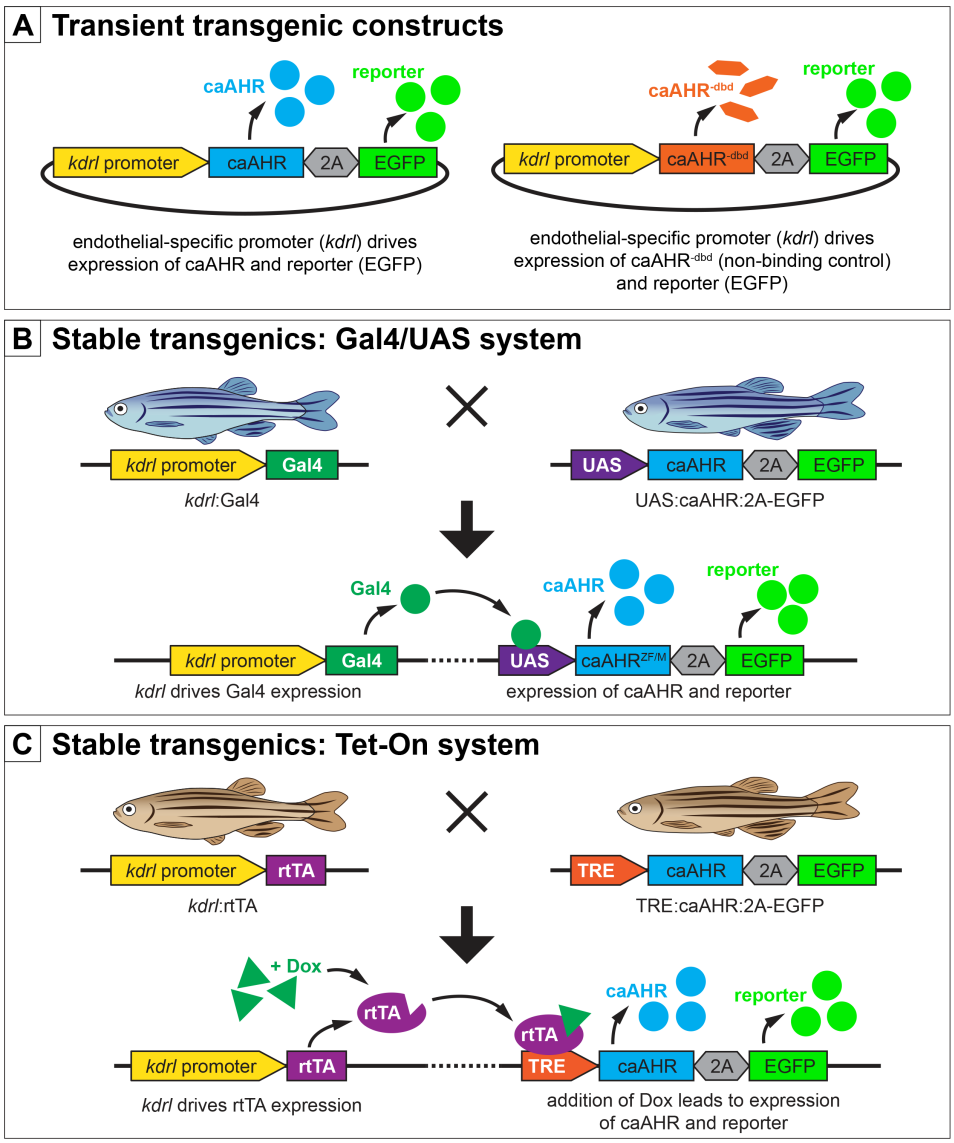

Figure 1. Schematic of transient and stable transgenic constructs for endothelial-specific expression of constitutively activated AHR (caAHR)

(A) Diagram of plasmid constructs for producing transient transgenic embryos. The *kdrl* promoter drives expression of caAHR (left), with a reporter (2A-EGFP), or a nonbinding control version of caAHR^{-dbd} (right), with a reporter (2A-EGFP). (B) Schematic describing stable transgenic lines utilizing the

Gal4/UAS system. In one line the *kdrl* promoter drives expression of Gal4. In the other complimentary line, the UAS promoter drives expression of caAHR and a reporter (2A-EGFP). Crossing these two lines produces offspring that have endothelial-specific expression of both caAHR and a reporter protein. (C) Schematic describing stable transgenic lines utilizing the Tet-On system. Similar to the Gal4/UAS system, in one line the *kdrl* promoter drives expression of rtTA, while in the other line the TRE promoter drives expression of caAHR and a reporter (2A-EGFP). Offspring from crossing these two lines produce embryos that have endothelial-specific expression of caAHR signaling and reporter protein when doxycycline (Dox) is present. The Tet-On system allows for temporal as well as spatial control of caAHR expression.

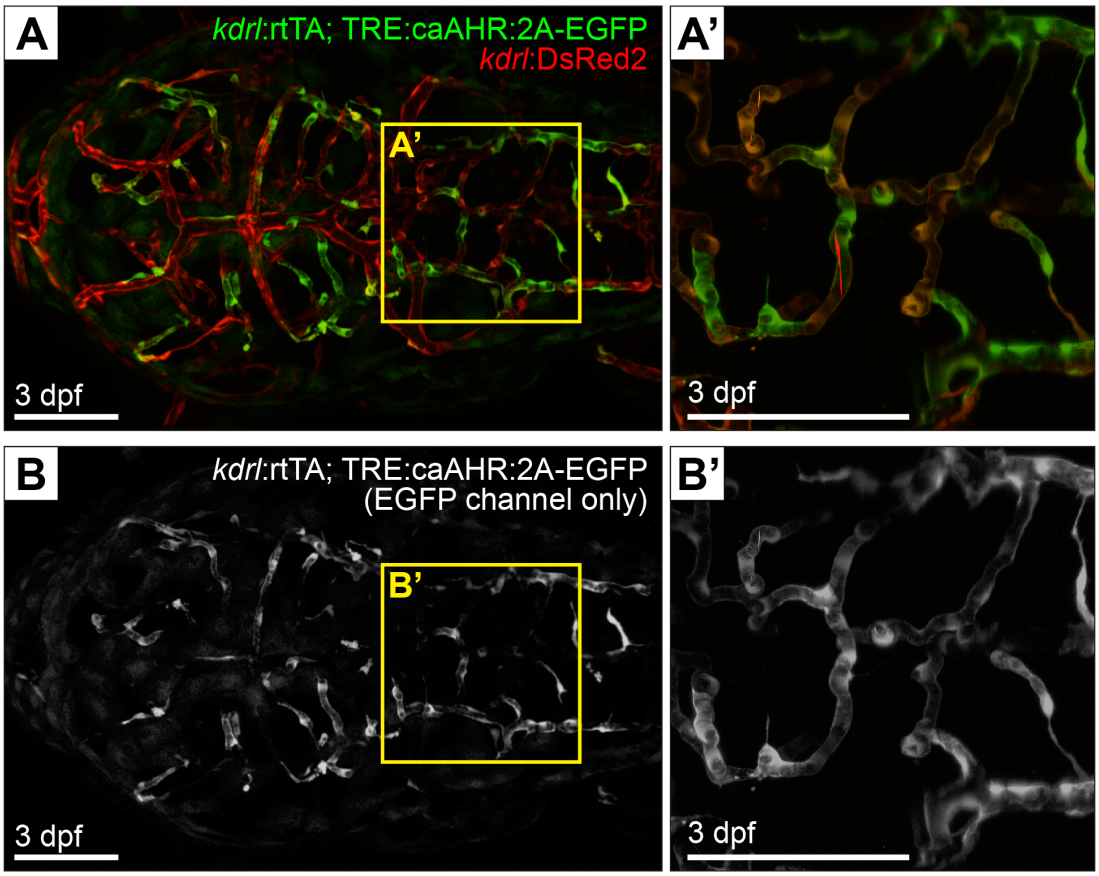

Figure 2. Endothelial-specific caAHR expression in a *kdrl*:rtTA; TRE:caAHR:2A-EGFP embryo

Offspring from crossing potential founder *kdrl*:rtTA and TRE:caAHR:2A-EGFP fish, with *kdrl*:DsRed transgenic background. Embryo was exposed to doxycycline beginning at 4 hpf and was assessed at 3 dpf for expression of the caAHR transgene, marked by EGFP expression. Images are maximum intensity projections from a confocal z-series collected *in vivo* using an inverted Nikon A1R scanning laser confocal microscope and analyzed using NIS-Elements AR4.30 software. (A', B') Higher magnification images of boxes in (A) and (B), respectively. (A-A') caAHR expression (green) is visible in blood vessels of the brain (red). (B-B') Green channel views of (A-A'), respectively. All images are orientated dorsally with anterior to the left. Scale bars = 100 μm.

Does TCDD have a direct effect on the swim bladder?

It is important to note that the work in Chapter II provides evidence that TCDD-induced cardiac dysfunction is sufficient to inhibit swim bladder inflation, however, this does not preclude the possibility that TCDD could also have direct effects on the swim bladder itself that contribute to swim bladder toxicity. Recently, a zebrafish CYP1A reporter line was developed (Kim *et al*., 2013). When exposed to TCDD the swim bladder was highlighted as an active site of CYP1A activity and, therefore, also a likely site of AHR activation (Kim *et al*., 2013). A tissue-specific approach is required in order to fully investigate whether the observed CYP1A expression reflects AHR-mediated gene misregulation leading to arrested swim bladder development. Similar to the strategy proposed for assessing the vascular endothelium as a target, one could assess the effects of AHR activation on the developing swim bladder by generating embryos expressing swim bladder-specific caAHR signaling or over-expression of AHR2. If TCDD is indeed exerting direct effects on the swim bladder then it is expected that the swim bladder-caAHR/AHR2 embryos would exhibit TCDD-like toxicity of the swim bladder: arrested development during the growth/elongation phase, thick chamber wall morphology, and lack of inflation by 120 hpf. Unfortunately, a swim bladder-specific marker has not yet been identified, although two enhancer-trap reporter lines exist (Winata *et al*., 2009). It is possible that these lines could be used in combination with non-specific swim bladder markers (e.g., *fgf10a*, *acta2*, *anxa5b*) in an intersectional gene expression approach to achieve the desired swim bladder-specific expression (Winata *et al*., 2009).

How does TCDD exposure and AHR2 activation interfere with vascular development in the eye and gut?

Work in Chapter V suggests that several of the TCDD-induced defects in the developing vasculature of the eye and gut are not secondary effects of TCDD-induced cardiac dysfunction. Studies have highlighted the roles of both Vegf and BMP signaling in vascular development, especially in the

SIVP (Koenig *et al.*, 2016; Goi and Childs, 2016). These signaling pathways should be investigated as potential targets of TCDD-induced AHR2-mediated toxicity. Inappropriately increased expression of Vegf signaling components (e.g., *vegfaa*/*b*, *vegfc*, *kdrl*) and BMP (e.g., *bmp4*) could lead to the overgrowth and mis-patterned phenotype observed in the SIVP of TCDD-exposed embryos. Expression patterns could be assessed using whole mount *in situ* hybridization and overall expression levels quantified using qRT-PCR. A zebrafish BMP activity reporter line has been developed by Dr. Hill and would be useful for assessing BMP signaling trends in the SIVP of TCDD-exposed fish (Wu *et al*., 2011). In addition, endothelial-specific caAHR or AHR2 transgenic fish lines could be utilized to examine whether the TCDD-induced effects in the eye and SIVP are truly independent of alterations in blood flow. If this is indeed the case, then endothelial-specific caAHR or AHR2 signaling would recapitulate the same vascular defects as in TCDD-exposed embryos.

How does TCDD exposure and AHR2 activation interfere with epicardial cell migration in the heart?

It was reported by Lanham *et al*. (2014) that *cmlc2*:caAHR zebrafish lacked an epicardium. Interestingly, it was also observed that *cmlc2*:caAHR zebrafish develop PE clusters, however these PE cells do not migrate to the heart (Plavicki and Lanham, unpublished data). Both myocardial caAHR expression and loss of cardiac contraction are sufficient to inhibit migration of epicardial cells, however, the mechanism preventing migration is unknown. Using scanning electron microscopy (SEM), high magnification images of isolated control and TCDD-treated zebrafish hearts indicate that the myocardial surface of the heart is altered by TCDD exposure (Figure 3). TCDD is known to down-regulate expression of *sox9b* in the heart and jaw, which is a transcription factor that influences deposition of extracellular matrix (ECM) (Hofsteen *et al*., 2013a; Xiong *et al.*, 2008; Burns *et al.*, 2015). Thus, one could investigate whether altered expression of key ECM components in the myocardium affects

epicardial cell migration, both *in vivo* with morpholino oligonucleotide injections, or *in vitro* using the assay developed in Chapter IV. Work in Chapter IV demonstrated that myocardial *tbx5* expression is an important factor in epicardial cell migration. Other genes of interest could be similarly investigated, including: α4-integrin and VCAM1, a receptor-ligand pair essential for PE budding and migration in mouse (Sengbush *et al*., 2002); PDGFα, which is involved in heart development in the chick and affects epicardial migration in the mouse (Bax *et al*., 2009, 2010); and PDGFRβ, which has been shown to promote cell migration in mouse (Mellgren *et al*., 2008).

Even though TCDD toxicity and AHR biology has been the focus of decades of research, there are still many questions left un-answered. Advances in genetic approaches and technology have enabled increasingly precise methods to investigate the mechanisms of AHR signaling and its role in development and toxicity. Future work will continue to improve our understanding of this complex but important pathway.

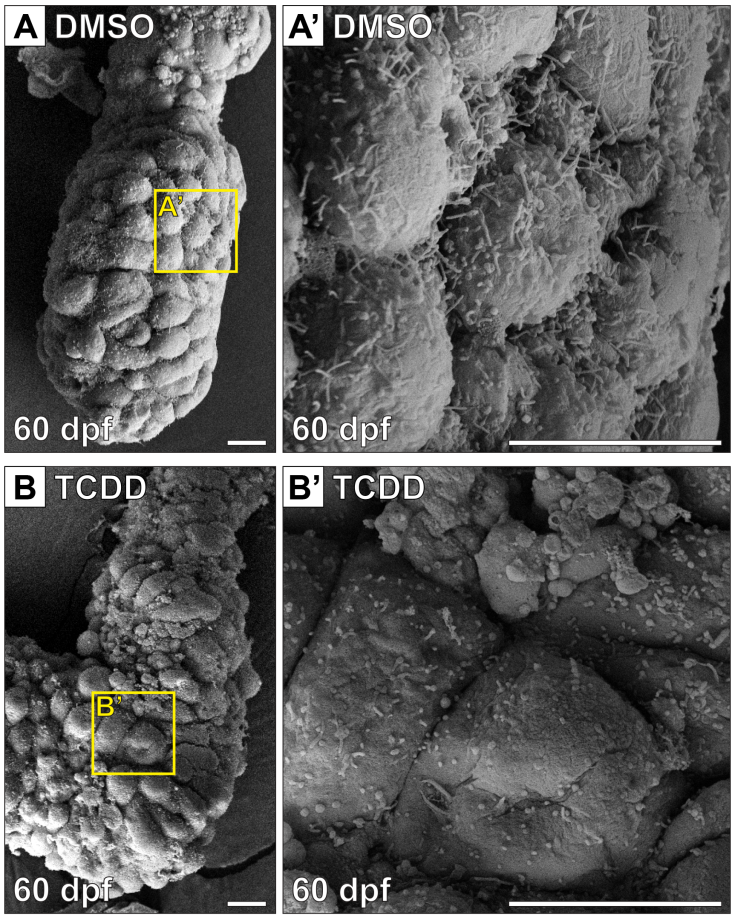

Figure 3. TCDD exposure alters the surface topography of the heart myocardium

Embryos were exposed to (A) DMSO (0.1%, vehicle control), or (B) TCDD (1 ng/ml; 1 hour, waterborne) at 4 hpf and hearts were isolated at 60 hpf and imaged using scanning electron microscopy (SEM). (A) and (B) show views centered on the ventricle. (A') and (B') are higher magnification images of the boxes in (A) and (B), respectively. (A) Many long villi-like structures are present on the surface of the DMSO-exposed myocardium, extending between cells. (B) In contrast, similar villi-like structures are absent from the surface of the TCDD-exposed myocardium and instead small round spheres are present. Overall the TCDD-exposed heart appears to have a smoother myocardial surface with fewer structures. Representative images are shown (n = 5). Scale bars = 10 μm.

REFERENCES

Abnet, C.C., Tanguay, R.L., Heideman, W., Peterson, R.E., 1999. Transactivation activity of human, zebrafish, and rainbow trout aryl hydrocarbon receptors expressed in COS-7 cells: Greater insight into species differences in toxic potency of polychlorinated dibenzo-*p*-dioxin, dibenzofuran, and biphenyl congeners. *Toxicol. Appl. Pharmacol*. 159, 41-51.

Akerboom, J., Chen, T.W., Wardill, T.J., Tian, L., Marvin, J.S., Mutlu, S., Calderón, N.C., Esposti, F., Borghuis, B.G., Sun, X.R., Gordus, A., Orger, M.B., Portugues, R., Engert, F., Macklin, J.J., Filosa, A., Aggarwal, A., Kerr, R.A., Takagi, R., Kracun, S., Shigetomi, E., Khakh, B.S., Baier, H., Lagnado, L., Wang, S.S., Bargmann, C.I., Kimmel, B.E., Jayaraman, V., Svoboda, K., Kim, D.S., Schreiter, E.R., and Looger, L.L., 2012. Optimization of a GCaMP Calcium Indicator for Neural Activity Imaging. *J. Neurosci.* 32, 13819-13840

Andreasen, E.A., Hahn, M.E., Heideman, W., Peterson, R.E., Tanguay, R.L., 2002a. The zebrafish (*Danio rerio*) aryl hydrocarbon receptor type 1 is a novel vertebrate receptor. *Mol*. *Pharmacol*. 62, 234-249.

Andreasen, E.A., Spitsbergen, J.M., Tanguay, R.L., Stegeman, J.J., Heideman, W., Peterson, R.E., 2002b. Tissue-specific expression of AHR2, ARNT2, and CYP1A in zebrafish embryos and larvae: effects of developmental stage and 2,3,7,8-tetrachlorodibenzo-*p*-dioxin exposure. *Toxicol*. *Sci*. 68, 403-419.

Antkiewicz, D.S., Burns, C.G., Carney, S.A., Peterson, R.E., Heideman, W., 2005. Heart malformation is an early response to TCDD in embryonic zebrafish. *Toxicol*. *Sci*. 84, 368-377.

Antkiewicz, D.S., Peterson, R.E., Heideman, W., 2006. Blocking expression of AHR2 and ARNT1 in zebrafish larvae protects against cardiac toxicity of 2,3,7,8- tetrachlorodibenzo-*p*-dioxin. *Toxicol*. *Sci*. 94, 175-182.

Bartman, T., Walsh, E.C., Wen, K., McKane, M., Ren, J., Alexander, J., Rubenstein, P.A., Stainier, D.Y.R., 2004. Early myocardial function affects endocardial cushion development in zebrafish. *PLoS Biol.* 2, 673-681.

Bax, N.A., Lie-Venema, H., Vicente-Steijn, R., Bleyl, S.B., Van Den Akker, N.M., Maas, S., Poelmann, R.E., Gittenberger-de Groot, A.C., 2009. Platelet-derived growth factor is involved in the differentiation of second heart field-derived cardiac structures in chicken embryos. *Dev. Dyn*. 238, 2658-69.

Bax, N.A., Bleyl, S.B., Gallini, R., Wisse, L.J., Hunter, J., Van Oorschot, A.A., Mahtab, E.A., Lie-Venema, H., Goumans, M.J., Betsholtz, C., Gittenberger-de Groot, A.C., 2010. Cardiac malformations in Pdgfralpha mutant embryos are associated with increased expression of WT1 and Nkx2.5 in the second heart field. *Dev*. *Dyn*. 239, 2307-17.

Begemann, G., Gibert, Y., Meyer, M., Ingham, P.W., 2002. Cloning of zebrafish T-box genes tbx15 and tbx18 and their expression during embryonic development. *Mech. Dev*. 114, 137-141.

Belair, C.D., Peterson, R.E., Heideman, W., 2001. Disruption of erythropoiesis by dioxin in the zebrafish. *Dev*. *Dyn*. 222, 581-594.

Bello, S.M., Heideman, W., Peterson, R.E., 2004. 2,3,7,8-Tetrachlorodibenzo-*p*-dioxin inhibits regression of the common cardinal vein in developing zebrafish. *Toxicol. Sci*. 78, 258-266.

Brade, T., Pane, L.S., Moretti, A., Chien, K.R., Laugwitz, K.L., 2013. Embryonic heart progenitors and cardiogenesis. *Cold Spring Harbor Perspect. Med*. 3, a013847.

Burns, F.R., Peterson, R.E., Heideman, W., 2015. Dioxin disrupts cranial cartilage and dermal bone development in zebrafish larvae. *Aquat Toxicol*. 164, 52-60.

Cantrell, S.M., Lutz, L.H., Tillitt, D.E., Hannink, M., 1996. Embryotoxicity of 2,3,7,8-tetrachlorodibenzo-*p*-dioxin (TCDD): the embryonic vasculature is a physiological target for TCDD-induced DNA damage and apoptotic cell death in Medaka (*Orizias latipes*). *Toxicol. Appl. Pharmacol*. 141, 23-34.

Carney, S.A., Chen, J., Burns, C.G., Xiong, K.M., Peterson, R.E., Heideman, W., 2006. Aryl hydrocarbon receptor activation produces heart-specific transcriptional and toxic responses in developing zebrafish. *Mol. Pharmacol*. 70, 549-561.

Choudhary, M., Kazmin, D., Hu, P., Thomas, R.S., McDonnell, D.P., Malek, G., 2015. Aryl hydrocarbon receptor knock-out exacerbates choroidal neovascularization via multiple pathogenic pathways. *J. Pathol.* 235, 101-112.

Dong, W., Teraoka, H., Yamazaki, K., Tsukiyama, S., Imani, S., Imagawa, T., Stegeman, J.J., Peterson, R.E., Hiraga, T., 2002. 2,3,7,8-tetrachlorodibenzo-*p*-dioxin toxicity in the zebrafish embryo: local circulation failure in the dorsal midbrain is associated with increased apoptosis. *Toxicol. Sci*. 69, 191-201.

Drummond, I.A., Majumdar, A., Hentschel, H., Elger, M., Solnica-Krezel, L., Schier, A.F., Neuhauss, S.C., Stemple, D.L., Zwartkruis, F., Rangini, Z., Driever, W., 1998. Early development of the zebrafish pronephros and analysis of mutations affecting pronephric function. *Development* 125, 4655-4667.

Elonen, G.E., Spehar, R.L., Holcombe, G.W., Johnson, R.D., Fernandez, J.D., Erickson, R.J., Tietge, J.E., Cook, P.M., 1998. Comparative toxicity of 2,3,7,8-tetrachlorodibenzo-*p*-dioxin to seven freshwater fish species during early life stage development. *Environ. Toxicol. Chem.* 17, 472-483.

Fransen, M.E., Lemanski, L.F., 1990. Epicardial development in the axolotl, *Ambystoma mexicanum*. *Anat. Rec*. 226, 228-236.

Gittenberger-de Groot, A.C., Winter, E.M., Bartelings, M.M., Goumans, M.J., DeRuiter, M.C., Poelmann, R.E., 2012. The arterial and cardiac epicardium in development, disease and repair. *Differentiation* 84, 41-53.

Goi, M., Childs, S.J., 2016. Patterning mechanisms of the sub-intestinal venous plexus in zebrafish. *Dev. Biol*. 409, 114-128.

Guiney, P.D., Walker, M.K., Spitsbergen, J.M., Peterson, R.E., 2000. Hemodynamic dysfunction and cytochrome P4501A mRNA expression induced by 2,3,7,8- tetrachlorodibenzo-*p*-dioxin during embryonic stages of lake trout development. *Toxicol. Appl. Pharmacol*. 168, 1-14.

Hankinson, O., 1995. The aryl hydrocarbon receptor complex. *Annu. Rev. Pharmacol. Toxicol*. 35, 307-340.

Hatcher, C.J., Diman, N.Y.G., Kim, M.S., Pennisi, D., Song, Y., Goldstein, M.M., Mikawa, T., Basson, C.T., 2004. A role for Tbx5 in proepicardial cell migration during cardiogenesis. *Physiol. Genomics* 18, 129-140.

Henry, T.R., Spitsbergen, J.M., Hornung, M.W., Abnet, C.C., Peterson, R.E., 1997. Early life stage toxicity of 2,3,7,8-tetrachlorodibenzo-*p*-dioxin in zebrafish (*Danio rerio*). *Toxicol. Appl. Pharmacol*. 142, 56-68.

Hofsteen, P., Plavicki, J., Johnson, S.D., Peterson, R.E., Heideman, W., 2013a. Sox9b is required for epicardium formation and plays a role in TCDD-induced heart malformation in zebrafish. *Molec. Pharmacol*. 84, 353-360.

Hofsteen, P., Plavicki, J., Peterson, R.E., Heideman, W., 2013b. Epicardium formation as a sensor in toxicology. *J. Dev. Biol*. 1, 112-125.

Hornung, M.W., Spitsbergen, J.M., Peterson, R.E., 1999. 2,3,7,8-Tetrachlorodibenzo-*p*-dioxin alters cardiovascular and craniofacial development and function in sac fry of rainbow trout (*Oncorhynchus mykiss*). *Toxicol. Sci*. 47, 40–51.

Isogai, S., Horiguchi, M., Weinstein, B.M., 2001. The vascular anatomy of the developing zebrafish: an atlas of embryonic and early larval development. *Dev. Biol*. 230, 278-301.

Kawamura, T., Yamashita, I., 2002. Aryl hydrocarbon receptor is required for prevention of blood clotting and for the development of vasculature and bone in the embryos of medaka fish, *Oryzias latipes*. *Zool. Sci*. 19, 309-319.

King-Heiden, T.C., Mehta, V., Xiong, K.M., Lanham, K.A., Antkiewicz, D.S., Ganser, A., Heideman, W., Peterson, R.E., 2012. Reproductive and developmental toxicity of dioxin in fish. *Mol. Cell. Endocrinol*. 354, 121-138.

Kim, K.H., Park, H.J., Kim, J.H., Kim, S., Williams, D.R., Kim, M.K., Do Jung, Y., Teraoka, H., Park, H.C., Choy, H.E., Shin, B.A., 2013. Cyp1a reporter zebrafish reveals target tissues for dioxin. *Aquat. Toxicol*. 134, 57-65.

Koenig, A.L., Baltrunaite, K., Bower, N.I., Rossi, A., Stainier, D.Y.R., Hogan, B.M., Sumanas, S., 2016. Vegfa signaling promotes zebrafish intestinal vasculature development through endothelial cell migration from the posterior cardinal vein. *Dev. Biol*. 411, 115-127.

Komiyama, M., Ito, K., Shimada, Y., 1987. Origin and development of the epicardium in the mouse embryo. *Anat. Embryol*. 176, 183-189.

Lahvis, G.P., Lindell, S.L., Thomas, R.S., McCuskey, R.S., Murphy, C., Glover, E., Bentz, M., Southard, J., Bradfield, C.A., 2000. Portosystemic shunting and persistent fetal vascular structures in aryl hydrocarbon receptor-deficient mice. *Proc. Natl. Acad. Sci. U.S.A*. 97, 10442-10447.

Lanham, K.A., Plavicki, J., Peterson, R.E., Heideman, W., 2014. Cardiac myocyte-specific AHR activation phenocopies TCDD-induced toxicity in zebrafish. *Toxicol. Sci.* 141, 141-54.

Lee, G.H., Chang, M.Y., Hsu, C.H., Chen, Y.H., 2011. Essential roles of basic helix-loop-helix transcription factors, Capsulin and Musculin, during craniofacial myogenesis of zebrafish. *Cell. Mol. Life Sci*. 68, 4065-4078.

Liu, J., Stainier, D.Y., 2010. Tbx5 and Bmp signaling are essential for proepicardium specification in zebrafish. *Circ. Res*. 106, 1818-1828.

Männer, J., 1992. The development of pericardial villi in the chick embryo. *Anat. Embryol*. 186, 379-385.

McGuire, J., Okamoto, K., Whitelaw, M.L., Tanaka, H., Poellinger, L., 2001. Definition of a dioxin receptor mutant that is a constitutive activator of transcription: Delineation of overlapping repression and ligand binding functions within the PAS domain. *J. Biol. Chem*. 276, 41841-41849.

Mehta, V., Peterson, R.E., Heideman, W., 2008. 2,3,7,8-Tetrachlorodibenzo-*p*-dioxin exposure prevents cardiac valve formation in developing zebrafish. *Toxicol. Sci*. 104, 303–311.

Mellgren, A.M., Smith, C.L., Olsen, G.S., Eskiocak, B., Zhou, B., Kazi, M.N., Ruiz, F.R., Pu, W.T., Tallquist, M.D., 2008. Platelet-derived growth factor receptor beta signaling is required for efficient epicardial cell migration and development of two distinct coronary vascular smooth muscle cell populations. *Circ. Res*. 103, 1393-401.

Nahirney, P.C., Mikawa, T., Fischman, D.A., 2003. Evidence for an extracellular matrix bridge guiding proepicardial cell migration to the myocardium of chick embryos. *Dev. Dyn*. 227, 511-523.

Nath, A.K., Ryu, J.H., Jin, Y.N., Roberts, L.D., Dejam, A., Gerszten, R.E., Peterson, R.T., 2015. PTPMT1 inhibition lowers glucose through succinate dehydrogenase phosphorylation. *Cell Rep*. 10, 694-701.

Ortiz-Delgado, J.B., Sarasquete, C., 2004. Toxicity, histopathological alterations and immunohistochemical CYP1A induction in the early life stages of the seabream, *Sparus aurata*, following waterborne exposure to B(a)P and TCDD. *J. Mol. Histol*. 35, 29-45.

Peralta, M., Steed, E., Harlepp, S., González-Rosa, J.M., Monduc, F., Ariza-Cosano, A., Cortés, A., Rayón, T., Gómez-Skarmeta, J.L., Zapata, A., Vermot, J., 2013. Heartbeat-driven pericardiac fluid forces contribute to epicardium morphogenesis. *Curr. Biol*. 23, 1726-1735.

Peterson, R.E., Theobald, H.M., Kimmel, G.L., 1993. Developmental and reproductive toxicity of dioxins and related compounds: cross-species comparisons. *Crit. Rev. Toxicol*. 23, 283-335.

Planchart, A., Mattingly, C.J., 2010. 2,3,7,8-Tetrachlorodibenzo-*p*-dioxin upregulates FoxQ1b in zebrafish jaw primordium. *Chem. Res. Toxicol*. 23, 480-487.

Plavicki, J., Hofsteen, P., Peterson, R.E., Heideman, W., 2013. Dioxin inhibits zebrafish epicardium and proepicardium development. *Toxicol. Sci*. 131, 558-567.

Poland, A., Glover, E., Kende, A.S., 1976. Stereospecific, high affinity binding of 2,3,7,8-tetrachlorodibenzo-*p*-dioxin by heaptic cytosol. Evidence that the binding species is receptor for induction of aryl hydrocarbon hydroxylase. *J. Biol. Chem.* 251, 4936-4946.

Prasch, A.L., Teraoka, H., Carney, S.A., Dong, W., Hiraga, T., Stegeman, J.J., Heideman, W., Peterson, R.E., 2003. Aryl hydrocarbon receptor 2 mediates 2,3,7,8- tetrachlorodibenzo-*p*-dioxin developmental toxicity in zebrafish. *Toxicol. Sci*. 76, 138-150.

Prasch, A.L., Tanguay, R.L., Mehta, V., Heideman, W., Peterson, R.E., 2006. Identification of zebrafish ARNT1 homologs: 2,3,7,8-tetrachlorodibenzo-*p*-dioxin toxicity in the developing zebrafish requires ARNT1. *Mol. Pharmacol*. 69, 776-787.

Rodgers, L.S., Lalani, S., Runyan, R.B., Camenisch, T.D., 2008. Differential growth and multicellular villi direct proepicardial translocation to the developing mouse heart. *Dev. Dyn*. 237, 145-152.

Schmidt, J. V., Bradfield, C.A., 1996. Ah receptor signaling pathways. *Annu. Rev. Cell Dev. Biol*. 12, 55-89.

Sehnert, A.J., Huq, A., Weinstein, B.M., Walker, C., Fishman, M., Stainier, D.Y.R., 2002. Cardiac troponin T is essential in sarcomere assembly and cardiac contractility. *Nat. Genet*. 31, 106-10.

Sengbusch, J.K., He, W., Pinco, K.A., Yang, J.T., 2002. Dual functions of α4β1 integrin in epicardial development initial migration and long-term attachment. *J. Cell Biol*. 157, 873-882.

Serluca, F.C., 2008. Development of the proepicardial organ in zebrafish. Dev. Biol. 315, 18-27.

Serluca, F.C., Fishman, M.C., 2001. Pre-pattern in the pronephric kidney field of zebrafish. Development 128, 2233-2241.

Shimizu, Y., Ito, Y., Tanaka, H., Ohshima, T., 2015. Radial glial cell-specific ablation in the adult Zebrafish brain. *Genesis* 53, 431-439.

Takahashi, M., Yamagishi, T., Narematsu, M., Kamimura, T., Kai, M., Nakajima, Y., 2014. Epicardium is required for sarcomeric maturation and cardiomyocyte growth in the ventricular compact layer mediated by transforming growth factor β and fibroblast growth factor before the onset of coronary circulation. *Congenit. Anom*. 54, 162-171.

Tanguay, R.L., Abnet, C.C., Heideman, W., Peterson, R.E., 1999. Cloning and characterization of the zebrafish (*Danio rerio*) aryl hydrocarbon receptor. *Biochim. Biophys. Acta* 1444, 35-48.

Teraoka, H., Dong, W., Okuhara, Y., Iwasa, H., Shindo, A., Hill, A.J., Kawakami, A., Hiraga, T., 2006. Impairment of lower jaw growth in developing zebrafish exposed to 2,3,7,8-tetrachlorodibenzo-*p*-dioxin and reduced hedgehog expression. *Aquat. Toxicol*. 78, 103-113.

Teraoka, H., Ogawa, A., Kubota, A., Stegeman, J.J., Peterson, R.E., Hiraga, T., 2010. Malformation of certain brain blood vessels caused by TCDD activation of Ahr2/Arnt1 signaling in developing zebrafish. *Aquat. Toxicol*. 99, 241-247.

Weeke-Klimp, A., Bax, N.A., Bellu, A.R., Winter, E.M., Vrolijk, J., Plantinga, J., Maas, S., Brinker, M., Mahtab, E.A., Gittenberger-de Groot, A.C., van Luyn, M.J., 2010. Epicardium-derived cells enhance proliferation, cellular maturation and alignment of cardiomyocytes. *J. Mol. Cell. Cardiol*. 49, 606-616.

Winata, C.L., Korzh, S., Kondrychyn, I., Zheng, W., Korzh, V., Gong, Z., 2009. Development of zebrafish swimbladder: The requirement of Hedgehog signaling in specification and organization of the three tissue layers. *Dev. Biol*. 331, 222-36.

Winata, C.L., Korzh, S., Kondrychyn, I., Korzh, V., Gong, Z., 2010. The role of vasculature and blood circulation in zebrafish swimbladder development. *BMC Dev. Biol*. 10, 3.

Wu, M.Y., Ramel, M.C., Howell, M., Hill, C.S., 2011. SNW1 is a critical regulator of spatial BMP activity, neural plate border formation, and neural crest specification in vertebrate embryos. *PLoS Biol*. 9, e1000593.

Xiong, K.M., Peterson, R.E., Heideman, W., 2008. Aryl hydrocarbon receptor-mediated downregulation of Sox9b causes jaw malformations in zebrafish embryos. *Mol*. *Pharmacol*. 74, 1544-1553.

Yin, A., Korzh, S., Winata, C.L., Korzh, V., Gong, Z., 2011. Wnt signaling is required for early development of zebrafish swimbladder. *PloS One* 6, e18431.